AD NUMBER

AD843334

NEW LIMITATION CHANGE

TO

Approved for public release, distribution unlimited

FROM

Distribution authorized to U.S. Gov't. agencies and their contractors; Administrative/Operational Use; OCT 1968. Other requests shall be referred to Rome Air Development Center, Attn: FMCRR, Griffiss AFB, NY 13440.

AUTHORITY

RADC USAF ltr, 31 Jan 1974

RADC-TR-68-221
Final Report

ACTIVE ELEMENT ARRAY

P. Ver Planck
W. Ku
T. Glynn

Sylvania Electronic Systems
Applied Research Laboratory

TECHNICAL REPORT NO. RADC-TR- 68-221
October 1968

Rome Air Development Center
Air Force Systems Command
Griffiss Air Force Base, New York

When US Government drawings, specifications, or other data are used for any purpose other than a definitely related government procurement operation, the government thereby incurs no responsibility nor any obligation whatsoever; and the fact that the government may have formulated, furnished, or in any way supplied the said drawings, specifications, or other data is not to be regarded, by implication or otherwise, as in any manner licensing the holder or any other person or corporation, or conveying any rights or permission to manufacturer, use, or sell any patented invention that may in any way be related thereto.

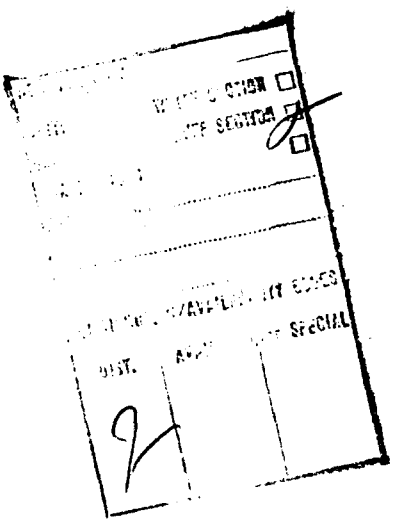

Do not return this copy. Retain or destroy.

ACTIVE ELEMENT ARRAY

Ver Planck
W. Ku
T. Glynn

Sylvania Electronic Systems
Applied Research Laboratory

AFLC, GAFB, N.Y., 1 Nov 78-6

FOREWORD

This final report was prepared by the Applied Research Laboratory, Sylvania Electronic Systems, 40 Sylvan Road, Waltham, Massachusetts, 02154, under Contract No. F30602-67-C-0189, Project 4519, Project 451901. The work was done under the direction of Rome Air Development Center, Griffiss Air Force Base, New York 13440. Project Monitor of this contract was Anthony Snyder, EMCRR. This report covers work conducted from 2 February 1967 to 16 April 1968.

This technical report has been reviewed and is approved.

Approved: Anthony F. Snyder
ANTHONY F. SNYDER
Project Engineer

Approved: Richard M. Cosel
RICHARD M. COSEL
Colonel, USAF
Chief, Communications Division

FOR THE COMMANDER: Irving J. Gabelman
IRVING J. GABELMAN
Chief, Advanced Studies Group

ABSTRACT

This report describes the Active Element Array study which was conducted to determine the feasibility of constructing a 16-element microwave retrodirective array employing spiral antennas and bilateral tunnel diode amplifiers.

A number of significant results were obtained. The shunt-diode type of amplifier originally proposed was shown to be impractical for small arrays because of its inherent mismatch. Computed patterns for the 4 x 4 case showed little evidence of retrodirectivity, and there were even "blind angles" at which no return was received at all. The amplifier mismatch problem can be eliminated if other bilateral circuits are used; unfortunately, all of these circuits contain at least two active devices, and are roughly equivalent in complexity to two unilateral amplifiers. In addition, there is a gain limitation imposed by the inherent mismatch of the antenna elements which is peculiar to bilateral-amplifier arrays. The gain of a unilateral array is limited only by the inter-antenna isolation. For the cavity-backed spiral antennas constructed under the present contract, the inter-antenna isolation exceeded the mismatch return loss by as much as 30 dB, so that the 6-dB gain advantage of the bilateral scheme was totally negated by the mismatch-imposed gain limitation.

The results of this study indicate that future investigations should concentrate on Van Atta arrays composed of a few well-isolated antenna elements interconnected by high-gain unilateral amplifiers. Use of superregenerative circuits should be considered as a means of attaining very high gains and frequency conversion with a minimum of complexity. Avalanche diodes and microwave transistors are particularly attractive for this application.

TABLE OF CONTENTS

TABLE OF CONTENTS (Continued)

TABLE OF CONTENTS (Continued)

TABLE OF CONTENTS (Continued

TABLE OF CONTENTS (Continued)

LIST OF ILLUSTRATIONS

LIST OF ILLUSTRATIONS (Continued)

LIST OF ILLUSTRATIONS (Continued)

LIST OF ILLUSTRATIONS (Continued)

LIST OF ILLUSTRATIONS (Continued)

EVALUATION

This effort was to determine feasibility of building a two-dimensional retrodirective array with bilateral amplifiers integral with the interconnecting transmission lines. Considerable time was spent in obtaining an equiangular spiral antenna with good circularity and VSWR's compatible with the gain specifications of the amplifiers. Calculations showed that unilateral amplifiers have a gain advantage, due to antenna mismatch, over an array utilizing bilateral amplifiers. In addition, the calculations showed that a large array of bilateral units gave the desired retrodirective beam but for appreciable array spacing "blind angles" appeared where no retrodirective beam is formed. For these reasons the contractor abandoned the bilateral concept and concentrated on optimizing arrays utilizing unilateral amplifiers.

A number of design considerations for active Van Atta arrays were analyzed, including choice of antenna type, array layout, amplifier type, and choice of interconnection scheme.

Many amplifier types were analyzed assuming non-ideal hybrids and circulators. The resulting mismatch is shown to have a very severe effect on overall array performance. Consideration was also given to the effects of mutual coupling on array performance.

In summary, this report contains an extensive theoretical analysis of Van Atta arrays and should provide users with an excellent reference text in the design of arrays of this nature.

Anthony F. Snyder

ANTHONY F. SNYDER
Project Engineer

SECTION I

INTRODUCTION

This technical report presents the findings and accomplishments of a 12 month study of active Van Atta arrays conducted under Contract No. F30602-67-C-0189. The intent of the investigation was to determine the feasibility of constructing a lightweight 16-element planar Van Atta array which would act as a retroreflector for incident microwave signals. The array was to consist of 8 pairs of spiral antennas, the antennas of each pair being interconnected via a tunnel diode amplifier. The design frequency was 4.5 GHz, with gain and bandwidth objectives of 18 dB and 200 MHz, respectively. Consideration was limited to bilateral amplifiers, so that each antenna element would be used both in receiving and transmitting, with a consequent 6-dB gain increase over the more conventional array employing unidirectional amplifiers. Topics to be investigated included array stability, bistatic array patterns, and the use of various amplifier-integration techniques.

The array design as originally proposed contained some very significant flaws which gradually became apparent during the course of the study program. The amplifier for a typical array element was to consist simply of a biased tunnel diode shunting the interconnecting transmission line at its center. This type of amplifier is particularly easy to integrate into a planar array, especially when compared to more conventional tunnel-diode amplifiers employing circulators or hybrids. Computed pattern data in paragraph 4.4.5 show that arrays using this type of amplifier operate according to the qualitative theory only if the number of elements is quite large. While an 8 x 8 array works well, the retrodirective performance of a 4 x 4 array is very poor.

The difficulty with the shunt-diode configuration lies in the fact that a significant portion of the amplified wave from the tunnel diode is returned to the input antenna and reradiated, rather than conducted to the conjugate antenna as required in the Van Atta array. In large arrays, this reflected energy forms a specular beam; however, for small numbers of elements the specular and retrodirected beams interact strongly, producing a broad, smeared pattern.

There are several well-known circuits which achieve bilateral amplification and yet are well matched at their ports; the hybrid-coupled tunnel diode amplifier is one which appeared to be ideal for the present application. Carefully matched terminations must be provided for any type of bidirectional amplifier, since reflections due to termination mismatch can cause positive feedback and consequent instability. In a bilateral Van Atta array, antenna mismatch has the same effect as increased antenna coupling.

A significant part of the present investigation was concerned with the development of a planar equiangular spiral antenna which had an acceptable pattern shape and circularity, together with the near-perfect match required for use with bidirectional amplifiers. At the same time, it was desired that the antenna assume a form suitable for integration into an inexpensive, lightweight array. After extensive experimentation, a resistance-terminated, cavity-backed antenna was developed which had a VSWR of less than 1.043 over a 14 percent band centered at 4.3 GHz, but weighed 1 lb., 5 oz. A second antenna was built to test the reproducibility of the match. The VSWR of the second model was also very low, but its detailed behavior as a function of frequency was substantially different from that of the first model. Even with the best of machining techniques, it is unrealistic to expect that a VSWR of 1.04 can be achieved consistently, particularly when the interconnecting cable and amplifier connector are included.

The mutual coupling between the two spiral antennas was determined over a range of frequencies for several different spacings, and found to vary from -30 dB to -60 dB. It is important to note that the return loss of one antenna due to its 1.04 VSWR is only 34 dB. The comparison of the numerical magnitudes of return loss and mutual coupling clearly favors the use of unidirectional amplifiers instead of bidirectional amplifiers, since much higher gains can be achieved in the former case, regardless of the antenna VSWR. The 6-dB gain advantage of the bidirectional scheme is thus completely negated by the effects of antenna mismatch for any case where antenna return loss exceeds the largest mutual coupling magnitude.

Section II summarizes a number of design considerations for active Van Atta arrays, including choice of antenna type, array layout, amplifier type, and choice of interconnection scheme. Section III deals with the development of a matched, cavity-backed spiral antenna element suitable for use in a bilateral Van Atta array. Detailed experimental data are presented on the pattern,

VSWR, and mutual coupling characteristics of the final antenna models. Section IV develops a detailed theory of the radiation properties of Van Atta arrays. Expressions are developed for the radar cross section of an arbitrary N-pair array, and the pattern of linear uniformly spaced arrays employing various types of amplifiers.

Extensive computed data are presented for all types of Van Atta arrays, particular attention being paid to the shunt-diode-amplifier case. Section V deals with the circuit properties of a number of different bilateral amplifier schemes. The circulator-coupled unilateral amplifier is included for completeness. One important result of the section, contained in paragraph 5.2, is the demonstration that a perfectly matched 2-port bilateral amplifier cannot be built using only one tunnel diode. Any single-diode amplifier with gain must return a significant portion of the amplified signal back to the input port. In an active Van Atta array, this returned energy degrades the retrodirected pattern. Paragraphs 5.3 and 5.4 summarize the behavior of several different types of bilateral and unilateral amplifiers built with nonideal hybrids and circulators. Mismatch effects are shown to be particularly severe.

Section VI deals with the stability of the entire Van Atta array and brings out the important effects of antenna mismatch and mutual coupling on array performance. Section VII contains a number of conclusions and recommendations on the design of active Van Atta arrays.

SECTION II

GENERAL DESIGN CONSIDERATIONS FOR AN ACTIVE VAN ATTA ARRAY

2.1 DESIRABLE CHARACTERISTICS FOR A RETRODIRECTIVE ARRAY

In this section we review briefly the properties of an ideal Van Atta array and indicate how these properties are affected by the choice of antenna type, spacing, array layout, amplifier type, etc. Results of the present investigation will be included where they apply.

By definition, a retrodirective array is an assembly of antennas which re-transmits an incident wavefront back toward the sender, regardless of the latter's position in space. An ideal array would have a constant radar cross section over all angles, so that the power level returned to the sender would not depend on the array's orientation. These considerations dictate a spherical configuration with broad-beam antenna elements pointing out in all directions. Unfortunately, the Van Atta scheme for achieving retrodirectivity by connecting conjugate pairs of antennas together by equal lengths of transmission line works only for linear or planar antenna arrangements. To obtain spherical coverage with one of these arrays, one must use an approximation of some sort, such as a polyhedron with independent planar arrays on each surface. The wider the angular coverage of the component arrays, the smaller the number of surfaces required. One can, of course, envision applications where a more limited coverage would suffice; for example, a ground beacon for use with an aircraft radar should have good coverage at low angles of elevation and be omni-directional in azimuth. Coverage at high angles can be less because of reduced distance to the aircraft, and only one hemisphere need be covered. For this particular application, a vertical linear array of omni-directional cylindrical dipoles would be ideal.

It is desirable for a Van Atta array to have as large a radar cross section σ as possible so that it can be "seen" at long distances. Paragraph 4.2.4 shows that σ varies with the square of the number of elements and the square of the amplifier gain used. Clearly, the amplifier gain cannot be made arbitrarily large because of the presence of positive feedback in the form of antenna mutual coupling. A frequency offset between the receiving and transmitting bands may be necessary if very high gains are to be achieved.

If a Van Atta array is used as part of a secure communication link, then the returned beam should be very narrow and pointed directly at the interrogator. A linear Van Atta array such as the ground beacon mentioned earlier will scatter uniformly in azimuth with a narrow elevation beamwidth, so that any aircraft at the same elevation angle as the interrogator would also receive the returned signal. The same type of spurious radiation can result from a planar array in which the element spacing is greater than 1/2 wavelength, so that grating lobes appear. An array which employs amplifiers in its interconnecting transmission lines will transmit both a retrodirective and a specular beam if the amplifiers are not matched to the antenna elements.

2.2 CONSIDERATIONS IN THE CHOICE OF AN ANTENNA ELEMENT

The angular coverage of a planar Van Atta array can only be as large as that of its component antennas; thus a very broad-beam antenna must generally be used. If an array is to be oriented more or less randomly with respect to the interrogator, the array antenna should be circularly polarized rather than linear, so that input waves of arbitrary linear polarization can be received and re-transmitted. Circular polarization for both the interrogator and the array is clearly the optimum choice. Finally, it should be possible to pack the antenna elements close together without an intolerable amount of mutual coupling, so that grating lobes can be avoided and the array will be reasonably compact.

The planar cavity-backed equiangular spiral is a good choice for the antenna element, in view of the considerations mentioned above. In addition, the spiral can be matched over a wide frequency range so that use of reflection-type amplifiers is feasible. Unfortunately, very little information on the design of practical cavity-backed spirals is available. A great deal of experimentation is required to develop an element with a clean, circularly polarized pattern which is at the same time electrically small in diameter and well matched.

In the present investigation a very well matched spiral antenna element was developed which had a reasonably good pattern. The mutual coupling between a pair of these elements was measured and found to be very small, anywhere from -30 dB to -60 dB depending on spacing and frequency. We found it necessary to make the antenna some 3/4 wavelengths in diameter for high efficiency, and

that the rather large cavity center post required to contain the matching network degraded the pattern somewhat.

2.3 ARRAY LAYOUT

The geometry of the element-pair layout in a Van Atta array would seem to be of prime importance in determining its retrodirective properties. In fact, the present study has shown (see paragraph 4.2.3) that the retrodirective cross section of a planar Van Atta array measured from a particular elevation angle is independent of the element pair arrangement. It is, of course, necessary to maintain the elements of each pair in conjugate positions, the element at (x,y) being connected to that at (-x,-y). Azimuthal variation of the element patterns is assumed nil.

Variations in element arrangement and spacing cause the width of the retrodirected beam to vary, and may cause the appearance of grating lobes. These characteristics of the Van Atta array are easy to understand when one observes that, in the retrodirective direction, all of the transmitting antennas are radiating in phase, regardless of their position in the plane of the array.

The difference between one array layout and another is manifested in the appearance of grating lobes, different mutual coupling between elements, and in the detailed behavior of the radiation pattern off the retrodirective direction. The "retrodirective beamwidth" is very much a function of arrangement and spacing. For closely spaced elements, the returned beam is relatively broad, while the converse is true for widely separated elements. Beamwidth considerations could be important if the transmitter and receiver are not at exactly the same angular position, or if a pointing error is present in the array due to mechanical or electrical imperfections.

2.4 CHOICE OF AMPLIFIER TYPE

Several types of amplifiers are suitable for use in the interconnecting lines of an active Van Atta array. The choice of an amplifier type is based on considerations of antenna-element mutual coupling, element mismatch, array performance desired and, most important of all, cost.

The simplest type of Van Atta array employs unilateral amplifiers in the interconnection cables, so that the antennas connected to the amplifier inputs are used exclusively for receiving the incident wave, and those connected to the amplifier outputs for re-transmitting the retrodirected beam. The stability of this class of array is a function only of the amplifier gains and the various cross-couplings between transmitting and receiving elements. A detailed analysis of the stability problem is presented in Section VI. Qualitatively, one can state that the gain per amplifier is bounded by the reciprocal of the largest mutual-coupling magnitude.

It is evident that the unilateral-amplifier scheme does not make the most efficient use of the array aperture, since only half the total number of elements are active as transmitters or receivers. Use of matched bilateral amplifiers would allow each antenna element to act simultaneously as a transmitter and as a receiver. Effectively, a bilateral-amplifier array is equivalent to two unilateral-amplifier arrays superimposed on one another, so that the retrodirective gain is higher by a factor of 4 (6 dB). The unfortunate flaw in this scheme is that the antenna elements must be extremely well matched to the transmission lines and the bilateral amplifier, since the amplifier makes no distinction between a radiation input to one of the antennas and a reflection due to antenna mismatch. The latter reflections act like additional positive feedback in the unilateral-amplifier case, so that the gain stability is degraded. A major result of the present investigation was to show that, in the case of cavity-backed spirals, the gain limitation imposed by antenna-element return loss is much more serious than that imposed by antenna mutual coupling alone. Thus, the unilateral amplifier scheme is preferable to any type of bilateral scheme on a gain-stability basis, in addition to being preferable because of circuit simplicity.

Originally our intention was to use a bilateral amplifier consisting of a shunt negative resistance at the center of the interconnecting line. The feasibility of this scheme was demonstrated for a two-pair array by Snyder at RADC.[1] This type of amplifier is bilateral, but has the property that the amplified output wave is applied equally to both antennas, with the result that both a specular and retrodirected beam are formed. Further, the analysis of paragraph 4.4.5 shows that there may be a "blind" angle for which the return from the array disappears, though at other angles it operates as expected from the qualitative theory. Also, unless

the number of element pairs is large, significant beam-pointing errors occur. Circuit considerations show that this "shunt-diode" amplifier scheme requires four times (6 dB) more amplifier gain than the matched-amplifier case (paragraph 5.3.3). For these reasons, the shunt-diode amplifier was abandoned in favor of the matched bilateral amplifier.

2.5 TRANSMISSION-LINE AND INTERCONNECTION CONSIDERATIONS

The uses to which a practical active Van Atta array could be put depend very strongly on how light in weight and inexpensive it could be made. A planar, stripline construction in which the spiral antennas, amplifiers, and interconnecting lines were etched on a single piece of copper-clad dielectric would be ideal. Small metal cups could be used on the back of the spirals for cavities. It would first appear that line-crossing problems would arise in connecting each element to its conjugate; however, it is a simple matter to devise a planar arrangement of lines in which no crossings occur, though the lines connecting the outer antennas need to be much longer than the lines connecting the central ones (see Figure 1). The phase delays of the various lines could be equalized by making the line lengths increase in steps of one wavelength, or by meandering the inner lines, or both.

Our experiments with stripline edge-fed spirals met with little success because of pattern problems and high VSWR (see paragraph 3.3.5). In retrospect, the use of resistive terminations and spirals of lower expansion rates might have yielded better results. However, precision matching of the antenna would still have been extremely difficult since there is no practical way to make VSWR measurements directly in the stripline itself. The stripline-to-coax transitions available have VSWR's which are prohibitive. If one were to use circulator-coupled, unidirectional amplifiers instead of bidirectional amplifiers, the antenna matching problem would largely disappear, and the edge-fed planar spiral approach might become very attractive. Circulators with suitable characteristics can now be made less than 1/4 inch in diameter.[2]

The requirement for bidirectional amplifiers demands that each antenna be very carefully matched to the interconnecting lines, and that the number of connectors be held to an absolute minimum. We adopted 0.141-inch semirigid copper-jacketed cable for the interconnections, since it is mechanically stable and the characteristic impedance can be held to close tolerances. We used the

rather large N-type connector on the antenna model both for convenience in VSWR measurements and because of the need for mechanical precision in the machining of the matching network. The resulting antenna achieved the desired VSWR with bandwidth to spare, but can hardly be recommended for inclusion in a lightweight array.

In summary, it does not appear to be feasible at present to build the well-matched antennas and circuit components required in a bidirectional-amplifier Van Atta array without incurring the weight and size penalties of coaxial components. Relaxation of the matching requirement through the use of circulator-coupled unilateral amplifiers would allow the use of modern integrated-microwave-circuit technology throughout, with consequent savings in size and weight.

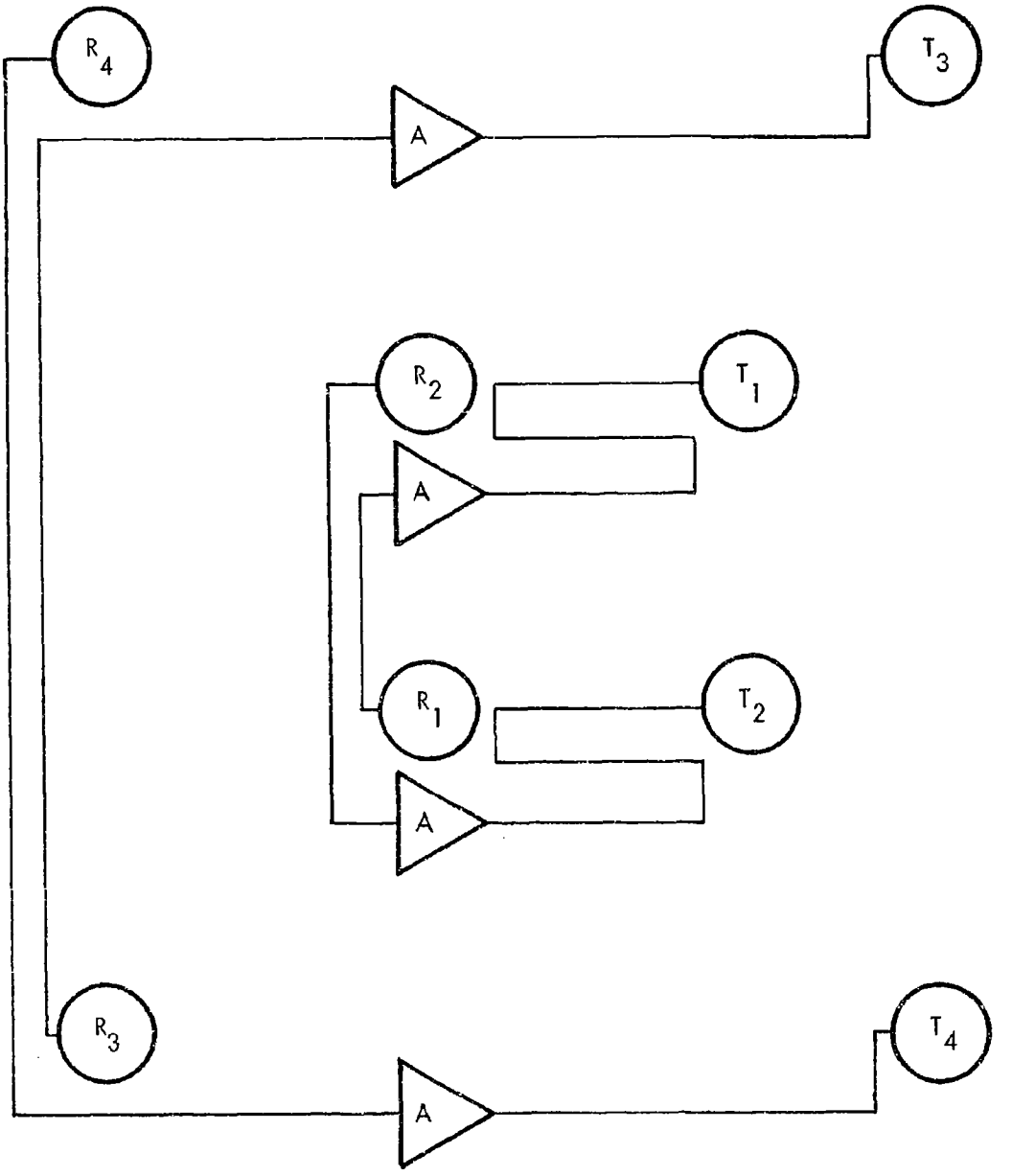

Figure 1. Planar Van Atta Array

BLANK PAGE

SECTION III

ANTENNA DEVELOPMENT

3.1 SUMMARY

An important part of the present investigation was concerned with developing a suitable radiating element for the Van Atta array. Consideration was limited to planar equiangular spirals because of their broad beam, circular polarization, and frequency-independent impedance characteristics. As discussed in paragraph 2.1, coverage of one hemisphere was desired, so that some sort of reflector had to be placed behind the spiral element.

The literature on spiral antennas is very sparse, particularly with regard to proven cavity-backed designs for the microwave region. The published theory appears to be entirely inadequate for the treatment of reflector-backed spirals. After considerable experimentation, we arrived at a suitable antenna design utilizing a resistance-terminated self-complementary spiral of expansion rate 1.4 per turn mounted over a cavity 1/4 wavelength deep at 4.5 GHz. A special center-post design was used to provide loading at the feed region of the antenna, and acted as the outer conductor for the coaxial feed line and matching network. A VSWR of less than 1.043 was achieved over a 14 percent bandwidth centered at 4.3 GHz.

A series of measurements was made of the mutual coupling between a pair of cavity-backed spiral antenna elements. The measured isolation ranged from 32 dB to 50 dB over 4.1 GHz to 4.9 GHz, with the antennas at their minimum spacing of 1.14 wavelength. The magnitude of the isolation sets an upper limit on the amplifier gain which can be used in an active Van Atta array; comparison of the isolation with the return loss of the individual elements determines whether a bidirectional amplifier scheme is practical or not. A VSWR of 1.05 corresponds to a return loss of 32.25 dB. Even for the exceptionally well-matched antennas we have constructed, the stable gain which can be obtained with a unidirectional amplifier far exceeds that achievable with any bidirectional scheme.

Paragraph 3.2 summarizes the results of the theory of planar equiangular spirals, and is mainly derived form Rumsey.[3] Paragraph 3.3 describes our initial experiments which were based on theoretical predictions. Our results were rather poor, and led us to seek outside assistance. Discussions with engineers at SES-West led to the design of the matched, resistance-terminated, cavity-backed antennas described in paragraph 3.4. Finally, a series of mutual coupling measurements was carried out on a pair of our antennas, as described in paragraph 3.5. Isolations exceeding 50 dB were measured at some frequencies. No advantage in using cross-polarized spirals could be discerned.

3.2 BRIEF REVIEW OF THE THEORY OF PLANAR EQUIANGULAR SPIRALS

The planar equiangular spiral antenna has been extensively studied by Dyson[4] and Rumsey[3] at the University of Illinois. The two-arm spiral pictured in Figure 2 consists of two metal arms of angular width α, separated by spaces of angular width $180^{\circ} - \alpha$.

The arms are generated by rotating the spiral curve

$$r = ke^{a\phi}$$

through an angle α. The expansion rate 'f' per turn is given by

$$fr = ke^{a(\phi + 2\pi)}$$

$$\therefore \quad f = e^{a2\pi}$$

An infinite spiral antenna may be described by two angles. One is the arm width α, and the other the angle $A = \cot^{-1}(a)$ which the radius vector makes with the tangent to the spiral curve. Scaling the antenna does not change it, except for rotation. Thus, the radiation characteristics are independent of frequency.

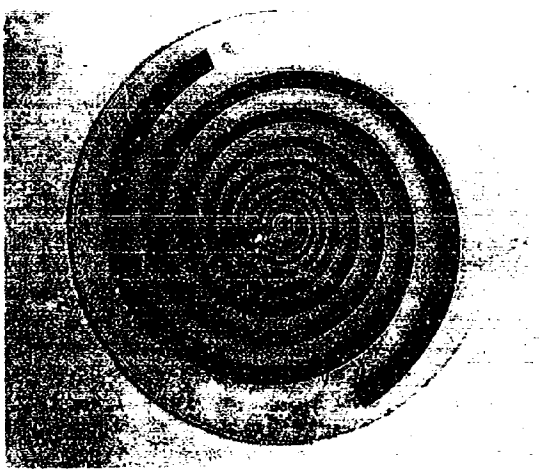

Figure 2. Two-Arm Equiangular Spiral Etched on Dielectric
$\alpha = 75°$, $f = 1.75$

It has been theorized, and fairly well substantiated experimentally, that the equiangular spiral radiates principally from a narrow annular zone one wavelength in circumference, similar to a loop antenna terminated in a matched load. As the wavelength is increased and decreased, the active region expands and contracts accordingly. Outside the active region, the attenuation of the waves on the antenna is extremely rapid. A finite equiangular spiral will behave in an approximately frequency-independent manner provided the active region is large enough to be outside the central terminal region, yet small enough to be at least half a turn or so away from the extermities of the antenna.

A two-arm spiral driven from a balanced line will radiate in the so-called fundamental mode, yielding an electric field pattern approximating two equal spheres touching at the feed point. That is, the radiation field varies as cos θ, where θ is measured from the normal to the antenna. Theory predicts that the field strength should vanish in the plane of the antenna, and that the polarization should be circular everywhere. For the self-complementary antenna, in which the arms and spaces are of equal angular width ($\alpha = 90^{o}$), the terminal impedance can be shown to be 189 ohms (Rumsey, [3] p. 27). No such simple statement can be made about the $\alpha \neq 90^{o}$ case, though one would expect antennas with $\alpha < 90^{o}$ to be inductive.

3.3 INITIAL ANTENNA EXPERIMENTS

3.3.1 Introduction

It appeared to us on the basis of Rumsey's work that almost any spiral antenna we built would radiate a cos θ pattern with nearly perfect circular polarization. Particularly important were the predictions that high expansion rates (up to f = 7 per turn) could be used, and that the attenuation of the currents on the arms outside the radiating zone was so fast that no special termination of the arms was required. We were also under the impression that the antenna element impedance could be matched directly to whatever value we desired by altering the arm width angle α, and that a simple ground plane one-quarter wavelength behind the antenna would direct all the

radiation forward without severely altering the pattern or the circular polarization. Our initial antenna models had very poor patterns and high polarization ratios, probably due to feed unbalance. Later, on the advice of engineers at SES-West, we tried larger-diameter, cavity-backed antennas having a very low expansion rate and terminated in a ring of resistive material. These antennas were far more successful than our earlier models, and formed the basis for a series of mutual coupling measurements. For completeness, we are including pictures and descriptions of some of our more successful early models, as well as a discussion of the cavity-backed, terminated units.

3.3.2 Tapered Coaxial Balun

Our initial experiments used baluns of the mode-converter type described by Duncan and Minerva.[5] The balun consists of a length of coaxial cable whose outer conductor is gradually cut away along its length, exposing the center conductor and finally degenerating into a two-wire line. The coaxial sheath is cut in such a way that the line impedance has a Chebyshev distribution along its length to minimize the VSWR for a fixed length, as in a tapered-line transformer. Measurements on the terminated, back-to-back pair of tapered baluns shown in Figure 3 indicated a VSWR of less than 1.2 from 3.2 GHz to 4.6 GHz. At 4.5 GHz the insertion loss was only 0.5 dB, indicating that little if any energy was being lost by radiation. We had designed the balun for a maximum VSWR of 1.035 for frequencies above 3.0 GHz, and suspect that the beads used to support the center conductor probably caused most of the reflections.

Tapered coaxial baluns present an interesting fabrication problem. We manufactured them by soldering the coaxial cable into a hole drilled in a slab of brass, then cutting away the brass and cable sheath together along the prescribed contour with an abrasive drum. The brass guide thus formed was used repeatedly to generate a series of nearly identical baluns. The best results on the sheath were obtained when the teflon insulation was removed prior to sanding; this was accomplished by cooling the cable in liquid nitrogen, then withdrawing the teflon and the center conductor. In some baluns, the dielectric was reinserted after cutting, often with considerable difficulty.

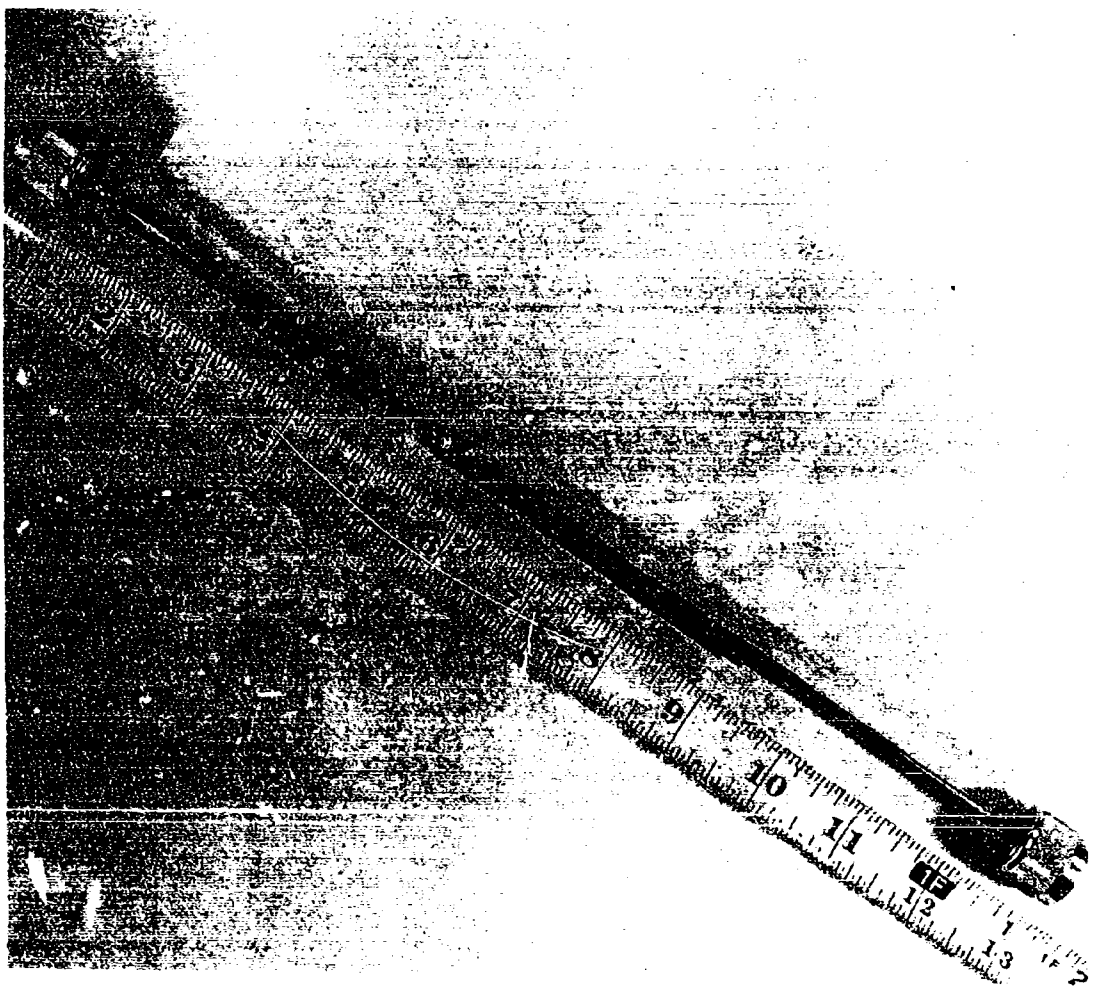

Figure 3. Back-to-Back Coaxial Baluns

3.3.3 Unbacked, Coaxial-Balun-Fed Antenna Models

Figure 4 shows an antenna model of the type tried initially. The very first model had a near perfect match over the range 2 to 4.6 GHz, the VSWR being less than 1.05 in spots, and nowhere greater than 1.6. A pattern test indicated considerable radiation in the plane of the antenna, where theory assured us there could be none. We had employed an electrically short, linearly taped balun filled with dielectric, and believed the radiation to be coming from it. In retrospect, it was undoubtedly the unterminated, high-expansion-rate spiral which caused the undesired radiation.

Later models of the "open" type were similarly unsuccessful. Decreasing the thickness of the antenna-backing dielectric from 1/16 inch to 1/32 inch, then to 0.01 inch improved the polarization ratio (circularity) somewhat. Tests of spirals with various numbers of turns, arm thickness, and expansion rates always gave patterns which had substantial radiation in the antenna plane (see Figure 5).

3.3.4 Flat-Plate Backed Antennas

Initially it was felt that the Van Atta array could take the form of a set of unenclosed spirals backed by a common ground plane. It was therefore of interest to test single antennas over a ground plane to see what effects could be observed on the radiation pattern and the impedance.

The coaxial, mode-converter balun was considerably longer than 1/4 wavelength at 4.5 GHz, so that it was not practical to put the ground plane that close to the spiral. It was reasoned that the behavior of an antenna with a ground plane 5/4 wavelength behind it would be similar, at least on axis. Figure 6 shows one of the patterns we took in this manner. Note the multilobe character of the pattern, caused by interference of the direct and reflected beams at various angles.

Recessing the balun within a 3/8-inch pipe allowed us to move the ground plane up close to the antenna, so that the multiple-lobing effect disappeared. The addition of a circular ring surrounding the antenna afforded some additional pattern improvement. The model is shown in Figure 7, and one of the

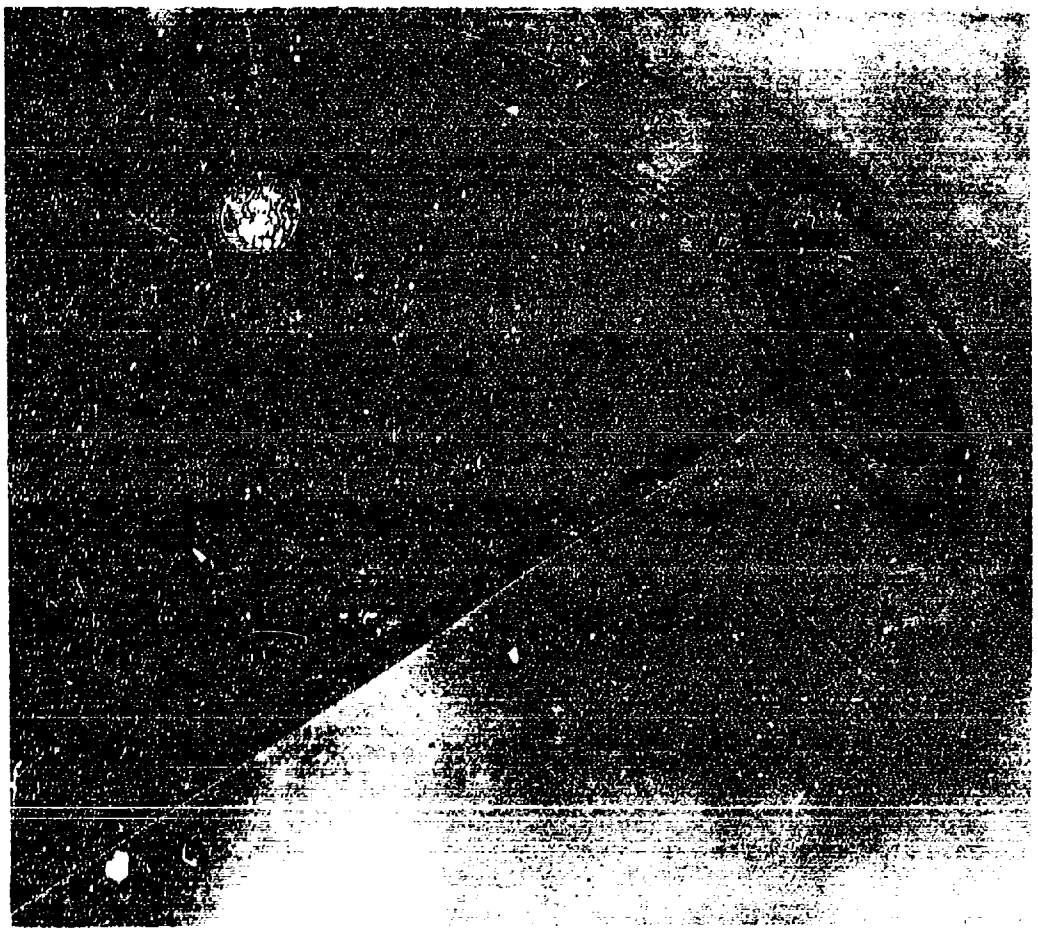

Figure 4. Unbacked, Coaxial-Balun-Fed Model

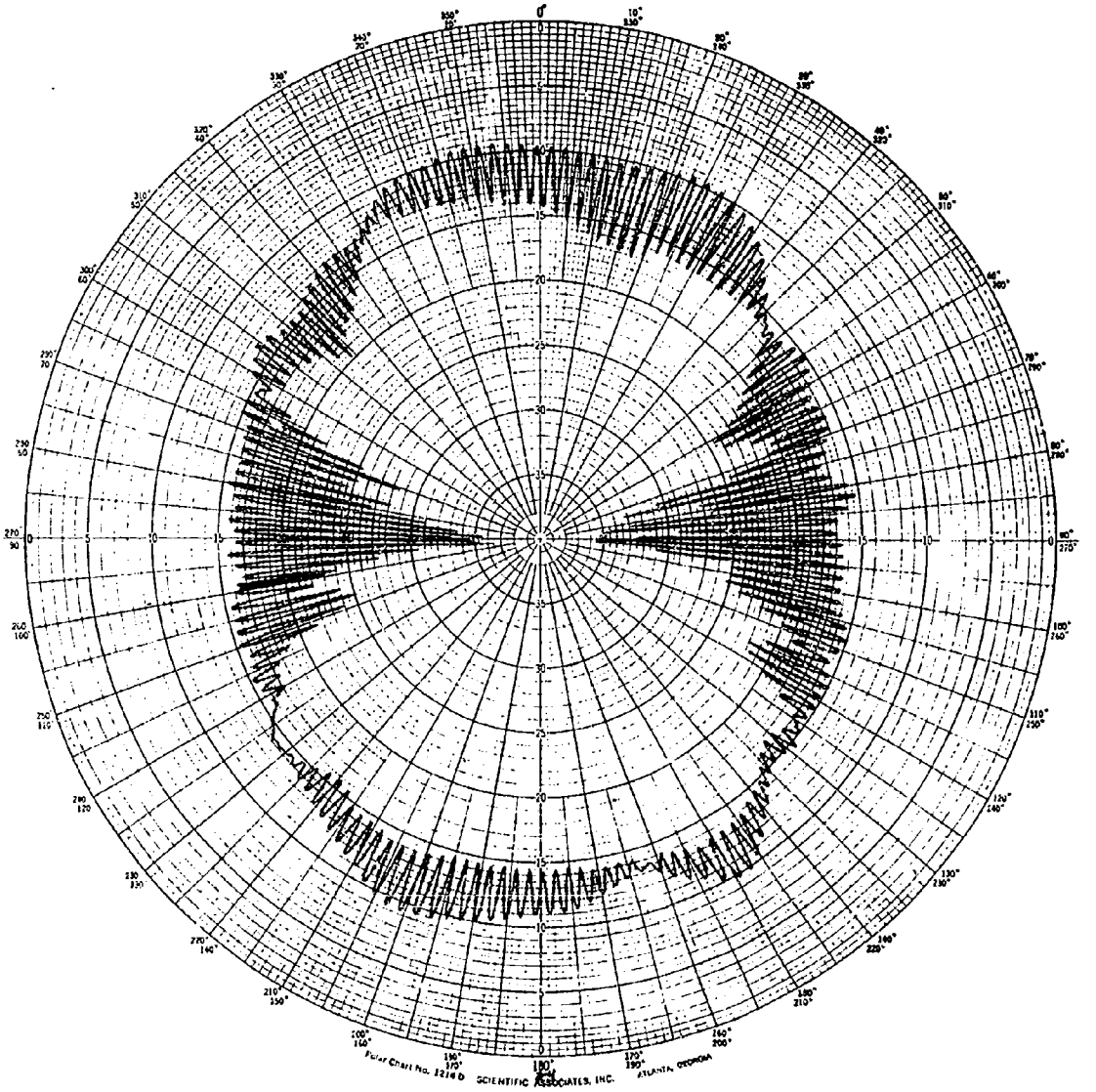

Figure 5. Pattern of the Unbacked, Coaxial-Balun-Fed Model

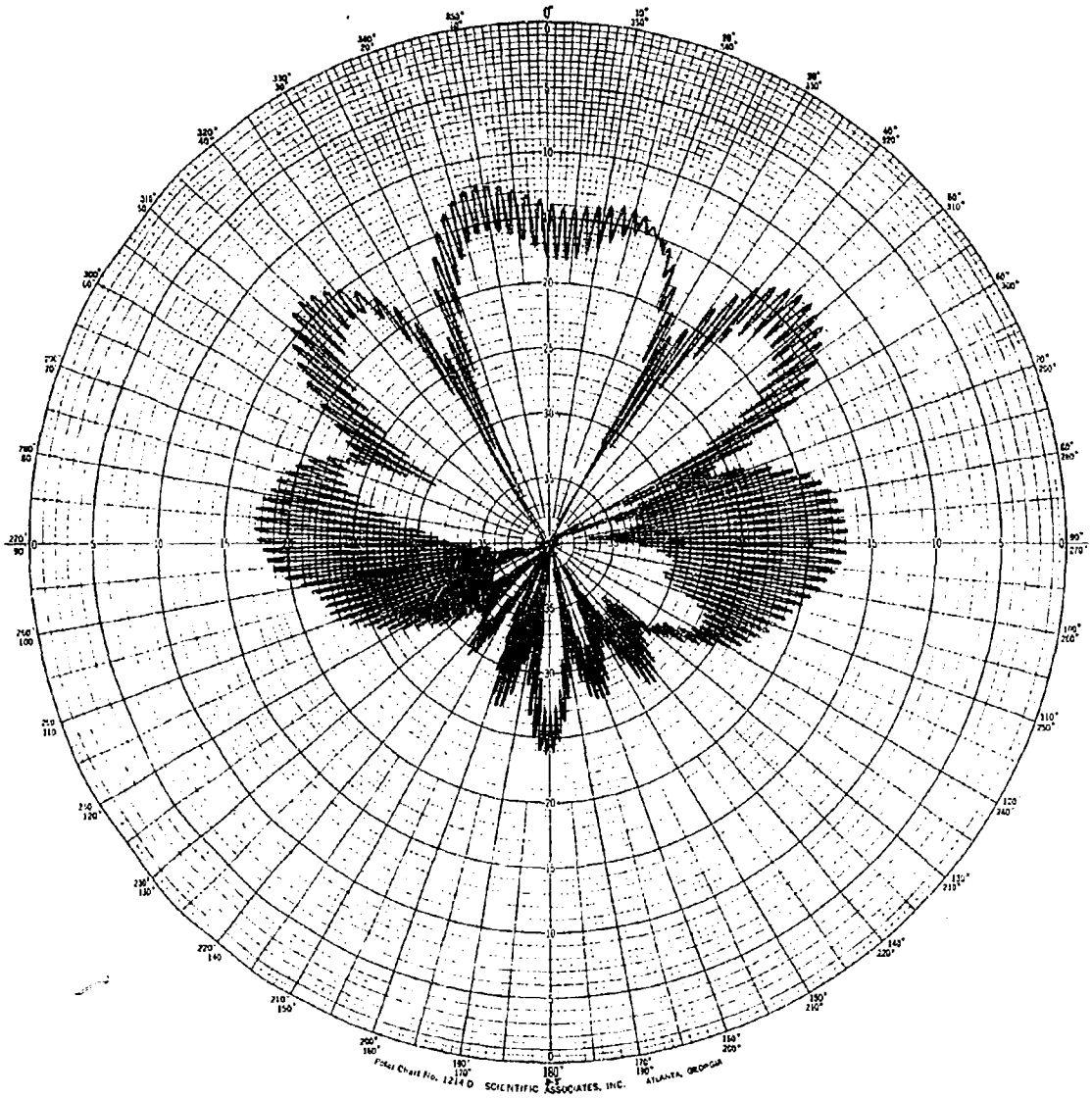

Figure 6. Pattern of Spiral 5/4 λ above Ground Plane

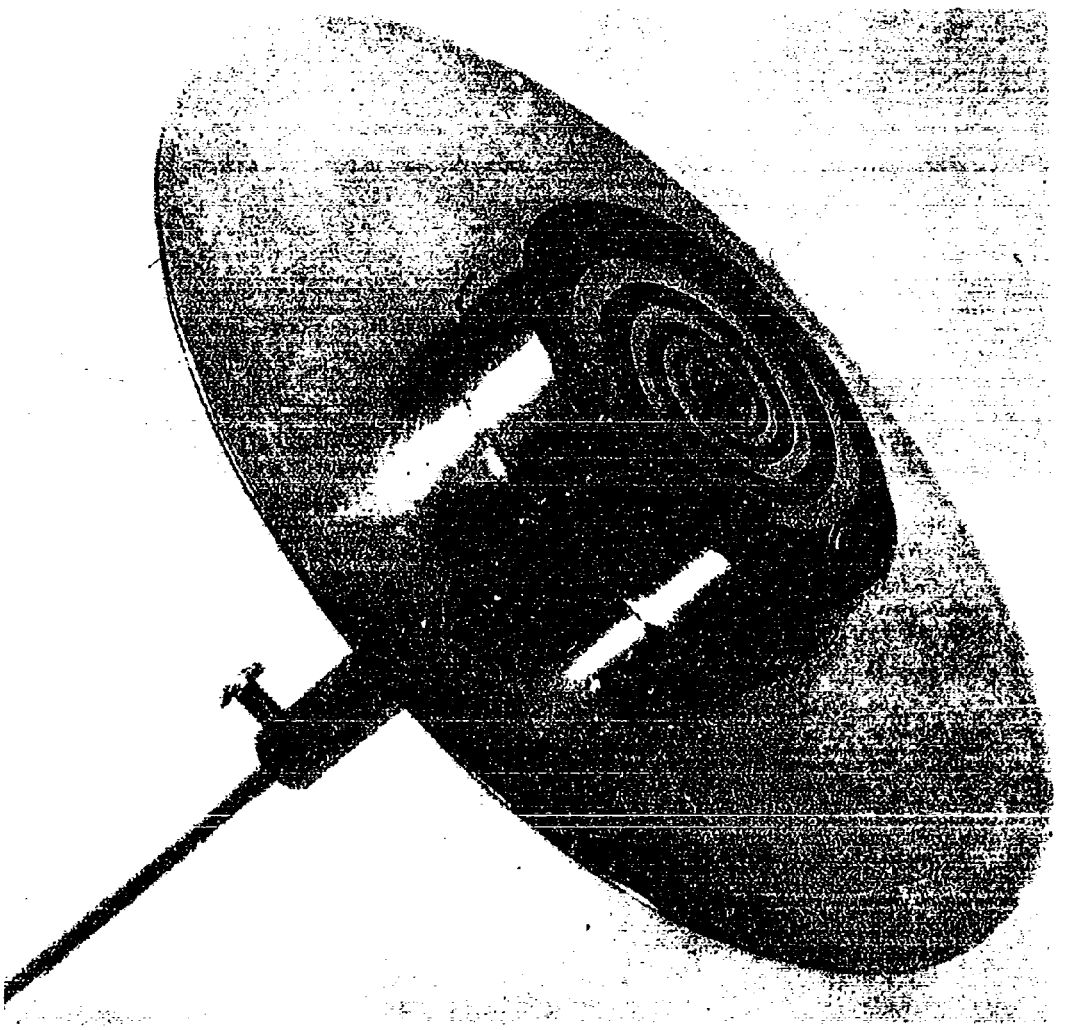

Figure 7. Recessed-Balun Model

better patterns is shown in Figure 8. Although the pattern shape and circularity were good at 3.95 GHz, comparable results could not be obtained at the design frequency of 4.5 GHz.

3.3.5 Stripline Antennas

The rather discouraging results obtained with the coaxial-balun-fed antennas led us to try a completely different approach, that of the infinite-balun feed used by Dyson.[4] In this feed scheme, a coaxial cable is soldered along one arm of a two-arm slot antenna, and the center conductor led across the gap at the center of the antenna and bonded to the second arm. A dummy cable may be soldered to the second arm to preserve symmetry.

It was of course impractical to solder cables along the arms of our tiny antennas. Instead, we tried two different stripline approaches which used the relatively wide spiral arms as "ground planes" for a narrow feed conductor.

The first model, shown in Figure 9, was a microstrip-fed slot etched on a single piece of 1/32-inch copper-clad dielectric. The transition from a 50-ohm microstrip to a 0.141-inch coaxial line was made by means of a butt joint at the edge of the board. Tests of a pair of these joints indicated an excellent match. The microstrip line was etched on the opposite side of the dielectric from one of the copper arms of the slot antenna. A dummy line was placed opposite the other arm to preserve symmetry. At the center of the spiral, the driven microstrip line was soldered to the end of the second spiral arm, thereby forming an "infinite" balun. The width of the microstrip line was tapered gradually over the length of the spiral in such a way that the original 50-ohm unsymmetrical line became a 150-ohm symmetrical, parallel-plate line at the center crossover point.

Figure 10 shows a pattern taken with the microstrip antenna. The pattern shape and circularity were very poor when compared to those of the cavity-backed antennas studied earlier.

In an effort to improve the pattern of the planar-type spiral antenna, the symmetrical Tri-plate design shown in Figure 11 was tried. This antenna consisted of two slot antennas back-to-back, with a Tri-plate transmission line running along the

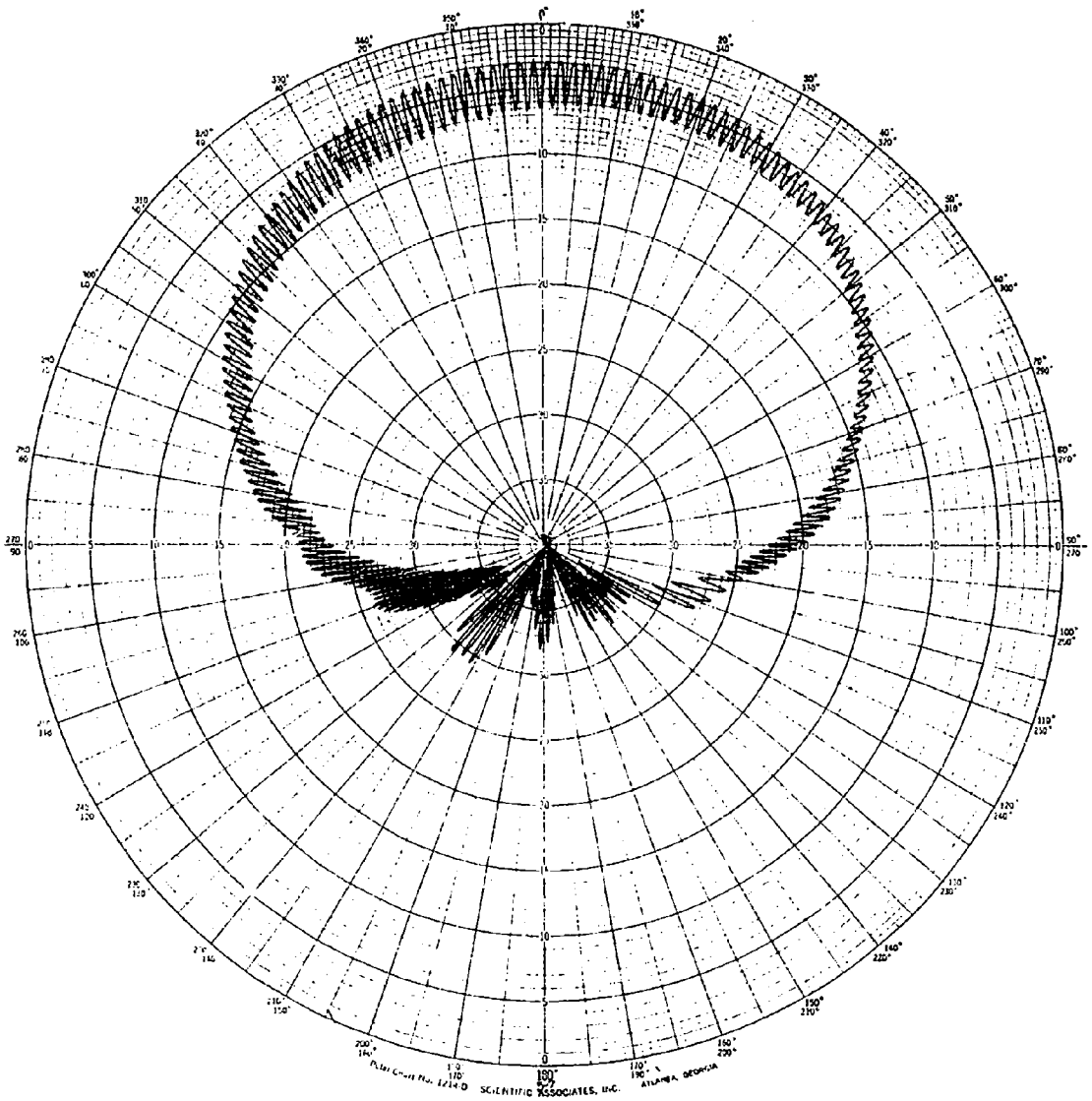

Figure 8. Pattern of the Recessed-Balun Model

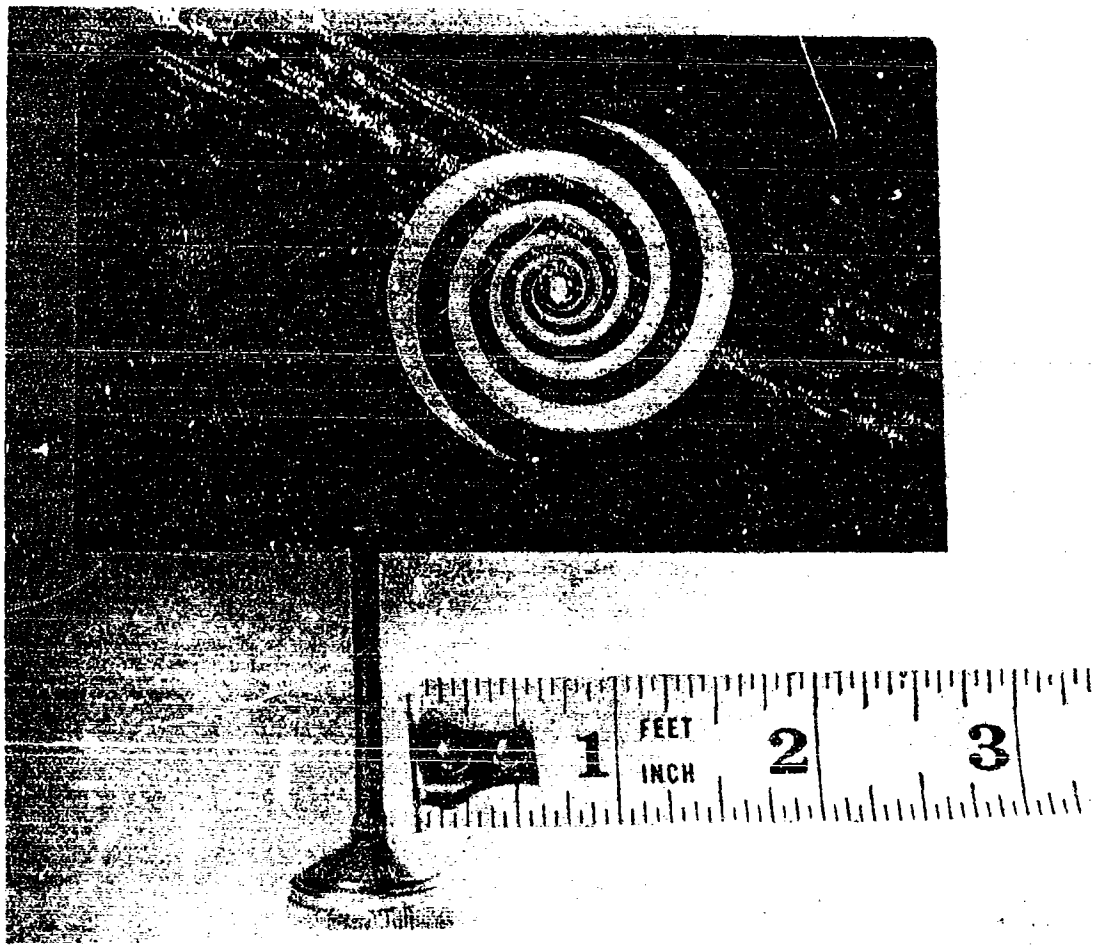

Figure 9. Microstrip-Fed Slot Antenna

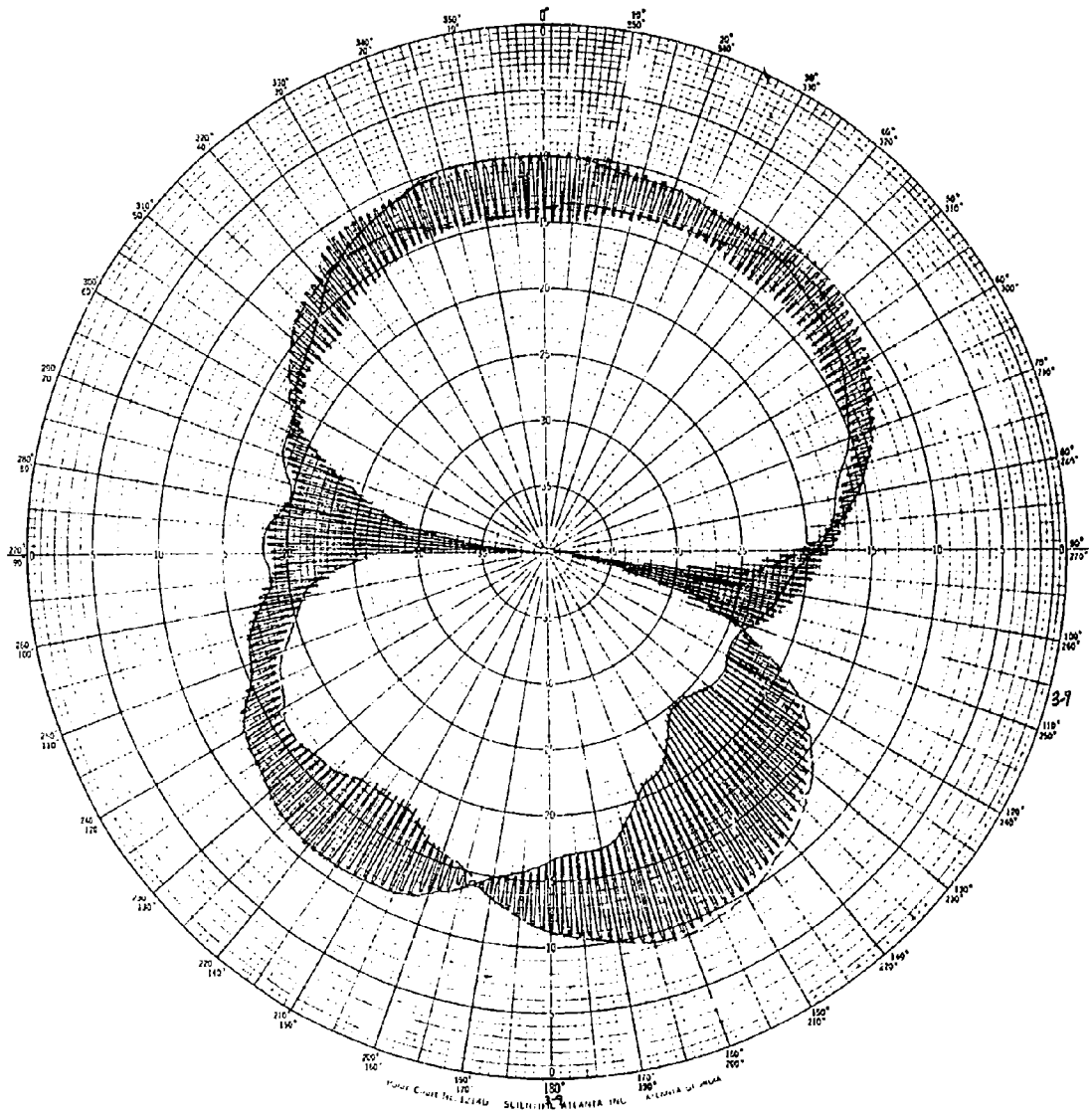

Figure 10. Pattern of the Microstrip-Fed Slot Antenna

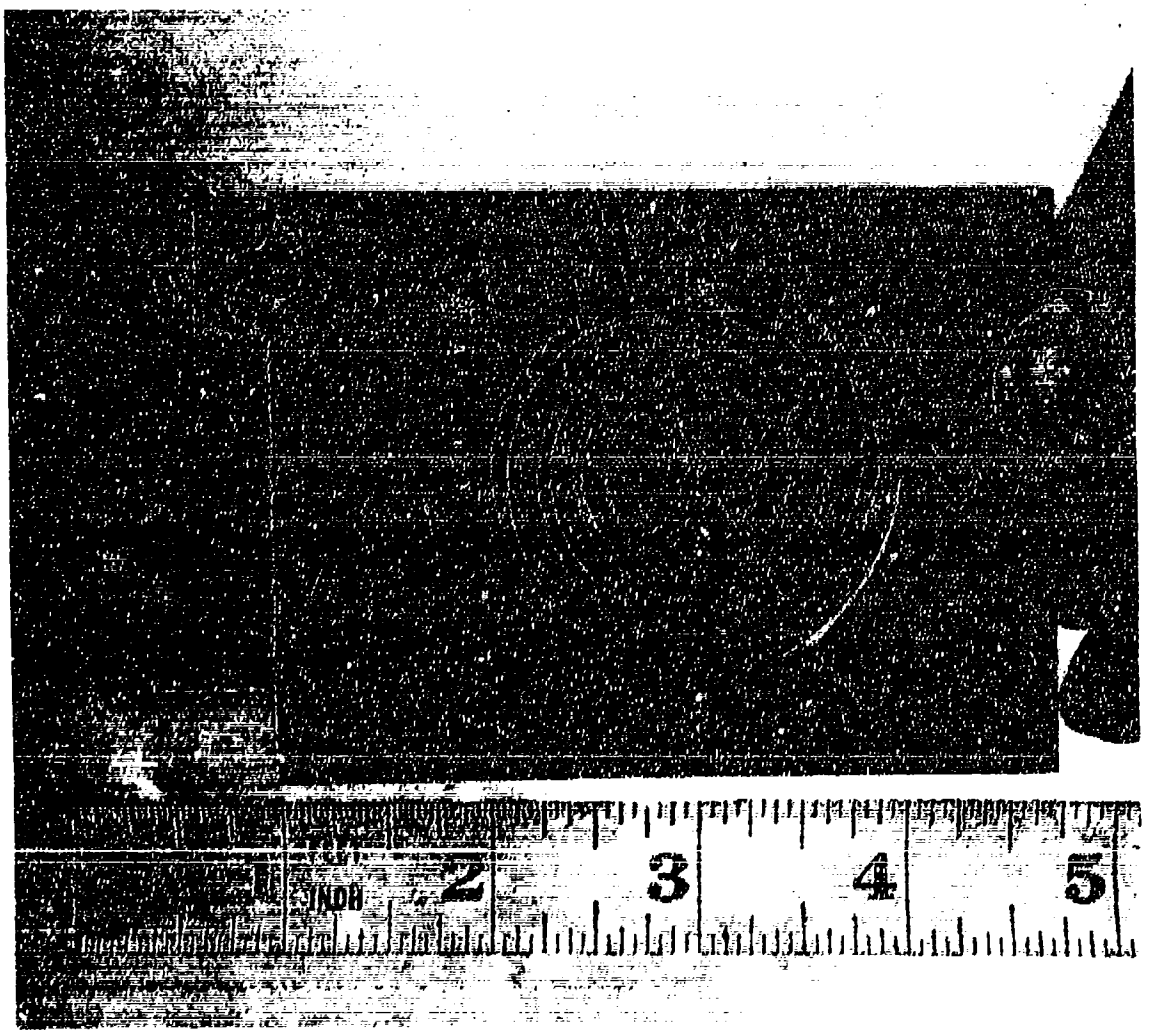

Figure 11. Triplate-Fed Slot Antenna

spiral arms and sandwiched between them. The two slot antennas were connected in parallel by bridging corresponding arms together at the center. At the central feed point, the Tri-plate line was connected across the gap to the opposite antenna arm. As in the case of the microstrip antenna, the transmission line impedance was tapered smoothly from 50 ohms at the antenna periphery to about 180 ohms at the center.

Pattern tests with the Tri-plate antenna indicated behavior similar to that of the microstrip model. A marked dependence of circularity on excitation frequency was noticed, as well as a periodic impedance variation. These effects suggest that the Tri-plate transmission line was coupling to the antenna slots along their entire length, rather than just at the feed point as was intended. Such coupling could be reduced by bonding the two antenna arms (Tri-plate ground planes) together periodically, as well as by drastically reducing the dielectric thickness. Neither technique seemed practical, so we returned to the cavity-backed spiral design.

3.3.6 Conical-Cavity-Backed Antenna

Concurrent with the study of the stripline antennas, we continued the development of a cavity-backed unit. The adjustable aluminum conical cavity shown in Figure 12 was designed so that the surface of the cone was always 1/4 wavelength behind the assumed one-wavelength-circumference radiating zone of the spiral. It was reasoned that this approach would give us a broadband reflector which would not affect the pattern or impedance of the spiral as drastically as a flat plate. As in previous models, a tapered, mode-converter balun was recessed into the center of the cavity.

We obtained one pattern at 4.0 GHz which showed a polarization ratio of better than 1.5 dB over a 220° beamwidth, and better than 3 dB over 220° (see Figure 13). Unfortunately, these results could not be repeated. It was noted that the pattern symmetry and circularity were extremely sensitive to mechanical displacement of the balun and the antenna. This led us to conclude that the balun was being distorted, destroying its balance.

At this point we learned of cavity-backed spiral work being done at SES-West, and discussions with their engineers cleared up many of our difficulties.

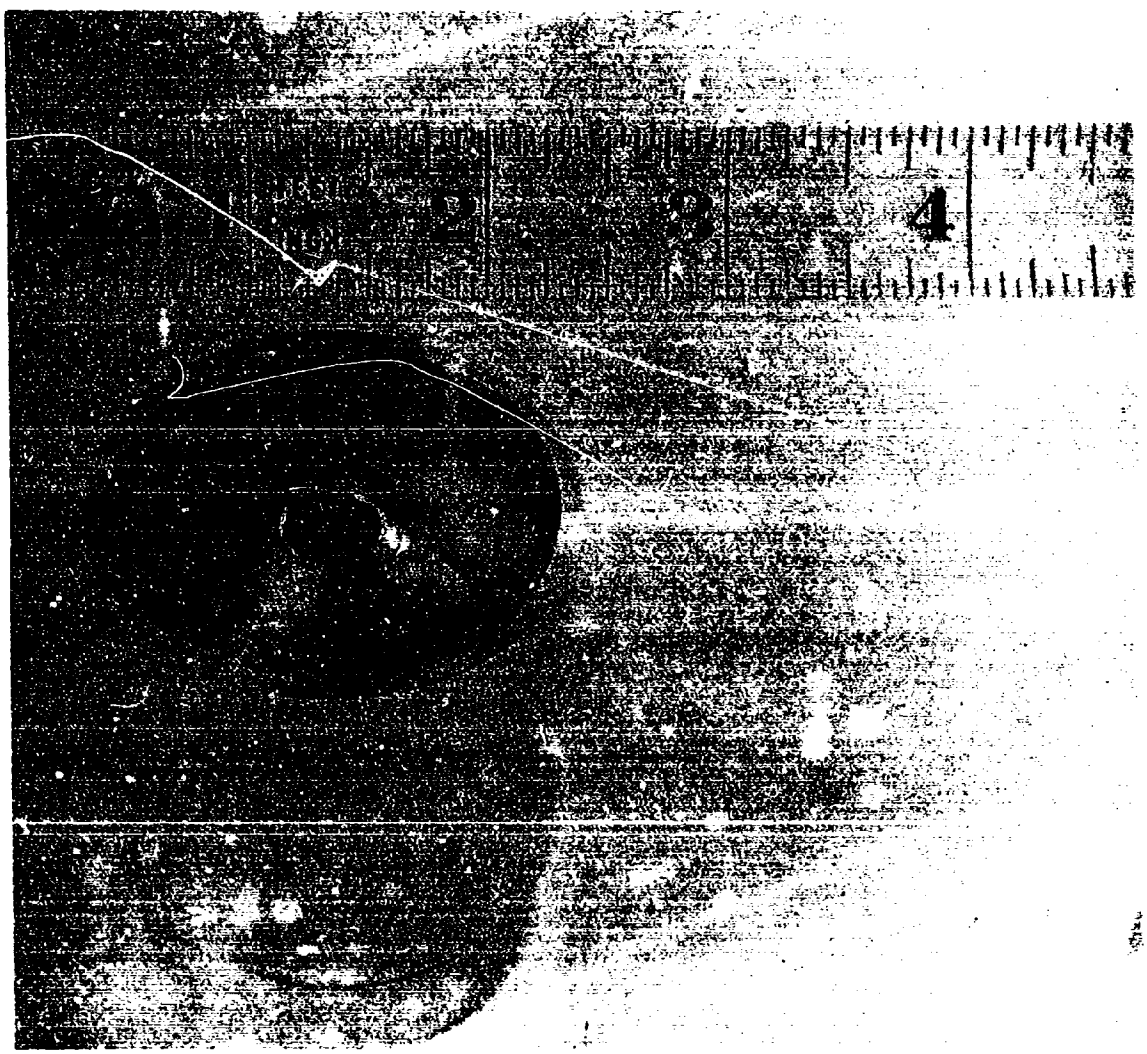

Figure 12. Adjustable Conical Cavity

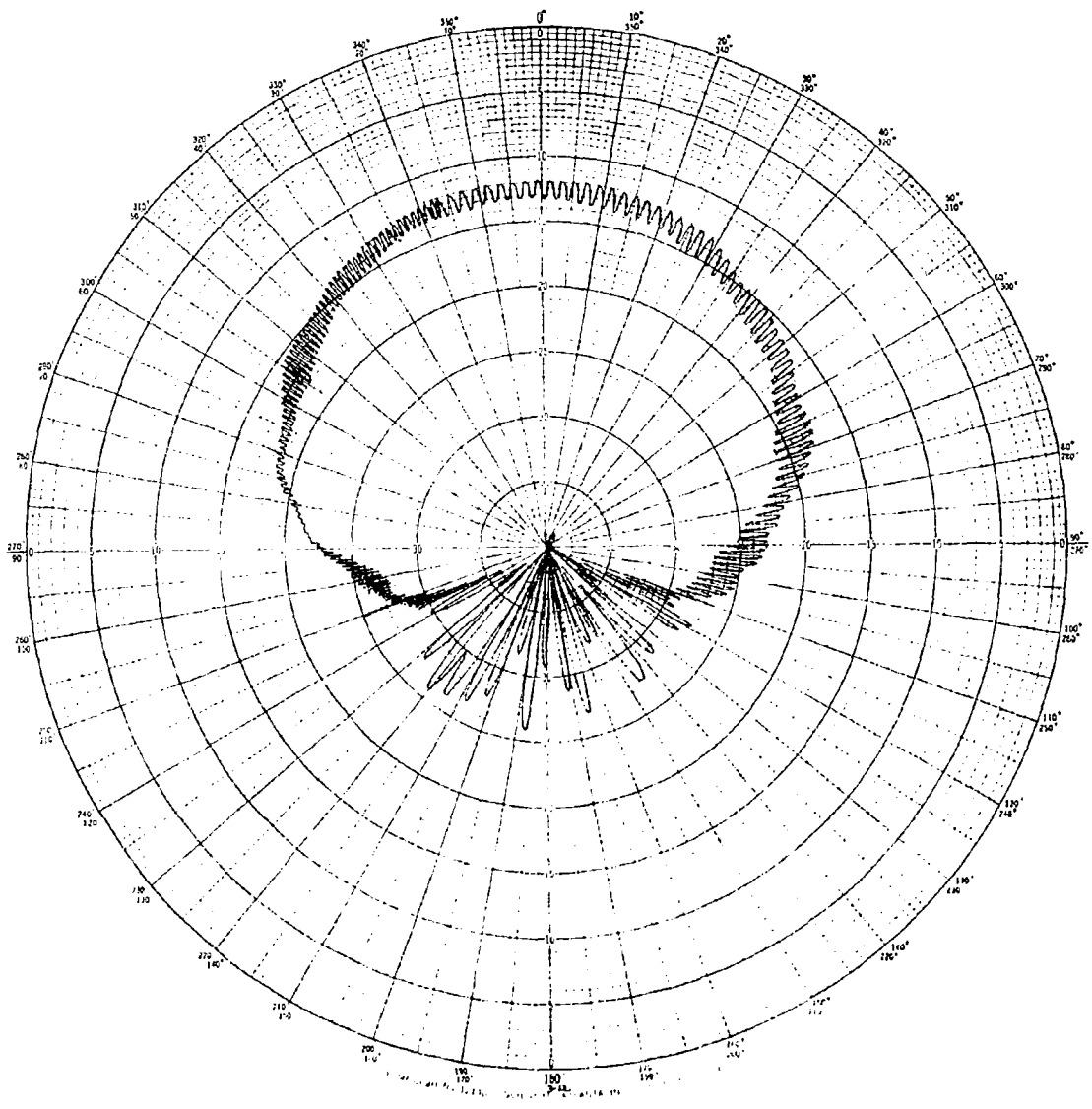

Figure 13. Pattern of the Conical-Cavity Backed Antenna

3.4 TERMINATED, CAVITY-BACKED SPIRAL ANTENNAS

3.4.1 Discussions with Engineers at SES-West

Conversations with members of the Antenna Department at SES-West, Mountain View, California, revealed many shortcomings in our initial approach to the problem of building a well-matched cavity-backed spiral antenna for 4.5 GHz. Most of the information was from the previous experimental experience of the individuals, which, while unpublished and with little theoretical basis, nonetheless enabled them to construct spiral antennas with exceptionally clean patterns and low polarization ratios.

We learned that although theory predicts a very high rate of current attenuation along the arms of an equiangular spiral, in practice it has been found necessary to place an annulus of resistive material around the edges of the antenna to get good performance. It is also necessary to use multiturn spirals of very low expansion rate, contrary to theoretical predictions.

The cavity design suggested to us was a right-circular cylinder from 0.18 0.28 wavelengths deep, and about two wavelengths in circumference. Substantially better patterns can be had through the use of an absorber-lined cavity, though at reduced gain.

The investigators at SES-West have completely separated the "antenna problem" from the "balun problem." They feed their spirals (2-arm, 4-arm, 6-arm, and conical) by means of very small (0.047 inch) 50-ohm coaxial cables phased appropriately. Their feed for a conical spiral consists of two cables soldered inside a small brass tube, the two center conductors being attached to the spiral arms. Behind the antenna, the cables are brought out separately to a special double-ridged-waveguide balun. In this balun, two -3 dB outputs 180° out-of-phase are obtained from probes inserted into opposite sides of a double-ridged waveguide operating in the $TE_{1,0}$ mode. The latter mode is generated by a conventional coax-to-waveguide probe transition. The balun has a VSWR of less than 1.4:1 over the 2.5 - 5.0 GHz band. Over most of the band, the output amplitude balance is better than 0.1 dB and the phases are within 2° of perfect opposition.

3.4.2 Cavity-Backed Spiral Fed by Push-Pull Cables

Several new ideas were incorporated in the cavity-backed spiral of Figure 14. We used a multiturn, self-complementary spiral of very low expansion rate.[1] The spiral was considerably larger than any we had been able to make on our oscilloscope, and was much more logarithmic toward the center. The antennas were made on 1/32-inch glass-reinforced polystyrene dielectric, coated on one side with 1 oz copper.[2] The expansion rate was only 1.4 per turn, where we had been using rates of from 1.75 to 2.5 previously. The antenna was terminated with a washer made of 0.025-inch Filmohm metal-film resistance card whose resistance was 377 ohms per square.[3]

Our first terminated cavity-backed antenna was fed from the center conductors of two 0.085-inch copper-jacketed cables mounted inside a 3/8-inch pipe. The two cables were drived in push-pull from a 180° hybrid T. The cavity was a right-circular cylinder 3/4 wavelength in diameter and 1/4 wavelength deep at 4.5 GHz. The pattern we obtained is shown in Figure 15. Substantial asymmetry was evident, but the circularity was good. The pattern falls off more slowly with angle than expected for a spiral operating in the first mode. We suspect that the two drive cables were not of exactly the same electrical length, resulting in a partially unbalanced drive for the antenna, and consequent excitation of the broad-beam second spiral mode. The difficulties involved with precisely phasing the cables, coupled with the necessity for providing a well-matched 180° hybrid and its associated connectors, encouraged us to try some simpler balun schemes.

3.4.3 Chebyshev-Balun-Fed, Cavity-Backed Spiral

We next tried the short, linearly tapered, dielectric-filled coaxial balun shown in Figure 16. This "Chebyshev balun" was very similar to the one used in the AEL Model ASN 533A Archimedes spiral antenna. The pattern obtained in this case

1. The antenna negative was kindly supplied by Sam Kuo of SES-West.
2. Custom Po... CR, Custom Materials Inc., Chelmsford, Mass.
3. Filmohm Corp., 37-11 47th Avenue, Long Island City, N. Y.

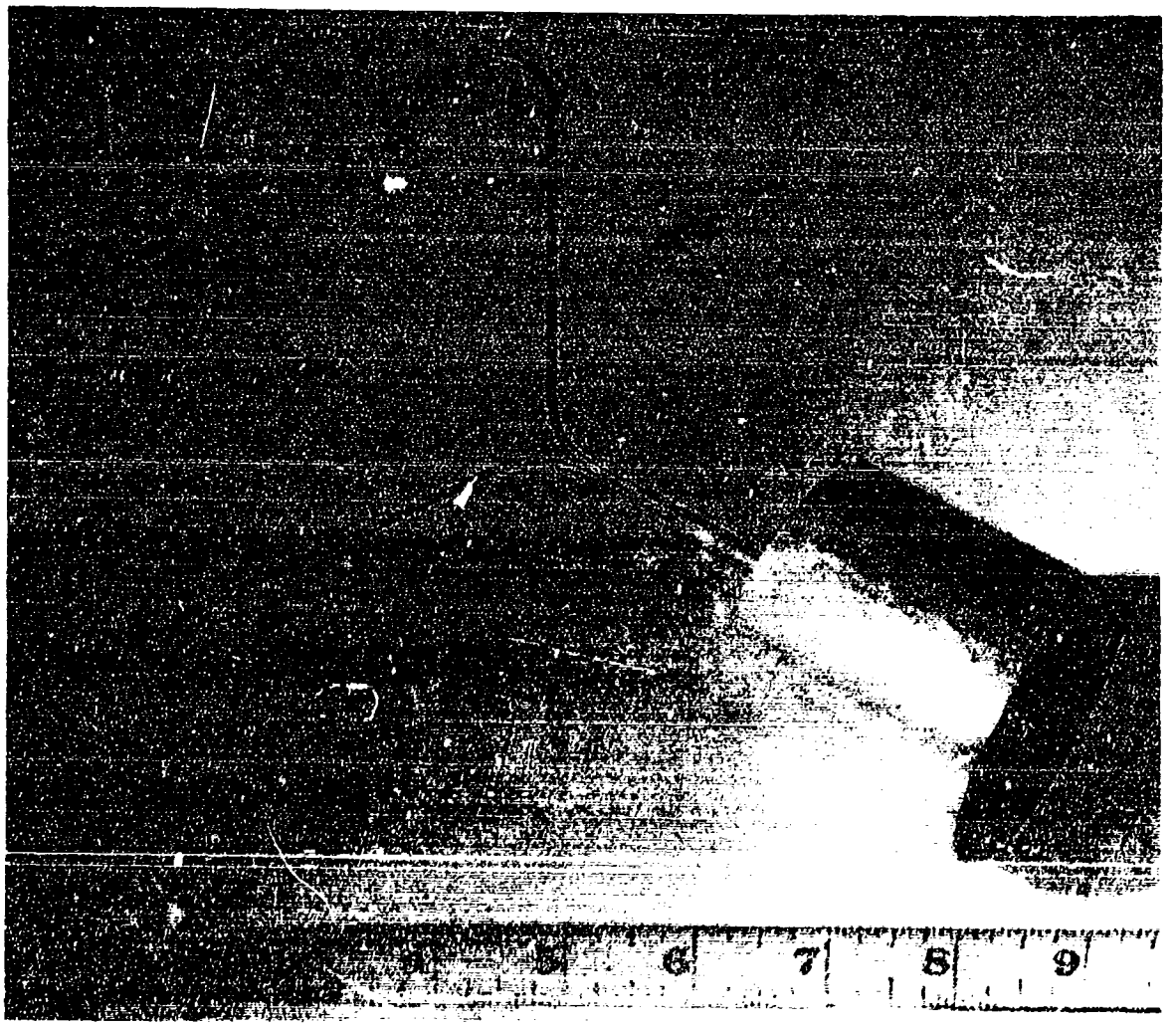

Figure 14. Cavity-Backed Spiral with Push-Pull Feed

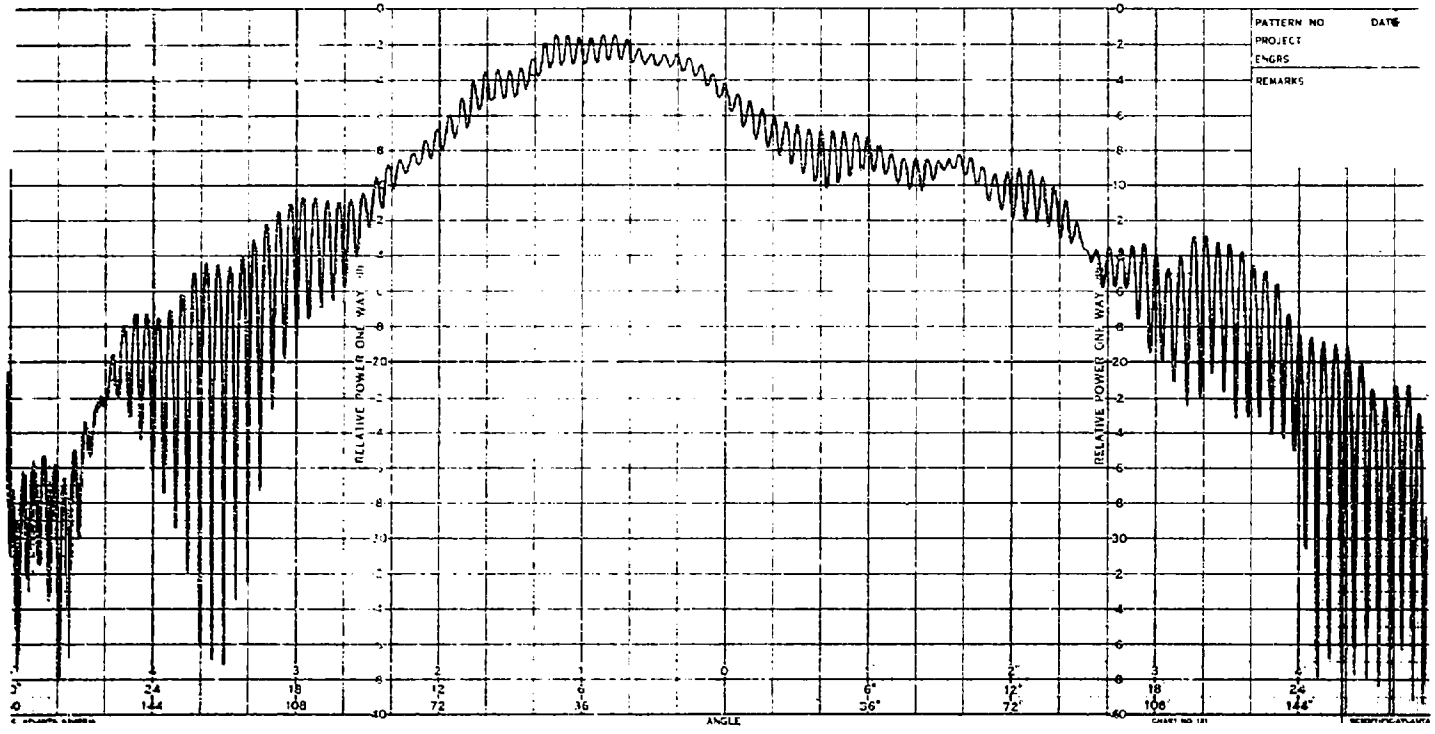

Figure 15. Pattern of the Push-Pull Cavity Backed Spiral

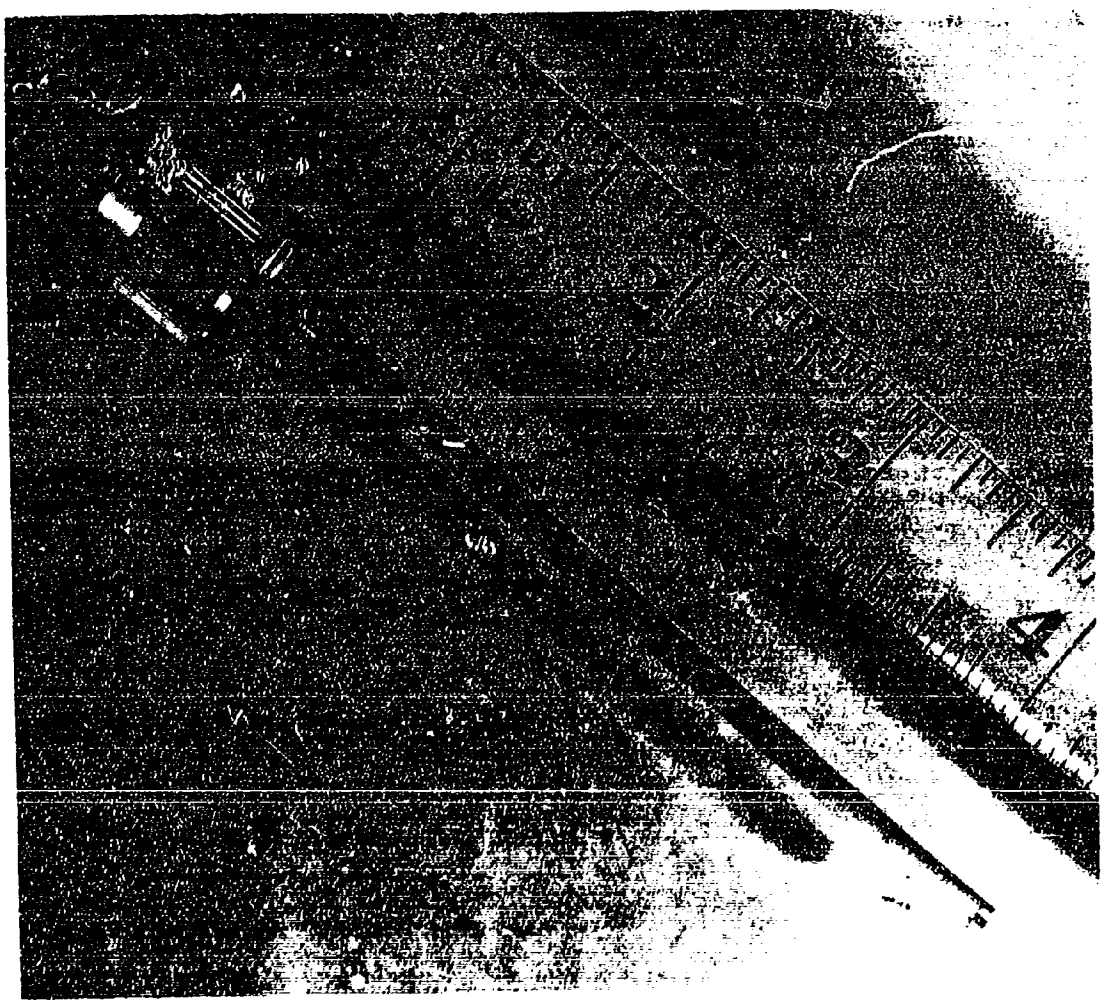

Figure 16. Chebyshev Balun

(see Figure 17) had better symmetry and circularity than in the case of the two-cable model, but we still were not obtaining the cos θ roll-off of the pattern with angle which is characteristic of the spiral operating in its lowest mode.

3.4.4 Tapered-Center-Post, Cavity-Backed Spiral

Our first really successful cavity-backed spiral is shown in Figure 18. In this model the cavity and "balun" were machined together out of a single piece of brass for mechanical reproducibility. This model had no balun as such, the two arms of the spiral being connected, respectively, to the inner and outer conductors of a coaxial line built into the center post of the cavity (see Figure 19). A conical top was provided on the center post with the idea that some capacitive loading at the antenna's terminal region would help cancel the inductance introduced there by the wire connections to the arms. This loading scheme has been used to match dipole antennas.[4] As it turned out, the loading was not sufficient to yield a purely resistive impedance, but the technique was later used successfully in another model. The pattern of this tapered-center-post model at 4.5 GHz is shown in Figure 20. The polarization ratio is less than 0.5 dB over a 100° beamwidth, and the 3-dB beamwidth is 70°. Some asymmetry of the roll-off with angle is evident, probably due to the slight offset of the spiral center from the cavity center. (This offset resulted because the center conductor of the input coaxial line was connected directly to one arm of the spiral, rather than to the geometric center of the antenna.)

We had intended to build a matching network within the center post of the cavity to match the antenna impedance to 50 ohms in the vicinity of the 4.5-GHz design frequency. The antenna impedance (referred to the plane of the antenna) is plotted on a Smith Chart in Figure 21. When viewed as a function of the operating frequency, the impedance is rather widely "spread," indicating that a complicated matching network would be required to transform the impedance to 50 ohms over a broadband.

4. A. Stratoti, Sanders Associates, private communication.

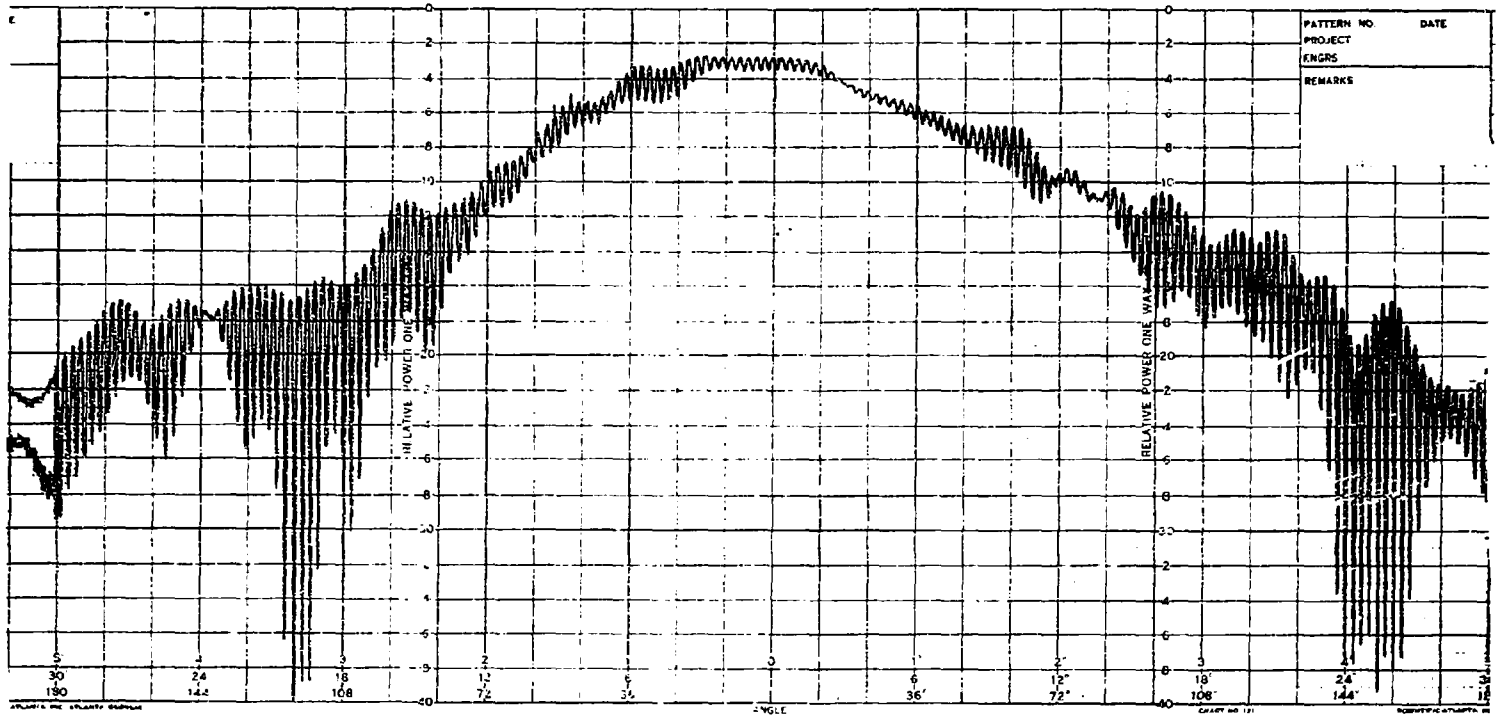

Figure 17. Pattern of the Chebyshev-Balun Fed, Cavity-Backed Spiral

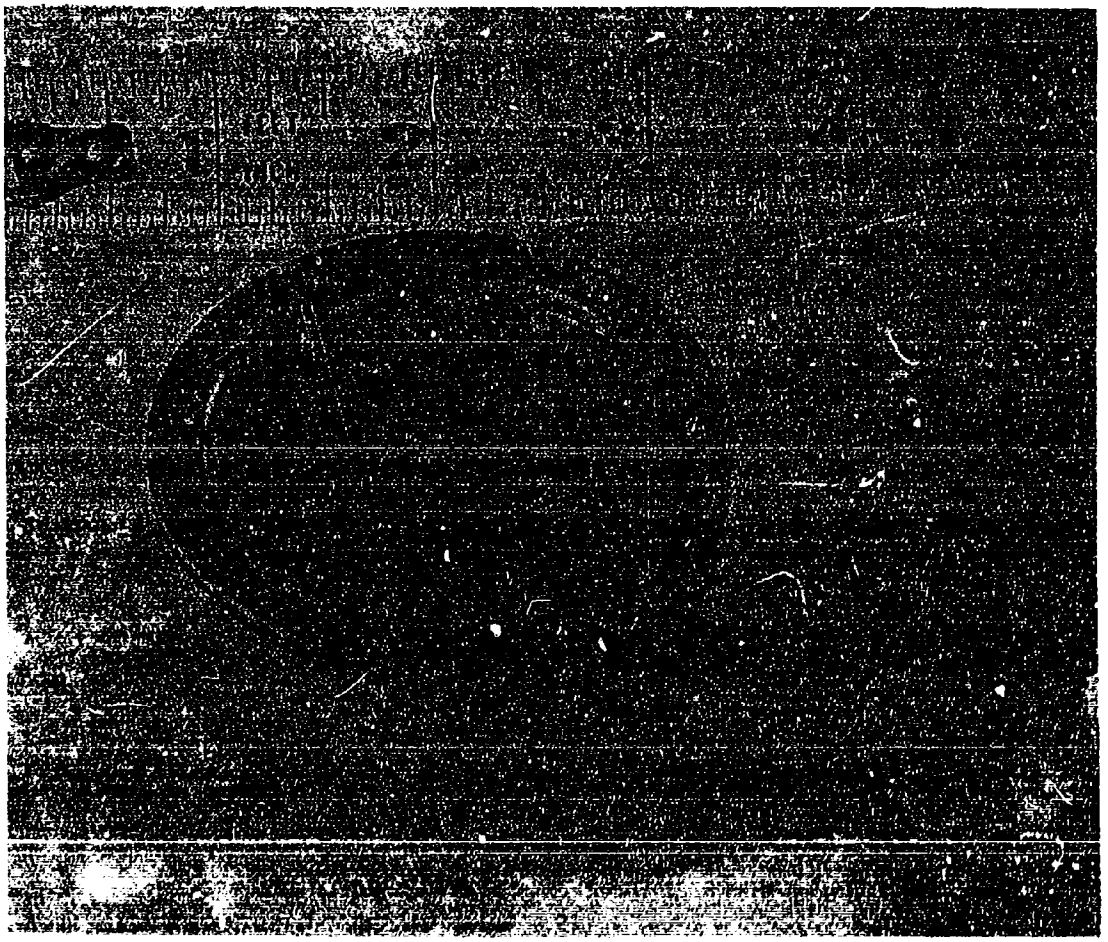

Figure 18. Tapered-Center Post Antenna

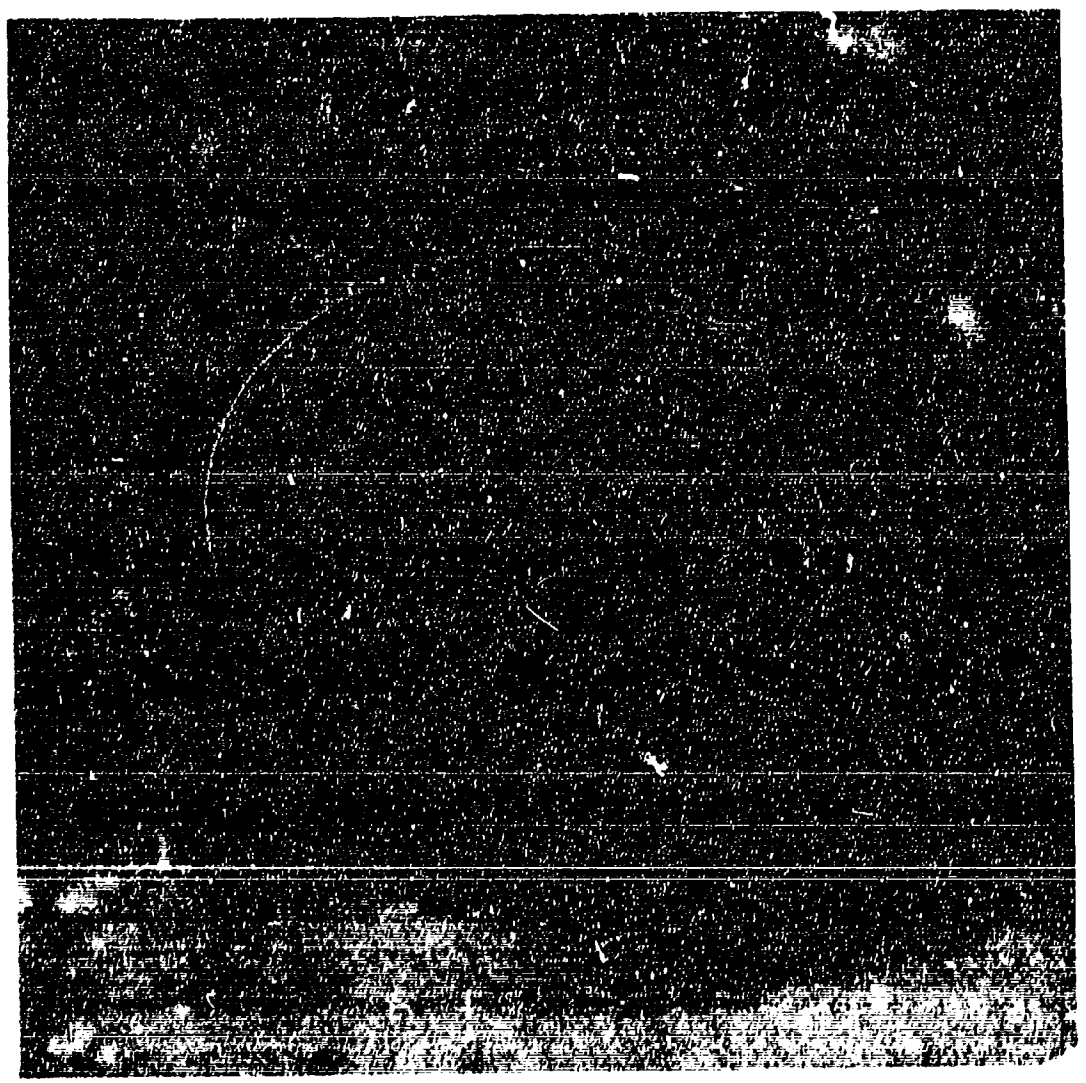

Figure 19. Cavity Showing Tapered Center Post

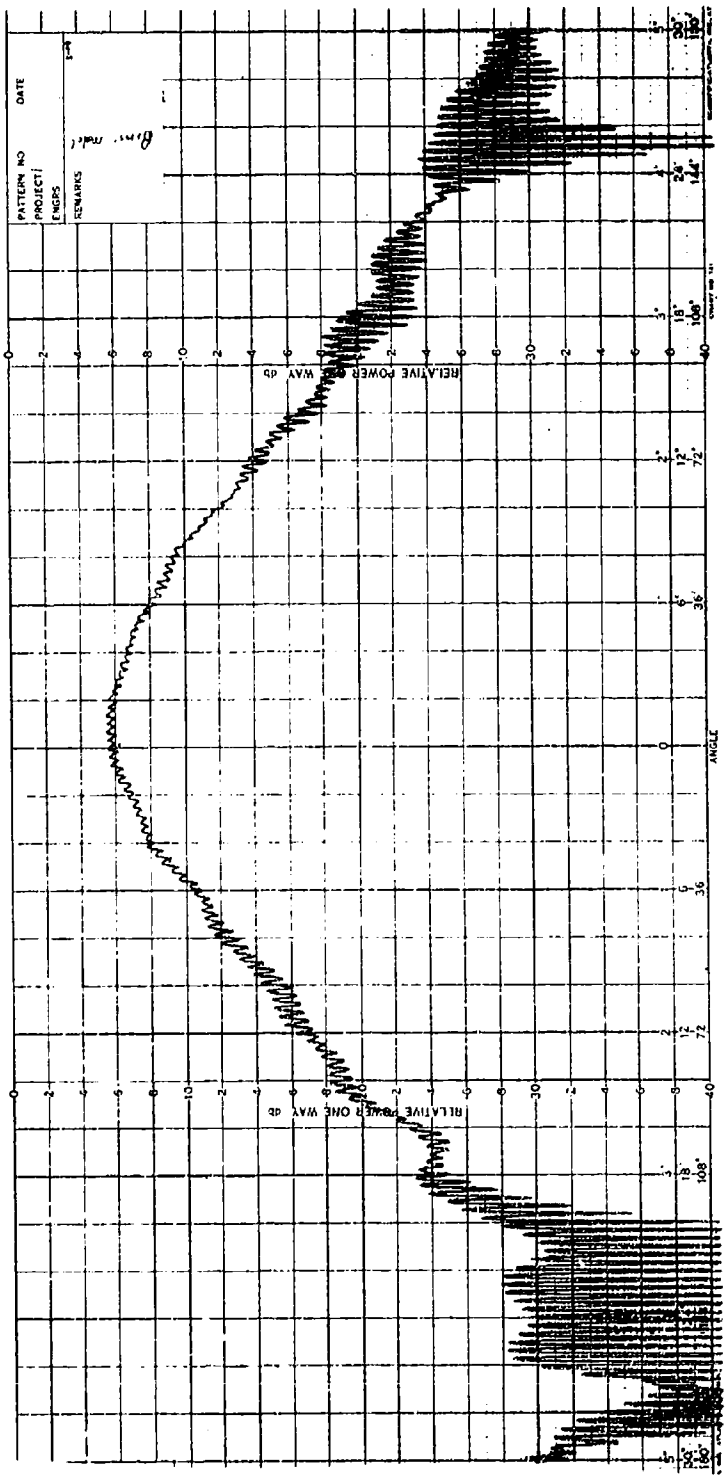

Figure 20. Pattern of the Tapered-Center-Post, Cavity-Backed Spiral

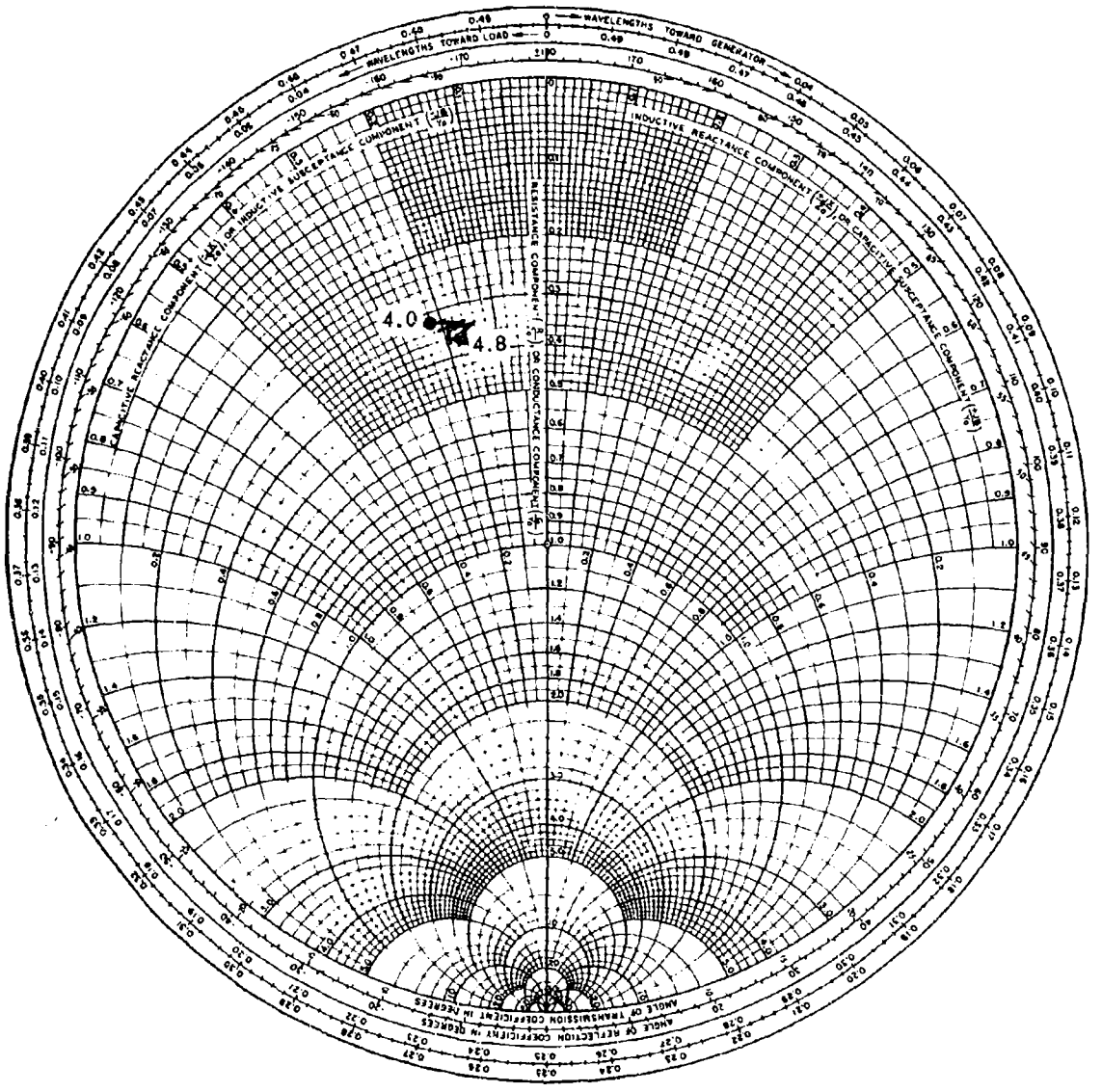

Figure 21. Impedance of Tapered-Center-Post Antenna

The poor impedance behavior and the pattern asymmetry led us to try the model described in paragraph 3.4.5. The center post proved to be very useful as a matching element, and a reasonable pattern was obtained at the same time.

3.4.5 The Final, Matched Cavity-Backed Spiral

The antenna described in this section and shown in Figure 22 differed from the one described in the previous section in two important respects. First, in an attempt to remove some of the pattern asymmetry noted with the earlier model, we offset the coaxial drive line in the center post so that the spiral could be centered with respect to the cavity. Second, the capacitive loading provided at the center of the antenna by the center post was made much heavier by eliminating the bevel entirely. Later, a very slight bevel (5^{o}) was introduced which yielded an antenna impedance which was almost constant over the 4.2 to 4.8 GHz range. It was then a relatively simple matter to match the latter impedance to 50 ohms. Our final experimental tests yielded a VSWR of less than 1.043 over the 4.0 to 4.6 GHz range. In the following paragraphs we will describe the antenna more fully.

Figure 23 is a detailed drawing of the antenna cavity, complete with matching network and beveled center post. The cavity diameter is 3/4 wavelength at 4.5 GHz, and the depth is 1/4 wavelength. Not shown are the antenna itself and the resistive terminating washer. The antenna is fed with two 0.018-inch O.D. pins spaced 0.065-inch apart. One pin is grounded to the cavity, while the other forms the center conductor of the 0.056-inch O.D. coaxial feed line. The impedance is kept at 50 ohms as the line proceeds through two increases in diameter, first to 0.143-inch O.D. then to 0.384-inch O.D. A section of 15-ohm (0.259-inch I.D.) line 1/4 wavelength long at 4.5 GHz follows, then 1/4 wavelength of 26.5-ohm line (0.205-inch I.D.). The 26.5-ohm line is then transformed to 50 ohms, and the latter line enters the UG58A/U connector.

Before the matching network could be designed, detailed data on the cavity-mounted antenna's impedance versus frequency was needed. This was obtained from standing-wave measurements at the UG58A/U connector, with a constant impedance 50-ohm line inside the cavity center post. The data were plotted on a

Figure 22. Matched, Cavity-Backed Spiral Antennas

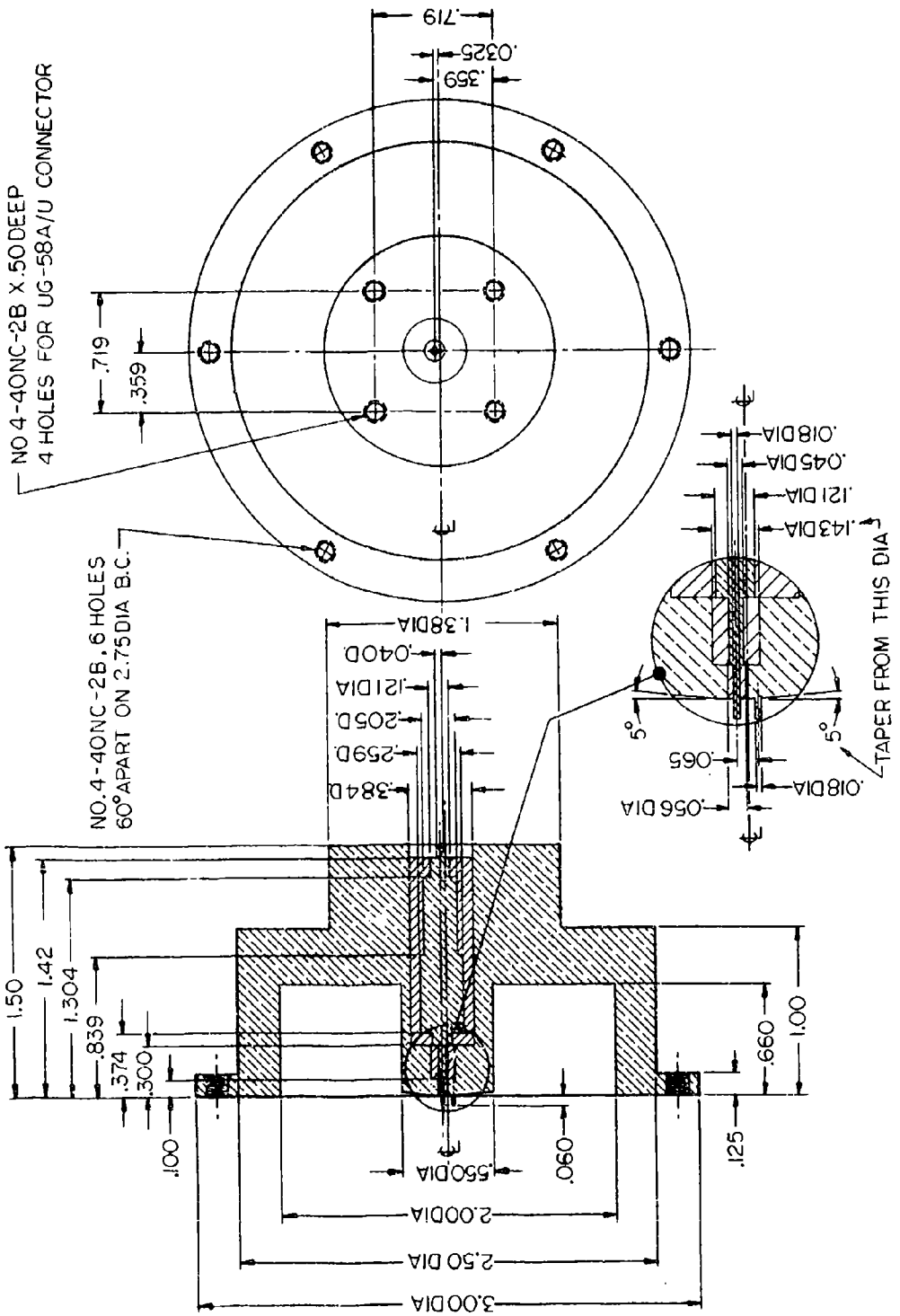

Figure 23. Detailed Drawing of the Matched, Cavity-Backed Spiral

Smith chart and referred to the antenna plane, ignoring the effects of the discontinuities caused by the two abrupt diameter reductions. Figure 24 shows that the normalized impedance $Z(\omega)$ was "spread" rather badly. The admittance, however, lies along a constant conductance contour, ranging from 0.39+j0.44 at 4.2 GHz to 0.39+j0.28 at 4.8 GHz. The corresponding shunt resistance is 128 ohms, compared with a theoretical value of 189 ohms for a self-complementary spiral in free space. Curiously, the shunt susceptance decreases with frequency, though it remains positive. We are at a loss to interpret this behavior in terms of a lumped model. The center post had a flat top for these measurements, so that considerable capacitance was present between the antenna arms and the post. We believe that a sort of radial transmission line was formed, with an abrupt discontinuity at the post edge. The effect of this discontinuity was reduced by beveling the top of the post at the 5^{o} angle, as shown in the detailed drawing, Figure 23. The effect of this change was a nearly perfect merging of all the normalized admittance points in the 4.2 to 4.8 GHz range to the value 0.32 + j0.29, the equivalent shunt resistance component being 156 ohms. We suspect that at least some of the change of admittance was due to unavoidable differences in the way the antenna was soldered on to the terminals in the two sets of measurements.

Figure 25 shows the antenna impedance group plotted on a Smith Chart as a small square centered at 1.75 - j1.5. The next step was to devise a broadband matching network to transform the antenna impedance to 50 ohms. For ease of manufacture, it was decided that the matching would be accomplished using a cascade of lines of different characteristic impedances, rather than with stubs. Rotation of a tightly grouped impedance plot through a fixed length of line inevitably spreads out the plot, since the impedance points corresponding to higher frequencies rotate farther than those at the low end of the band. To achieve a truly broadband match, the spreading must be compensated for by "inverting" the impedance through a quarter-wave line, so that further rotation will tend to merge the impedance points as 50 ohms is reached.

The steps we followed are sketched on the Smith Chart of Figure 25. Rotation of the antenna impedance group through 0.2 wavelength (at 4.5 GHz) of line transformed the group to the real axis of the chart, but spread the points so that the 4.2 GHz point was at 0.3 - j0.075, while the 4.8-GHz point was at

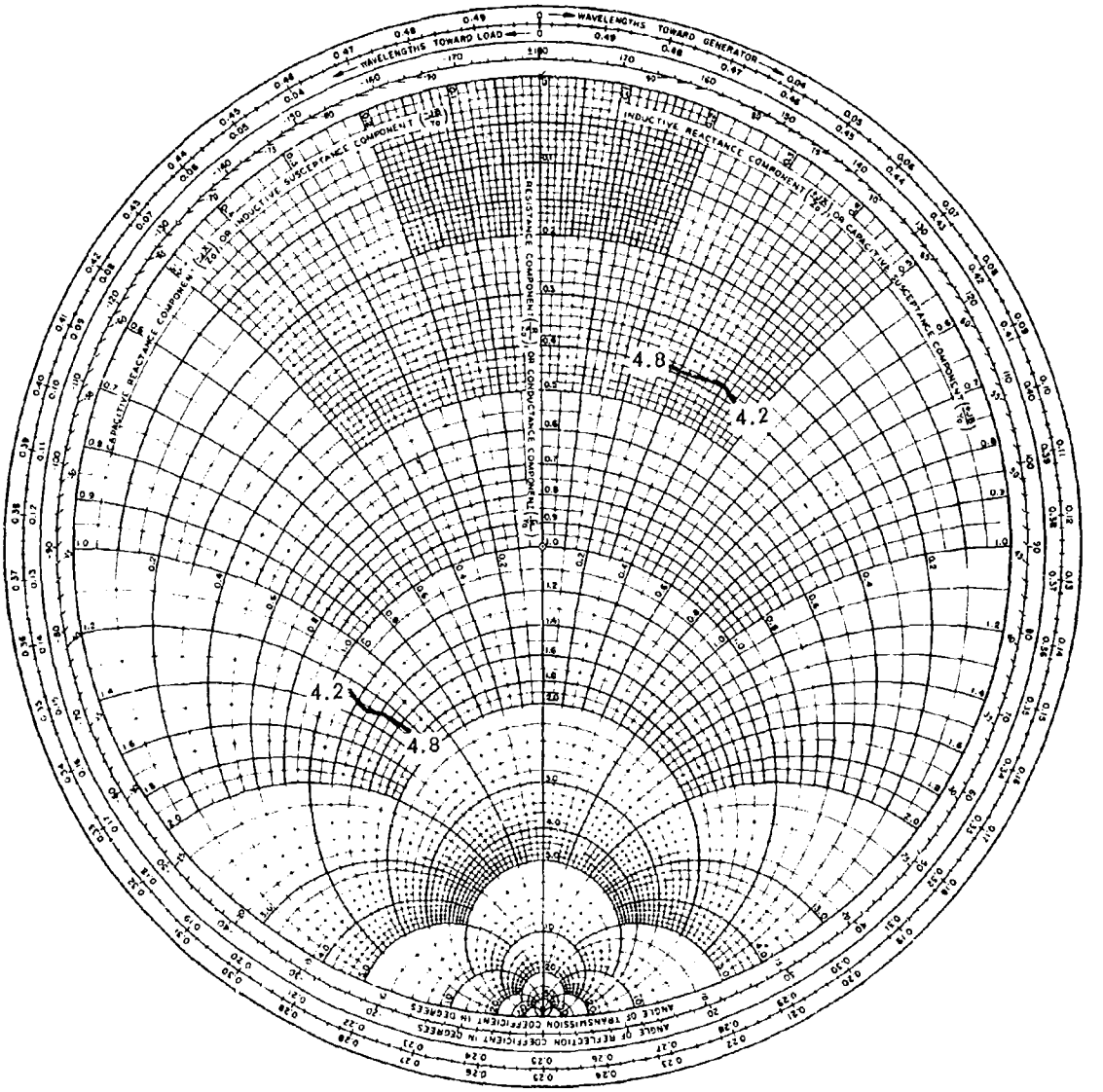

Figure 24. Impedance and Admittance of the Cavity-Backed Spiral Antenna Prior to Matching

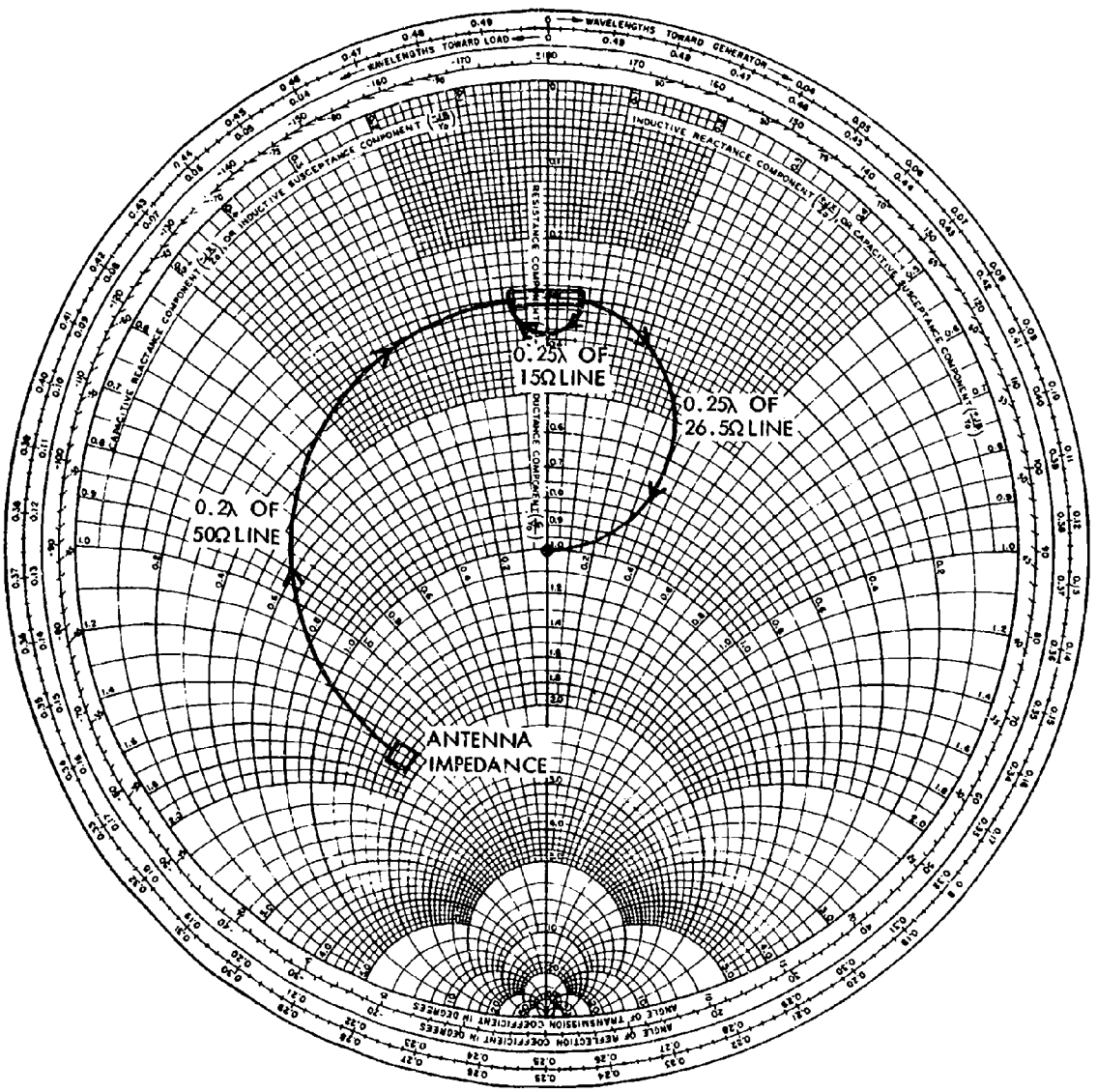

Figure 25. Matching Procedure for the Cavity-Backed Spiral

0.3 + j0.08. These points were transformed to their complex conjugates by a quarter-wave rotation through a line of characteristic impedance 0.3 (i.e., 15 ohms). Finally, the impedance was rotated through a quarter wavelength of 26.5-ohm line to the 50-ohm center of the chart. The "spreading" of impedance points caused by the final rotation was just sufficient to bring all the points together at the center of the Smith Chart. It is important to note parenthetically that the operation shown on the Smith Chart of Figure 25 could not all be accomplished on one chart as we have indicated, because three different characteristic impedances were involved. The points resulting from the 0.2-wavelength rotation of the antenna impedance on a 50-ohm chart were transferred to a 15-ohm chart, rotated through a quarter wavelength to invert the impedance spread, then transferred to a 26.5-ohm chart and rotated to 50 ohms. Needless to say, a fair amount of "cut and try" was necessary to choose both the configuration and the line lengths and impedances used. This would undoubtedly be a fertile area for the use of computer optimization procedures, if such procedures could be devised.

Measured data on the matched equiangular spiral are presented in Figures 26 and 27. The VSWR is less than 1.043 over a band extending from 4.0 GHz to 4.6 GHz, a bandwidth of 600 MHz, or 14 percent of the 4.3-GHz center frequency. A second antenna was built to test the reproducibility of these results, and to permit measurement of the coupling between two antennas as a function of frequency and separation. The second antenna's impedance is plotted in Figure 28. The two Smith Chart plots are substantially different near the design center frequency of 4.5 GHz. The first antenna had a VSWR of 1.015 there, while the second's is 1.11. At 4.3 GHz, the second antenna's VSWR is 1.035, comparing favorably with the 1.029 measured on the first antenna. It should be noted that the measurement of such small VSWR's is subject to errors because of residual reflections in the slotted line and connectors. In fact, the typical VSWR of a pair of the latest type N connectors is 1.08 at 5.0 GHz.[5] In general, every pair of connectors will behave differently, and even the same pair cannot be relied upon to yield the same VSWR consistently. It is random behavior of this sort which limits the gain which can be had reproducibly in any system using reflection amplifiers. Quantitative discussion of this limitation is presented in paragraph 5.3.

5. General Radio Co., Catalog, p. 78.

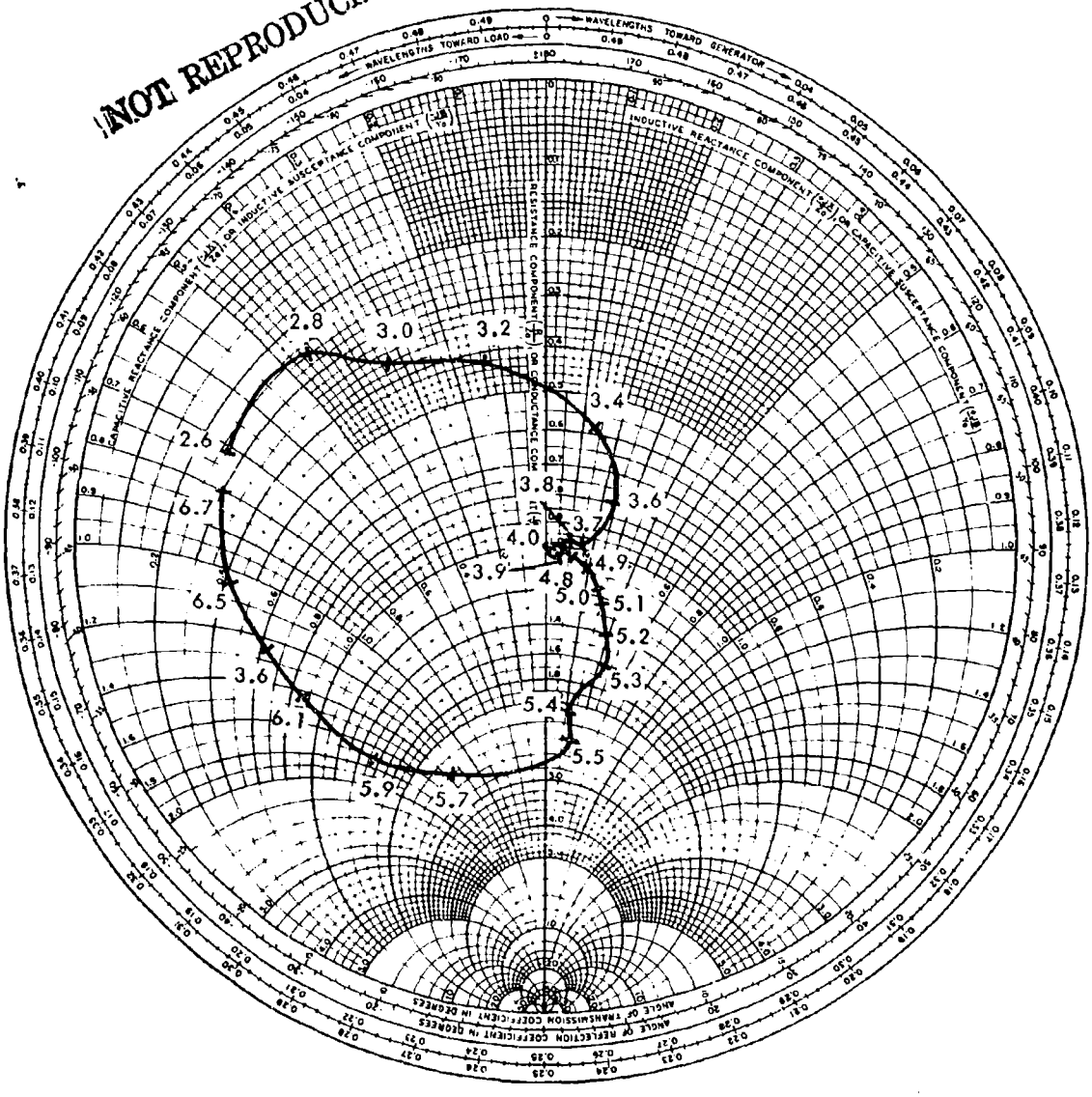

Figure 26. Impedance of the Matched Cavity-Backed Spiral, 2.6 GHz to 6.7 GHz

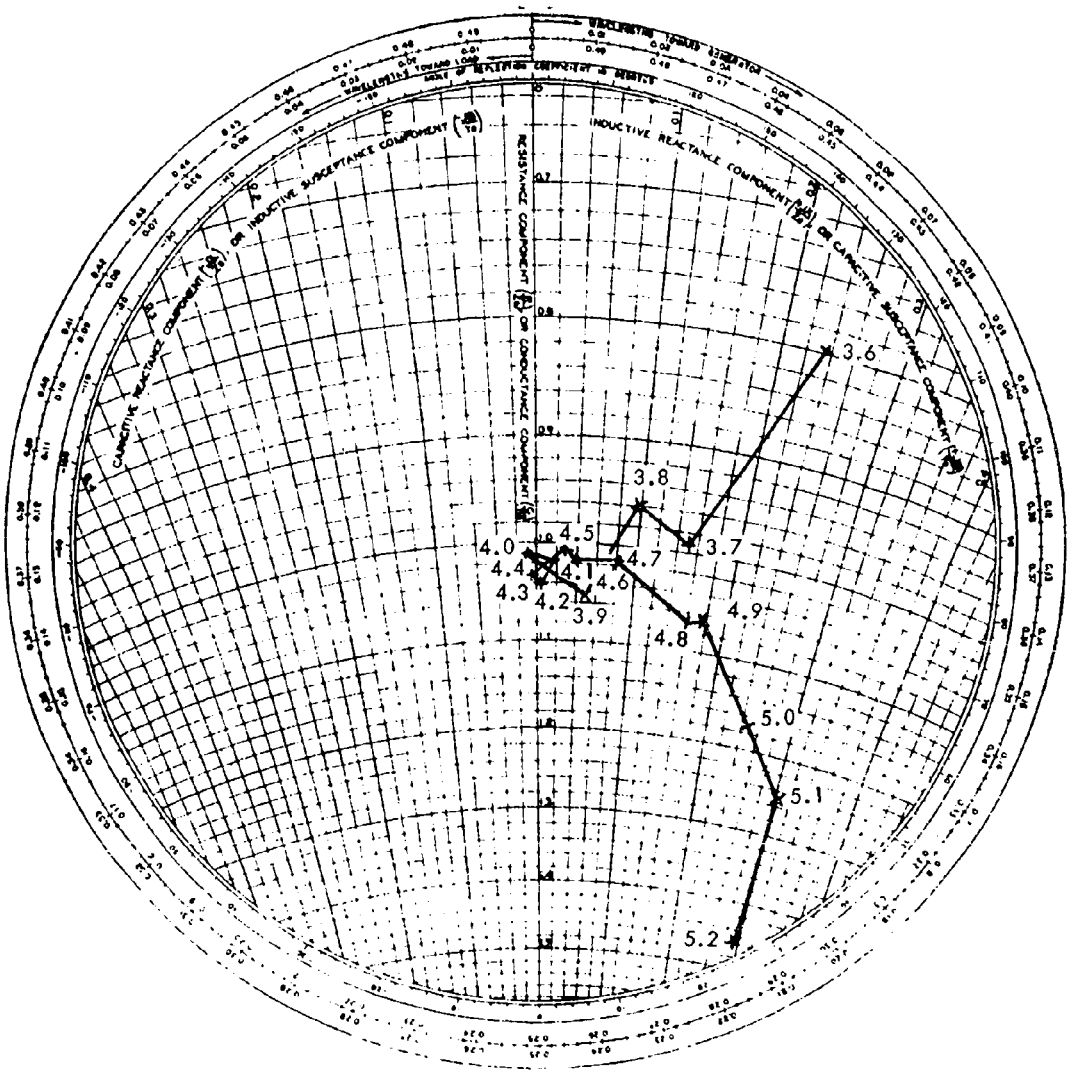

Figure 27. Impedance of the Matched, Cavity-Backed Spiral, 3.6 GHz to 5.2 GHz

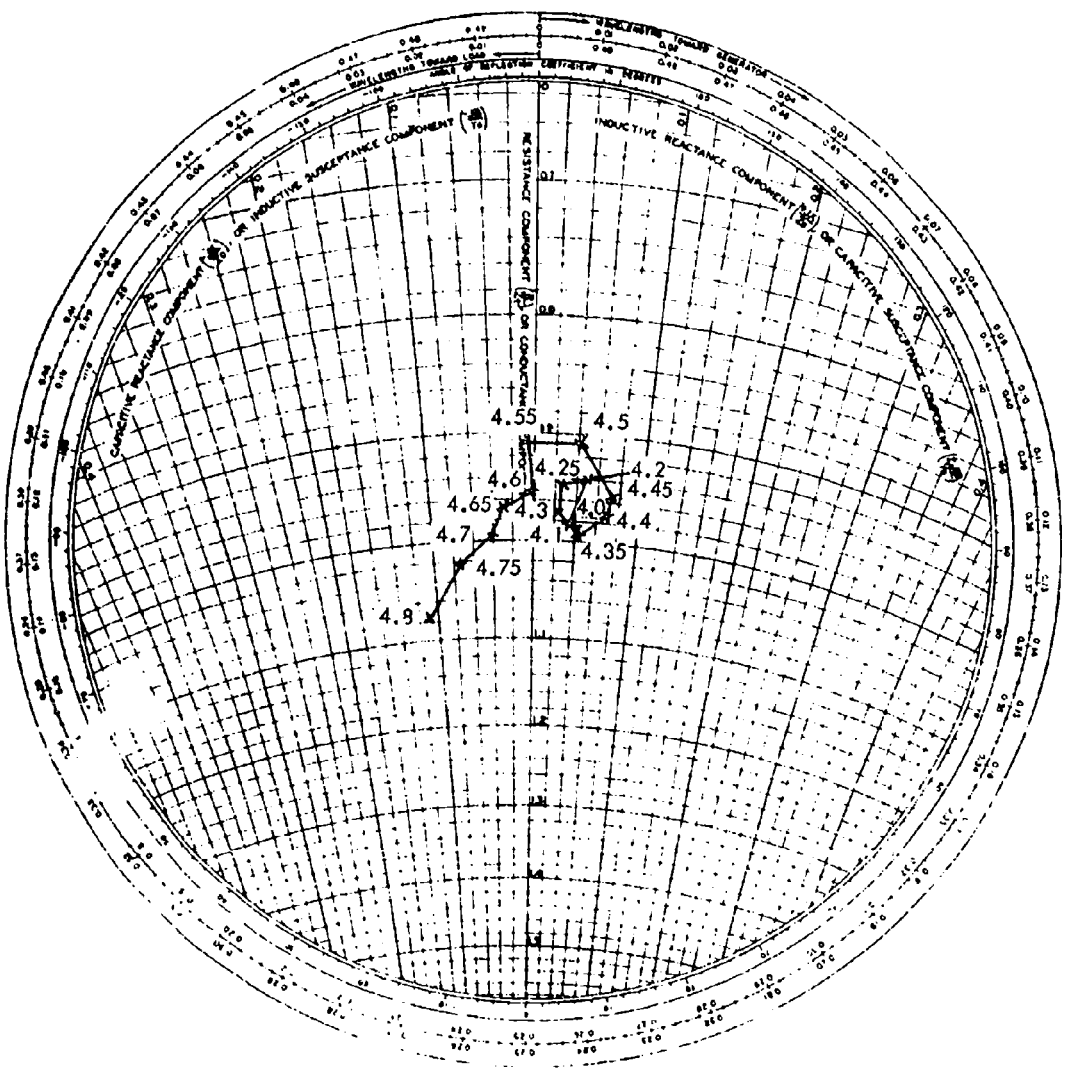

Figure 28. Impedance of the Second Matched Antenna

A pattern taken with the matched spiral is shown in Figure 29. The symmetry and circularity are somewhat poorer than obtained in Figure 20, perhaps due to the proximity of the center post to the center of the antenna. Some compromise is evidently necessary between pattern and impedance match.

3.5 MUTUAL COUPLING BETWEEN CAVITY-BACKED SPIRALS

3.5.1 Qualitative Theory

The mutual coupling between any two antennas can theoretically be calculated exactly. The exact technique is to set up an integral equation for the tangential $\vec{E}$ field at any point on either antenna as a function of the current distributions on both antennas. By setting this tangential $\vec{E}$ field equal to zero (for a perfectly conducting antenna) or $\vec{J}/\sigma$ [current density/antenna conductivity], one arrives at an integral equation in $\vec{J}$ alone which can be solved numerically if not analytically.[6,7] Once the currents are known with a given driving condition the mutual impedance can be derived easily. This calculation has been performed analytically only for a very few simple antennas. King has performed the calculation for dipoles and Vee antennas arbitrarily oriented.[8] Such calculation has never been done for any antenna as complex as an equiangular spiral antenna.

Since the $\vec{E}$ field at a distance 'r' along a ground plane from an antenna varies as $\frac{1}{r}$ [radiation term], $\frac{1}{r^2}$ [induction or near field term] or $\frac{1}{\sqrt{r}}$ [ground wave term], the mutual coupling should vary in the same way. Actually this is approximately true except for a superimposed resonant behavior that causes the coupling to vary periodically with the distance. Combining all of these effects one soon realizes that for a complicated system like two equiangular spirals in a ground plane the only way to arrive at the mutual coupling is to either 1) Solve the integral equation numerically, (Very difficult to set up and very expensive to run. It could involve the inversion of a 1000 x 1000 matrix for this case) or 2) Measure the coupling experimentally, which we did.

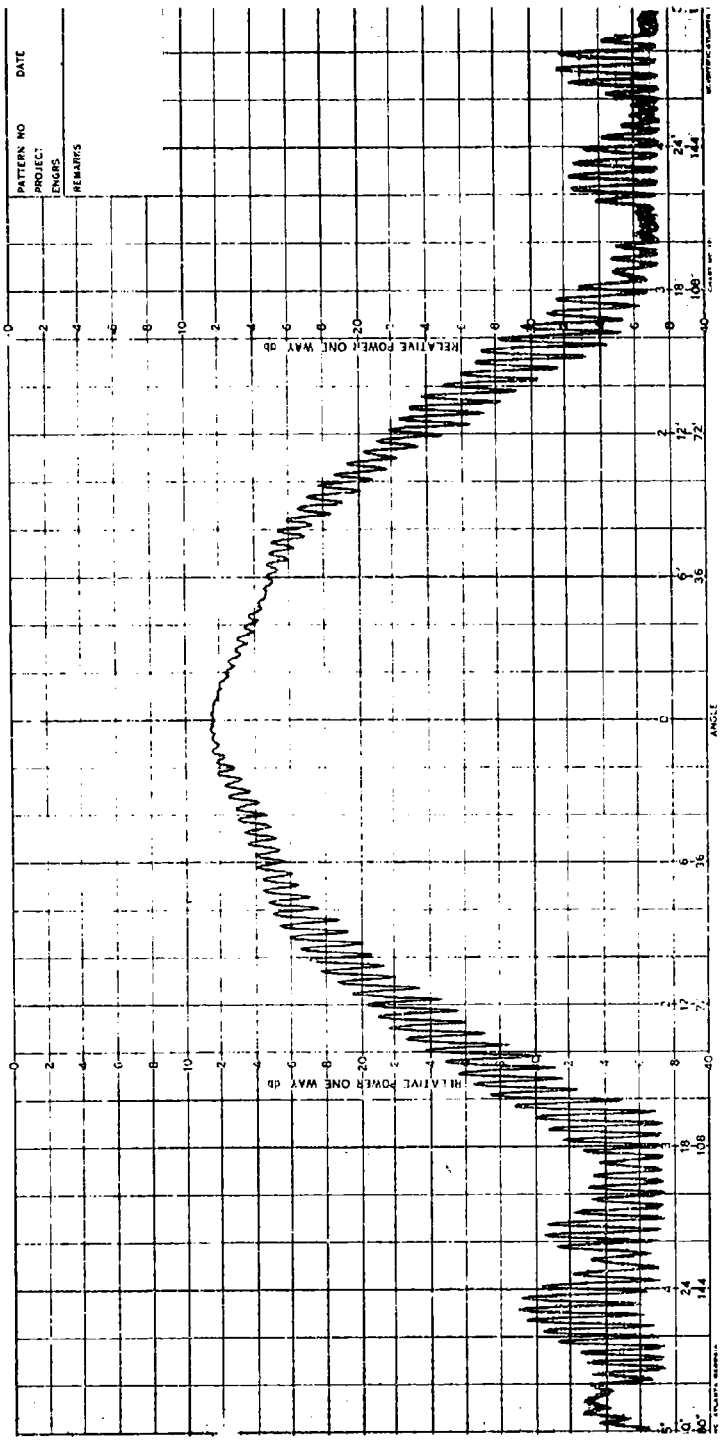

Figure 29. Pattern of Matched Cavity-Backed Spiral at 4.5 GHz

3.5.2 Experimental Coupling Measurements

In order to get a quantitative idea about the limitations on Van Atta array performance imposed by mutual coupling, we performed a series of measurements using the two matched antennas described in paragraph 3.4.5. The antennas were mounted in a series of two-hole ground planes, and the coupling between them measured as a function of frequency. The antenna assembly was pointed into a microwave anechoic chamber to simulate a free-space environment. Figure 30 shows the antennas at their minimum spacing of 3 inches center-to-center.

The measurements were carried out as follows. The transmitting antenna was fed from a leveled, frequency-swept generator, and a sample of the transmitted wave was tapped off with a directional coupler. The signal from the coupler was passed through a calibrated attenuator and applied to one of a pair of matched, wideband detectors (HP423A). The receiving antenna was connected directly to the other detector. The two detector output voltages were subtracted in an oscilloscope differential amplifier, and the attenuator used to obtain zero output at each of the measurement frequencies. The sum of the attenuator reading and the directional coupler's coupling value gave the isolation between the antennas. The quantity measured is actually the squared magnitude of the scattering coefficient $|S_{21}|^2$ between the transmitting antenna (port 1) and the receiving antenna (port 2), as the following argument shows. The power incident on port 1, or $|a_1|^2$, is sampled by the directional coupler which ignores the reflected power $|b_1|^2$. The output port (2) is terminated in the matched detector, which senses $|b_2|^2$ and generates no reflected power $|a_2|^2$. The ratio $|b_2|^2/|a_1|^2$ is, by definition, $|S_{21}|^2$. If desired, the transfer impedance $Z_{21}(\omega)$ can be calculated from $S_{21}(\omega)$ using the following relationship, valid for any matched two port terminated in matched loads at both ports:

$$Z_{21}(\omega) = 2RS_{21}(\omega)$$

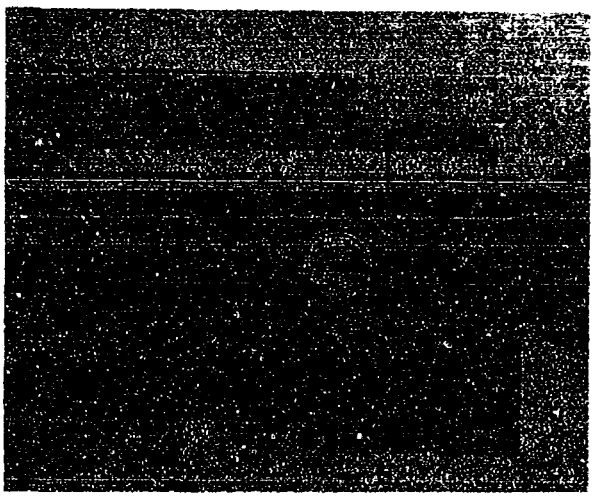

Figure 30. Matched Antennas Mounted for Mutual-Coupling Measurements

Extensive data were taken with the antenna mounted in plates of the type shown in Figure 30. Four different center-to-center spacings were used. The smallest was 3 inches, or 1.14 wavelengths at 4.5 GHz, set by the cavity diameter. Denoting this minimum spacing by 'd,' the other spacings were $\sqrt{2}d$, 2d, and $\sqrt{5}d$. These values are the four shortest interantenna distances in an array where the antennas are located on a grid of squares whose edge dimension is 'd.'

Figure 31 is a plot of the isolation between two antennas of like polarization for spacings of d and 2d. For both spacings the variation in the isolation is substantial over the matched operating band of the antenna. With the antennas at the minimum spacing 'd,' the isolation ranges from 32 dB at 4.0 GHz to 50 dB at 4.9 GHz. The data for twice the minimum spacing follows a very similar trend as a function of frequency. At 4.0 GHz, the isolation is 39 dB, while at 4.9 GHz it is 56.5 dB. In the vicinity of the 4.5 GHz design-center frequency, both isolations vary rapidly indeed.

Figure 32 shows the isolation between two antennas of like polarization over the range 3.0 to 5.0 GHz, for all four antenna separations. Note that the isolation is not always an increasing function of spacing. At 4.0 GHz, the isolation at a separation of $\sqrt{2}d$ is some 10 dB higher than that at 2d. Near 4.5 GHz, the isolation at the minimum spacing 'd' is higher than it is at $\sqrt{2}d$.

To test the conjecture that antennas of opposite polarizations should exhibit higher isolations, the data reported in Figure 33 were taken. Contrary to expectation, the isolation values for the cross-polarized case follow the same trend as the like-polarized case, and the isolation values are nearly the same. No clear-cut advantage for the cross-polarized case is evident; in fact, at 4.0 GHz, the isolation of the like-polarized antennas is higher by 3.5 dB.

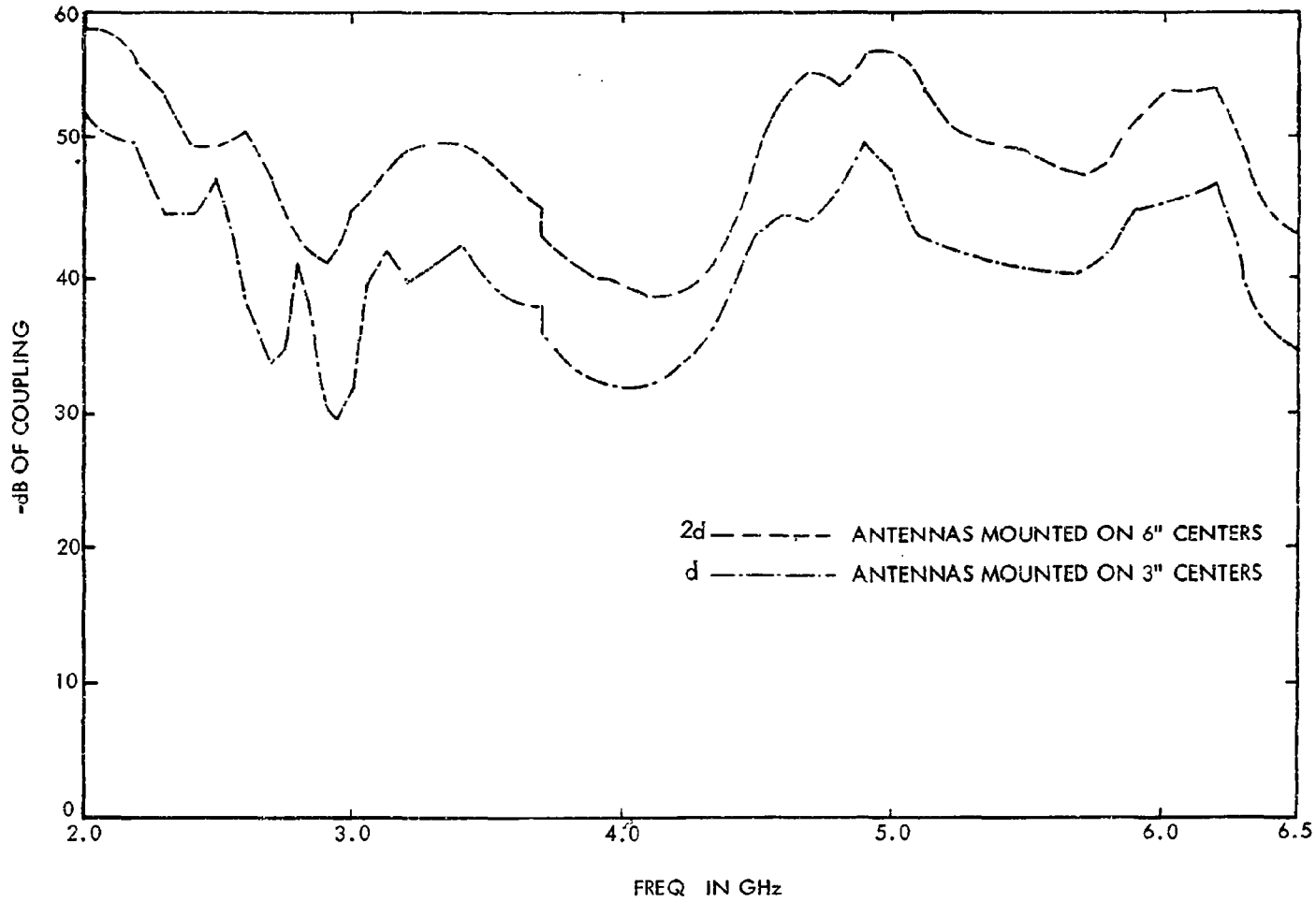

Figure 31. Isolation Between Two Spirals of Like Polarizations, 2.0 GHz to 6.5 GHz

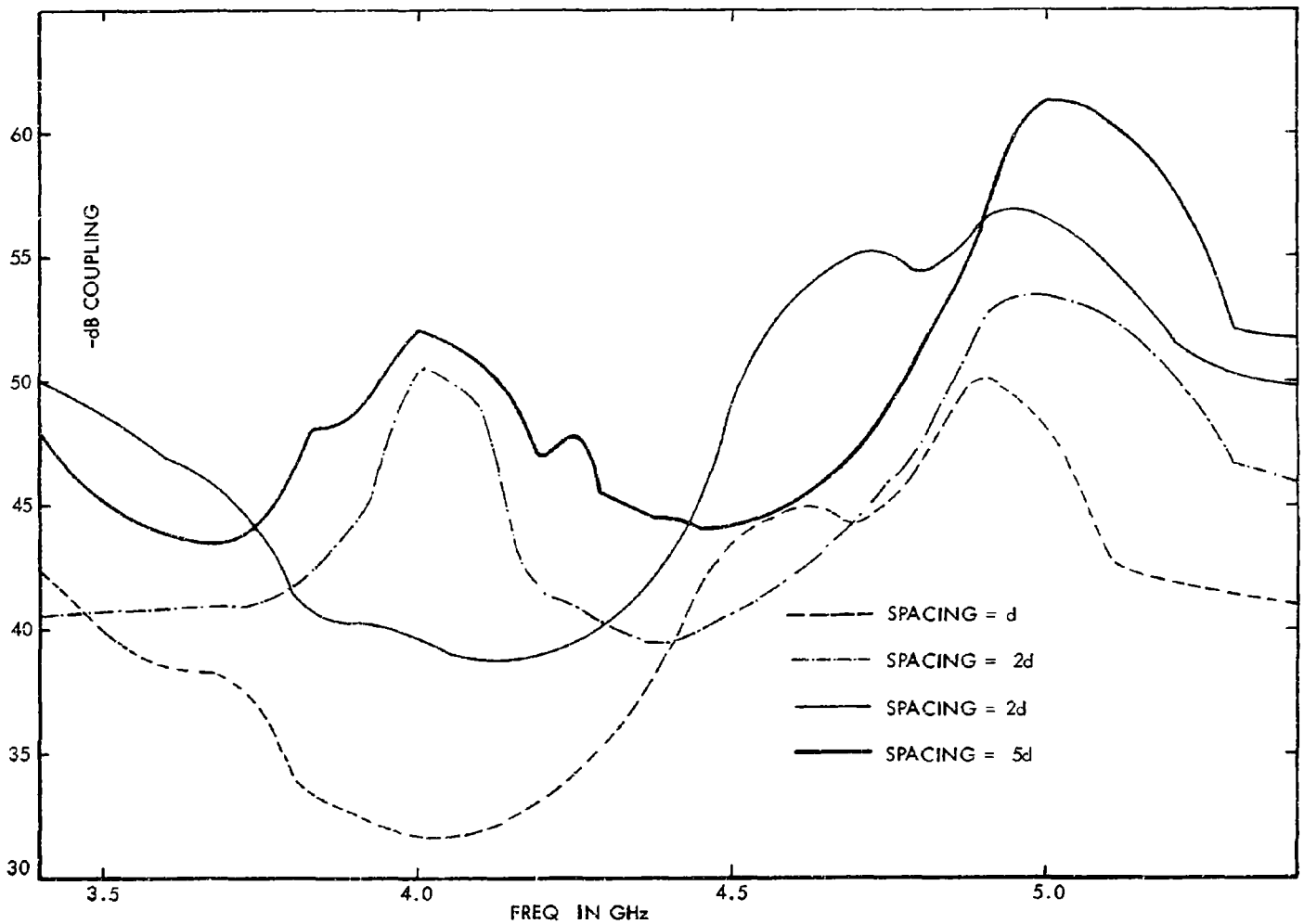

Figure 32. Isolation Between Two Spirals of Like Polarizations, 3.4 GHz to 5.4 GHz

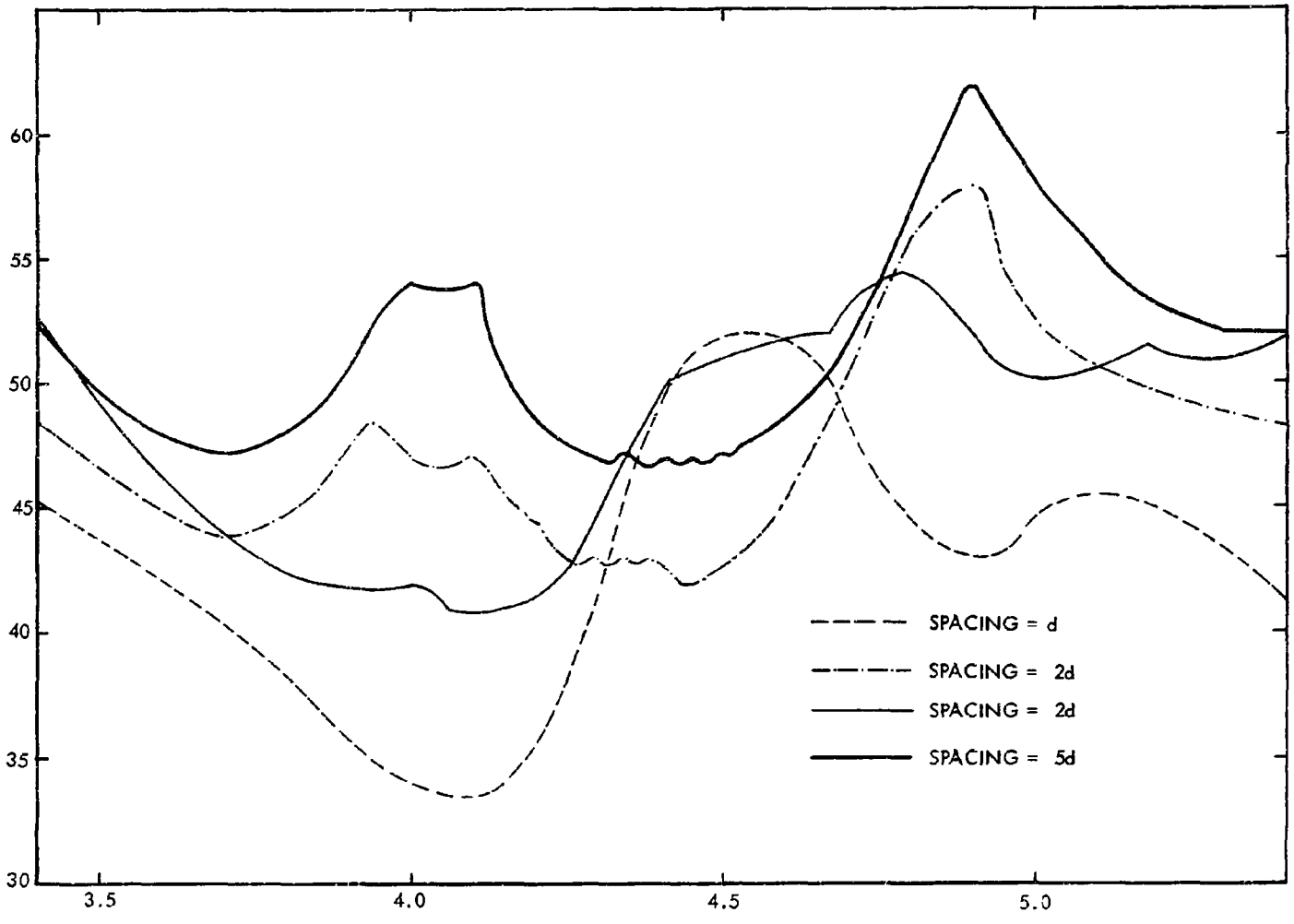

Figure 33. Isolation Between Spiral Antennas Having Opposite Polarizations

SECTION IV

RADIATION PROPERTIES OF ACTIVE VAN ATTA ARRAYS

4.1 INTRODUCTION

The Van Atta array is the simplest form of retrodirective array. In his patent, Van Atta shows that an array in which antisymmetrically located elements are connected by equal-length transmission lines is a discrete analog of the well-known corner reflector.[9] The array absorbs a plane wave striking it from any direction, and after a short delay retransmits a plane wave back in the incident direction. The Van Atta array is thus an elementary "adaptive" antenna array.

The principle which gives the Van Atta array its retrodirective property can be explained using Figure 34. The figure shows a linear Van Atta array in which the elements are spaced by 'd' and interconnected by cables of a common length 'L.' The central element (0) is terminated in an open-circuited cable of length L/2. Inspection of Figure 34 shows that the propagation delay from each point on the incident wavefront to the conjugate point on the same wavefront is constant. Thus, the delay from the point marked (+1) to the nearest antenna element is $2\delta/c$, the cable delay is L/c, and the delay from the conjugate antenna element to the wavefront point (-1) is $4\delta/c$, for a total delay of $(6\delta + L)/c$. Exactly the same delay occurs between points (+2) and (-2), (+3) and (-3), and (0), (0). This equality of propagation delays obtains regardless of the incident angle, θ, so that the array acts like a mirror to a plane wave arriving from any direction. The above plausibility argument neglects the energy scattered by the antenna elements. The scattered power forms a specular beam at $(-\theta)$, and is usually negligible in an array containing high gain, matched amplifiers.

One of the first analyses of the Van Atta array was done by Sharp and Diab.[10] They studied a passive array using dipoles as elements, and calculated its radar cross section. Their result for σ is too large by a factor of two, since they neglected scattering. Davies et al.[11] have written a good review paper in which they discuss acoustic arrays, circular arrays, and active arrays using beam steering and frequency shifting. Their

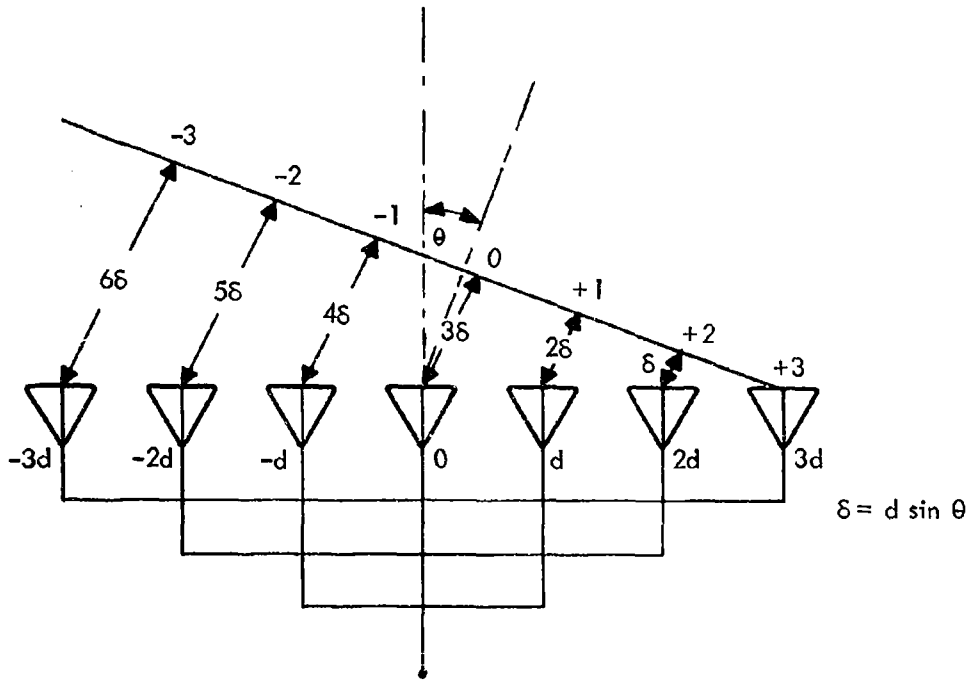

Figure 34. Linear Van Atta Array

main contributions to array theory is the simplified calculation they present for the pattern of a Van Atta array. A special issue of the IEEE Transactions on Antennas and Propagation was devoted to adaptive antennas, and contains several excellent papers on Van Atta arrays.[12]

The analysis presented in paragraph 4.2 gives a derivation of the radar cross section of a Van Atta array employing unilateral amplifiers. The cross section is shown to be independent of the element-pair arrangement in the array plane. Paragraph 4.3 considers the detailed pattern behavior of active Van Atta arrays.

A general linear array consisting of uniformly spaced elements interconnected by mismatched bilateral amplifiers is studied in paragraph 4.3.1. It is shown that the pattern of any planar array can be calculated using an equivalent linear array. The results of this analysis are specialized to various amplifier types of interest in paragraph 4.4, and a number of computed patterns are presented. Finally, paragraph 4.5 discusses the use of advanced array theory in the synthesis of Van Atta arrays for special purposes.

4.2 CALCULATION OF THE RADAR CROSS SECTION OF A GENERAL VAN ATTA ARRAY

In this section we calculate the radar cross section of a Van Atta array consisting of N pairs of identical circularly-polarized elements interconnected by matched unidirectional amplifiers of gain A. The calculation proceeds in several steps. Paragraph 4.2.1 calculates the electric field $\vec{E}(\theta,r)$ emitted by one of the antenna elements when it is used as a transmitter. Paragraph 4.2.2 studies the same antenna used as a receiver. The results of these two sections are used in paragraph 4.2.3 to calculate the electric-field return ratio, or "gain," of the Van Atta array in the retrodirective direction. Finally, in paragraph 4.2.4, the return ratio is used to compute the array's radar cross section.

4.2.1 Calculation of $\vec{E}(\theta,r)$ for a Single Antenna Element Used as a Transmitter

An antenna whose terminal voltage is V will radiate an electric field $\vec{E}(\theta,r)$ whose amplitude varies linearly with V, inversely with distance r, and with some angular dependence $F(\theta)$, thus:

$$\left|\vec{E}(\theta,r)\right| = \frac{V}{r} F(\theta) C \qquad (1)$$

For simplicity, the pattern will be assumed to vary only with the polar angle θ. The function $F(\theta)$ is the antenna's voltage pattern, normalized to 1 at the beam peak. The quantities $\vec{E}(\theta,r)$ and V are complex amplitudes, and an $e^{j\omega t}$ time dependence is understood.

To evaluate the dimensionless constant C, the total power supplied to the antenna will be equated to the total power radiated. The radiated power P_r is computed by integrating the normal component of the Poynting vector $\vec{S}(\theta,r)$ over a sphere of radius r centered at the antenna:

$$\vec{S}(\theta,r) = \frac{1}{2} \mathrm{Re}\left|\vec{E}(\theta,r) \times \vec{H}^*(\theta,r)\right| = \frac{\left|\vec{E}(\theta,r)\right|^2}{2Z_0} \vec{i}_r \qquad (2)$$

Z_0 = Impedance of free space = 377 ohms

$$P_r = \int_S \int \vec{S}(\theta,r) \cdot \vec{ds} = \int_0^{2\pi} \int_0^{\pi} \frac{\left|\vec{E}(\theta,r)\right|^2}{2Z_0} \vec{i}_r \cdot \vec{i}_r \, r^2 \sin\theta \, d\theta \, d\phi$$

$$= \int_0^{2\pi} \int_0^{\pi} \left(\frac{1}{2Z_0}\right) \frac{|V|^2}{r^2} C^2 F^2(\theta) \, r^2 \sin\theta \, d\theta \, d\phi$$

$$= \frac{|V|^2 C^2}{2Z_0} \int_0^{2\pi} \int_0^{\pi} F^2(\theta) \sin\theta \, d\theta \, d\phi \qquad (3)$$

The directivity D of an antenna is defined as:

$$D = \frac{4\pi \left|E_{max}\right|^2}{\int_0^{2\pi}\int_0^{\pi} \left|E(\theta,\phi)\right|^2 \sin\theta d\theta d\phi} = \frac{4\pi}{\int_0^{2\pi}\int_0^{\pi} F^2(\theta) \sin\theta d\theta d\phi} \tag{4}$$

The radiated power P_r can be rewritten in terms of D, thus:

$$P_r = \frac{|V|^2 C^2}{Z_0 D} 2\pi \tag{5}$$

The average power P_s supplied to the terminals of the antenna is:

$$P_s = \frac{1}{2} \mathrm{Re}[VI^*] = \frac{|V|^2}{2R} \tag{6}$$

In writing Eq. (6) we have assumed that the antenna's impedance is real. If the antenna is perfectly efficient, then R is just the radiation resistance, and we can equate the power supplied to the power radiated:

$$\frac{|V|^2}{2R} = \frac{|V|^2 C^2}{Z_0 D} 2\pi \tag{7}$$

$$\therefore C = \sqrt{\frac{Z_0 D}{4\pi R}} \tag{8}$$

Thus, the magnitude of the electric field $\vec{E}(\theta,r)$ radiated from a matched, perfectly efficient antenna is

$$\left|\vec{E}(\theta,r)\right| = \frac{|V|}{r}\sqrt{\frac{DZ_0}{4\pi R}}\,F(\theta) \tag{9}$$

Equation (9) can be rewritten in a more convenient form using the power gain function $G(\theta)$:

$$G(\theta) \triangleq D\,F^2(\theta) \tag{10}$$

$$\therefore \left|\vec{E}(\theta,r)\right| = \frac{|V|}{r}\sqrt{\frac{G(\theta)Z_0}{4\pi R}} \tag{11}$$

4.2.2 Calculation of the Terminal Voltage of an Antenna Excited by $\vec{E}(\theta,r)$

The receiving properties of the antenna studied in paragraph 4.2.1 are now investigated. The antenna is again assumed to be 100 percent efficient, and matched so that its terminal impedance is identical to its radiation resistance R. In addition, the antenna is terminated in a matched load, i.e., a resistor of value R. We wish to calculate the terminal voltage V caused by an electric field $\vec{E}(\theta,r)$ incident on the antenna. This is done by equating the power intercepted by the antenna's effective aperture to one-half the power dissipated in the resistor. The other half of the incident power is, of course, scattered.

The intercepted power P_i is given by the surface integral of the normal component of the Poynting vector $\vec{S}(r,\theta)$ over the effective aperture A_{eff} of the antenna, thus:

$$P_i = \int_{A_{eff}} \int \vec{S}(\theta,r) \cdot \vec{ds}$$

$$= \int_{A_{eff}} \int \frac{|\vec{E}(\theta,r)|^2}{2Z_0} \vec{i}_r \cdot \vec{i}_r \, dA$$

$$= \frac{1}{2Z_0} \left|\vec{E}_{inc}(\theta)\right|^2 A_{eff} \tag{12}$$

The received power P_r delivered to the load resistor is:

$$P_r = \frac{1}{2} \mathrm{Re}[VI^*] = \frac{|V|^2}{2R} \tag{13}$$

Equating half the intercepted power to the received power yields an expression for the magnitude of the terminal voltage:

$$\frac{|V|^2}{2R} = \frac{1}{4Z_0} \left|\vec{E}_{inc}(\theta)\right|^2 A_{eff}$$

$$|V| = \left|\vec{E}_{inc}(\theta)\right| \sqrt{\frac{R\, A_{eff}}{2Z_0}} \tag{14}$$

It is well known that the effective area of an antenna in a particular direction is related to its gain in that direction, thus:

$$A_{eff}(\theta) = \frac{G(\theta)\, \lambda^2}{4\pi} \tag{15}$$

The desired expression for the voltage at the terminals of a matched antenna excited by an incident electric field $\vec{E}_{inc}(\theta)$ is obtained by substituting Eq. (15) into Eq. (14).

$$|V| = \left|\vec{E}_{inc}(\theta)\right| \sqrt{\frac{R\,\lambda^2\,G(\theta)}{8\pi Z_0}} \qquad (16)$$

4.2.3 Electric-Field Return Ratio of a Van Atta Array

The results of the two previous sections will now be used to compute the electric-field return ratio $\vec{E}(\theta,r)/\vec{E}_{inc}(\theta)$ for a typical element pair in a Van Atta array. The return ratio for an array of N element pairs is then shown to be simply N times the return ratio for a single pair, independent of the arrangement of the conjugate pairs in the array.

A typical conjugate pair in a Van Atta array consists of a receiving antenna element, a unidirectional amplifier whose voltage gain is 'A,' and a transmitting antenna. It is assumed that the amplifier and interconnecting transmission line constitute a matched load for the receiving antenna. From Eq. (16), the voltage applied to the amplifier input due to an electric $\vec{E}_{inc}(\theta)$ striking the receiving antenna is:

$$|V| = \left|\vec{E}_{inc}(\theta)\right| \sqrt{\frac{R\,\lambda^2\,G(\theta)}{8\pi Z_0}} \qquad (17)$$

This voltage is amplified by A and applied to the transmitting antenna, which in turn radiates an electric field $\vec{E}(\theta,r)$ given by Eq. (11):

$$\left|\vec{E}(\theta,r)\right| = \frac{A|V|}{r} \sqrt{\frac{G(\theta)\,Z_0}{4\pi\,R}} \qquad (18)$$

If the receiving and transmitting antennas are identical, the electric-field return ratio for a single conjugate pair is:

$$\left|\frac{\vec{E}(\theta,r)}{\vec{E}_{inc}(\theta)}\right| = \frac{A\,\lambda\,G(\theta)}{4\pi\sqrt{2}\,r} \qquad \text{(single pair)} \qquad (19)$$

The conjugate arrangement of antenna elements in a Van Atta array causes all of the transmitting antennas to radiate in phase in the retrodirective (θ) direction. If we assume identical antenna elements, antenna orientations (θ) and transmission-path delays, then an array of N element pairs will have a return ratio just N times that of a single pair:

$$\left|\frac{\vec{E}(\theta,r)}{\vec{E}_{inc}(\theta)}\right| = \frac{A\,N\,\lambda\,G(\theta)}{4\pi\sqrt{2}\,r} \qquad \text{(N - pair array)} \qquad (20)$$

Equation (20) tacitly assumes that the pattern $G(\theta)$ for an isolated antenna does not change when N antennas are arrayed, or equivalently that there is no mutual coupling between elements. As a consequence, the gain of the array is just $NG(\theta)$, independent of spacing.[20,21] For spacings of a few wavelengths, however, the array gain varies with spacing in a complex manner, and $NG(\theta)$ can then be regarded only as an approximation to the actual gain.[22,23]

4.2.4 Radar Cross Section of a Van Atta Array

The radar cross section σ of a Van Atta array is easily calculated from Eq. (20) for the electric-field return ratio. The hypothetical scatterer used in the definition of radar cross section intercepts a power $|\vec{S}_{inc}|\sigma$ from the radar, and scatters it uniformly in all diretions. The resulting power per unit area $|\vec{S}_{rec}|$ received by the radar is:

$$\left|\vec{S}_{rec}\right| = \frac{\left|\vec{S}_{inc}\right|\sigma}{4\pi\,r^2} \qquad (21)$$

Therefore,

$$\sigma = 4\pi r^2 \frac{\left|\vec{S}_{rec}\right|}{\left|\vec{S}_{inc}\right|} \tag{22}$$

For the Van Atta array, the ratio of the two power densities is given by the square of the electric-field return ration, Eq. (20). Thus, the radar cross section of the array is:

$$\sigma = \frac{A^2 N^2 \lambda^2 G^2(\theta)}{8\pi} \tag{23}$$

For a passive Van Atta array, Eq. (23) reduces to 1/2 the result obtained by Sharp and Diab.[10] The latter authors assumed in their derivation that all of the intercepted power was retrodirected, which is incorrect. Each antenna element is terminated in a matched load (the conjugate antenna), so that half the intercepted power is lost to scattering.

4.3 PATTERN ANALYSIS OF ACTIVE VAN ATTA ARRAYS

In this section the problem of calculating the bistatic pattern of an active Van Atta array is considered. A linear, uniformly spaced array employing mismatched bilateral amplifiers is studied in paragraph 4.3.1. Patterns are derived for arrays having both even and odd symmetry. Paragraph 4.3.2 demonstrates how the linear theory can be used for two-dimensional array calculations. Detailed application of the analytical results to specific arrays is contained in paragraph 4.4.

4.3.1 Pattern Analysis of a Linear Van Atta Array Using Bilateral Amplifiers

The Van Atta array to be studied in this section is shown in Figure 35. The array elements are omnidirectional radiators

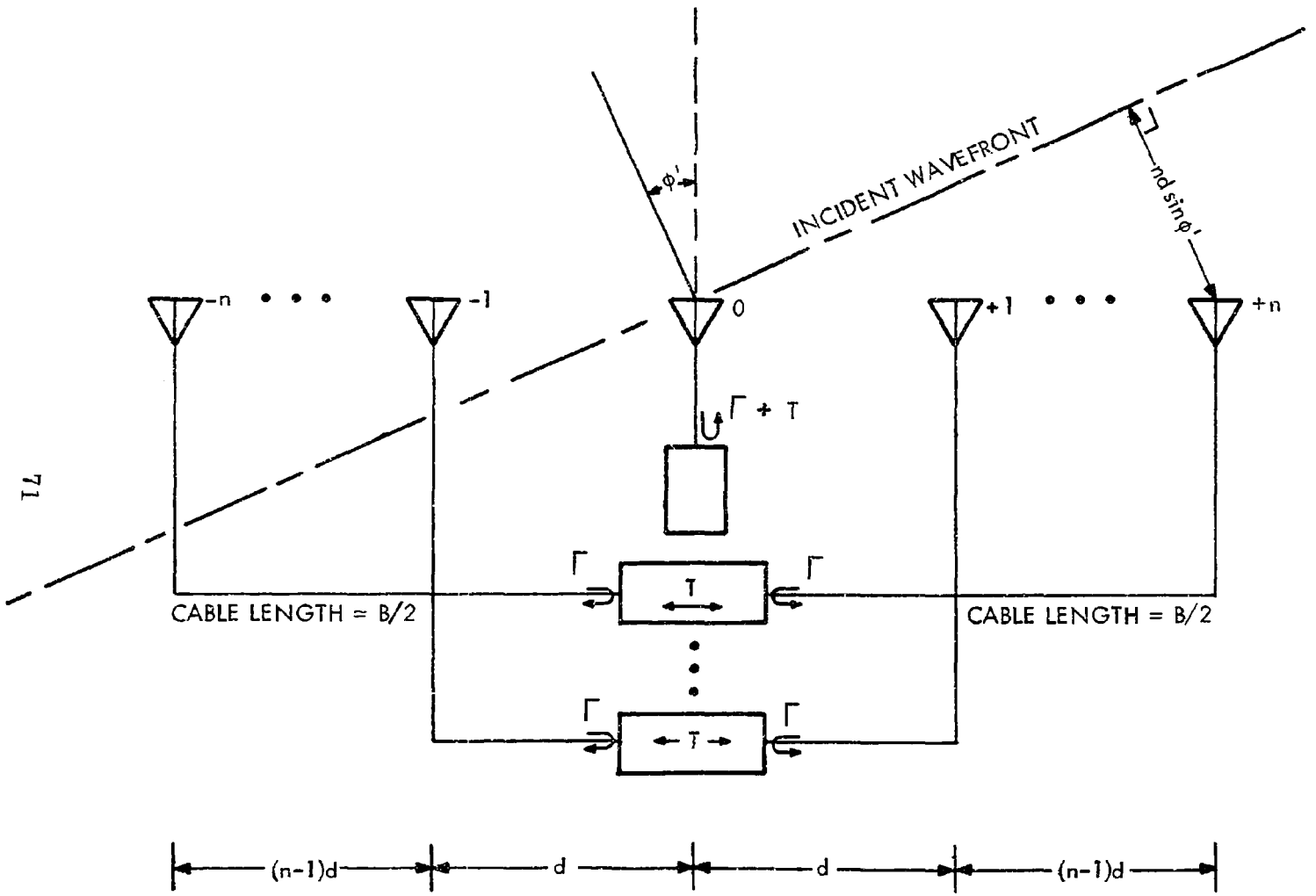

Figure 35. Bilateral Van Atta Array

spaced uniformly along a line. At the center of each of the interconnecting cables is a symmetrical, bilateral amplifying device which has a voltage reflection coefficient Γ at each port, and a voltage cross-transmission of T between opposite ports. We will first derive the bistatic pattern for an array using identical amplifiers whose Γ and T are arbitrary, then specialize the results to cover several cases of interest.

Consider a plane wave incident on the linear array from the ϕ' direction as shown in Figure 35. If the voltage V_0' induced on the center element is used as a phase reference, then the voltage V_n' on the n^{th} element will be:

$$V_n' = V_0' e^{j2n\pi d \sin\phi'/\lambda} \tag{24}$$

This induced voltage travels down the transmission line to the amplifier. A portion Γ of the incident wave is returned to the original antenna, while a portion T is carried to the conjugate antenna. The wave striking the $-n^{th}$ element is similarly reflected and transmitted by the amplifier, so that the total voltage V_n returned to the n^{th} antenna is:

$$V_n = \Gamma V_n' e^{-j2\pi B/\lambda} + T V_{-n}' e^{-j2\pi B/\lambda} \tag{25}$$

$$= V_0' e^{-j2\pi B/\lambda} \left[\Gamma_e e^{j\frac{2n\pi d}{\lambda} \sin\phi'} + T e^{-j\frac{2n\pi d}{\lambda} \sin\phi'} \right] \tag{26}$$

Equations (25) and (26) include a term $e^{-j2\pi B/\lambda}$ to account for the cable delay. Amplifier delay can be included in T by making it complex.

The n^{th} antenna radiates into space an electric field E_n whose magnitude is proportional to the applied voltage V_n. If the phase of the electric field from the center antenna is taken to be 0 in the far field, then the E field due to the n^{th} antenna is:

$$E_n = C' V_n e^{j\frac{2n\pi d}{\lambda} \sin \phi} \tag{27}$$

The total E field of the array is found by substituting Eq. (26) for V_n into Eq. (27) and summing over the 2N + 1 antenna elements, thus:

$$E = C' V_0 e^{-j\frac{2\pi B}{\lambda}} \sum_{n=-N}^{+N} \left[\Gamma e^{j\frac{2n\pi d}{\lambda}(\sin\phi + \sin\phi')} + T e^{j\frac{2n\pi d}{\lambda}(\sin\phi - \sin\phi')} \right] \tag{28}$$

If the constants in front of the summation sign are collected into a new constant C, and the summation performed, we have:

$$E = C\Gamma \frac{\sin\left[(2N+1)\frac{d\pi}{\lambda}(\sin\phi + \sin\phi')\right]}{\sin\left[\frac{d\pi}{\lambda}(\sin\phi + \sin\phi')\right]} + CT \frac{\sin\left[(2N+1)\frac{d\pi}{\lambda}(\sin\phi - \sin\phi')\right]}{\sin\left[\frac{d\pi}{\lambda}(\sin\phi - \sin\phi')\right]} \tag{29}$$

Equation (29) can be written more compactly as follows:

$$E = C\Gamma \frac{\sin Ka}{\sin a} + CT \frac{\sin Kb}{\sin b} \tag{30}$$

where

$$K = 2N + 1 = \text{total number of elements}$$

$$a = \frac{d\pi}{\lambda}(\sin\phi + \sin\phi')$$

$$b = \frac{d\pi}{\lambda}(\sin\phi - \sin\phi')$$

Equation (30) is the pattern of a Van Atta array containing an odd number of elements. The central element consists of a single antenna connected via a cable of length B/2 to a reflection amplifier whose reflection coefficient is $\Gamma + T$.

The pattern function appropriate for an array composed of an even number of elements (no central element) is most easily found by subtracting the patterns of two arrays containing an odd number of elements. This process is illustrated diagrammatically in Figure 36. If we begin with an odd array of $(2\ell-1)$ elements spaced by d/2, then subtract an odd array composed of $(\ell-1)$ elements spaced by d and centered at the same point, the result will be an even array of ℓ elements with spacing d. These steps are carried out mathematically in Eq. (31), using the notation of Eq. (30):

$$E = C\Gamma\left[\frac{\sin[2\ell-1)a/2]}{\sin(a/2)} - \frac{\sin[(\ell-1)a]}{\sin a}\right]$$

$$+ CT\left[\frac{\sin[(2\ell-1)b/2]}{\sin(b/2)} - \frac{\sin[(\ell-1)b]}{\sin b}\right] \qquad (31)$$

4.3.2 Extension of Linear-Array Theory to Planar Arrays

At first sight, the problem of calculating the pattern of a planar Van Atta array seems to be much more difficult than calculating the pattern of a linear array. In fact, however, the

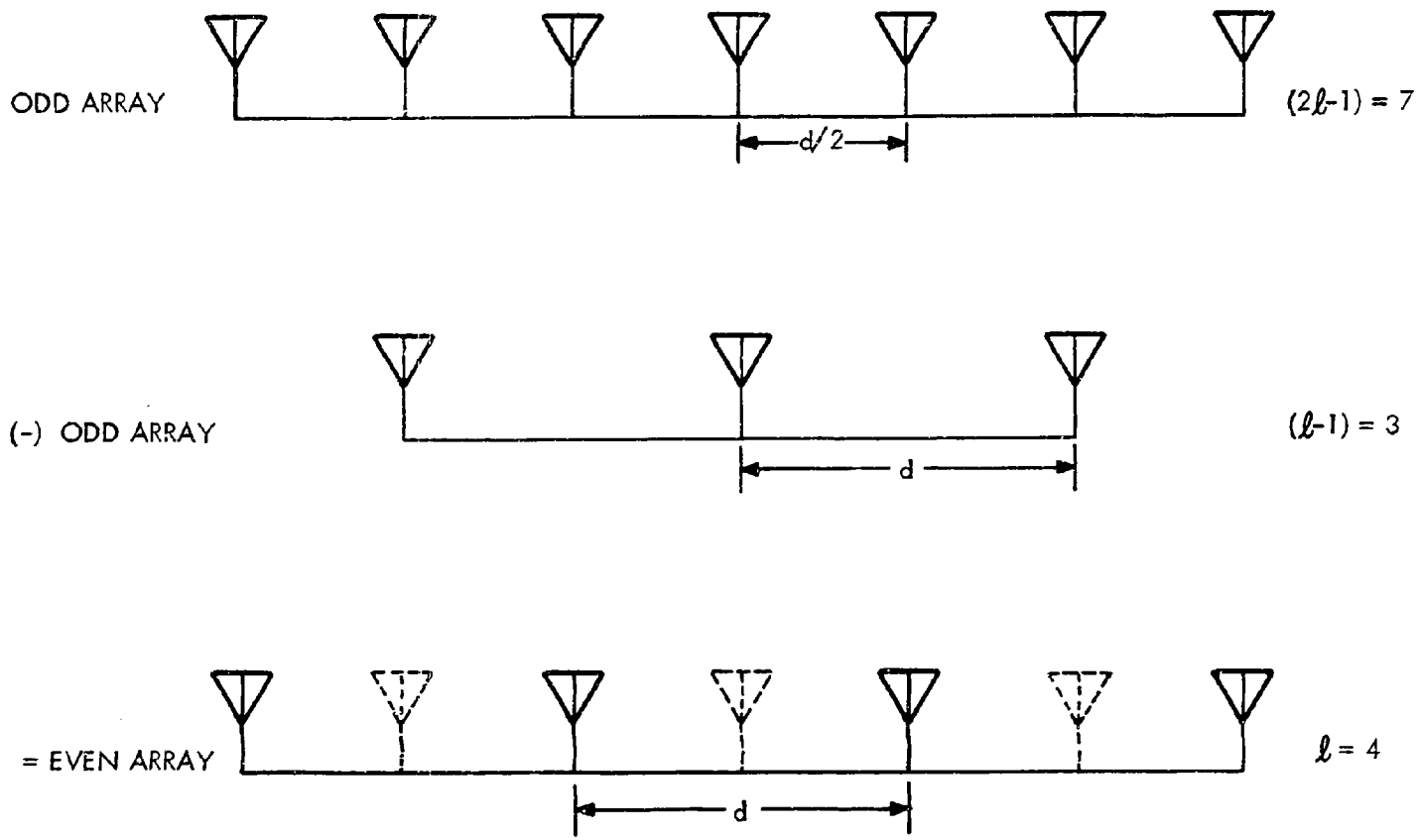

Figure 36. Array Subtraction

two-dimensional problem can often be reduced to the solution of two one-dimensional array problems.

First, consider the calculation of the pattern of an m x n-element rectangular array. The m rows of n elements each are assumed to be identical to one another, as are the n columns of 'm' elements. The rows are assumed to be perpendicular to the columns. The spacing of elements need not be uniform. In order to evaluate the pattern of the total array, we observe that the rectangular arrangement of m n antennas can be treated as a linear array of n "elements," each of the "elements" being itself a linear array of m antennas. The "element pattern" $F_m(\theta,\phi)$, of the m-element array is written in the usual way as the product of an m-term array factor $F_{am}(\phi)$ and an individual-antenna element pattern $F_e(\theta,\phi)$:

$$F_m(\theta,\phi) = F_{am}(\phi)F_e(\theta,\phi) \qquad (32)$$

where

$F_e(\theta,\phi)$ = antenna element pattern

$F_{am}(\phi)$ = array factor in the ϕ plane of a linear array of m omnidirectional radiators

If all of the n columns of m elements are identical, then each of the columns can be considered to be an element of a linear array lying in the θ plane, which is orthogonal to the ϕ plane. The appropriate array factor is then an n-term sum $F_{an}(\theta)$. The total rectangular-array pattern $F_t(\theta,\phi)$ is given by the product of $F_{an}(\theta)$ and the "element pattern" $F_m(\theta,\phi)$:

$$F_t(\theta,\phi) = F_m(\theta,\phi)F_{an}(\theta)$$

$$= F_{am}(\phi)F_{an}(\theta)F_e(\theta,\phi) \qquad \text{Q.E.D.} \qquad (33)$$

The above calculation applies only to rectangular arrays. If the array does not have this two dimensional symmetry, the pattern in any one plane perpendicular to the array can still be calculated from linear array theory, as the following argument shows. Consider the general planar array shown in Figure 37(a). It is desired to compute the pattern of this array in the θ plane, which is perpendicular to the array surface. A linear array whose far-field pattern in the θ-plane is identical to the array of Figure 37(a) is shown in Figure 37(b). The latter array was formed by moving the elements of the planar array into the θ-plane along perpendiculars to the θ-plane. The latter transformation clearly does not affect the relative far-field phases of individual elements, and therefore does not alter the θ-plane pattern. Note that a different equivalent linear array will, in general, be obtained for each orientation of the observation plane, requiring a separate pattern calculation to be made.

We conclude that the linear array theory is adequate for the treatment of planar arrays, at least in the usual approximation where mutual coupling effects are neglected.

4.4 COMPUTED ARRAY PATTERNS FOR VARIOUS AMPLIFIER TYPES

The array-pattern equations derived in paragraph 4.3.1 apply to a generalized bilateral-amplifier interconnection scheme. In this section, these analytical results are specialized to various particular cases of interest, and computed patterns are presented. The cases studied are the simple passive interconnection, matched unilateral and bilateral amplifier connections, the independent scatterer case, and various forms of the shunt-negative-conductance interconnection. Each of these interconnections can be described by assuming appropriate values for the amplifier's reflection coefficient Γ and transmission coefficient T. From Eq. (30), the voltage pattern of a Van Atta array employing a generalized bilateral interconnection is:

$$\left|E(\phi,\phi')\right| = \left|\Gamma \frac{\sin Ka}{\sin a} + T \frac{\sin Kb}{\sin b}\right| \qquad (34)$$

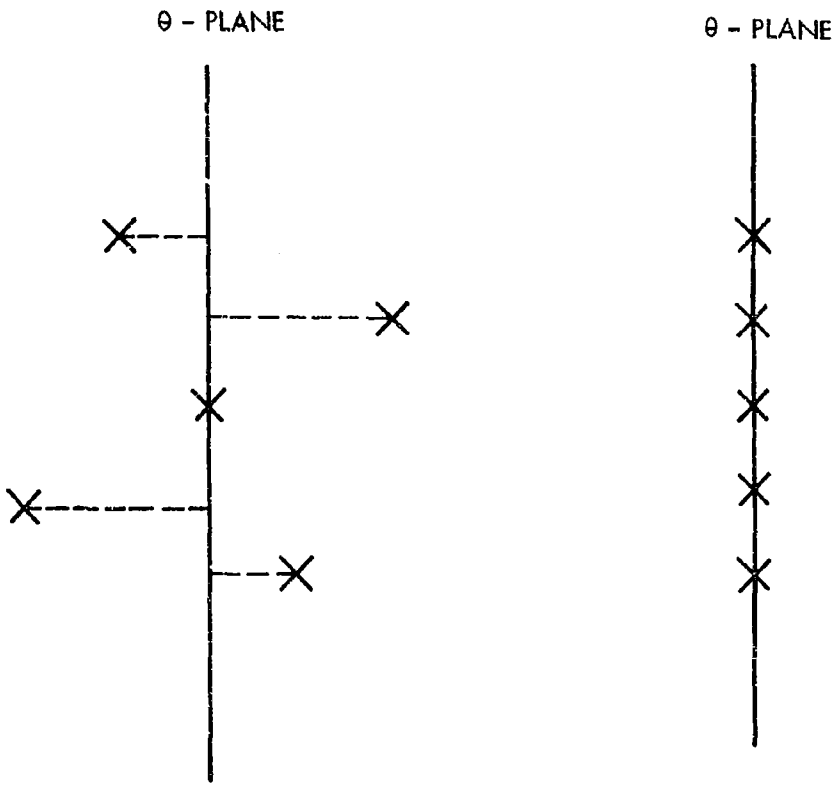

Figure 37. Two Arrays with Identical Patterns in the θ-Plane

where

$$a = \frac{d\pi}{\lambda}(\sin\phi + \sin\phi')$$

$$b = \frac{d\pi}{\lambda}(\sin\phi - \sin\phi')$$

This expression for $E(\phi, \phi')$ was plotted for a large number of special cases using the Applied Research Laboratory's CDC-3200 computer. The variables used and their ranges were:

ϕ' = incident angle = 0°, 15°, 30°, 60°

ϕ = array output angle = -90° to $+90^\circ$ in steps of 2°

K = total number of transmitting elements = 3, 5, 7, 11

d = element spacing in wavelengths = 1.0, 1.25

Γ = amplifier reflection coefficient

T = amplifier transmission coefficient

The quantity K refers to the number of active transmitting elements. K is odd because of the presence of a central element (see Figure 35). Even arrays are handled by the subtraction method of Eq. (31). In a bilateral array, all the antennas are used for both receiving and transmitting, so that the total number of array elements is equal to K; for a unilateral array (inherently even), the total number of antennas is 2K.

Equation (34) was plotted in a normalized form so that the maximum value on each graph was always 1. If desired the true peak value can be calculated from the return-ratio expression, Eq. (20). In several of the plots, a spurious dip occurs at $\phi' = \phi = 0^\circ$ because a division by 0 is indicated and the computer automatically generates an output of 2. The actual peak value can be ascertained approximately from the points at $\phi = \pm 2^\circ$. The discontinuity at 0° provides a convenient reference point for comparison of the various $\phi' = 0^\circ$ plots.

4.4.1 Patterns for the Passive or Matched-Amplifier Interconnection

Three important types of Van Atta array interconnection can be described by Eq. (34) if $\Gamma = 0$ and $T = A$, where A is a constant. The case of a matched, passive cable interconnection of conjugate antennas corresponds to $\Gamma = 0$, $T = 1$. If a matched, bilateral amplifier of voltage gain G is inserted in the cable, then $\Gamma = 0$ and $T = G$. Equation (34) was derived for a bilateral interconnection; however, it applies equally well to the case of a unilateral array with twice as many elements. A single set of normalized plots was computed from the following form of Eq. (34):

$$\left| E(\phi, \phi') \right| = \left| T \frac{\sin \frac{Kd\pi}{\lambda}(\sin\phi - \sin\phi')}{\sin \frac{d\pi}{\lambda}(\sin\phi - \sin\phi')} \right| \qquad (36)$$

Figures 38 and 39 show Eq. (36) plotted for incident angles ϕ' varying form 0° to 60°, with the total number of transmitting elements K being 3, 5, 7, and 11. The element spacing d is λ. The retrodirective property of Van Atta arrays is evident in each plot, since $\phi = \phi'$ at the beam peak. The true peak value is KT, obtained by taking the limit of Eq. (36) as ϕ approaches ϕ'. Note the appearance of grating lobes at large angles of incidence, as well as the increased directivity of the array as the number of elements is increased. Figure 40 and 41 show the effect of increasing the element spacing to 1.25 λ. The main beam is narrowed somewhat, but more sidelobes and grating lobes appear.

4.4.2 Pattern of the Independent Scatterer Case

It is a simple matter to generate the pattern of an active specular reflector by setting $\Gamma = 1$ and $T = 0$ in Eq. (34):

$$E(\phi, \phi') = \left| \Gamma \frac{\sin \frac{Kd\pi}{\lambda}(\sin\phi + \sin\phi')}{\sin \frac{d\pi}{\lambda}(\sin\phi + \sin\phi')} \right| \qquad (37)$$

An active specular array is simply an array of independent antennas, each of which is terminated in a reflection amplifier of gain Γ. The computer results for this case are shown in Figure 42. The plots for the individual scatterer case are exact mirror images of the bidirectional Van Atta case treated in paragraph 4.4.1, and similar comments apply concerning beamwidth, sidelobes, and grating lobes.

4.4.3 Patterns of the High Gain Shunt Diode Interconnection

This section and those which follow deal with various cases of the elementary shunt-negative-conductance interconnection originally proposed for the experimental Van Atta array. For any shunt-amplifier connection, the voltage must be continuous across the junction point, so that we have the following relation between Γ and T:

$$T = 1 + \Gamma \qquad (38)$$

It is computationally convenient to consider various special cases. For high levels of gain, $\Gamma \approx T$, and Eq. (34) becomes:

$$\left|E(\phi, \phi')\right| = \Gamma \left| \frac{\sin Ka}{\sin a} + \frac{\sin Kb}{\sin b} \right|$$

where

$$a = \frac{d\pi}{\lambda}(\sin\phi + \sin\phi')$$

$$b = \frac{d\pi}{\lambda}(\sin\phi - \sin\phi') \qquad (39)$$

Computed patterns for the high gain case are shown in Figures 43 and 44. For large numbers of elements, K = 7 and K = 11, the patterns exhibit the retrodirective (b=0, $\phi=\phi'$) and specular (a=0, $\phi=-\phi'$) peaks which are predicted from the qualitative theory. This desired behavior occurs only because the interference of the two terms in Eq. (39) is negligible in the vicinity of the two peaks. At lower values of K, the interaction of the two terms is much stronger. For K = 3 it is very difficult to distinguish the two peaks except at large angles of incidence. In general one can say that K must be ≥ 5 to obtain significant retrodirective action. These results are for an odd array, that is, an array of (K-1)/2 antenna pairs with their associated shunt amplifiers, plus a single central antenna terminated in a reflection amplifier. The even-array case is treated in paragraph 4.4.5.

4.4.4 Patterns for the Shunt Amplifier Interconnection at Intermediate Gains

As noted in paragraph 4.4.3, the condition $\Gamma + 1 = T$ always holds for the shunt-amplifier interconnection, regardless of gain. Two extremes have already been already been treated, namely the passive interconnection, for which $T = 1$ and $\Gamma = 0$, and the high-gain case, where $\Gamma \approx T$. Between these two cases there is a gradual transition between the purely retrodirective behavior of the passive case to the retrodirective-specular behavior of the high-gain case. For the intermediate-gain case, Eq. (34) becomes:

$$E(\theta,\phi) = \Gamma\frac{\sin Ka}{\sin a} + (1+\Gamma)\frac{\sin Kb}{\sin b} \qquad (40)$$

Figures 45 and 46 show the effect of increasing Γ on the formation of retrodirective and specular peaks. Equation (40) indicates that the magnitude of the retrodirective peak should be proportional to $1 + \Gamma$, while that of the specular peak should vary as Γ. As Γ increases we expect to see the specular peak gradually increase in size until it equals the retrodirective peak. For low numbers of elements (K), however, the interaction of the two terms in Eq. (40) is pronounced, and the specular peak does not appear. For K = 11, the separation between retrodirective and specular peaks is very clear.

Figure 47 shows the effect on the pattern caused by varying the incident angle ϕ' at an intermediate value of Γ, $\Gamma = 3.0$. The first four plots are for an element separation $d = \lambda$, and the next four are for $d = 1.25\ \lambda$. It is interesting to note that no specular peak is formed when $\Gamma = 3.0$ and $d = \lambda$. Increasing the separation d to $1.25\ \lambda$ reduces the interaction between terms, causing the specular beam to appear. In general, the width of the main beam is decreased by increasing any or all of the quantities Γ, ϕ', K, or d.

4.4.5 Pattern for the High Gain Shunt Amplifier Interconnection with an Even Number of Elements

In this section we calculate the pattern for the array interconnection originally proposed, namely an <u>even</u> high-gain shunt-amplifier array. As in paragraph 4.4.3, we approximate the high-gain case with the condition $\Gamma = T$. The even array can be handled by the array-subtraction technique discussed in paragraph 4.3.3, Eq. (31). However, for the present case it is computationally easier to modify Eq. (28) and invoke the condition $\Gamma = T$.

The pattern for an even array in which $\Gamma = T$ is found from Eq. (28) by summing over the odd-numbered elements and factoring out a common phase factor, thus:

$$E = C' V_0 e^{-j\frac{2\pi B}{\lambda}} \Gamma \sum_{\substack{n=-N \\ n\ \text{odd}}}^{+N} e^{j\frac{n\pi d}{\lambda}\sin\phi} \left[e^{j\frac{n\pi d}{\lambda}\sin\phi'} + e^{-j\frac{n\pi d}{\lambda}\sin\phi'} \right] \quad (41)$$

The quantity d in Eq. (41) has been redefined as twice the spacing in the original array, so that it now represents the even array's interelement separation. Equation (41) can be further simplified by collecting the constant terms in a new constant C, and combining the exponentials, thus:

$$E = C \sum_{\substack{n=-N \\ \text{odd}}}^{+N} e^{j\frac{n\pi d}{\lambda}\sin\phi}\left[2\cos\left(\frac{n\pi d}{\lambda}\sin\phi'\right)\right] \qquad (42)$$

Since the cosine is an even function of its argument, corresponding positive and negative terms in the summation can be combined. It is also convenient to introduce the total number of transmitting elements K:

$$E = 4C \sum_{\substack{n=1 \\ \text{odd}}}^{K=1} \cos\left(\frac{n\pi d}{\lambda}\sin\phi\right)\cos\left(\frac{n\pi d}{\lambda}\sin\phi'\right) \qquad (43)$$

Patterns computed from Eq. (43) are shown in Figures 48 to 51. The plots are normalized for each value of K to the largest beam-peak value calculated at one of the incoming angles ϕ'.

The first set of patterns, Figure 48, is for one element pair, or K = 2. Equation (43) reduces to:

$$E = 4C\cos\left[\frac{\pi d}{\lambda}\sin\phi\right]\cos\left[\frac{\pi d}{\lambda}\sin\phi'\right] \qquad (44)$$

All of the patterns are identical in form as ϕ is varied. The only effect produced by changing the incoming angle ϕ' is a change in magnitude of the pattern. An interesting phenomenon occurs at $\phi' = 30^{\circ}$. Since the assumed spacing $d = \lambda$, the second term vanishes, with the result that no radiation occurs in any direction!

$$E = 4C \cos[\pi \sin\phi]\cos[\phi \sin 30^{o}] = 0 \qquad (45)$$

Physically, this effect results because the voltage wave reflected back to a given antenna is exactly 180^{o} out of phase with the wave applied to the conjugate antenna, for the particular ϕ' and d chosen. We have, of course, neglected the 1 in the expression $1 + \Gamma = T$ in computing these patterns, and have also neglected the scattered power. The point is that no <u>gain</u> is realized from a single element pair of the high-gain shunt-amplifier type whenever $d \sin\phi'$ happens to be $\lambda/2$.

The second set of curves, Figure 49, is for a two-pair array, i.e., $K = 4$. For the particular spacing chosen, $d = \lambda$, there is no retrodirective peak for an incident angle $\phi' = 10^{o}$, but a peak appears when ϕ' is increased to 60^{o}. Once again at $\phi' = 30^{o}$ the returned pattern vanishes for all output angles ϕ, since both the $n = 1$ term and the $n = 3$ term in Eq. (43) are zero. Because of the periodicity of the cosine function, $\phi' = 30^{o}$ will be a "blind angle" for an even array of interelement spacing $d = \lambda$ regardless of the number of transmitting elements K, as shown in the computed patterns for $K = 4$, 8, and 16 (Figures 49, 50, and 51).

The patterns for $K = 8$ and $K = 16$ clearly show the retrodirective and specular beam peaks predicted by the qualitative theory. For $K \leq 4$, however, the beams interact to such a degree that the array can hardly be considered retrodirective at all.

It is instructive to determine whether or not an even, high-gain shunt-amplifier array can be made which does not have blind angles. From Eq. (43) the condition for the array pattern to vanish identically is:

$$\cos\left[\frac{n\pi d}{\lambda} \sin\phi'\right] = 0 \text{ for } n = 1,\ 3,\ 5 \qquad (46)$$

Vanishing of the $n = 1$ term is a necessary and sufficient condition for all terms to vanish, so that Eq. (46) can be replaced by:

$$\cos\left[\frac{\pi d}{\lambda}\sin\phi'\right] = 0$$

$$\frac{\pi d}{\lambda}\sin\phi' = \frac{\pi}{2}$$

$$\sin\phi' = \frac{\lambda}{2d} \qquad (47)$$

If there are to be no blind angles, then $\lambda > 2d$, i.e., the inter-element separation must be less than one-half wavelength.

4.4.6 Pattern of a 4 x 4 Square Van Atta Array

The pattern of a 16-element square Van Atta array of the type originally proposed can be found very easily by combining the results of paragraphs 4.4 and 4.3.2. Figure 52(a) shows a square-grid arrangement of 16 antennas, together with the conjugate-element interconnection. Figure 52(b) shows a linear array equivalent to the square array in the θ-plane, generated by moving the various antennas into the θ-plane along perpendiculars, by the method of paragraph 4.3.2. The equivalent linear array consists of two pairs of elements interconnected via amplifiers having a gain of 4G, where G is the gain of the amplifiers in the original 4 x 4 array.

Patterns for the two-pair equivalent linear array were calculated in paragraph 4.4. If the amplifiers are of the matched bidirectional or unidirectional type, the appropriate patterns can be calculated by the subtraction method of paragraph 4.3.1. The patterns for the high gain shunt-diode amplifier are shown in Figure 49. The latter patterns can hardly be classed as "retro-directive," except for very large angles of incidence ϕ'. Also evident is the "blind spot" at $\phi' = 30^{\circ}$.

4.5 APPLICATION OF ADVANCED ARRAY THEORY TO VAN ATTA ARRAYS

The concepts of advanced ray theory (beam steering, amplitude tapering, beam synthesis, etc.) can be applied to the Van Atta

array, provided some care is taken when applying these concepts and interpreting the results.

4.5.1 Beam Steering

The standard method of steering the beam of an array is to introduce progressive phase shifts into the transmitting elements, according to the formula,

$$\Delta\phi_n = \frac{nd2\pi}{\lambda} \sin \Delta\theta_1 \tag{48}$$

where $\Delta\phi_n$ is the phase shift added to the n^{th} element to produce a beam shift of $\Delta\theta_1$. This is a straightforward technique that produces only a small change in gain. In applying beam steering to the Van Atta array it must be remembered that the beam is shifted from its original position, i.e., the beam will be shifted from the retrodirective direction by an amount $\Delta\theta_1$.

Another beam-steering method of recent interest involves applying equal positive and negative phase shifts to two conjugate antennas in a large array. This technique is useful for producing small beam shifts, and requires only two phase shifters of relatively low precision. Recently, we have derived an equation for the amount of beam shift in such an array.[13]

$$\Delta \sin \theta_1 = \frac{3}{4\pi dN^3}(2m - 1) \sin \Delta\phi_m$$

where

m = element pair number ($1 < m < N/2$)

$\Delta\phi_m$ = change in the phase of the m^{th} element pair

$N = \frac{1}{2}$ number of elements in the array $N > 5$

d = element spacing in wavelengths

$\Delta \sin \theta_1$ = resultant shift in the sine of the main beam angle θ_1

As an application of single-element beam steering, consider a 10-element array with the elements spaced by one wavelength. Shifting the phase of the end elements by $\pm 90^{\circ}$ will move the beam peak about 1°.

4.5.2 Amplitude Tapering

The beam shape and sidelobe levels of a conventional phased array are controlled by varying the amplitude of the signals applied to the various elements. The same type of amplitude tapering can be accomplished in a Van Atta array through changing the gains of the various interconnecting amplifiers. For any one angle (measured with respect to the array normal) it is possible to design tapered distributions to optimize various performance criteria (i.e., Binomial, Taylor, Dolph-Chebyshev, etc.). However, at present there is no theory available for designing a fixed distribution for minimizing sidelobe levels over a range of beam angles. In a conventional phased array one can vary the amplitude distribution according to the scan angle, which is known a priori. Such is, of course, not the case with a Van Atta array, where the incoming angle may assume any value whatever.

4.5.3 Problems Unique to the Van Atta Array

One of the main difficulties with the theory of Van Atta arrays is the scattered power. The wave incident on the array has,

at best, half of its power absorbed, the rest being reradiated. The reradiated portion will form a specular beam (mirror image beam) of the following form:

$$S(\theta) = A(\theta)\, T(\theta)$$

where

$S(\theta)$ is the array scattered pattern

$A(\theta)$ is the array pattern pointing in the mirror image direction

$T(\theta)$ is the scattered pattern of one individual element

$A(\theta)$ is a well-known calculable function, but $T(\theta)$ is known only for a very few cases. It should be emphasized that $T(\theta)$ is <u>not</u> equal to the ordinary element radiation pattern because the current distribution on the antenna is not the same as it would be if the antenna were driven at its terminals. Because of this difficulty the scattered power has been ignored in our calculations. This is usually a valid procedure when dealing with active Van Atta arrays, since the active pattern will be greater than the scattered pattern by the gain of the amplifier. Some recent work by Lewis[14] discusses a method of disposing of the scattering effect by interferometer techniques.

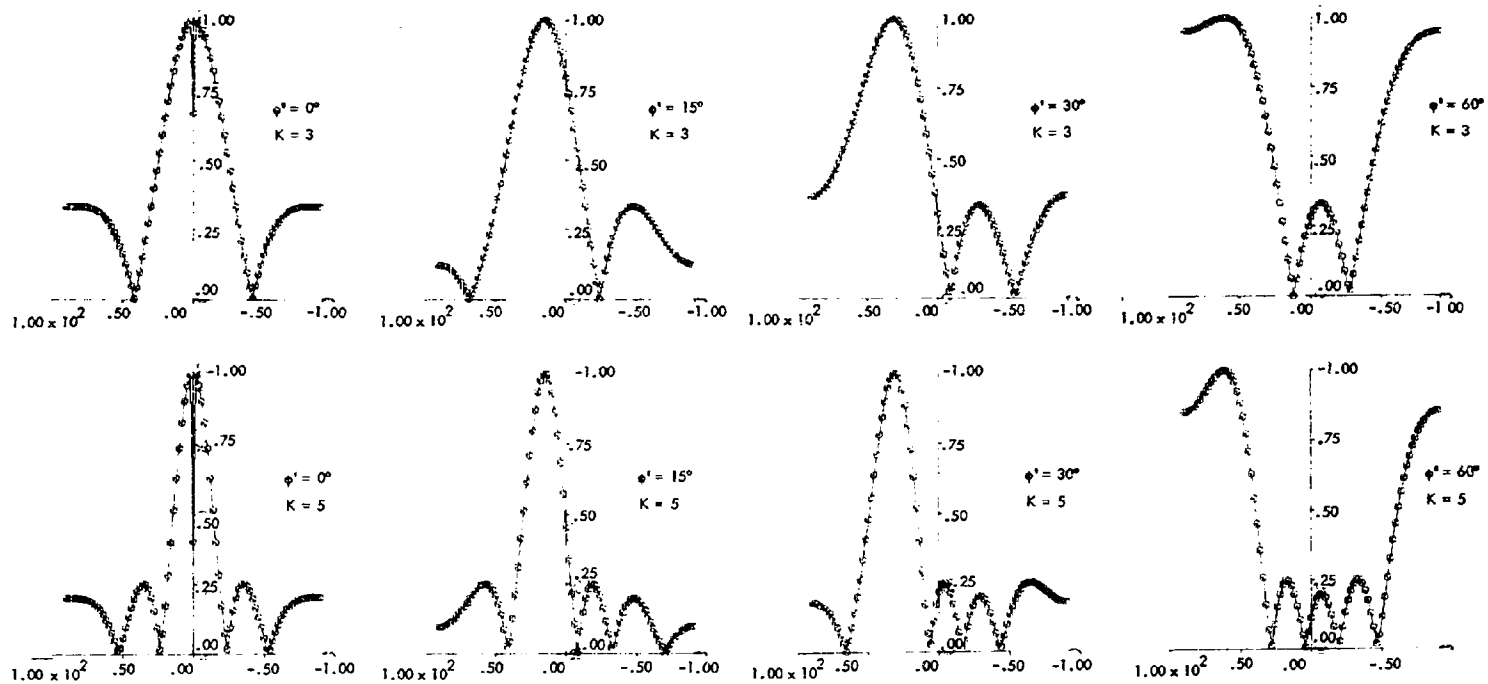

Figure 38. Patterns for Passive or Matched-Amplifier Interconnection ($T = 1$, $\Gamma = 0$, $d = \lambda$)

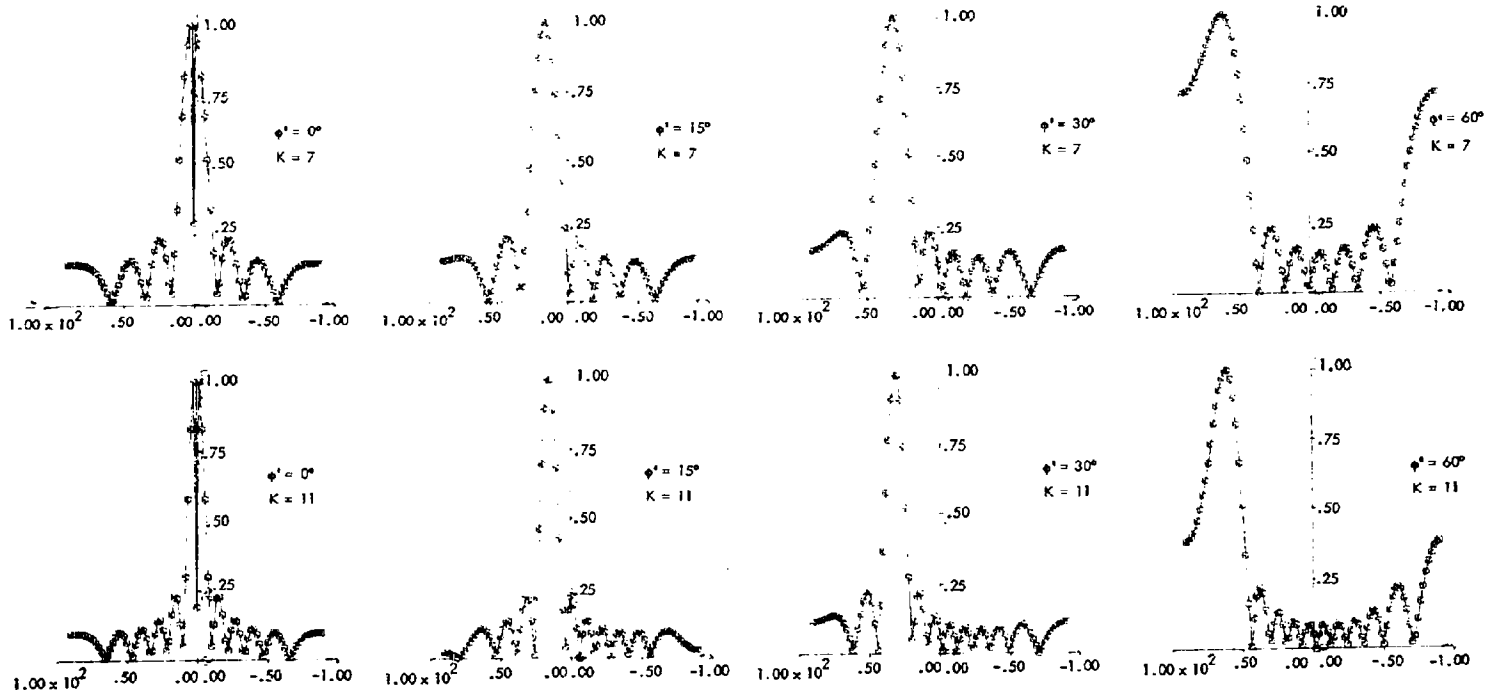

Figure 39. Patterns for Passive or Matched-Amplifier Interconnection (T = 1, Γ = 0, d = λ)

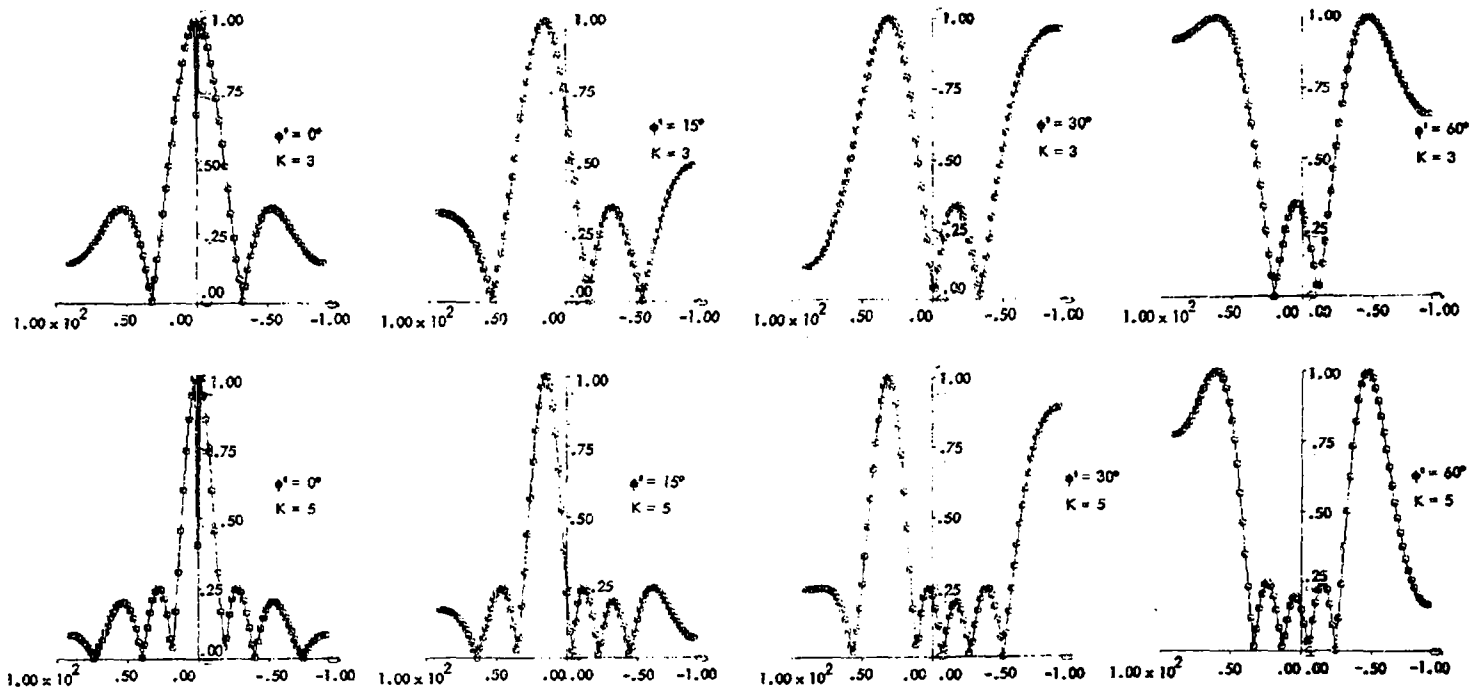

Figure 40. Patterns for Passive or Matched-Amplifier Interconnection ($T = 1$, $\Gamma = 0$, $d = 1.25\lambda$)

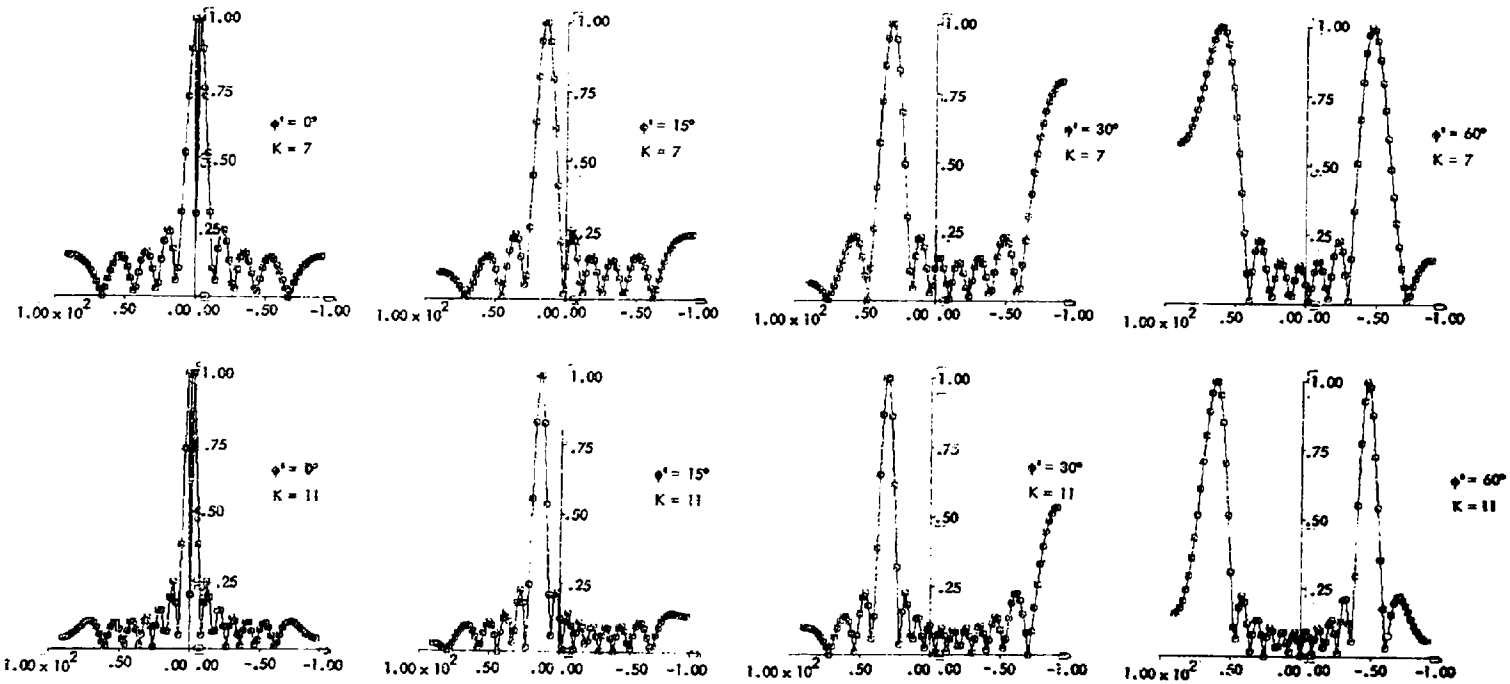

Figure 41. Patterns for Passive or Matched-Amplifier Interconnection ($T = 1$, $\Gamma = 0$, $d = 1.25\lambda$)

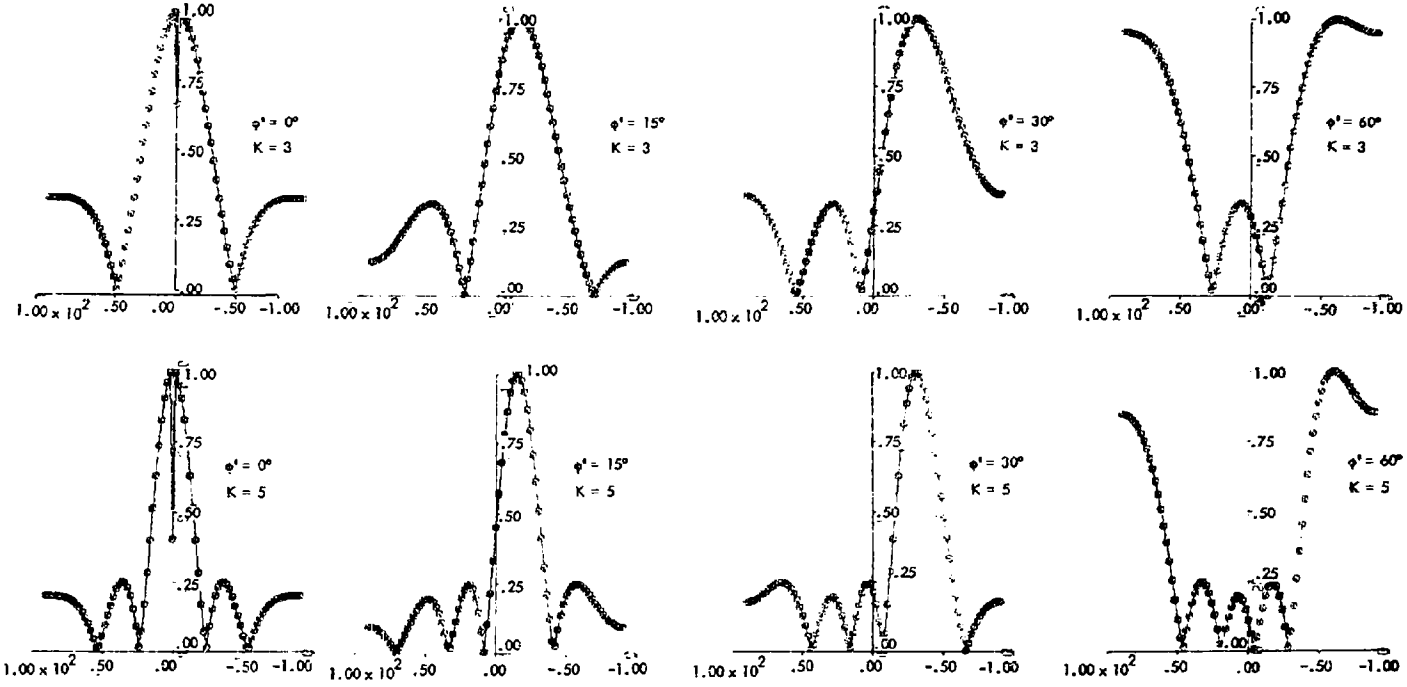

Figure 42. Patterns for Individual Scatterer Case ($T = 0$, $\Gamma = 1$, $d = \lambda$)

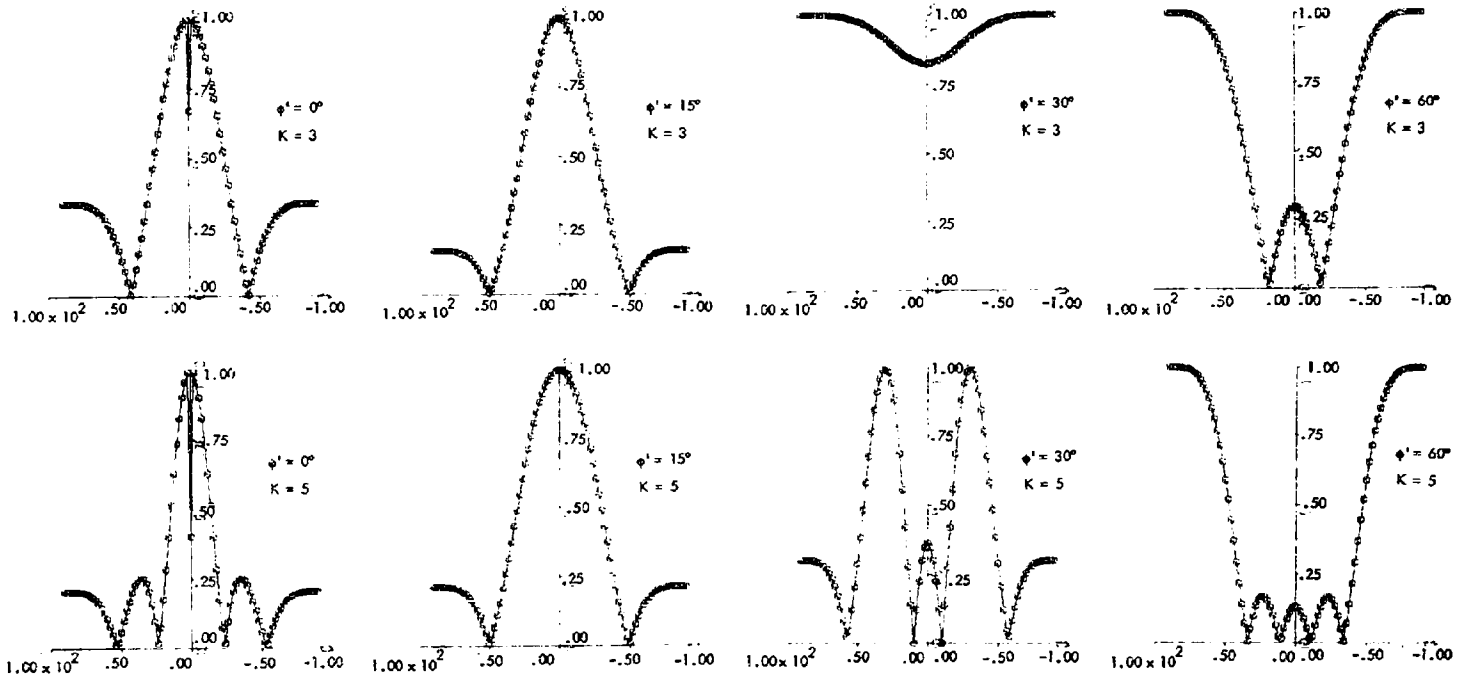

Figure 43. Patterns for High Gain Shunt Diode Connection ($\Gamma = 1$, $T = 1$, $d = \lambda$)

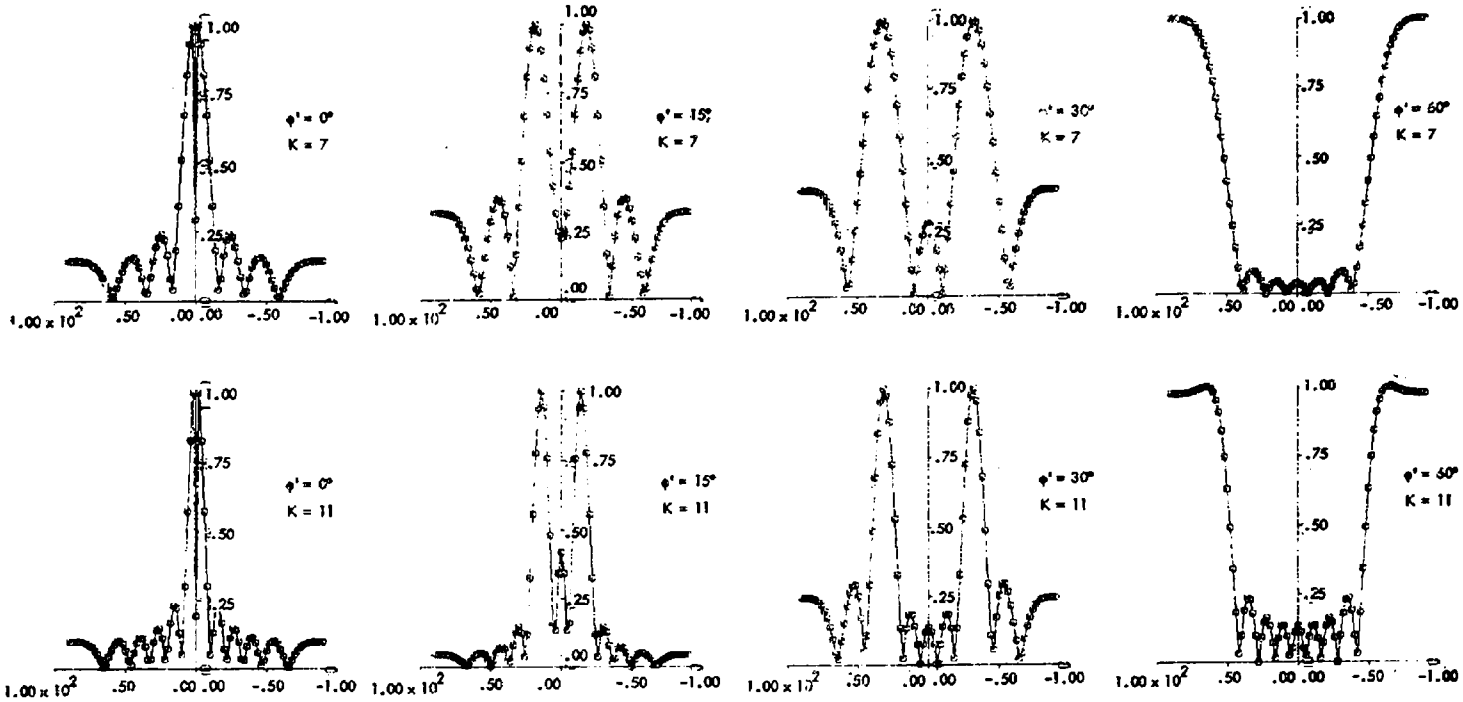

Figure 44. Patterns for High Gain Shunt Diode Connection ($\Gamma = 1$, $T = 1$, $d = \lambda$)

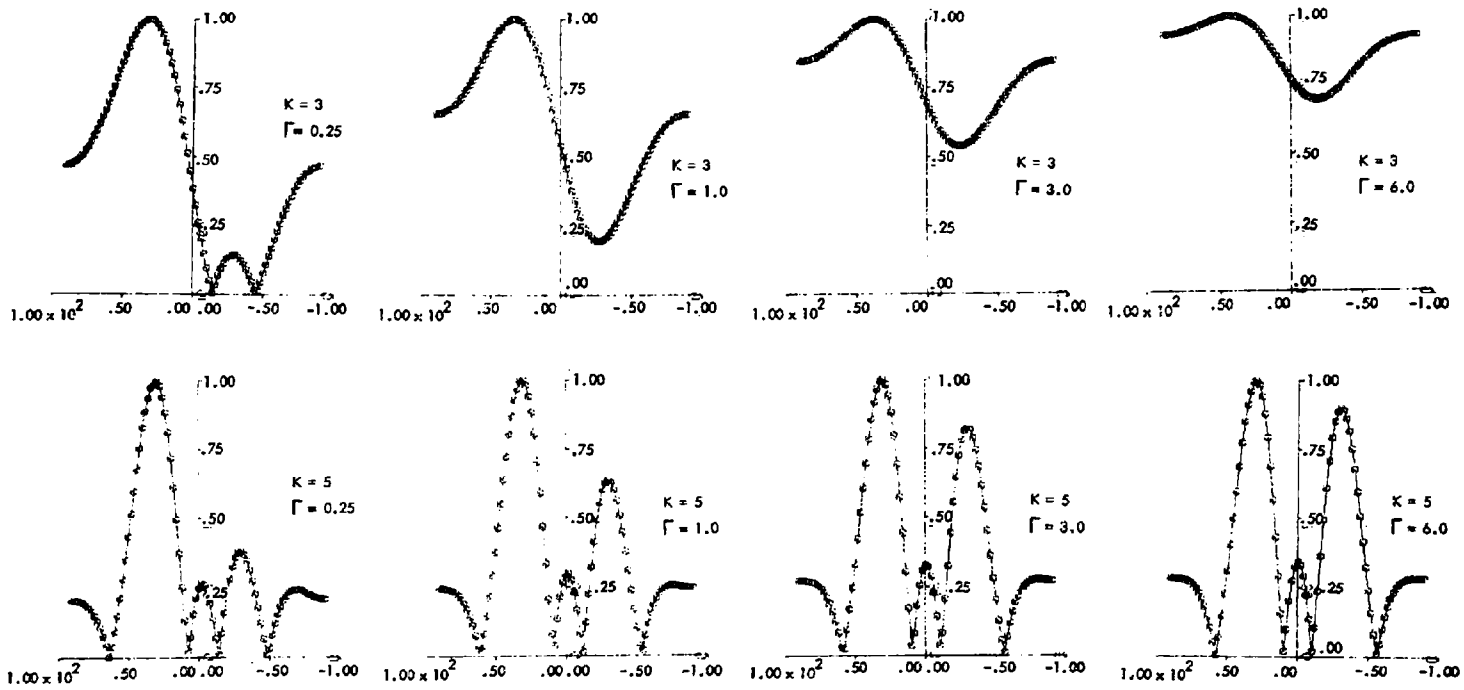

Figure 45. Patterns for the Shunt Diode Connection at Intermediate Gains (d = λ , φ = 30°, K = 3, 5)

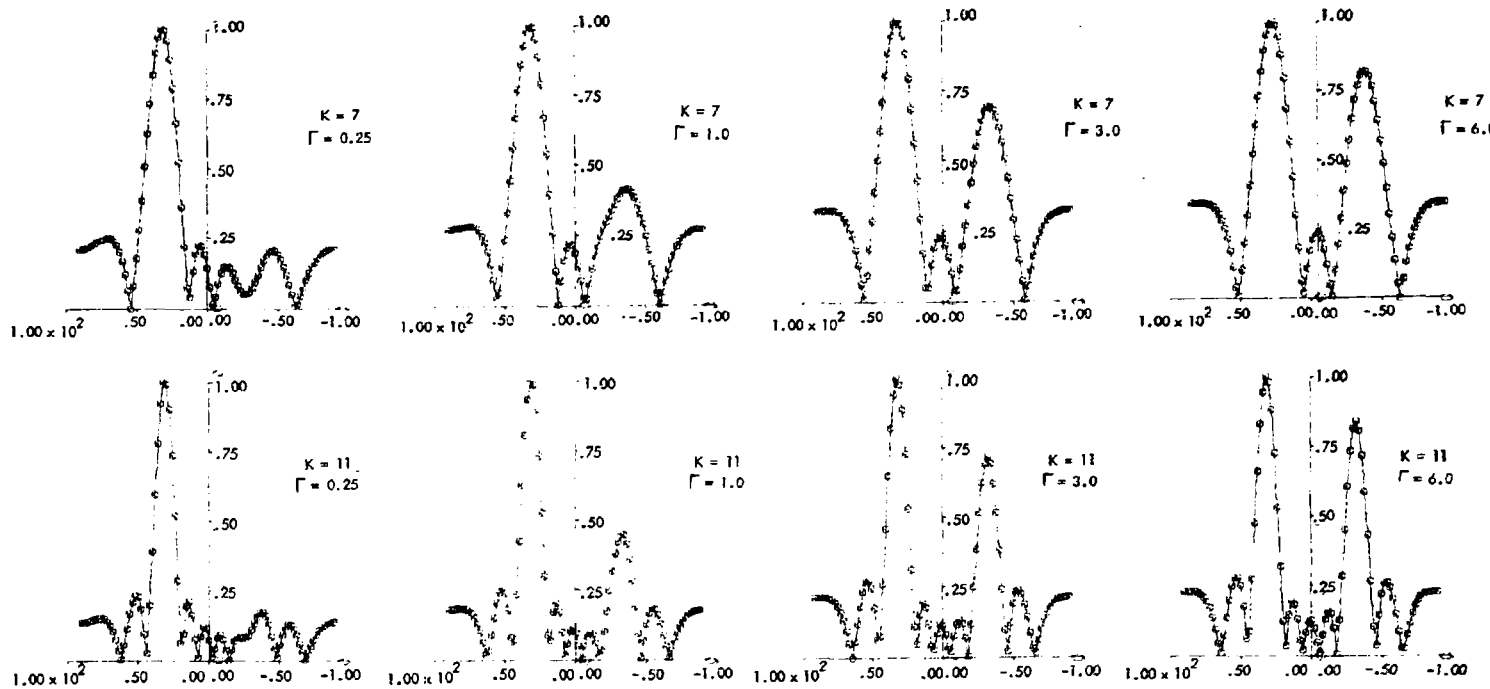

Figure 46. Patterns for the Shunt Diode Connection at Intermediate Gains ($d = \lambda$, $\phi = 30°$, K = 7, 11)

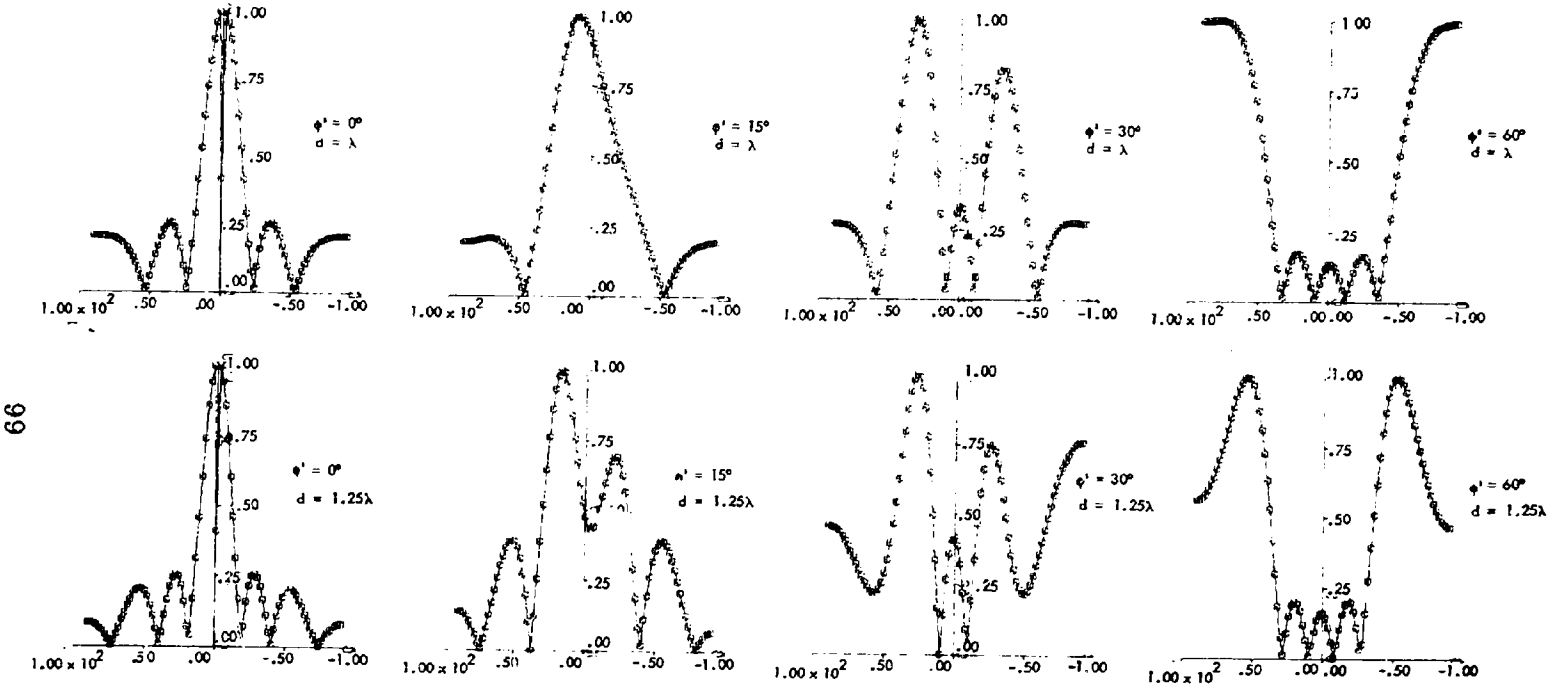

Figure 47. Patterns for the Shunt Diode Case Showing the Effects of Increased Element Spacing (K = 5, Γ = 3)

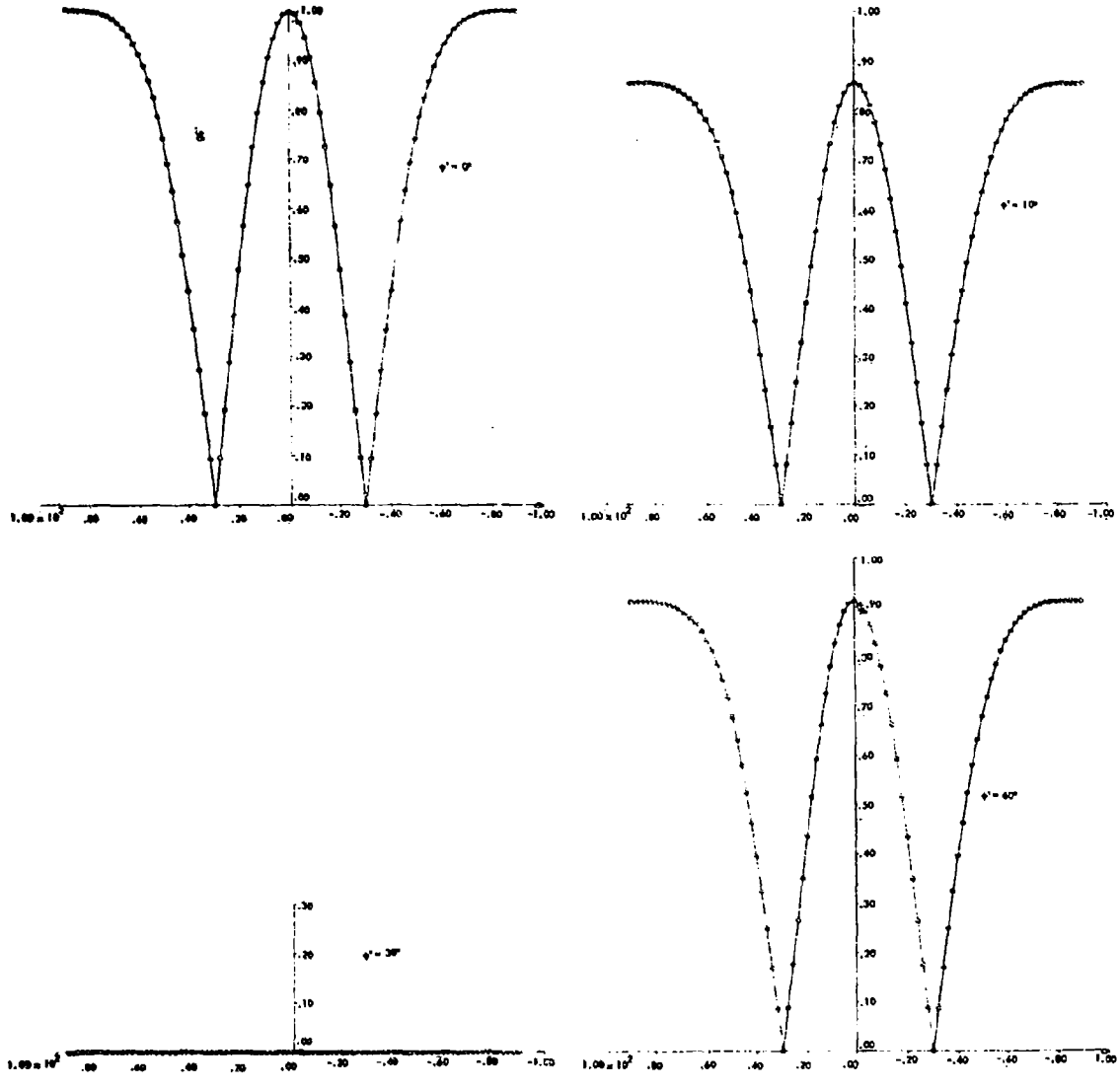

Figure 48. Patterns for the High-Gain Shunt Diode Interconnection
(Even Array, 1 Antenna Pair, $d = \lambda$)

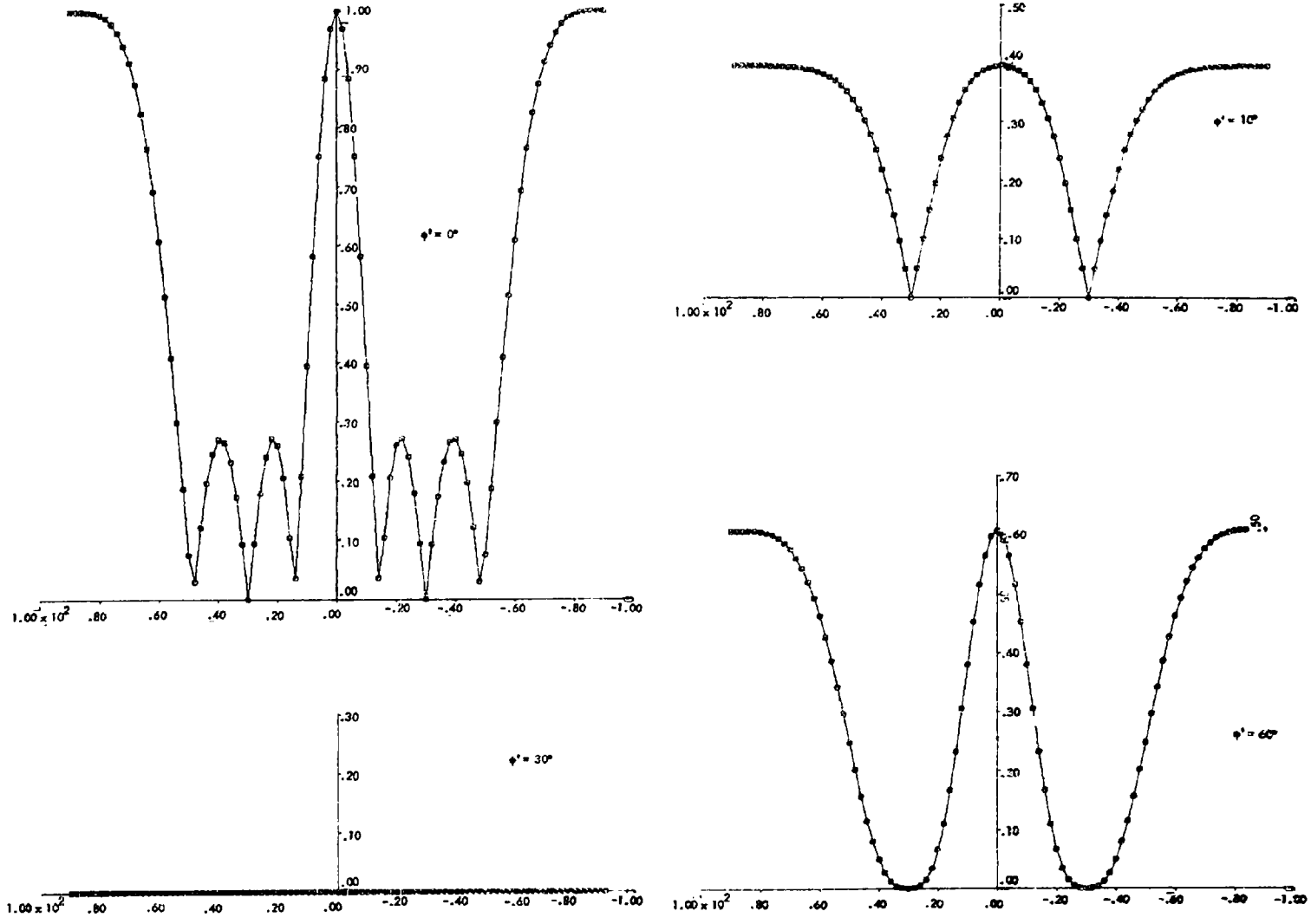

Figure 49. Patterns for the High-Gain Shunt Diode Interconnection (Even Array, 2 Antenna Pairs, d = λ)

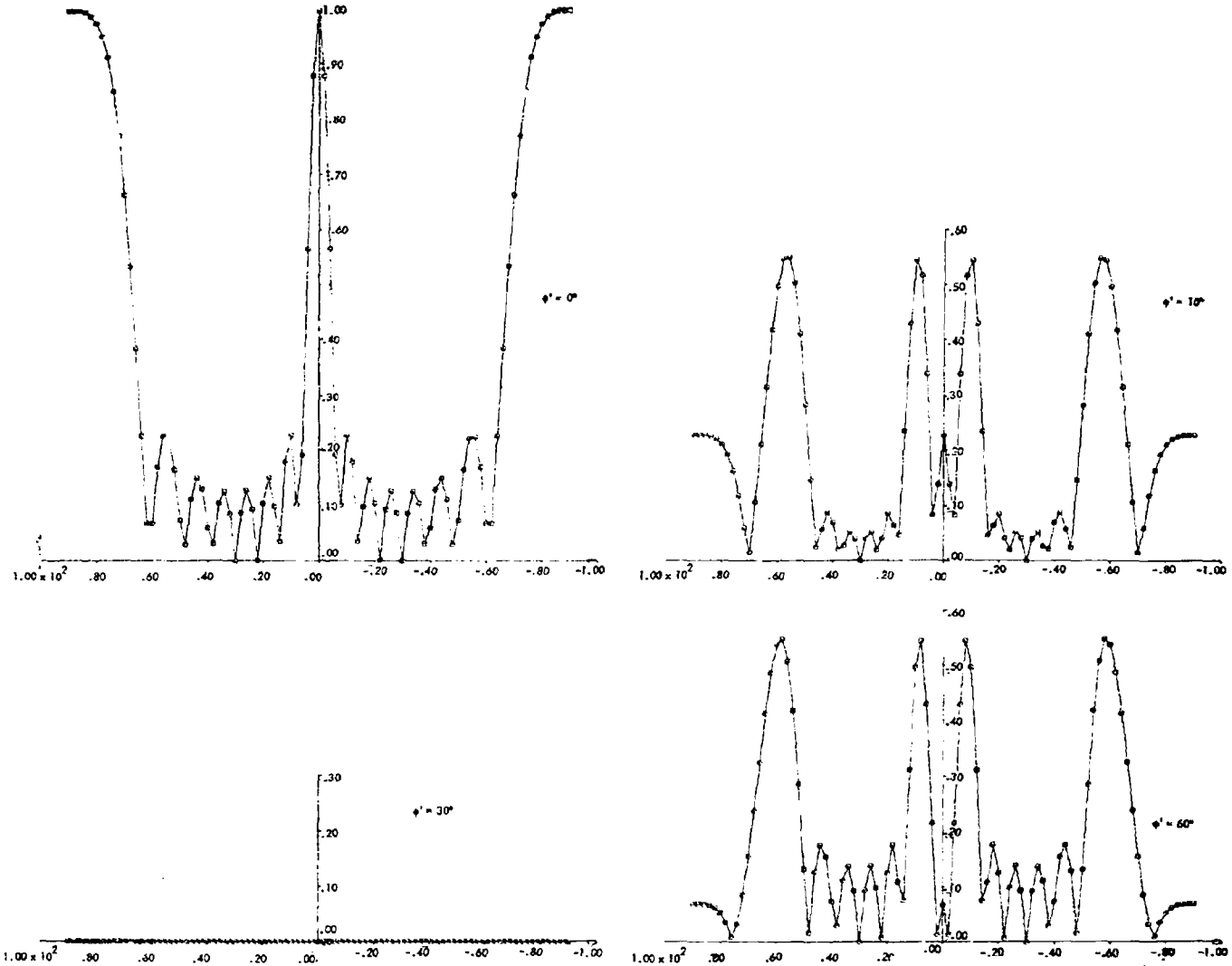

Figure 50. Patterns for the High-Gain Shunt Diode Interconnection (Even Array, 4 Antenna Paris, d = λ)

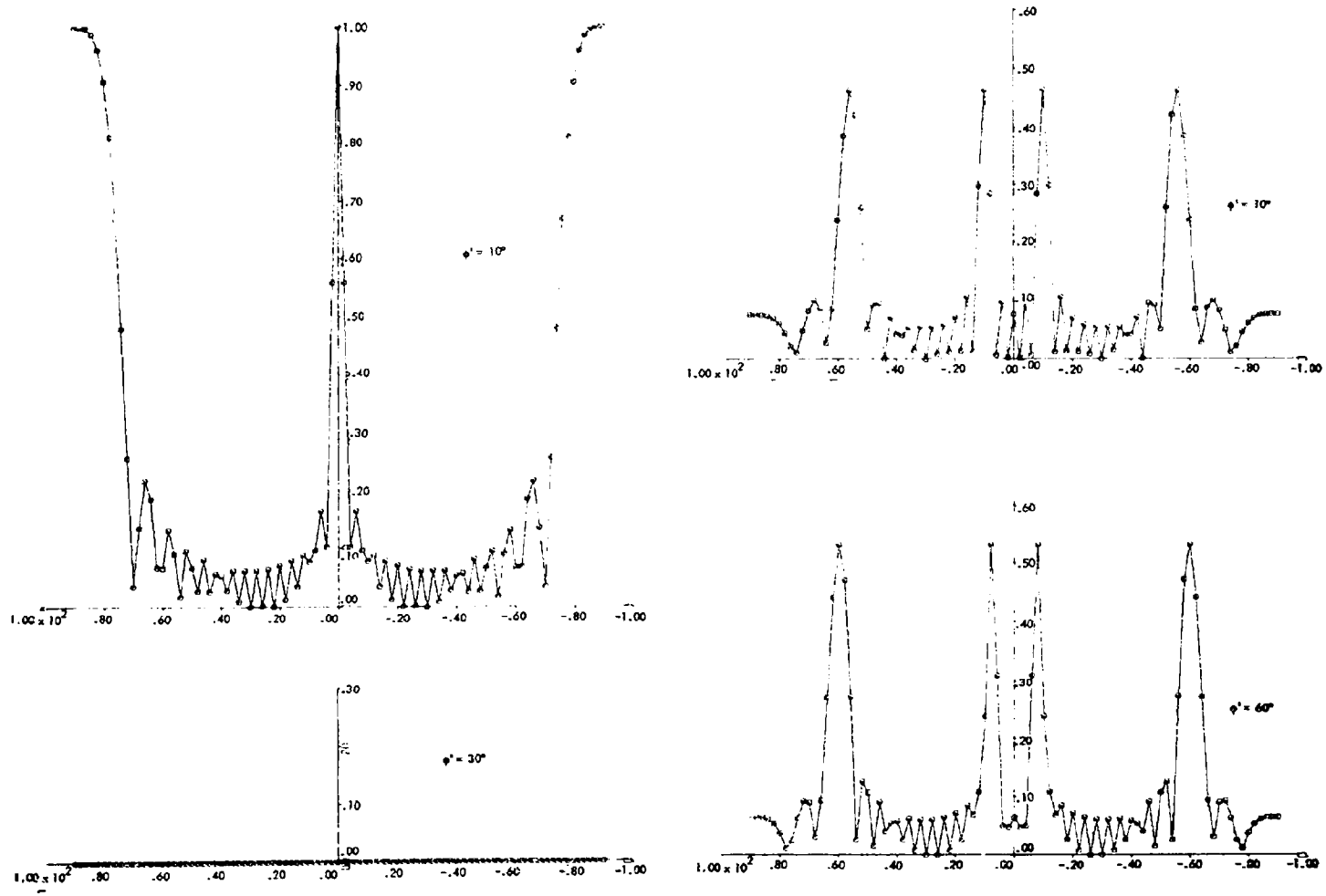

Figure 51. Patterns for the High-Gain Shunt Diode Interconnection (Even Array, 8 Antenna Pairs, d = λ)

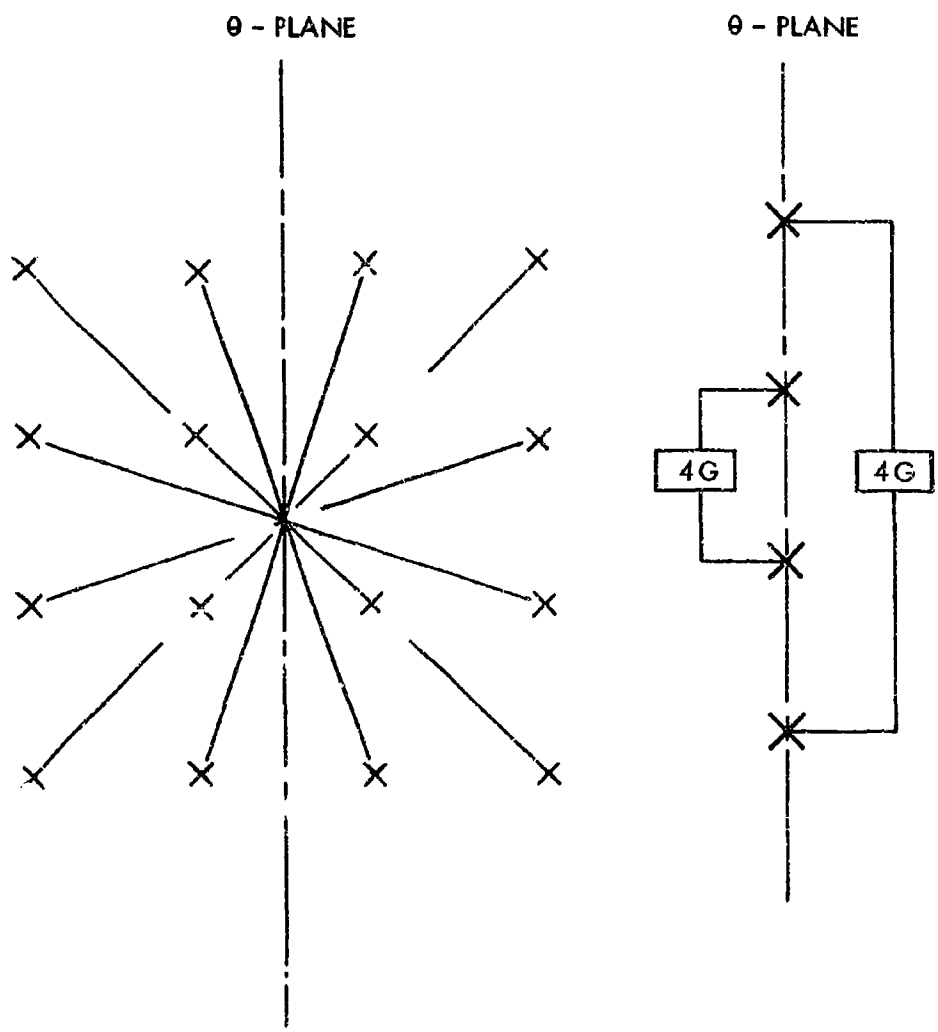

Figure 52. Transformation of 16-Element Square Array to an Equivalent Linear Array

SECTION V

BILATERAL-AMPLIFIER DESIGN CONSIDERATIONS

5.1 THE SHUNT NEGATIVE-CONDUCTANCE AMPLIFIER

Originally it was proposed that the active Van Atta array utilize amplifiers consisting of a single biased tunnel diode shunting the interconnecting transmission line at its midpoint. An obvious shortcoming of this scheme is that the amplified output wave from the diode is applied equally to both antennas, regardless of the direction from which the input came, so that both a retrodirected beam and a specular beam are formed by the array. The analysis of paragraph 4.4.5 revealed some more serious difficulties, namely the existence of "blind angles" for which no retrodirected return could be obtained, and very poor beam formation and pointing in arrays containing only a few elements. Also, the gain-sensitivity of the shunt-diode amplifier is poorer than that of other types of bilateral amplifiers. All of the above difficulties are caused by the severe input mismatch of the shunt-diode amplifier. The portion of the amplified wave from the tunnel diode which is returned to the input antenna is wasted as far as the retrodirected beam is concerned, and may even cancel out the retrodirected beam entirely at certain angles. These effects are absent in the passive Van Atta array, where the antennas are matched to the transmission line. We are therefore led to consider various other types of negative-conductance amplifiers which are bilateral and matched at the input and output, so that a signal incident on one antenna will be amplified and conducted to the other antenna with no reflections occuring anywhere along the way.

5.2 THE IMPOSSIBILITY OF CONSTRUCTING A MATCHED BILATERAL AMPLIFIER USING A SINGLE NEGATIVE CONDUCTANCE

The simplest type of bilateral amplifier for the interconnecting lines of the Van Atta array can be represented as a lossless, reciprocal 3-port network with one of the ports terminated in a tunnel diode, as shown in Figure 53. In this section, it is shown that if we require both antenna ports

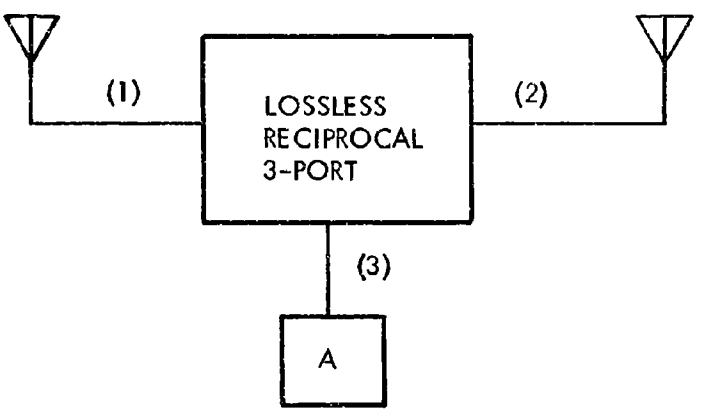

Figure 53. Bilateral Amplifiers with a Lossless Reciprocal 3-Port Coupling Network

to be matched, then it is not possible to obtain any power gain from this system no matter how much inherent gain the amplifier may possess. The consequence of this somewhat surprising result is that there exists an unavoidable tradeoff between the minimum reflection factor (or mismatch) at the antenna ports and the achievable gain of the active array element.

The basic problem we are considering is the design of the physically realizable lossless reciprocal 3-port coupling network shown schematically in Figure 53. This 3-port network interconnects the two conjugate antennas with a bilateral tunnel diode reflection amplifier. An equivalent circuit is shown in Figure 54, in which the parasitic capacitance of the tunnel diode and the matching network are incorporated into the lossless 3-port. Let the 3-port be represented by its scattering matrix defined by

$$\underline{S} = \begin{bmatrix} S_{11} & S_{12} & S_{13} \\ S_{12} & S_{22} & S_{23} \\ S_{13} & S_{23} & S_{33} \end{bmatrix} \tag{49}$$

Since the 3-port is lossless, the matrix $\underline{S}$ must be unitary; i.e.,

$$\underline{S}\,\underline{S}^* = \underline{1} \tag{50}$$

or

$$\underline{S}^* = \underline{S}^{-1} \tag{51}$$

where the asterisk denotes complex conjugate transpose and the superscript "-1" denotes the inverse.

In Figure 54, a_i and b_i represent, respectively, the incident and reflected wave at the i^{th} port ($i = 1, 2, 3$). The normaliz-

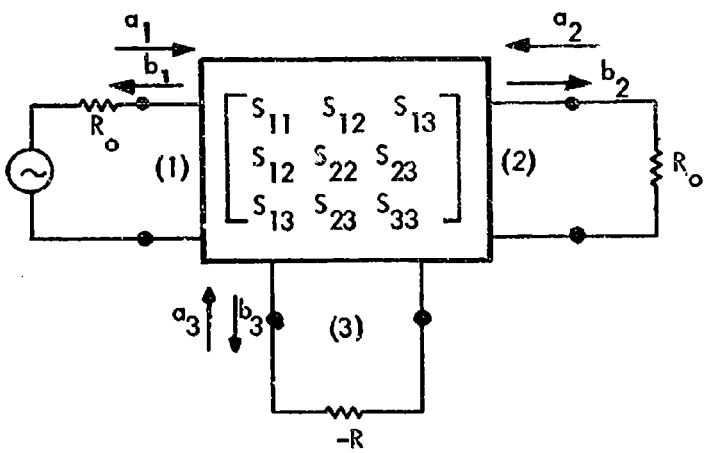

Figure 54. Schematic of a Bilateral Amplifier Using a Lossless Reciprocal 3-Port Coupled Negative Resistance Amplifier

ing numbers used in defining the scattering matrix are R_a (the impedance of the antenna, assumed to be real) at ports 1 and 2, and R (magnitude of the negative resistance of the tunnel diode) at port 3.

Using this normalization scheme, we have $a_2 = 0$ and $b_3 = 0$. It can be shown that the transducer power gain between the antenna at port 1 (the source) and the antenna at port 2 (the load) is given by

$$G_t = \frac{|S_{12}|^2}{|S_{33}|^2} \tag{52}$$

Note that if the 3-port is nonreciprocal then we can choose $|S_{12}|$ and $|S_{33}|$ independently. In fact, we can then make $|S_{12}| = 1$ and the gain reduces simply to $G_t = |\rho|^2$, where $\rho = 1/S_{33}$. In our present problem, the 3-port is <u>constrained</u> to be reciprocal.

As stated previously, the lossless nature of the reciprocal 3-port requires that the matrix $\underline{S}$ of Eq. (49) be unitary. This means that the following conditions must be satisfied:

$$|S_{11}|^2 + |S_{12}|^2 + |S_{13}|^2 = 1 \tag{53}$$

$$|S_{12}|^2 + |S_{22}|^2 + |S_{23}|^2 = 1 \tag{54}$$

$$|S_{13}|^2 + |S_{23}|^2 + |S_{33}|^2 = 1 \tag{55}$$

$$S_{11}\overline{S}_{12} + S_{12}\overline{S}_{22} + S_{13}\overline{S}_{23} = 0 \tag{56}$$

$$S_{11}\bar{S}_{13} + S_{12}\bar{S}_{23} + S_{13}\bar{S}_{33} = 0 \tag{57}$$

$$S_{12}\bar{S}_{13} + S_{22}\bar{S}_{23} + S_{23}\bar{S}_{33} = 0 \tag{58}$$

In addition to these unitary conditions, we shall require that the antenna ports 1 and 2 be matched when the other port is terminated in the antenna impedance R_a and port 3 is terminated in -R. This means that the input reflection factor at ports 1 and 2 must be zero; i.e.,

$$S_{in1} = \frac{b_1}{a_1} = 0 \quad \text{(Port 1 matched)} \tag{59}$$

and

$$S_{in2} = \frac{b_2}{a_2} = 0 \quad \text{(Port 2 matched)} \tag{60}$$

It can be shown that the matched condition at port 1, Eq. (59), together with the fact that port 3 is terminated in -R yields the condition

$$S_{11}S_{33} - S_{13}^2 = 0 \tag{61}$$

Furthermore, invoking Eq. (51), we have

$$\bar{S}_{22} = \frac{\left(S_{11}S_{33} - S_{13}\right)^2}{\det\,[\underline{S}]} \tag{62}$$

Thus, from Eqs. (61) and (62), we have the interesting result that

$$S_{22} = 0 \tag{63}$$

which states that in the circuit configuration of Figures 53 or 54, where port 3 is terminated in a negative resistance, the requirement of a match at port 1 results in S_{22} being identically equal to zero.

Additional conditions are derived as follows. Taking the sum of Eqs. (53) and (55) and subtracting Eq. (54), we obtain

$$\left|S_{11}\right|^2 + 2\left|S_{13}\right|^2 + \left|S_{33}\right|^2 = 1 \tag{64}$$

From Eq. (61), we see that $\left|S_{13}\right|^2 = \left|S_{11}S_{33}\right|$. Substitution of this result into Eq. (64) yields

$$\left|S_{33}\right| = 1 - \left|S_{11}\right| \tag{65}$$

Since, from Eq. (63), $S_{22} = 0$, Eq. (56) and (58) become

$$S_{11}\bar{S}_{12} + S_{13}\bar{S}_{23} = 0 \tag{66}$$

$$S_{12}\bar{S}_{13} + S_{23}\bar{S}_{33} = 0 \tag{67}$$

From these two relations, we find that

$$\bar{S}_{33} = \frac{S_{12}^2 \bar{S}_{11}}{S_{23}^2} \tag{68}$$

Taking the amplitude of this equation, we have

$$\left|S_{33}\right| = \frac{\left|S_{12}\right|^2 \left|S_{11}\right|}{\left|S_{23}\right|^2} \tag{69}$$

From Eq. (69), coupled with Eqs. (54) and (65), we obtain

$$\left|S_{11}\right| = \left|S_{23}\right|^2 \tag{70}$$

and

$$\left|S_{33}\right| = \left|S_{12}\right|^2 \tag{71}$$

Combining these results, we have

$$S_{22} = 0$$

$$\left|S_{33}\right| = \left|S_{12}\right|^2 = 1 - \left|S_{11}\right| = 1 - \left|S_{23}\right|^2 \tag{72}$$

These are the constraints derived for a physically realizable lossless reciprocal 3-port with port 1 matched and port 3 terminated in -R. An interesting consequence of the condition contained in Eq. (71) is that the transducer power gain expression, Eq. (52), now reduces to

$$G_t = \frac{1}{|S_{33}|} \tag{73}$$

An analogous derivation by imposing the condition that port 2 is matched results in the following relations

$$S_{11} = 0$$

$$|S_{33}| = |S_{12}|^2 = 1 - |S_{22}| = 1 - |S_{13}|^2 \tag{74}$$

From Eqs. (72), (73), and (74), we see that the simultaneous match conditions at ports 1 and 2 result in $S_{11} = S_{22} = 0$ and $|S_{33}| = 1$, or $G_t = 1$. Thus, we arrive at the following interesting conclusion:

> For the circuit shown in Figure 53, the requirement of simultaneous match at the antenna ports renders the transducer power gain to be identically equal to unity (no power gain). In fact, port 3, at which the reflection amplifier is connected, is completely decoupled from the antennas.

The last part of the above statement can be shown by combining conditions (72) and (73). We have

$$\underline{S} = \begin{bmatrix} 0 & S_{12} & 0 \\ S_{12} & 0 & 0 \\ 0 & 0 & S_{33} \end{bmatrix} \tag{75}$$

where

$$\left|S_{12}\right| = 1 \text{ and } \left|S_{33}\right| = 1 \tag{76}$$

The conclusion stated here is derived by imposing only the simultaneous match at the antenna ports and the realizability conditions. In other words, we can make the conclusive statement that: No physically realizable lossless reciprocal 3-port exists which will provide match at the antenna ports and gain at the same time.

The immediate consequence of the above result is that there is an inevitable tradeoff between the minimum allowable reflection factor (or mismatch) at the antenna ports and the achievable gain of the active array element. The synthesis problem is shown in Figure 55. The lossless reciprocal 3-port is constrained to be symmetrical with respect to the tunnel diode reflection amplifier port. Let S_0 be the reflection factor at port 1 and port 2. We have the relations that

$$S_{in1} = \frac{S_{11}S_{33} - S_{13}^2}{S_{33}} = S_0 \tag{77}$$

and

$$S_{in2} = \frac{S_{22}S_{33} - S_{23}^2}{S_{33}} = S_0 \tag{78}$$

In addition,

$$\left|S_{11}\right| = \left|S_{22}\right| = \left|S_0\right|\left|S_{33}\right| \tag{79}$$

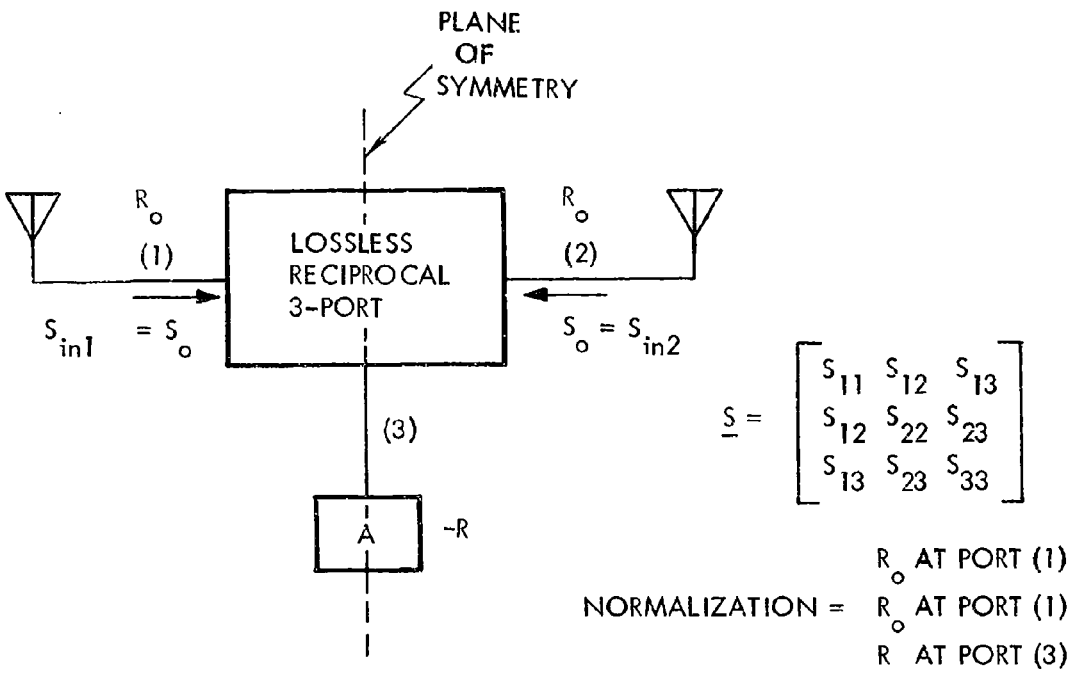

S_o = REFLECTION FACTOR AT PORT 1 (PORT 2) WHEN PORT 2 (PORT 1) IS LOADED BY ANTENNA IMPEDANCE AND PORT 3 IS TERMINATED BY THE TD REFLECTION AMPLIFIER DENOTED BY SYMBOL A.

Figure 55. Synthesis Problem of the Lossless Reciprocal 3-Port Coupling Network

With a prescribed amount of allowable mismatch at the antenna ports (prescribed $|S_0|$), it is desired to design a physically realizable, lossless reciprocal 3-port (symmetrical with respect to port 3) such that the transducer power gain,

$$G_t = |S_{12}|^2 / |S_{33}|^2 \tag{80}$$

is maximized.

To illustrate the procedure, consider a specific lossless reciprocal 3-port defined by

$$\underline{S} = \begin{bmatrix} \frac{1}{3} & -\frac{2}{3} & -\frac{2}{3} \\ -\frac{2}{3} & \frac{1}{3} & -\frac{2}{3} \\ -\frac{2}{3} & -\frac{2}{3} & \frac{1}{3} \end{bmatrix} \tag{81}$$

which is normalized to 1 ohm (R_o) at each of the three ports. Under a change of normalization with port 3 normalized to $r = R/R_o$ and defining the reflection coefficient

$$\Gamma = \frac{r - 1}{r + 1} \tag{82}$$

the scattering matrix under this set of normalizations is given by

$$\underline{S} = \frac{1}{(3-\Gamma)} \begin{bmatrix} (1+\Gamma) & -2(1-\Gamma) & -2\sqrt{1-\Gamma^2} \\ -2(1-\Gamma) & (1+\Gamma) & -2\sqrt{1-\Gamma^2} \\ -2\sqrt{1-\Gamma^2} & -2\sqrt{1-\Gamma^2} & (1-3\Gamma) \end{bmatrix} \quad (83)$$

The transducer power gain for this specific example is given by

$$G_t = \left| \frac{S_{12}}{S_{33}} \right|^2 = \left| \frac{2(\Gamma - 1)}{(1 - 3\Gamma)} \right|^2 \quad (84)$$

Substitution of the parameters in Eq. (83) into Eqs. (77) or (78) yields

$$S_1 = S_{in1} = S_{in2} = \frac{1 + \Gamma}{3\Gamma - 1} \quad (85)$$

For $\Gamma = \frac{1}{2}$,

$$G_t = (2)^2 = 4; \text{ and } S_o = 3$$

For $\Gamma = \frac{5}{12}$,

$$G_t = (4.67)^2 = 21.8; \text{ and } S_o = 5.67$$

The tradeoff between gain and mismatch is made evident. In fact, for this example, $\sqrt{G_t} = S_o - 1$.

5.3 ANALYTICAL RESULTS ON THE DESIGN OF BILATERAL NEGATIVE RESISTANCE AMPLIFIERS

5.3.1 Introduction

This section presents analytical results on the design of bilateral (bidirectional) negative resistance amplifiers. Three basic configurations for this class of reflection amplifier using one-port negative resistance elements are considered; namely,

I. Direct-Coupled (Figure 56)

II. Hybrid-Coupled (Figure 57)

III. 4-Port Circulator-Coupled (Figure 58)

The results contained in this section are applicable to any one-port negative resistance element including tunnel diodes and avalanche diodes, denoted in general by their impedance z_D.

The important common feature of all these amplifier configurations is their bilateral property; i.e., the input and the output of the overall negative resistance amplifier are indistinguishable. In Figures 56, 57, and 58, the symmetry of the input and output port and the interchangeability of their roles is clearly evident. Note that it is impossible to derive a bilateral amplifier configuration using a single 3-port circulator and a single negative resistance element. However, this does not mean that nonreciprocal coupling networks and/or unilateral 2-port active devices cannot be used in an overall bilateral amplifier; for example, in Figure 58 a 4-port circulator and two negative resistance elements are used to obtain the required bilateral property. In addition, Figures 59 and 60 show bilateral amplifiers which use two unilateral 2-port amplifiers coupled by hybrids and circulators. In the latter case, both nonreciprocal coupling networks (circulators) as well as unilateral active 2-ports are used, but the overall amplifier is indeed bilateral assuming identical active devices.

With the advent of transistor amplifiers in the low microwave frequency range, the configurations shown in Figures 59 and 60 are practical realizations of the bilateral amplifier in an active Van Atta array in which all the elements are used for

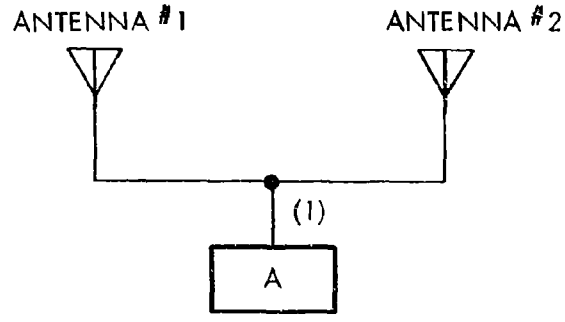

(a)

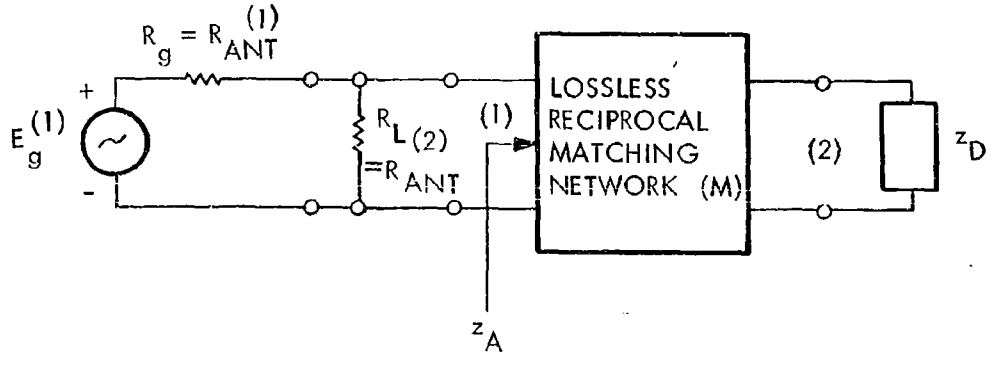

(b)

Figure 56. Direct-Coupled Bilateral Negative Resistance Amplifier

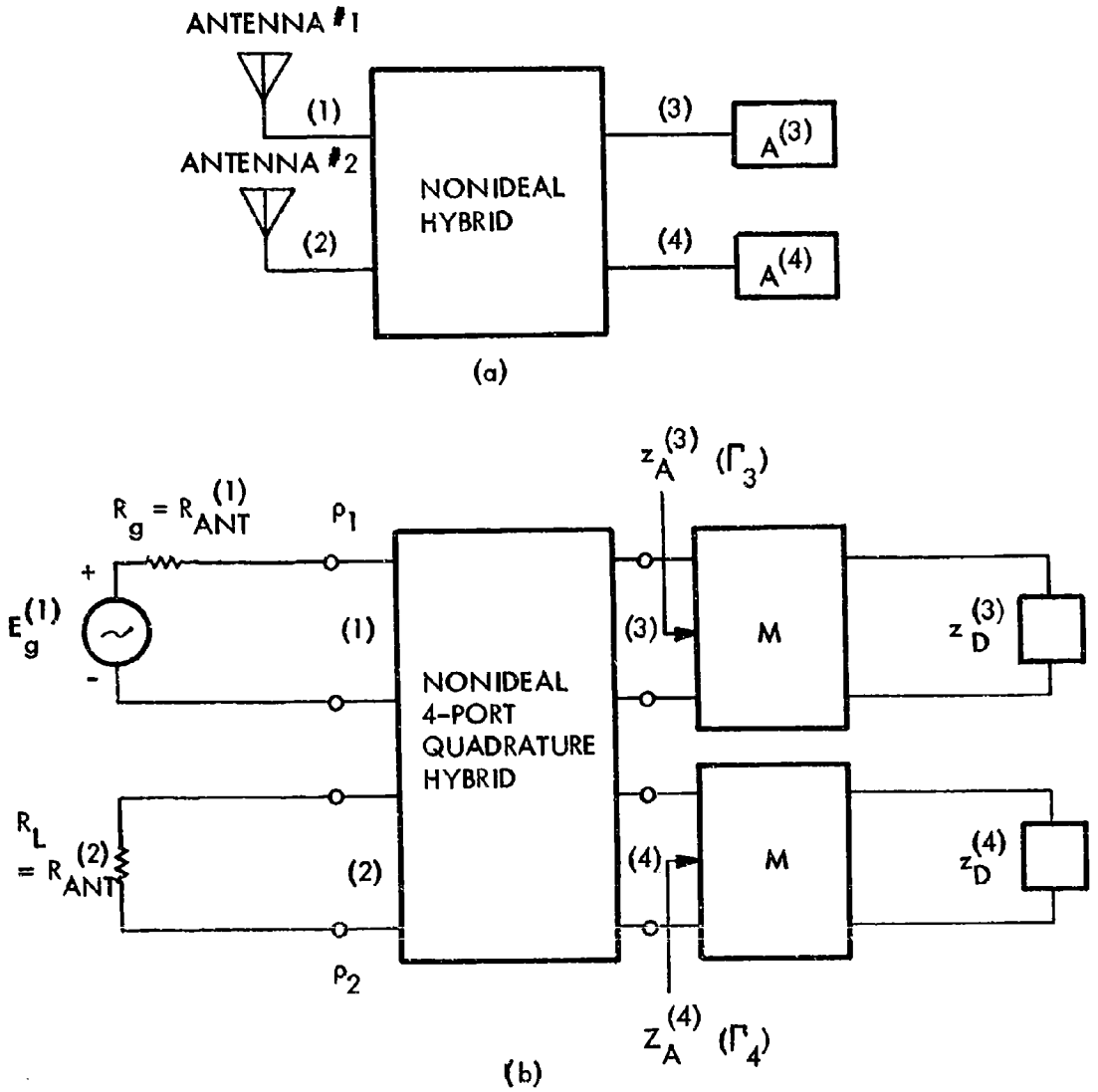

Figure 57. Bilateral Amplifier Using a Practical 4-Port Quadrature Hybrid and Two Negative Resistance Amplifiers

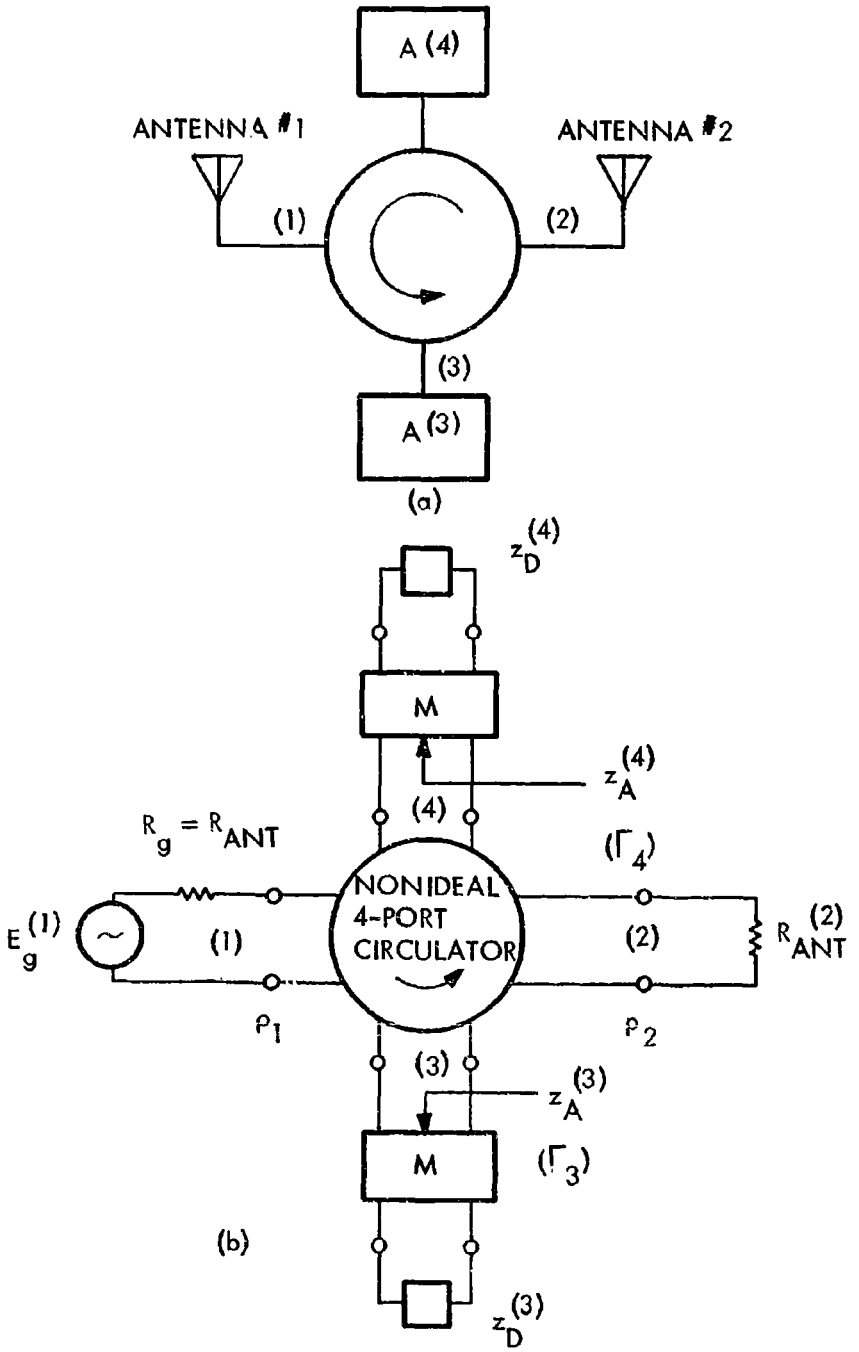

Figure 58. Bilateral Amplifier Using a Practical 4-Port Circulator and Two Negative Resistance Amplifiers

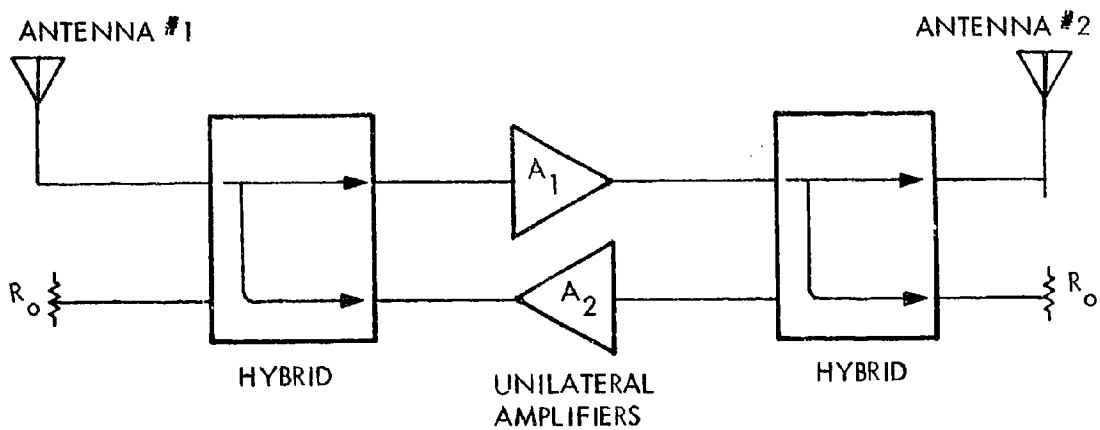

Figure 59. Hybrid-Coupled Bidirectional Amplifier Using Two Unilateral Amplifiers

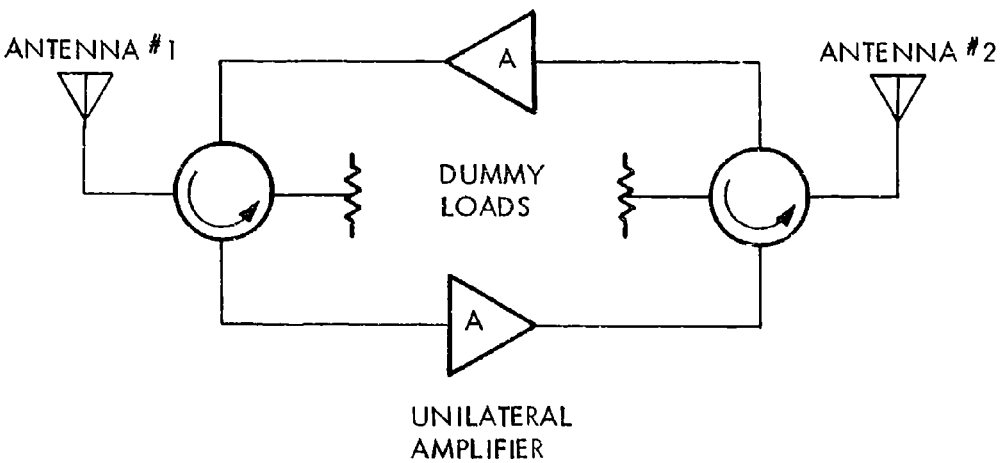

Figure 60. Bilateral Amplifier Using Two Circulators and Two Unilateral Amplifiers

both transmitting and receiving. These two configurations have also been studied, and the results are summarized in this section.

The design of unilateral (unidirectional) negative resistance amplifiers is treated in the next section. The techniques used in the design of both bilateral and unilateral amplifiers are very similar. Except for the simple direct-coupled case treated in paragraph 5.3.3, a unified approach using an equivalent active 2-port representation is employed to simplify the derivations as well as to provide an overall insight into the inherent properties of the various amplifier configurations.

As a starting point, we shall first present in paragraph 5.3.2 the basic properties of an active two-port. These results will be used throughout subsequent sections. It should be noted that the mutual coupling among the antenna elements has not been taken into account in the results presented in paragraphs 5.3 and 5.4. The effects of the mutual coupling on the stability (and gain) of the active Van Atta array are studied in Section VI.

The usual idealized assumptions on the source, the load, and the coupling networks are not used in this work so that the results are valid under very general and practical conditions. The results show clearly the effects of mismatched source, mismatched load, and practical hybrid and circulator parameters on the performance of the amplifiers. It is shown that the gain, bandwidth, and the important stability conditions are all critically dependent on these parameters. For brevity, most of the derivations for the results presented here will be omitted. Also omitted are results for quarter-wave coupled and reactive power-divider coupled bilateral amplifiers.

5.3.2 Equivalent Active 2-Port Representation [15]

Consider the general linear nonreciprocal 2-port shown in Figure 61. Let a_1 and a_2 denote the incident waves and b_1 and b_2 the reflected waves at the respective ports, and let the scattering matrix of the 2-port be defined with respect to some convenient positive normalization number R_0, at both ports 1 and 2.

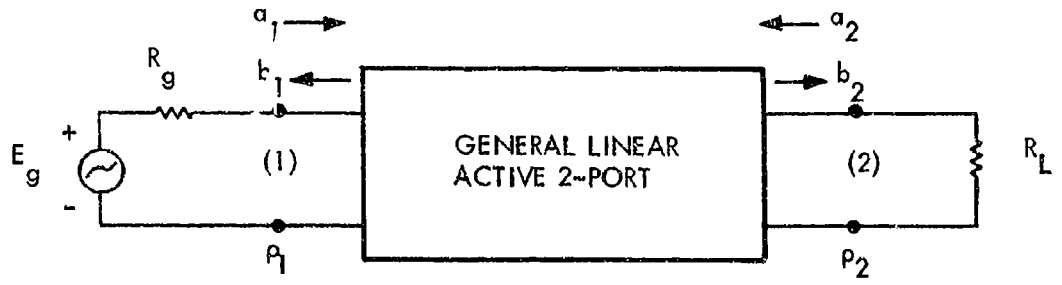

$$\hat{\underline{S}} = \begin{bmatrix} \hat{S}_{11} & \hat{S}_{12} \\ \hat{S}_{21} & \hat{S}_{22} \end{bmatrix}$$

Figure 61. General Linear Active 2-Port Network

Then

$$\begin{bmatrix} b_1 \\ b_2 \end{bmatrix} \quad \begin{bmatrix} \hat{S}_{11} & \hat{S}_{12} \\ \hat{S}_{21} & \hat{S}_{22} \end{bmatrix} \quad \begin{bmatrix} a_1 \\ a_2 \end{bmatrix} \tag{86}$$

The ports are terminated in real but arbitrary source and load impedances and the reflection factors of these terminations are represented by ρ_1 and ρ_2, which are again normalized to R_0. We now proceed to derive the transducer power gain of the general 2-port as a function of the scattering coefficients and the input and output reflection factors.

The transducer power gain denoted by $G_t(\omega)$ is defined to be the ratio of the actual power dissipated in the load P_L to the maximum available power from the source P_M. Thus,

$$G_t(\omega) = \frac{P_L}{P_M} = \frac{R_L \left| I_2 \right|^2}{\frac{\left| E_g \right|^2}{4R_g}} \tag{87}$$

where I_2 is the current through the load and the other quantities are defined in Figure 61. Defining the input and output reflection factors, respectively, as

$$\rho_1 = \frac{R_g - R_0}{R_g + R_0} \tag{88}$$

and

$$\rho_2 = \frac{R_L - R_0}{R_L + R_0} \tag{89}$$

then

$$P_L = |b_2|^2 - |a_2|^2 = |b_2|^2 \left(1 - |\rho_2|^2\right) \tag{90}$$

and

$$P_M = \frac{|a_1 - \rho_1 b_1|^2}{1 - |\rho_1|^2} \tag{91}$$

Substitution of Eqs. (90) and (91) into Eq. (87) yields

$$G_t(\omega) = \frac{|b_2|^2 \left(1 - |\rho_1|^2\right)\left(1 - |\rho_2|^2\right)}{|a_1 - \rho_1 b_1|^2} \tag{92}$$

From the defining equations of the active 2-port given by Eq. (86) and using $a_2 = \rho_2 b_2$, we have

$$\frac{a_1 - \rho_1 b_1}{b_2} = \frac{1}{\hat{S}_{21}}\left[\left(1 - \rho_1 \hat{S}_{11}\right)\left(1 - \rho_2 \hat{S}_{22}\right) - \hat{S}_{12}\hat{S}_{21}\rho_1\rho_2\right] \tag{93}$$

Therefore, the general transducer power gain expression, Eq. (92), is given by

$$G_t(\omega) = \frac{|\hat{S}_{21}|^2 \left(1 - |\rho_1|^2\right)\left(1 - |\rho_2|^2\right)}{|1 - \rho_1 \hat{S}_{11} - \rho_2 \hat{S}_{22} + \rho_1\rho_2 \det(\underline{\hat{S}})|} \tag{94}$$

where

$$\det(\hat{\underline{S}}) = \hat{S}_{11}\hat{S}_{22} - \hat{S}_{12}\hat{S}_{21} \tag{95}$$

For the case where both the input (source) and the output (load) are perfectly matched, then Eq. (94) reduces simply to

$$G_t(\omega) = \left|\frac{b_2}{a_1}\right|^2 = \left|\hat{S}_{21}\right|^2 \quad \text{(Matched Source and Load)} \tag{96}$$

A particularly interesting application of the linear active 2-port theory is the absolute stability criterion. It is known that for real frequencies a linear nonreciprocal 2-port is absolutely stable (arbitrary input and output termination) if and only if

$$1 - \left|\hat{S}_{11}\right|^2 - \left|\hat{S}_{12}\hat{S}_{21}\right|^2 \geq 0 \tag{97}$$

or

$$1 - \left|\hat{S}_{22}\right|^2 - \left|\hat{S}_{12}\hat{S}_{21}\right| \geq 0 \tag{98}$$

and

$$1 - \left|\hat{S}_{11}\right|^2 - \left|\hat{S}_{22}\right|^2 - 2\left|\hat{S}_{12}S_{21}\right| + \left|\det(\hat{\underline{S}})\right|^2 \geq 0 \tag{99}$$

In addition, it is known that if the 2-port is reciprocal ($\hat{S}_{12} = \hat{S}_{21}$) then it is absolutely stable if and only if it is passive.

For potential stability, the denominator of Eq. (94) must not be equal to zero, i.e.,

$$1 - \rho_1 \hat{S}_{11} - \rho_2 \hat{S}_{22} + \rho_1 \rho_2 \det(\hat{\underline{S}}) \neq 0 \tag{100}$$

This is a potential stability criterion which depends explicitly on the input and output mismatches. A sufficient real-frequency condition for potential stability is given by

$$\left| \rho_1 \hat{S}_{11} + \rho_2 \hat{S}_{22} - \rho_1 \rho_2 \det(\hat{\underline{S}}) \right| < 1 \tag{101}$$

The results contained in this section will be applied to the various reflection amplifier configurations.

5.3.3 Direct-Coupled Case

The transducer power gain for the direct-coupled amplifier used in Figure 56 is given by

$$G_t = \frac{1}{4} (1 - \zeta^2)(1 - \rho)^2 \left| \frac{1 + \Gamma_0}{1 - \rho \Gamma_0} \right|^2 \tag{102}$$

where

$$\Gamma_0 \equiv \frac{z_A - R_0}{z_A + R_0} \tag{103}$$

$$\zeta \equiv \frac{R_g - R_L}{R_g + R_L} \tag{104}$$

$$\rho \equiv \frac{R_1 - R_0}{R_1 + R_0} \quad , \qquad R_1 \equiv \frac{R_g R_L}{R_g + R_L} \tag{105}$$

Reference is made to Figure 56 in which the function z_A is defined. The quantity R_0 is an arbitrary positive normalizing impedance. The factor of $\frac{1}{4}$ in Eq. (102) accounts for the inherent 6 dB loss for the direct-coupled configuration. The quantity Γ_0 as defined in Eq. (103) is the reflection coefficient of the tunnel diode reflection amplifier normalized to R_0. The parameter ζ accounts for the difference between the two antenna impedances; i.e., it is a measure of difference of $R_g = R_{ANT}^{(i)}$ and $R_L = R_{ANT}^{(j)}$ where i, j = 1, 2 and i ≠ j. The parameter ρ accounts for the mismatch of the antenna impedance. All of these parameters may be functions of frequency.

For $R_g = R_L = R_{ANT}$ (assume identical antennas), then $\zeta = 0$, and Eq.(102) reduces to

$$G_t = \frac{1}{4}(1 - \rho)^2 \left| \frac{1 + \Gamma_0}{1 - \rho\Gamma_0} \right|^2 \tag{106}$$

where

$$\rho \equiv \frac{\frac{R_{ANT}}{2} - R_0}{\frac{R_{ANT}}{2} + R_0} \tag{107}$$

Relations (102) and (106) show explicitly the effects of antenna mismatch. It affects both the gain and stability of the amplifier and must be taken into account. For stability, the denominator of Eqs. (102) or (106) cannot vanish for all frequencies.

For the matched case, $\rho = 0$ ($R_{ANT} = 2\ R_0$), then Eq. (106) reduces to

$$G_t = \frac{1}{4}\left|1 + \Gamma_0\right|^2 \quad \text{(Matched Case)} \tag{108}$$

For the high gain case, Eq. (106) can be approximated by

$$G_t \cong \frac{1}{4}(1 - \rho)^2 \left|\frac{\Gamma_0}{1 - \rho\Gamma_0}\right|^2 \quad \text{(High Gain Case)} \tag{109}$$

Finally, for the case of matched antennas and high gain, we have

$$G_t \cong \frac{1}{4}\left|\Gamma_0\right|^2 \quad \text{(Matched and High Gain Case)} \tag{110}$$

5.3.4 Hybrid-Coupled Bilateral Amplifiers

For the hybrid-coupled bilateral amplifier shown in Figure 59, the nonideal quadrature hybrid is defined in terms of its scattering parameters normalized with R_0 at all of its ports. We have

$$\underline{S}^{(c)} = \begin{bmatrix} \gamma & \beta & \frac{1}{\sqrt{2}} & \alpha_1 e^{j\theta_1} & \frac{1}{\sqrt{2}} & \alpha_2 \\ \beta & \gamma & \frac{1}{\sqrt{2}} & \alpha_2 e^{j\theta_2} & \frac{-1}{\sqrt{2}} & \alpha_1 \\ \frac{1}{\sqrt{2}} & \alpha_1 e^{j\theta_1} & \frac{1}{\sqrt{2}} & \alpha_2 e^{j\theta_2} & \gamma & \beta \\ \frac{1}{\sqrt{2}} & \alpha_2 & \frac{-1}{\sqrt{2}} & \alpha_1 & \beta & \gamma \end{bmatrix} \tag{111}$$

In Eq. (111), the parameters γ, β, α_1, α_2, θ_1, and θ_2, which may all be functions of frequency, give a measure of the characteristics of the nonideal quadrature hybrid. The parameter γ is the reflection coefficient, and β is a measure of the isolation. Parameters α_1 and α_2 are measures of the forward insertion loss. Finally, β_1 and β_2 are measures of the nonideal phase quadrature.

For an ideal quadrature hybrid, these parameters attain their limiting values given by

$$\begin{aligned} &\gamma = 0 \text{ (Perfectly matched)} \\ &\beta = 0 \text{ (Infinite isolation)} \\ &\alpha_1 = \alpha_2 = 1 \text{ (Ideal 3-dB power division)} \\ &\theta_1 = \theta_2 = \frac{\pi}{2} \text{ (Ideal phase quadrature)} \end{aligned} \tag{112}$$

In Figure 57, Γ_3 and Γ_4 are defined as the reflection factors at port 3 and 4, respectively; i.e.,

$$\Gamma_3 = \frac{Z_A^{(3)} - R_0}{Z_A^{(3)} + R_0} \tag{113}$$

and

$$\Gamma_4 = \frac{Z_A^{(4)} - R_0}{Z_A^{(4)} - R_0} \tag{114}$$

Since $\mathrm{Re}\left[Z_A^{(3)}\right]$ and $\mathrm{Re}\left[Z_A^{(4)}\right]$ are negative in the frequency band of interest, the magnitudes of Γ_3 and Γ_4 are greater than unity.

Partitioning the matrix $\underline{S}^{(c)}$ into 2 x 2 submatrices as

$$\underline{S}^{(c)} = \left[\begin{array}{c|c} \underline{S}_{11}^{(c)} & \underline{S}_{12}^{(c)} \\ \hline \underline{S}_{21}^{(c)} & \underline{S}_{22}^{(c)} \end{array}\right] \tag{115}$$

and defining the diagonal matrix

$$\underline{\Gamma} = \text{diag}\left[\Gamma_3,\ \Gamma_4\right] \tag{116}$$

then it can be shown that the scattering matrix of the equivalent active 2-port is given by

$$\hat{\underline{S}} = \underline{S}_{11}^{(c)} + \underline{S}_{12}^{(c)}\left[\underline{\Gamma}^{-1} - \underline{S}_{22}^{(c)}\right]^{-1}\underline{S}_{21}^{(c)} \tag{117}$$

where the superscript "-1" denotes the inverse of the matrix.

Identifying Eq. (111) with Eq. (115) and substituting into Eq. (117) we obtain

$$\hat{S}_{11} = \gamma + \frac{1}{2\eta}\left[\alpha_1^2\, e^{j2\theta_1}\left(\frac{1}{\Gamma_4} - \gamma\right) + \alpha_2^2\left(\frac{1}{\Gamma_3} - \gamma\right) + 2\alpha_1\alpha_2\beta\, e^{j\theta_1}\right] \tag{118}$$

$$\hat{S}_{22} = \gamma + \frac{1}{2\eta}\left[\alpha_1^2\left(\frac{1}{\Gamma_3} - \gamma\right) + \alpha_2^2\, e^{j2\theta_2}\left(\frac{1}{\Gamma_4} - \gamma\right) - 2\alpha_1\alpha_2\beta\, e^{j\theta_2}\right] \tag{119}$$

$$\hat{S}_{12} = \hat{S}_{21} = \beta + \frac{1}{2\eta}\left[\alpha_1\alpha_2\, e^{j(\theta_1+\theta_2)}\left(\frac{1}{\Gamma_4} - \gamma\right) - \alpha_1\alpha_2\left(\frac{1}{\Gamma_3} - \gamma\right)\right.$$

$$\left. + \alpha_2^2\beta\, e^{j\theta_2} - \alpha_1^2\beta\, e^{j\theta_1}\right] \qquad (120)$$

where

$$\eta \equiv \frac{1}{\Gamma_3\Gamma_4}\left[1 - \gamma\left(\Gamma_3 + \Gamma_4\right) + \left(\gamma^2 - \beta^2\right)\Gamma_3\Gamma_4\right] \qquad (121)$$

Finally, substitution of Eqs. (118) - (121) into Eq. (94) gives the transducer power gain of the hybrid-coupled bilateral negative resistance amplifier. Note that since the equivalent active 2-port in reciprocal, the hybrid-coupled amplifier cannot be absolutely stable. For given input and output mismatches, substitution of Eqs. (118) - (121) into Eq. (101) results in a sufficient condition for potential stability of the device.

Note that ρ_1 and ρ_2 (which are measures of the antenna mismatches) and all the hybrid parameters significantly affect both the gain and the stability of the device. The performance of the device is also dependent on whether the negative resistance amplifiers (Γ_3 and Γ_4) are identical or not.

5.3.4.1 Ideal Hybrid, Mismatched Source and Load

For an ideal quadrature hybrid defined by Eq. (112), Eqs. (118) -(121) reduce to

$$\hat{S}_{11} = \hat{S}_{22} = \frac{1}{2}\left(\Gamma_4 - \Gamma_3\right)$$

$$\hat{S}_{12} = \hat{S}_{21} = -\frac{1}{2}(\Gamma_3 + \Gamma_4)$$

and the transducer power gain is given by Eq. (94) as

$$G_t(\omega) = \frac{\frac{1}{4}\left|\Gamma_3 + \Gamma_4\right|^2 \left(1 - \left|\rho_1\right|^2\right)\left(1 - \left|\rho_2\right|^2\right)}{\left|1 - \frac{1}{2}(\rho_1 + \rho_2)(\Gamma_4 - \Gamma_3) - \rho_1\rho_2\Gamma_2\Gamma_3\Gamma_4^2\right|} \tag{122}$$

This expression isolates the effects of input and output mismatch as well as the fact that the two negative resistance elements (Γ_3 and Γ_4) are not identical. If, in addition, Γ_3 and Γ_4 are assumed to be identical ($\Gamma_3 = \Gamma_4 = \Gamma_0$), then

$$G_t(\omega) = \frac{\left|\Gamma_0\right|^2 \left(1 - \left|\rho_1\right|^2\right)\left(1 - \left|\rho_2\right|^2\right)}{\left|1 - \rho_1\rho_2\Gamma_0^2\right|^2} \tag{123}$$

A sufficient stability condition for this case is expressed by

$$\left|\rho_1\rho_2\Gamma_0^2\right| < 1 \tag{124}$$

5.3.4.2 Practical Hybrid, Matched Source and Load

For perfectly matched source and load, the transducer power gain is given by

$$G_t(\omega) = \left|S_{12}\right|^2 = \left[\beta + \left\{\frac{\alpha_1\alpha_2\left|e^{j(\theta_1+\theta_2)}\left(1 - \gamma\Gamma_3\right) - \left(1 - \gamma\Gamma_4\right)\right| - \beta\Gamma_3\Gamma_4\left(\alpha_2^2\, e^{j\theta_2} + \alpha_1^2\, e^{j\theta_1}\right)}{2\left|1 - \gamma\left(\Gamma_3 + \Gamma_4\right) + \left(\gamma^2 - \beta^2\right)\Gamma_3\Gamma_4\right|}\right\}\right]^2 \tag{125}$$

This expression shows only the effects of the nonideal hybrid. Note that the hybrid parameters γ and β, which give measure of matching and isolation, respectively, are important in the gain expression as well as in the stability property of the amplifier. For $\Gamma_3 = \Gamma_4 = \Gamma_0$, the sufficient condition for stability given by Eq.[4](101) becomes

$$\left|2\gamma\Gamma_0 - \left(\gamma^2 - \beta^2\right)\Gamma_0^2\right| < 1 \tag{126}$$

5.3.4.3 Ideal Hybrid, Matched Source and Load

For an ideal hybrid and matched source and load, the transducer power gain is given by

$$G_t = \frac{1}{4}\left|\Gamma_3 + \Gamma_4\right|^2 \tag{127}$$

If, in addition, $\Gamma_3 = \Gamma_4 = \Gamma_0$, then

$$G_t = \left|\Gamma_0\right|^2 \tag{128}$$

This final, highly idealized result is the one usually used in the literature.

5.3.5 Circulator-Coupled Bilateral Amplifiers

A practical 4-port circulator can be expressed in terms of its scattering matrix as

$$\underline{S}^{(c)} = \begin{bmatrix} \gamma & \eta & \beta_1 & \alpha_2 \\ \eta & \gamma & \alpha_2 & \beta_1 \\ \alpha_1 & \beta_2 & \gamma & \eta \\ \beta_2 & \alpha_1 & \eta & \gamma \end{bmatrix} \tag{129}$$

where γ, β's and α's represent, respectively, the reflection coefficient, the isolation, and the forward insertion loss parameters. In addition, the parameter η is the coupling coefficient of the symmetrically located ports.

For an ideal 4-port circulator, these parameters attain their limiting parameters as follows:

$$\begin{aligned} &\gamma = 0 \text{ (Perfectly matched)} \\ &\beta_1 = \beta_2 = 0 \text{ (Infinite isolation)} \\ &\alpha_1 = \alpha_2 = 1 \text{ (Lossless)} \\ &\eta = 0 \text{ (Perfectly decoupled)} \end{aligned} \tag{130}$$

In Figure 58, Γ_3 and Γ_4 are defined as in Eqs. (113) and (114). Using the same procedure presented in paragraph 5.3.4, we can derive the scattering parameters of the equivalent active 2-port as

$$\hat{S}_{11} = \gamma + \frac{1}{\Delta}\left\{\beta_1\left[\alpha_1\left(\frac{1}{\Gamma_4} - \gamma\right) + \eta\beta_2\right] + \alpha_2\left[\beta_2\left(\frac{1}{\Gamma_3} - \gamma\right) + \eta\alpha_1\right]\right\} \tag{131}$$

$$\hat{S}_{22} = \gamma + \frac{1}{\Delta}\left\{\alpha_2\left[\beta_2\left(\frac{1}{\Gamma_4} - \gamma\right) + \eta\alpha_1\right] + \beta_1\left[\alpha_1\left(\frac{1}{\Gamma_3} - \gamma\right) + \eta\beta_2\right]\right\} \tag{132}$$

$$\hat{S}_{12} = \eta + \frac{1}{\Delta}\left\{\beta_1\left[\beta_2\left(\frac{1}{\Gamma_4} - \gamma\right) + \eta\alpha_1\right] + \alpha_2\left[\alpha_1\left(\frac{1}{\Gamma_3} - \gamma\right) + \eta\beta_2\right]\right\} \tag{133}$$

$$\hat{S}_{21} = \eta + \frac{1}{\Delta}\left\{\alpha_2\left[\alpha_1\left(\frac{1}{\Gamma_4} - \gamma\right) + \eta\beta_2\right] + \beta_1\left[\beta_2\left(\frac{1}{\Gamma_3} - \gamma\right) + \eta\alpha_1\right]\right\} \tag{134}$$

where

$$\Delta \equiv \frac{1}{\Gamma_3\Gamma_4}\left[1 - \gamma\left(\Gamma_3 + \Gamma_4\right) + \left(\gamma^2 - \eta^2\right)\Gamma_3\Gamma_4\right] \tag{135}$$

Substitution of the relations (131) to (135) into Eq. (94) yields the transducer power gain of the 4-port circulator-coupled bilateral negative resistance amplifier. Note that the equivalent active 2-port is nonreciprocal if $\Gamma_3 \neq \Gamma_4$. For this configuration to be truly bilateral, we require $\hat{S}_{12} = \hat{S}_{21}$; i.e., $\Gamma_3 = \Gamma_4$. This condition will not be imposed at the outset so that the effect of this condition on the device characteristics is made evident.

5.3.5.1 Ideal 4-Port Circulator, Mismatched Source and Load

For an ideal 4-port circulator defined by Eq. (130), then Eqs. (131) - (135) simplify to

$$\hat{S}_{11} = \hat{S}_{22} = 0$$

$$\hat{S}_{12} = \Gamma_4 \qquad (136)$$

$$\hat{S}_{21} = \Gamma_3$$

and the transducer power gain from antenna no. 1 to antenna no. 2 is given by Eq. (94) as

$$G_t^{(2-1)} = \frac{|\Gamma_3|^2 (1 - |\rho_1|^2)(1 - |\rho_2|^2)}{|1 - \rho_1 \rho_2 \Gamma_3 \Gamma_4|^2} \qquad (137)$$

Note that because of the presence of the source and load mismatches, the negative resistance amplifier at port 4 is coupled into the system (see Figure 58) and it affects both the gain and the stability of the device. Comparing Eq. (137) with Eq. (123), note the presence of the extra term in the denominator of Eq. (123). If the two negative resistance amplifiers are not identical, $(\Gamma_3 \neq \Gamma_4)$, then this term will make the gain sensitivity and stability more critical for the hybrid-coupled configuration, as compared to the 4-port circulator-coupled configuration. The effect of nonidentical negative resistance elements is manifested in the bilateral property of the overall amplifier. This is shown by comparing Eq. (137) with the transducer power gain from antenna no. 2 to antenna no. 1 given by

$$G_t^{(2-1)} = \frac{|\Gamma_4|^2 (1 - |\rho_1|^2)(1 - |\rho_2|^2)}{|1 - \rho_1 \rho_2 \Gamma_3 \Gamma_4|^2} \qquad (138)$$

If the negative resistance elements are not identical, then the two transducer power gain expressions are not exactly the same. However, stability of the device is not affected.

If $\Gamma_3 = \Gamma_4 = \Gamma_0$, then Eqs. (137) and (138) are identically given by

$$G_t^{(1-2)} = G_t^{(2-1)} = \frac{|\Gamma_0|^2\left(1 - |\rho_1|^2\right)\left(1 - |\rho_2|^2\right)}{\left|1 - \rho_1\rho_2\Gamma_0^2\right|^2} \tag{139}$$

which is the same as Eq. (123) for the ideal hybrid and $\Gamma_3 = \Gamma_4 = \Gamma_0$ case, and the stability condition contained in Eq. (124) also applies.

5.3.5.2 Practical 4-Port Circulator, Matched Source and Load

For perfectly matched sourced and load, the transducer power gain expressions are given by

$$G_t^{(1-2)} = \left|\hat{S}_{21}\right|^2 = \left|\eta + \left\{\frac{\alpha_2\left[\alpha_1\left(1-\gamma\Gamma_3\right) + \eta\beta_2\Gamma_3\Gamma_4\right] + \beta_1\left[\beta_2\left(1-\gamma\Gamma_4\right) + \eta\alpha_1\Gamma_3\Gamma_4\right]}{1-\gamma\left(\Gamma_3+\Gamma_4\right)+\left(\gamma^2-\eta^2\right)\Gamma_3\Gamma_4}\right\}\right|^2 \tag{140}$$

$$G_t^{(2-1)} = \left|\hat{S}_{12}\right|^2 = \left|\eta + \left\{\frac{\alpha_2\left[\alpha_1\left(1-\gamma\Gamma_4\right) + \eta\beta_2\Gamma_3\Gamma_4\right] + \beta_1\left[\beta_2\left(1-\gamma\Gamma_3\right) + \eta\alpha_1\Gamma_3\Gamma_4\right]}{1-\gamma\left(\Gamma_3+\Gamma_4\right)+\left(\gamma^2-\eta^2\right)\Gamma_3\Gamma_4}\right\}\right|^2 \tag{141}$$

Again, these two expressions are equal if $\Gamma_3 = \Gamma_4 = \Gamma_0$. For this case, the stability condition is given by

$$\left|2\gamma\Gamma_0 - \left(\gamma^2 - \eta^2\right)\Gamma_0^2\right| < 1 \tag{142}$$

5.3.5.3 Ideal 4-Port Circulator, Matched Source and Load

The transducer power gain from antenna no. 1 to antenna no. 2 is

$$G_t^{(1-2)} = |\Gamma_3|^2 \tag{143}$$

A similar development for the gain from antenna no. 2 to antenna no. 1 yields

$$G_t^{(2-1)} = |\Gamma_4|^2 \tag{144}$$

These results should be compared with Eq. (122) for the corresponding ideal hybrid-coupled case. If, in addition, $\Gamma_3 = \Gamma_4 = \Gamma_0$, then Eqs. (143) and (144) reduce to

$$G_t^{(1-2)} = G_t^{(2-1)} = |\Gamma_0|^2 \tag{145}$$

Detailed comparisons have been made of the results for the three basic bilateral amplifier configurations considered so far in this section. The following conclusions can be made:

1. There is an inherent 6-dB loss in the direct-coupled case.

2. The input and output mismatches and the parameters of the coupling networks significantly affect all the performance measures of the overall amplifier. Most important of these are the gain, the gain sensitivity, and the stability. Even without taking antenna mutual coupling into account, stability of the bilateral amplifier is severly limited by mismatches and coupling network parameters.

3. For a prescribed gain and given antenna mismatch, the gain sensitivity and stability of the direct-coupled case are inferior to the hybrid-coupled and the 4-port circulator-coupled cases.

4. Since we are considering the bilateral configuration, there is no inherent stability advantage of the 4-port circulator-coupled configuration over the hybrid-coupled configuration. The circulator-coupled is better with respect to the effects of the non-identical negative resistance amplifiers. It has been shown that the stability of the hybrid case is affected; whereas for the circulator case, only the bilateral property is affected.

5. For both the hybrid- and 4-port circulator-coupled cases, the most significant nonideal parameter is the reflection coefficient γ. Since presently available circulators exhibit larger mismatches than hybrids, this consideration will favor the hybrid-coupled case.

6. To point out the importance of the effects of the mismatch of both the antenna and the coupling network, it can be shown that assuming an amplifier gain of 20 dB and antenna and hybrid mismatch of VSWR of 1.05, a variation of the negative resistance value of 10 percent will render the device unstable at the operating frequency.

7. The expressions presented here are functions of frequency. Each of the stability conditions must be checked not only in the passband of the amplifier but also for all frequencies up to the resistive cutoff frequency of the tunnel diode.

5.3.6 A Class of Bilateral Amplifiers Using Hybrid- and Circulator-Coupled 2-Port Unilateral Amplifiers

A class of bilateral amplifiers using hybrid- and circulator-coupled 2-port unilateral amplifiers has also been analyzed. This particular class of bilateral amplifier is well known at low

frequencies and is used in two-way repeater telephone circuits. The basic active building blocks for this class of bilateral amplifiers are 2-port unilateral amplifiers such as TWT's or microwave transistor amplifiers which are presently available up to S-band frequencies.

Two of the basic configurations studied are shown in Figures 59 and 60. Practical models of the coupling networks and the unilateral amplifiers have been used in the analysis. Results obtained, however, are rather involved, in general, and will not be presented. For a special case in which the circulators in Figure 60 are assumed to be ideal, we have

$$G_t^{(1-2)} = \frac{\left|S_{21}^{(A_1)}\right|^2 \left(1 - |\rho_1|^2\right)\left(1 - |\rho_2|^2\right)}{\left|1 - \rho_1\rho_2\, S_{21}^{(A_1)}\, S_{21}^{(A_2)}\right|^2} \tag{146}$$

where $S_{21}^{(A_1)}$ and $S_{21}^{(A_2)}$ are the scattering parameters of the unilateral amplifiers A_1 and A_2, respectively.

If, in addition, the source and the load are matched, then

$$G_t^{(1-2)} = \left|S_{21}^{(A_1)}\right|^2 \tag{147}$$

$$G_t^{(2-1)} = \left|S_{21}^{(A_2)}\right|^2 \tag{148}$$

These results are similar to those presented previously on negative resistance bilateral amplifiers. For the corresponding ideal hybrid-coupled configuration shown in Figure 59, there is a 6-dB reduction in the transducer power gain expressions.

5.4 ANALYTICAL RESULTS ON VARIOUS TYPES OF UNILATERAL NEGATIVE RESISTANCE AMPLIFIERS

5.4.1 Introduction

In this section, some results on the design of unilateral (unidirectional) negative resistance amplifiers are presented. As applied to the active Van Atta array in the unilateral configuration, only half of the antenna elements are used for transmitting, while the conjugate elements are used for receiving. If the unilateral 2-port amplifiers are available, then no coupling network is needed and the realization is merely that shown in Figure 61 in which antenna no. 1 (receiving) is connected to port 1 and antenna no. 2 (transmitting) is connected to port 2. The scattering parameters $\hat{S}_{ij}$ are then those associated with the actual active 2-port such as a microwave transistor. Results are identical to those presented in paragraph 5.3.2. On the other hand, at frequencies above S-band, negative resistance elements such as tunnel diodes or avalanche diode amplifiers are needed together with some coupling network to realize the unilateral amplifier.

Three basic configurations of this class of unilateral amplifier using negative resistance elements are considered; namely,

I. Hybrid-Coupled Configuration with Isolator

II. 3-Port Circulator-Coupled (Figure 62)

III. 4-Port Circulator-Coupled (Figure 63)

The hybrid-coupled configuration has already been studied in paragraph 5.3.4. The only distinction here is that an isolator (or one-way line) is inserted in front of the load at port 2 of Figure 57. The results are contained in Eqs. (118) to (128) except that now with the isolator, $\hat{S}_{12}$ will equal zero in the ideal case and the device is absolutely stable under matched and ideal hybrid and isolator conditions.

5.4.2 3-Port Circulator-Coupled Unilateral Amplifier

A practical 3-port circulator can be represented in terms of its scattering matrix as

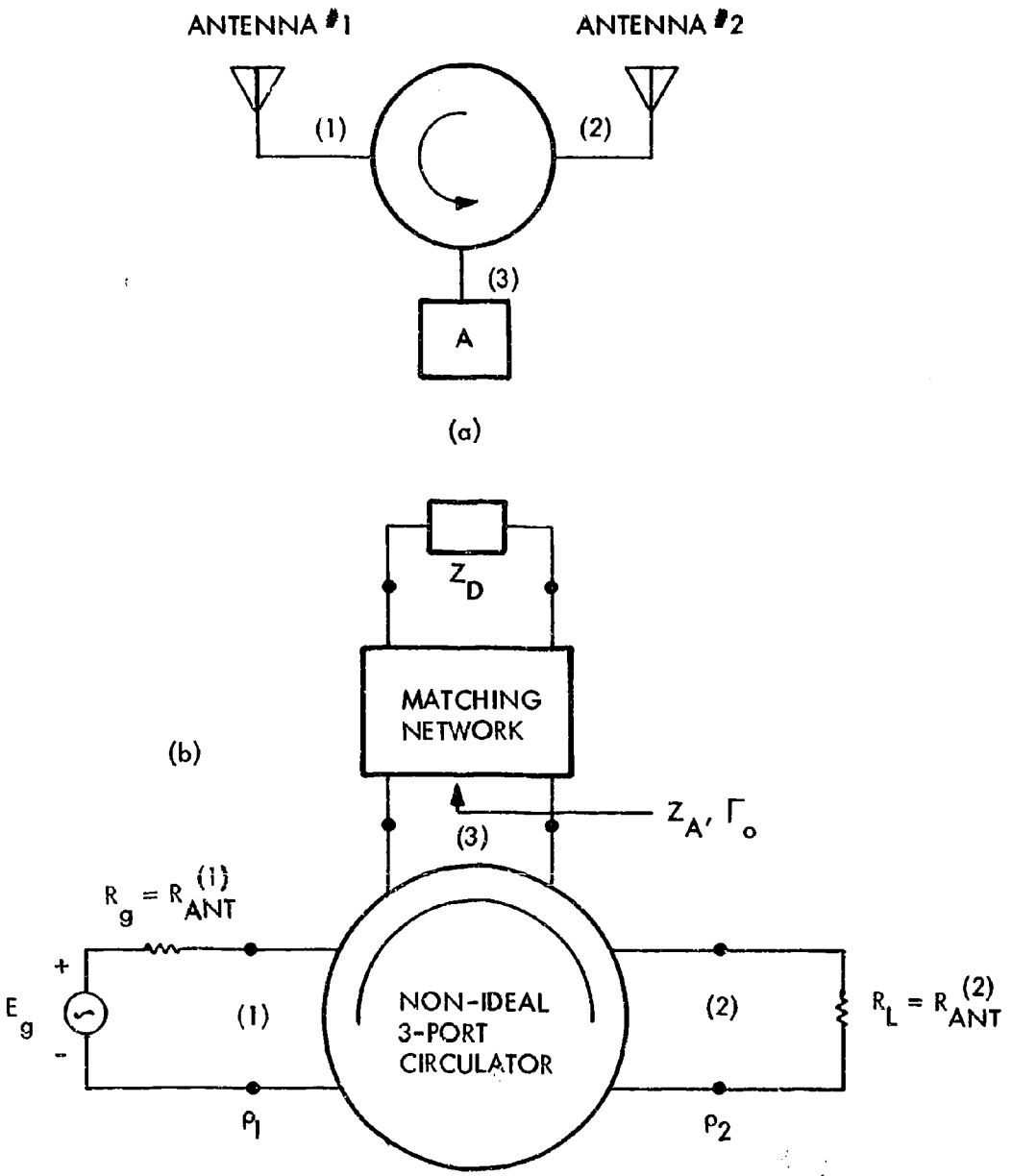

Figure 62. Circulator-Coupled Unilateral Amplifier Using a Practical 3-Port Circulator and One Negative Resistance Element

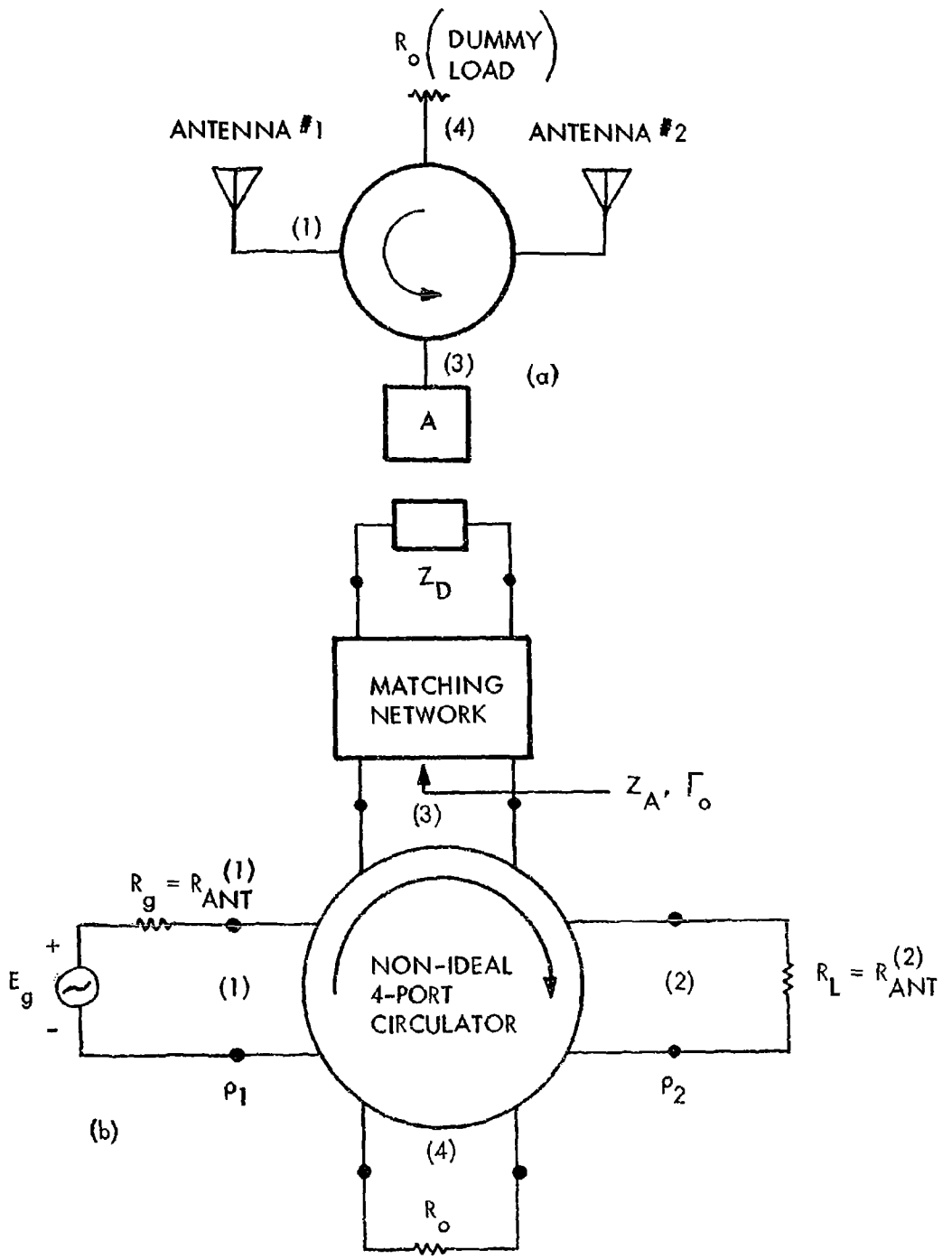

Figure 63. Circulator-Coupled Unilateral Amplifier Using a Practical 4-Port Circulator and One Negative Resistance Element

$$\underline{S}^{(c)} = \begin{bmatrix} \gamma & \alpha & \beta \\ \beta & \gamma & \alpha \\ \alpha & \beta & \gamma \end{bmatrix} \tag{149}$$

where the parameters γ, β, and α represent the reflection coefficient, the isolation, and the forward insertion loss, respectively. For an ideal 3-port circulator, we have

$$\begin{aligned} \gamma &= 0 \text{ (Perfectly matched)} \\ \beta &= 0 \text{ (Infinite isolation)} \\ \alpha &= 1 \text{ (Lossless)} \end{aligned} \tag{150}$$

The equivalent active 2-port is described by

$$\hat{S}_{11} = \hat{S}_{22} = \left(1 - \gamma\Gamma\right)^{-1}\left|\gamma + \left(\alpha\beta - \gamma^2\right)\Gamma\right| \tag{151}$$

$$\hat{S}_{12} = \left(1 - \gamma\Gamma\right)^{-1}\left|\alpha + \left(\beta^2 - \alpha\gamma\right)\Gamma\right| \tag{152}$$

$$\hat{S}_{21} = \left(1 - \gamma\Gamma\right)^{-1}\left|\beta + \left(\alpha^2 - \beta\gamma\right)\Gamma\right| \tag{153}$$

Substitution of Eqs. (151) to (153) into the transducer power gain expression (94) yields

$$G_t = \frac{\left|1 - \gamma\Gamma_0\right|^2 \left|\beta + \left(\alpha^2 - \beta\gamma\right)\Gamma_0\right|^2 \left(1 - \left|\rho_1\right|^2\right)\left(1 - \left|\rho_2\right|^2\right)}{\left|\left(1 - \gamma\Gamma_0\right)^2 - \left(\rho_1 + \rho_2\right)\left(1 - \gamma\Gamma_0\right)\left[\gamma + \left(\alpha\beta - \gamma^2\right)\Gamma_0\right] + \rho_1\rho_2\left\{\left[\gamma + \left(\alpha\beta - \gamma^2\right)\Gamma_0\right]^2 - \left[\alpha + \left(\beta^2 - \alpha\gamma\right)\Gamma_0\right]\left[\beta + \left(\alpha^2 - \beta\gamma\right)\Gamma_0\right]\right\}\right|^2} \tag{154}$$

5.4.2.1 Ideal 3-Port Circulator Except $\gamma \neq 0$

If the 3-port circulator is ideal except that $\gamma \neq 0$, then

$$\hat{S}_{11} = \hat{S}_{22} = \gamma$$

$$\hat{S}_{21} = 1 \tag{155}$$

$$\hat{S}_{21} = \left(1 - \gamma\Gamma_0\right)^{-1} \Gamma_0$$

and the transducer power gain is given by

$$G_t = \frac{\left|\Gamma_0\right|^2 \left(1 - \left|\rho_1\right|^2\right)\left(1 - \left|\rho_2\right|^2\right)}{\left|1 - \gamma\Gamma_0\right|^2 \left|1 - \left(\rho_1 + \rho_2\right)\gamma + \rho_1\rho_2\left[\gamma^2 - \Gamma_0\left(1 - \gamma\Gamma_0\right)^{-1}\right]\right|^2} \tag{156}$$

In this case, we can substitute Eq. (155) into Eqs. (97) to (99) to derive a stability criterion which is both necessary and sufficient for stability with arbitrary source and load mismatches.

For matched source and load,

$$G_t = \left| \frac{\Gamma_0}{1 - \gamma\Gamma_0} \right|^2 \tag{157}$$

This expression shows only the effect of the mismatch of the 3-port circulator. A sufficient condition for stability for this case is that

$$\left| \gamma\Gamma_0 \right| < 1 \tag{158}$$

5.4.2.2 Ideal 3-Port Circulator Except $\beta \neq 0$

If the 3-port circulator is ideal except that the isolation $\beta \neq 0$, then

$$\begin{aligned} \hat{S}_{11} &= \hat{S}_{22} = \beta\Gamma_0 \\ \hat{S}_{12} &= 1 + \beta^2\Gamma_0 \\ \hat{S}_{21} &= \beta + \Gamma_0 \end{aligned} \tag{159}$$

and

$$G_t = \frac{\left|\beta + \Gamma_0\right|^2 \left(1 - \left|\rho_1\right|^2\right)\left(1 - \left|\rho_2\right|^2\right)}{\left|1 - \left(\rho_1 + \rho_2\right)\beta\Gamma_0 - \rho_1\rho_2\left[\beta\left(1 + \beta^2\Gamma_0\right) + \Gamma_0\right]\right|^2} \tag{160}$$

For matched source and load,

$$G_t = \left|\beta + \Gamma_0\right|^2 \tag{161}$$

which shows that for matched source and load, there is no stability problem due to the fact that $\beta \neq 0$.

5.4.2.3 Ideal 3-Port Circulator, Mismatched Source and Load

For an ideal 3-port circulator, $\gamma = 0$, $\beta = 0$, and $\alpha = 1$, then

$$\hat{S}_{11} = \hat{S}_{22} = 0$$

$$\hat{S}_{12} = 1 \tag{162}$$

$$\hat{S}_{21} = \Gamma_0$$

and

$$G_t = \frac{\left|\Gamma_0\right|^2\left(1 - \left|\rho_1\right|^2\right)\left(1 - \left|\rho_2\right|^2\right)}{\left|1 - \rho_1\rho_2\Gamma_0\right|^2} \tag{163}$$

It is interesting to note that in the 3-port circulator-coupled case, even the assumption of ideal circulator will not guarantee absolute stability. This can be seen by substituting Eq. (161) into Eqs. (97) to (99). This is due to the mismatches at the source and the load. In this case a sufficient condition for stability is given by

$$\left|\rho_1\rho_2\Gamma_0\right| < 1 \tag{164}$$

5.4.2.4 Practical 3-Port Circulator, Matched Source and Load

For a practical 3-port circulator with $\gamma \neq 0$, $\beta \neq 0$, and $\alpha \neq 1$, but under matched source and load conditions, we have

$$G_t = \left| \beta + \frac{\alpha_2 \Gamma_0}{1 - \gamma \Gamma_0} \right|^2 \tag{165}$$

This expression shows only the effects of a nonideal 3-port circulator. A sufficient condition for stability is given by

$$\left| \gamma \Gamma_0 \right| < 1 \tag{166}$$

5.4.2.5 Ideal 3-Port Circulator, Matched Source and Load

Under ideal circulator and matched conditions, the gain is given simply by

$$G_t = \left| \Gamma_0 \right|^2 \tag{167}$$

5.4.3 4-Port Circulator-Coupled Unilateral Amplifier

A 4-port circulator-coupled unilateral amplifier is shown in Figure 63. The major difference in this configuration compared to the bilateral amplifier presented in Figure 58 is that now only one negative resistance element is used and one of the ports of the circulator is terminated in a dummy load. The scattering matrix of a practical 4-port circulator has also been given in Eq. (129). Based on this result, the equivalent active 2-port is represented by

$$\hat{S}_{11} = \left(1 - \gamma \Gamma_0\right)^{-1} \left| \gamma \left(1 - \gamma \Gamma_0\right) + \alpha_1 \beta_1 \Gamma_0 \right| \tag{168}$$

$$\hat{S}_{22} = \left(1 - \gamma\Gamma_0\right)^{-1}\left[\gamma\left(1 - \gamma\Gamma_0\right) + \alpha_2\beta_2\Gamma_0\right] \tag{169}$$

$$\hat{S}_{12} = \left(1 - \gamma\Gamma_0\right)^{-1}\left[\eta\left(1 - \gamma\Gamma_0\right) + \beta_1\beta_2\Gamma_0\right] \tag{170}$$

$$\hat{S}_{21} = \left(1 - \gamma\Gamma_0\right)^{-1}\left[\eta\left(1 - \gamma\Gamma_0\right) + \alpha_1\alpha_2\Gamma_0\right] \tag{171}$$

Substitution of Eqs. (168) to 171) into Eq. (94) yields the transducer power gain for this amplifier. This particular configuration has the useful property that it may be absolutely stable even with practical 4-port circulator parameters. The exact stability criterion is obtained by substituting the scattering parameters into Eqs. (97) to (99).

5.4.3.1 Ideal 4-Port Circulator Except $\gamma \neq 0$

If the 4-port circulator is ideal except that $\gamma \neq 0$, then

$$\hat{S}_{11} = \hat{S}_{22} = \gamma$$

$$\hat{S}_{12} = 0 \tag{172}$$

$$\hat{S}_{21} = \left(1 - \gamma\Gamma_0\right)^{-1}\Gamma_0$$

and

$$G_t = \frac{\left|\Gamma_0\right|^2\left(1 - \left|\rho_1\right|^2\right)\left(1 - \left|\rho_2\right|^2\right)}{\left|1 - \gamma\Gamma_0\right|^2\left|1 - \rho_1\gamma\right|^2\left|1 - \rho_2\gamma\right|^2} \tag{173}$$

Note that in the denominator, since $\rho_1 \leq 1$, $\rho_2 \leq 1$, and $\gamma \leq 1$, the only term that might lead to stability problems is $1 - \gamma\Gamma_0$. This is to be compared with Eq. (162) for the corresponding 3-port circulator case.

For matched source and load, the gain and stability conditions are identical to Eqs. (157) and (158) derived for the 3-port circulator-coupled configuration.

For the case where the 4-port circulator is ideal except that $\beta \neq 0$, results are similar to those presented in the corresponding 3-port circulator-coupled case.

5.4.3.2 Ideal 4-Port Circulator, Mismatched Source and Load

For an ideal 4-port circulator, the circulator parameters attain their ideal limits contained in Eq. (131). We have that

$$\hat{S}_{11} = \hat{S}_{22} = 0$$

$$\hat{S}_{12} = 0 \qquad (174)$$

$$\hat{S}_{21} = \Gamma_0$$

and

$$G_t = |\Gamma_0|^2 \left(1 - |\rho_1|^2\right)\left(1 - |\rho_2|^2\right) \qquad (175)$$

These results should be compared with Eqs. (161) and (162) for the 3-port circulator-coupled case. Note from Eq. (174) that this case actually corresponds to an ideal unilateral active 2-port with reverse transmission parameter $\hat{S}_{12}$ identically zero. In fact, this unilateral amplifier is absolutely stable for arbitrary source and load mismatches. This fact is also manifested

in the gain expression presented in Eq. (175). The presence of mismatches will reduce the gain, but the stability is not affected.

5.4.3.3 Practical 4-Port Circulator, Matched Source and Load

For this case, we have

$$G_t = \left| \eta + \frac{\alpha_1 \alpha_2 \Gamma_0}{1 - \gamma \Gamma_0} \right|^2 \qquad (176)$$

This result is similar to Eq. (165) and the sufficient stability condition (166) also applies.

Finally, under the ideal 4-port circulator and matched condition, the gain is identical to (167) for the 3-port circulator-coupled case.

5.4.4 Summary of Unilateral Amplifier Design Considerations

One of the major desirable features of the unilateral amplifier is that the stability of the device is inherently superior to the bilateral amplifier. It is known that a bilateral amplifier is absolutely stable if and only if it is passive. Thus, in active arrays, it is not possible to design stable bilateral amplifiers which are not functions of the source and load mismatches. On the other hand, we have shown in the previous sections that it is possible to design unilateral amplifiers which are absolutely stable.

For unilateral amplifiers, the two circulator-coupled configurations are superior to the hybrid-coupled case. The 4-port circulator-coupled case is, in general, superior to the 3-port circulator-coupled case. However, since in practice the 4-port circulator is realized by cascading two 3-port circulators, the parameters of the resulting 4-port circulators are, in general, worse than the corresponding parameters of the

3-port circulators. Even taking this fact into account, the overall performance of the 4-port circulator-coupled configuration should be the best realization for unilateral amplifiers in the high microwave frequencies. For frequencies at or below S-band, a transistor amplifier should definitely be used since it is unilateral without using any additional coupling networks.

The presence of inevitable mutual coupling of the antenna array imposes additional restrictions on the design of both the bilateral and the unilateral amplifiers. This important problem is studied in detail in Section VI.

BLANK PAGE

SECTION VI

STABILITY CRITERIA OF ACTIVE VAN ATTA ARRAYS

6.1 INTRODUCTION

This section presents some results on the stability of active Van Atta arrays with imbedded negative-resistance elements. The primary purpose of this study is to delineate clearly and rigorously the effects of the antenna mutual coupling on the behavior of active Van Atta arrays. In particular, explicit stability criteria are derived for a general class of active Van Atta arrays. Based on these stability criteria, definitive results are obtained concerning the limitations and various tradeoffs relating the size of the array, the amount of mutual coupling, and the gain of the system.

The material contained in this section is organized as follows: In paragraph 6.2, the stability of a general active array is formulated; paragraph 6.3 treats the case of an active array containing arbitrary numbers of independent 1-port active elements and shows that the stability problem can be solved elegantly using a matrix eigenvalue approach. In paragraph 6.4, it is shown that the stability problem of active Van Atta arrays can be reformulated so that the techniques presented in paragraph 6.3 can be applied. Finally, in paragraph 6.4, stability criteria for a number of specific active Van Atta arrays are presented.

6.2 STABILITY OF ACTIVE ANTENNA ARRAYS

Figure 64 shows schematically a general active array using n independent 1-port active elements. The antenna array can be characterized by its n x n impedance matrix

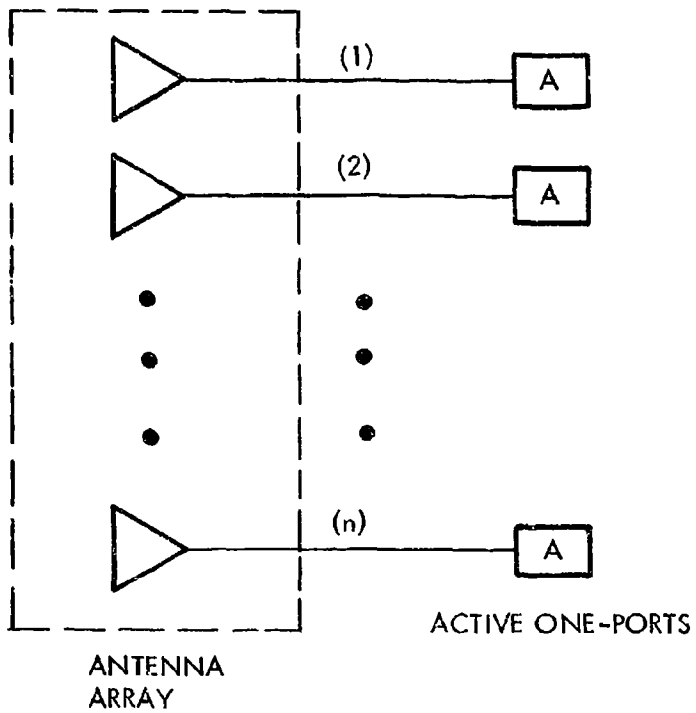

(a)

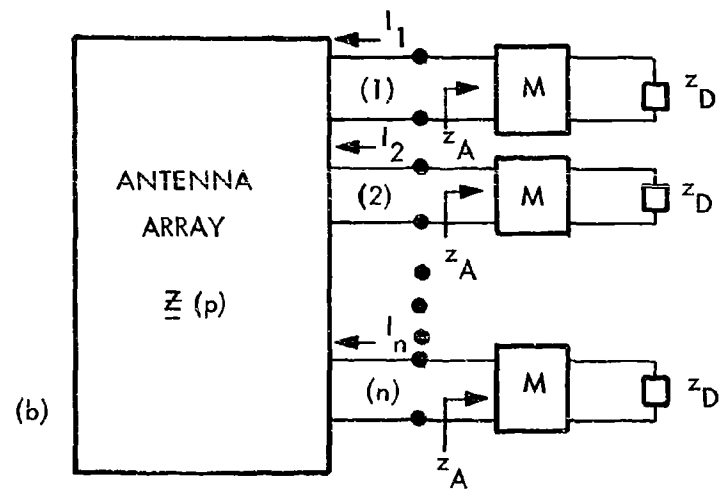

(b)

Figure 64. A General Active Antenna Array with n Imbedded Active One-Ports

$$\underline{Z}(p) = \begin{bmatrix} Z_{11}(p) & Z_{12}(p) & \cdots & Z_{1n}(p) \\ Z_{12}(p) & Z_{22}(p) & \cdots & Z_{2n}(p) \\ \vdots & \vdots & \ddots & \vdots \\ Z_{1n}(p) & Z_{2n}(p) & \cdots & Z_{nn}(p) \end{bmatrix} \qquad (177)$$

where the $Z_{ij}(p)$ are the self- and mutual-impedances of the anterna array and are considered to be artibrary functions of the complex frequency variable p. The matrix $\underline{Z}(p)$ is symmetric since the array is reciprocal. In addition, it is also passive since the active elements have been pulled out.

The only assumptions we shall impose on the antenna array are:

1. The self-impedances are identical, i.e.,

$$Z_{ii}(p) = Z_a(p), \; i = 1, 2, \ldots, n;$$

and the mutual-impedances differ only through a proportionality constant, i.e.,

$$Z_{ij}(p) = a_{ij} \, z_a(p), \; i,j = 1, 2, \ldots, n, \; i \neq j \; ;$$

2. The active elements are identical.

These assumptions amount to specifying that the active array is composed only of identical anternas and active elements. These assumptions are not very restrictive and are satisfied by a wide class of active arrays of interest. Note that the physical configuration of the array is not restricted and the self- and mutual-impedances denoted by $Z_a(p)$ and $z_a(p)$, respectively, can be arbitrary functions of the complex frequency variable, p.[6]

[6] These impedances do not have to be rational although rationality may be invoked for convenience.

Using these assumptions, Eq. (177) can be rewritten as

$$\underline{Z}(p) = \begin{bmatrix} Z_a(p) & a_{12}z_a(p) & \cdots & a_{1n}z_a(p) \\ a_{12}z_a(p) & Z_a(p) & \cdots & a_{2n}z_a(p) \\ \vdots & \vdots & \ddots & \vdots \\ a_{1n}z_a(p) & a_{2n}z_a(p) & \cdots & Z_a(p) \end{bmatrix} \tag{178}$$

and the active elements represented by

$$Z_A(p) = z_A(p)\underline{I} \tag{179}$$

where $z_A(p)$ is the impedance of the identical active elements and $\underline{I}$ is the n x n identity matrix.

Using some of the results published previously,[16] the stability of the active array shown in Figure 64 is governed by the determinantal equation

$$\det\left|\underline{Z}(p) + \underline{Z}_A(p)\right| = 0 \tag{180}$$

The active array is stable if this equation has no solution in the closed right-half p-plane, $\mathrm{Re}(p) \geq 0$.[7] Substitution of Eqs. (178) and (179) into Eq. (180) and factoring out the term $z_a(p)$ yields

7. Referring to Figure 64, this condition corresponds to the fact that the currents I_1, I_2, ..., I_n are identically zero.

$$\left[z_a(p)\right]^n \det \begin{bmatrix} \frac{Z_a(p)+z_A(p)}{z_a(p)} & a_{12} & a_{13} & \cdots & a_{1n} \\ a_{12} & \frac{Z_a(p)+z_A(p)}{z_a(p)} & a_{23} & \cdots & a_{2n} \\ \vdots & \vdots & & \ddots & \vdots \\ a_{1n} & a_{2n} & a_{3n} & \cdots & \frac{Z_a(p)+z_A(p)}{z_a(p)} \end{bmatrix} = 0 \tag{181}$$

A key step in our derivation is now to identify the main diagonal terms as

$$\frac{Z_a(p) + z_A(p)}{z_a(p)} = -\lambda(p) \tag{182}$$

and recognize that the stability problem can be formulated as an associated eigenvalue problem. Using Eq. (182), the determinantal equation (181) can be written simply as

$$\left[z_a(p)\right]^n \det\left[\underline{A} - \lambda(p)\, \underline{I}\right] = 0 \tag{183}$$

where $\underline{A}$ is an n x n <u>constant</u> matrix defined by

$$\underline{A} = \begin{bmatrix} 0 & a_{12} & a_{13} & \cdots & a_{1n} \\ a_{12} & 0 & a_{23} & \cdots & a_{2n} \\ \vdots & \vdots & 0 & & \vdots \\ \vdots & \vdots & \vdots & \ddots & \vdots \\ a_{1n} & a_{2n} & a_{3n} & \cdots & 0 \end{bmatrix} \tag{184}$$

Except for the factor $[z_a(p)]^n$ and the dependence of λ on p via Eq. (182), Eq. (183) is in the standard form of the characteristic equation of the matrix $\underline{A}$. For stability, we require Eq. (183) to have no roots in the entire closed right-half p-plane. A necessary condition for stability is obviously that $z_a(p)$ can have no zeros in the closed right-half p-plane [$z_a(p)$ cannot have poles in right-half plane since the antenna array is passive]. Attention is now concentrated on studying the eigenvalues of the constant matrix $\underline{A}$.

Let the eigenvalues of $\underline{A}$ be denoted by λ_i, i = 1, 2, ..., n. Discarding the factor, $[z_a(p)]^n$, Eq. (183) can be written equivalently as

$$\prod_{i=1}^{n} \left| \lambda(p) - \lambda_i \right| = 0 \tag{185}$$

Since the matrix $\underline{A}$ is real and symmetric, all the eigenvalues are <u>real</u>. The dominanting term of Eq. (185) as far as stability is concerned is the factor associated with the maximum positive eigenvalue denoted by λ_{max}.

Thus the stability problem of the active array shown in Figure 64 is now reduced simply to requiring that the equation

$$\lambda(p) - \lambda_{max} = 0 \tag{186}$$

must have no zeros in the closed right-half p-plane. Substituting Eq. (182) into Eq. (186), we obtain

$$\frac{Z_a(p) + z_A(p)}{z_a(p)} + \lambda_{max} = 0 \tag{187}$$

which, in effect, assumes the role of a "characteristic" equation for the stability of the active array, in the sense that it completely delineates the stability behavior of the active array.

6.3 STABILITY CRITERIA FOR ACTIVE ARRAYS WITH n IMBEDDED ACTIVE ONE-PORTS (17)

The general stability theory is now applied to several active arrays with n imbedded tunnel diode amplifiers. It is assumed that the tunnel diodes are identical, and represented by the usual lumped equivalent circuit consisting of r_s (spreading resistance), L (parasitic series inductance), C (junction capacitance), and -R (negative resistance). Denoting the diode impedance by $z_D(p)$, we have

$$z_D(p) = r_s + pL + \frac{R}{pRC - 1}$$

$$= \frac{p^2(LCR) + p\left(r_s CR - L\right) + \left(R - r_s\right)}{pRC - 1} \tag{188}$$

For simplicity, it is assumed that z_D is the same as z_A without considering explicitly the effect of the matching network (see Figure 64).

Consider first a simple antenna array in which it is assumed that the antenna impedance is real $\left(Z_a = R_a \text{ and } z_a = r_a\right)$ and that the mutual coupling exists only between antenna elements which are adjacent to one another. For this case, the n x n matrix $\underline{A}$ of Eq. (184) is given simply by

$$\underline{A} = \begin{bmatrix} 0 & 1 & & 0 \\ 1 & 0 & \ddots & \\ & \ddots & \ddots & 1 \\ 0 & & 1 & 0 \end{bmatrix} \tag{189}$$

The eigenvalues of this matrix can be obtained analytically for arbitrary n as

$$\lambda_i = -2 \cos\left(\frac{i\pi}{n+1}\right), \quad i = 1, 2, \ldots, n \tag{190}$$

Furthermore, the maximum eigenvalue is given by

$$\lambda_{max} = 2 \cos\left(\frac{\pi}{n+1}\right) \tag{191}$$

For example, $\lambda_{max} = \sqrt{2}$ for $n = 3$, $\lambda_{max} = 1.618$ for $n = 4$, and $\lambda_{max} = \sqrt{3}$ for $n = 5$, etc.

Substituting Eqs. (188) and (191) into Eq. (187), the stability criteria for this class of active array can be written analytically for arbitrary n as

$$2\left[\cos\left(\frac{\pi}{n+1}\right)\right]\left(\frac{r_a}{R}\right) + \frac{L}{R^2 C} < \frac{r_s + R_a}{R} < 1 - 2\left[\cos\left(\frac{\pi}{n+1}\right)\right]\left(\frac{r_a}{R}\right) \tag{192}$$

Before we treat the next class of active arrays, it should be mentioned that, in general, λ_{max} cannot be obtained analytically except for special cases. If all the elements of the matrix $\underline{A}$ are non-negative, then various bounds exist on λ_{max}. One of the simplest ones, due to Frobenius, states that[18]

$$k \leq \lambda_{max} \leq K \tag{193}$$

where k and K are, respectively, the minimum and maximum row sums of the non-negative matrix. Applying this result to Eq. (189), $k = 1$ and $K = 2$, independent of the size of the array n. Thus

$$1 \leq \lambda_{max} \leq 2 \tag{194}$$

for <u>any</u> n. The upper bound on λ_{max} can be used as a simple <u>sufficient</u> condition for stability regardless of the size of the array.

Consider a more general class of active array where mutual coupling between nonadjacent antenna elements exists. In particular, consider an array with equally spaced elements and assume that the mutual coupling varies inversely proportional to the square of the spacing of the elements. The n x n matrix $\underline{A}$ is now given by

$$\underline{A}_n = \begin{bmatrix} 0 & 1 & a_1 & a_2 & \cdots & a_{n-2} \\ 1 & 0 & 1 & a_1 & & \vdots \\ a_1 & & & & & \\ a_2 & & & & & \\ \vdots & & & & & a_2 \\ & & & & & a_1 \\ & & & & & 1 \\ a_{n-2} & \cdots & a_2 & a_1 & 1 & 0 \end{bmatrix} \tag{195}$$

where

$$a_k = \frac{1}{(k+1)^2}, \quad k = 1, 2, \ldots, n-2 \tag{196}$$

It is known that the maximum eigenvalue of an non-negative matrix is positive and it is bounded by the maximum and minimum row sums of the matrix. Let the maximum row sum be denoted by K. Then a sufficient condition for this class of active array is given by

$$K\left(\frac{r_a}{R}\right) + \frac{L}{R^2 C} < \frac{r_s + R_a}{R} < 1 - K\left(\frac{r_a}{R}\right) \tag{197}$$

For the purpose of illustration, consider n = 3. We have

$$\underline{A} = \begin{bmatrix} 0 & 1 & \frac{1}{4} \\ 1 & 0 & 1 \\ \frac{1}{4} & 1 & 0 \end{bmatrix} \tag{198}$$

The eigenvalues of $\underline{A}$ are

$$\lambda_1 = 1.545$$

$$\lambda_2 = -0.25$$

$$\lambda_3 = -1.245$$

Thus, $\lambda_{max} = 1.545$ for n = 3.[8] The minimum row sum is given by k = 1.25 and the maximum row sum is given by K = 2. Using the calculated λ_{max}, the exact stability criterion is obtained. Substitution of the maximum row sum K = 2 into Eq. (197) yields a sufficient condition for stability.

8. Note that for the first array with no nonadjacent coupling, the λ_{max} for n = 3 is given by $\lambda_{max} = \sqrt{2} = 1.414$. The present case yields more stringent stability criterion, as it should be.

For n = 4 (2 x 2 array), we have

$$\underline{A} = \begin{bmatrix} 0 & 1 & \frac{1}{4} & \frac{1}{9} \\ 1 & 0 & 1 & \frac{1}{4} \\ \frac{1}{4} & 1 & 0 & 1 \\ \frac{1}{9} & \frac{1}{4} & 1 & 0 \end{bmatrix} \tag{199}$$

The minimum and maximum row sums of this matrix are given, respectively, by k = 1.36 and K = 2.25. Thus, $1.36 \leq \lambda_{max} \leq 2.25$.

The eigenvalues for this class of $\underline{A}$ matrix for n up to 25 (5 x 5 array) have been calculated on the computer and the results are tabulated in Table 1.

It is interesting that it is possible to derive a simple sufficient condition for the stability of this class of active arrays which is independent of the size of the array and is valid for an infinite array of this type. The matrix $\underline{A}$ for general n is defined by Eqs. (195) and (196). As n approaches infinity, the minimum row sum of $\underline{A}$ approaches

$$k_{\infty} = \sum_{i=0}^{\infty} \frac{1}{(i)^2} = \frac{\pi^2}{6} = 1.667 \tag{200}$$

and the maximum row sum of A approaches

$$K_{\infty} = 2 \sum_{i=0}^{\infty} \frac{1}{(i)^2} = \frac{\pi^2}{3} = 3.334 \tag{201}$$

TABLE 1

COMPUTED MAXIMUM EIGENVALUES λ_{max} FOR
CASE 1: EQ. (189); CASE 2: EQ. (195) AND (196)

n	CASE 1	CASE 2
3	1.4142	1.5447
4	1.6180	1.8822
5	1.7320	2.1109
6	1.8019	2.2759
7	1.8478	2.4004
8	1.8794	2.4977
9	1.9021	2.5758
10	1.9190	2.6399
11	1.9319	2.6935
12	1.9419	2.7388
13	1.9499	2.7778
14	1.9563	2.8116
15	1.9616	2.8412
16	1.9659	2.8674
17	1.9696	2.8906
18	1.9727	2.9115
19	1.9753	2.9303
20	1.9777	2.9473
21	1.9796	2.9627
22	1.9814	2.9768
23	1.9829	2.9898
24	1.9842	3.0017
25	1.9854	3.0127

Thus, for an infinite array of this type,

$$k_\infty = 1.667 \leq \lambda_{max} \leq 3.334 = K_\infty \tag{202}$$

Clearly, for an array with arbitrary size, the maximum eigenvalue is bounded by $K_\infty = 3.334$. Therefore, for an array of this type, a sufficient condition which is <u>independent</u> of the array size is given by Eq. (197) in which K is replaced by K_∞ derived above.

Finally, we consider a class of array described by

$$\underline{A} = \begin{bmatrix} 0 & 1 & 1 & 1 & \cdots & 1 \\ 1 & 0 & \ddots & & & \vdots \\ 1 & \ddots & \ddots & \ddots & & \vdots \\ 1 & & \ddots & \ddots & \ddots & \vdots \\ \vdots & & & \ddots & \ddots & 1 \\ 1 & \cdots & \cdots & \cdots & 1 & 0 \end{bmatrix} \tag{203}$$

The model used in this class probably does not have the physical basis as do the previous two classes. It is treated here merely to illustrate the important effects of the mutual coupling on the stability of active arrays.

For this class of array, the problem can be solved analytically. Note that the minimum and maximum row sums of $\underline{A}$ in Eq. (203) are equal and are given by (n-1). Hence, the maximum eigenvalue is precisely equal to (n-1) and the stability criterion is contained in

$$(n-1)\left(\frac{r_a}{R}\right) + \frac{L}{R^2 C} < \frac{r_s + R_a}{R} < 1 - (n-1)\left(\frac{r_a}{R}\right) \tag{204}$$

In contrast to the previous two classes we have treated, Eq. (204) states that there exists a maximum array size such that any array of this type with n exceeding this maximum will be unstable. The fact that a maximum array size exists for this class of array is not surprising since, as defined in Eq. (203), the mutual couplings are equal. Therefore, as n increases, the effect of the mutual coupling will become increasingly important. Note that for the previous two classes (which represent more physically meaningful models for the antenna array), this is not the case. In fact, as n increases, the λ_{max} converges to a well-defined limit (for the first class, the limit is $\lambda_{max} = 2$ and for the second class, the limit is $\lambda_{max} = 3.334$), so that the stability is not critically dependent on the size of the array as n increases. This latter conclusion is also what one would expect for the array models we have chosen.

The stability criteria presented in this section contain design tradeoffs between r_a, n, and R_a determining, respectively, the amount of antenna mutual coupling, the size of the array, and the gain of the system. The bounds specified in the stability criteria are, of course, dependent on the parameters of the active elements. The mutual coupling coefficient denoted by r_a is a design parameter and is determined primarily by the antenna type and the physical configuration of the array.

6.4 STABILITY OF ACTIVE VAN ATTA ARRAYS

The stability theory and techniques presently in the previous sections can be applied to other classes of general active arrays. In this section, the stability of various configurations of active Van Atta arrays are studied. It is shown that the stability can again be formulated as a matrix eigenvalue problem. The mutual coupling of the antenna elements plays an important role in the stability of this class of active arrays.

Figure 65(a) shows an active bilateral Van Atta array using 2n antenna elements and n negative resistance amplifiers. The coupling networks denoted by C are lossless reciprocal 3-ports. The bilateral amplifiers used in this class of active array have been analyzed in paragraphs 5.2 and 5.3 (see Figures 53 to 55) and include the special case of the direct-coupled amplifiers shown in Figure 56. The schematic circuit diagram of this class of active

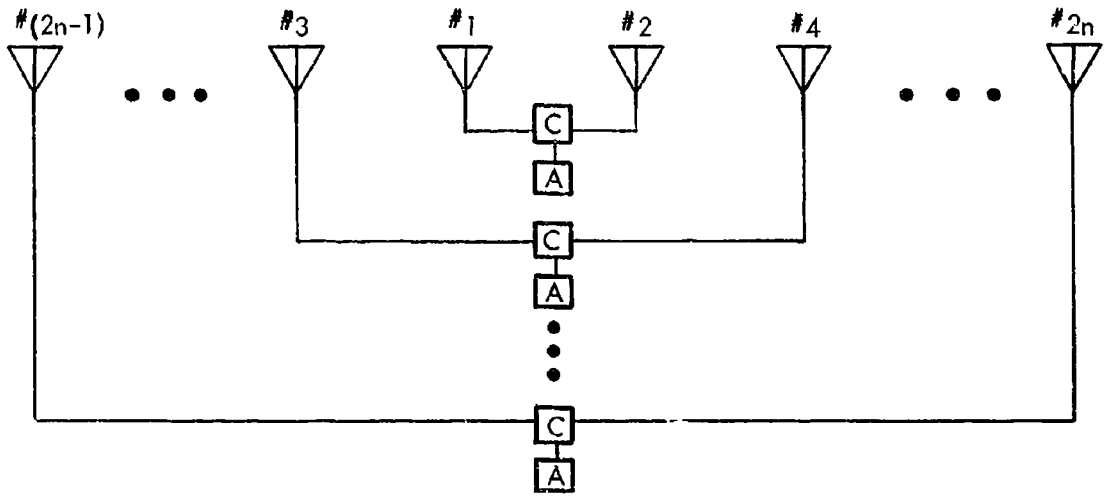

C: LOSSLESS RECIPROCAL 3-PORT

(a)

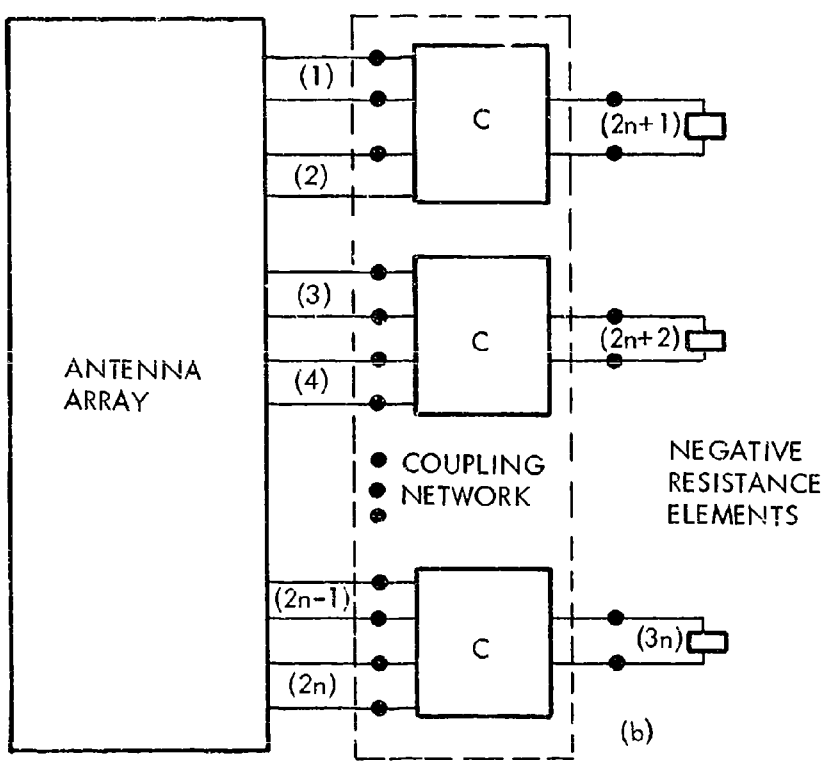

Figure 65. Active Bilateral Van Atta Array Using 3-Port Coupling Networks and n Negative Resistance Amplifiers

array is shown in Figure 65(b). Note that if we lump the coupling networks with the antenna array, which is represented by a 2n-port, then we obtain an equivalent passive n-port which is terminated in n independent negative resistance elements. The stability problem of this active array is now equivalent to the case studied in the previous section and the techniques involving the matrix eigenvalue can now be applied without any modification.

Figure 66 shows an active bilateral Van Atta array using 2n antenna elements and 2n bilateral negative resistance elements. The coupling networks are 4-port networks representing either quadrature hybrids or 4-port circulators. Note that this class of active Van Atta array is bilateral. The individual amplifier configurations have been studied in paragraphs 5.3.1 and 5.3.5. As shown in Figure 66(b), if we lump the 4-port coupling networks with the antenna array, then the problem reduces to that of an equivalent 2n-port terminated in 2n independent negative resistance elements.

An active unilateral Van Atta array using n 4-port circulator-coupled negative resistance amplifiers is shown in Figure 67(a). The individual unilateral amplifiers have been studied in paragraph 5.4.3. In Figure 67(b), the equivalent n-port is terminated in n independent negative resistance elements.

In these figures, the arrays are shown as linear equi-spaced arrays. This is done only for ease in illustration. The theory to be presented is applicable, in general, to arbitrary linear or planar array configurations. The only restriction to be placed on the form of mutual coupling is that stated in paragraph 6.2.

We now proceed to show that, in general, the stability problem of these active Van Atta arrays can be reduced to a matrix eigenvalue formulation. In the next section, explicit stability criteria of specific active Van Atta arrays are derived.

Consider a prescribed n-port defined by its n x n scattering matrix $\underset{\sim}{\tilde{S}}$.

$$\underset{\sim}{b} = \underset{\sim}{\tilde{S}}\, \underset{\sim}{a} \qquad (205)$$

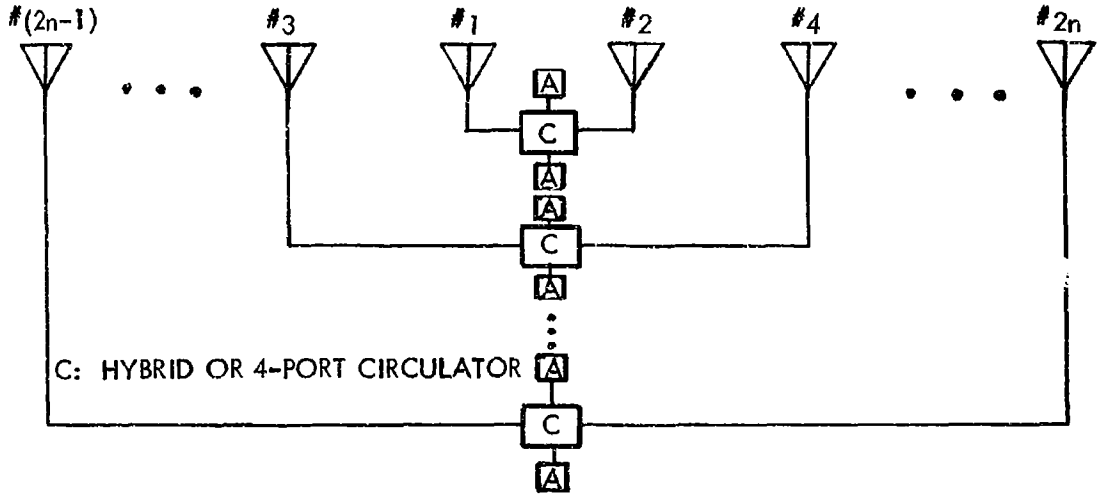

(a)

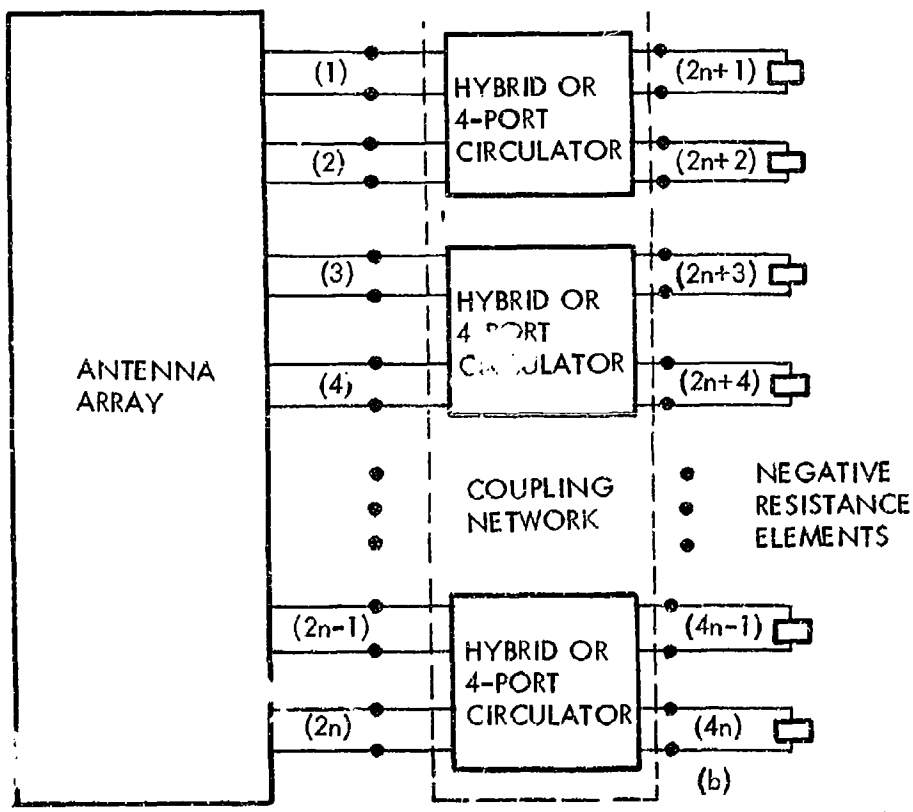

(b)

Figure 66. Active Bilateral Van Atta Array Using 2n Hybrid or 4-Port Circulator-Coupled Negative Resistance Amplifiers

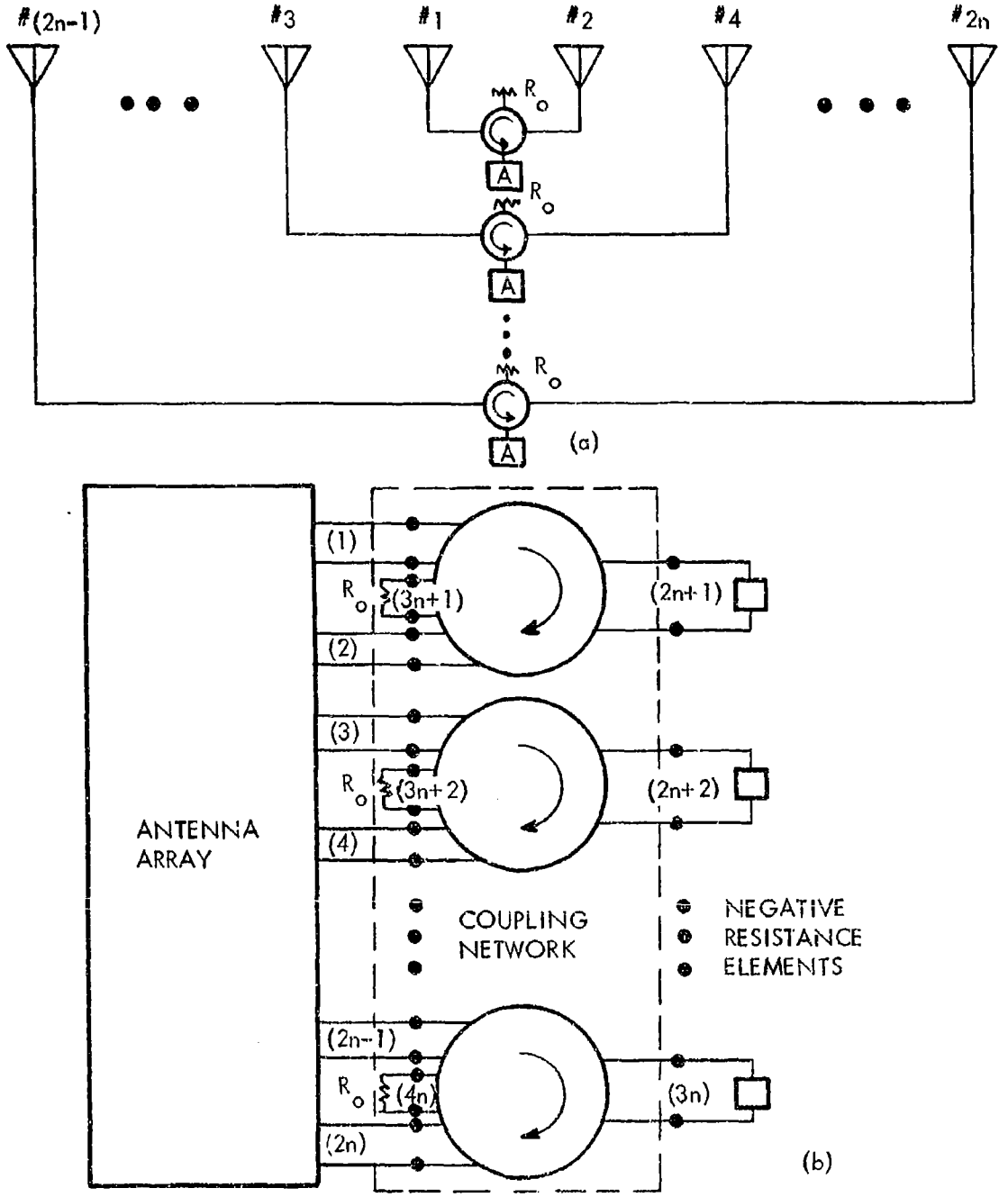

Figure 67. Active Unilateral Van Atta Array Using n 4-Port Circulator-Coupled Negative Resistance Amplifiers

If the n-port is terminated in n uncoupled impedances described by

$$a_i = \Gamma_i b_i, \quad i = 1, 2, \ldots, n \tag{206}$$

then

$$\underset{\sim}{b} = \underline{\Gamma}^{-1} \underset{\sim}{a} \tag{207}$$

$$\underline{\Gamma} = \text{diag}\left|\Gamma_1, \Gamma_2, \ldots, \Gamma_n\right| \tag{208}$$

Substitution of Eq. (207) into Eq. (205) yields

$$\underline{\tilde{S}}\, \underset{\sim}{a} = \underline{\Gamma}^{-1} \underset{\sim}{a}$$

or

$$\left[\underline{\tilde{S}} - \underline{\Gamma}^{-1}\right] \underset{\sim}{a} = \underset{\sim}{0} \tag{209}$$

For stability, the incident waves $\underset{\sim}{a}$ must be identically equal to zero. Thus, the determinantal equation

$$\det\left|\underline{S}(p) - \underline{\Gamma}^{-1}(p)\right| = 0 \tag{210}$$

must have no zero in the closed right-half p-plane, $\text{Re}(p) \geq 0$.

Let the n-port be the equivalent network incorporating the antenna array and the coupling networks, and let the terminating impedances correspond to the negative resistance elements; then the statement contained in Eq. (210) can be formulated as a matrix

eigenvalue problem if we assume that the negative resistance elements are identical. This formulation is equivalent to Eq. (180) which was based on the impedance matrix of the antenna array.

In Figures 65 to 67, the coupling networks are incorporated with the antenna array to derive an equivalent multiple-port network which is terminated in a set of uncoupled impedances denoted by the reflection coefficients Γ_i. Once this is done, it is clear that the general techniques presented in paragraphs 6.2 and 6.3 are applicable. It should be noted that we are treating active Van Atta arrays in which the active elements are composed of 1-port negative resistance amplifiers coupled by hybrids or circulators. We may use unilateral 2-port amplifiers as in Figure 67, but these unilateral amplifiers are realized by using 4-port circulators and 1-port reflection amplifiers. This decomposition is an important feature which allows us to apply the techniques to general antenna mutual coupling and nonideal coupling networks. If the unilateral amplifiers are actually transistor amplifiers, for example, then more elaborate techniques must be used to study the stability problem.

6.5 STABILITY CRITERIA OF SOME ACTIVE VAN ATTA ARRAYS

This section presents explicit stability criteria of some specific active Van Atta arrays. In particular, several configurations are analyzed in detail to compare Van Atta arrays using bilateral and unilateral amplifiers. It is shown that the effect of mutual coupling on the bilateral case is much more critical than the corresponding unilateral case. It should be emphasized that although only simple Van Atta arrays are treated in this section, the techniques presented here are applicable to Van Atta arrays of arbitrary complexity. In the more general case, numerical computations of matrix eigenvalues are necessary.

6.5.1 Two-Element Bilateral Case

Consider first the simplest case having two antenna elements with arbitrary mutual coupling. The active elements are either bilateral or unilateral as shown in Figures 68 and 69. In both cases, a 4-port circulator is used.

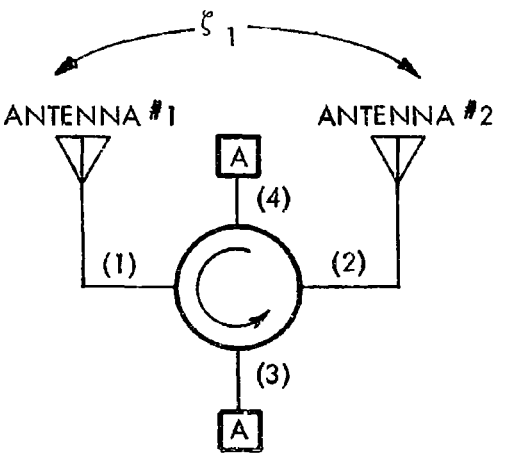

(a)

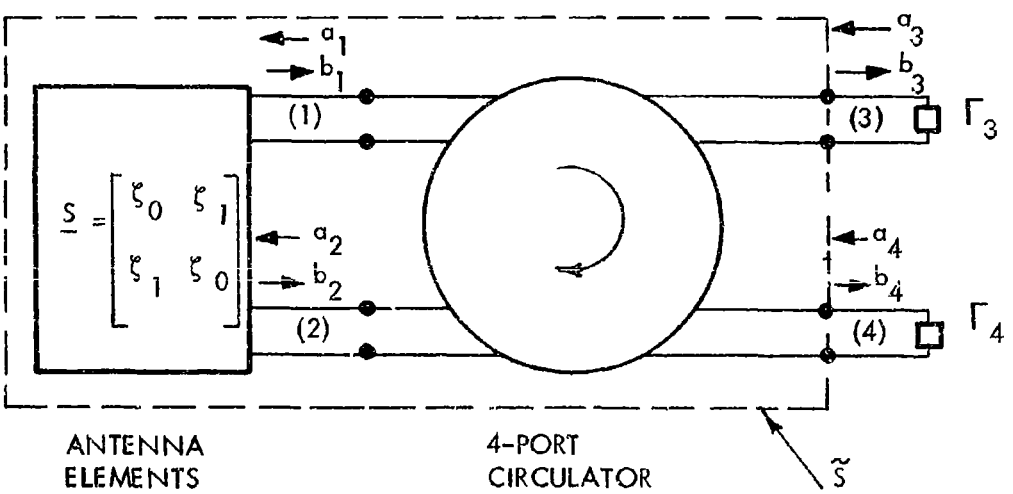

(b)

Figure 68. Two Element Bilateral Active Van Atta Array

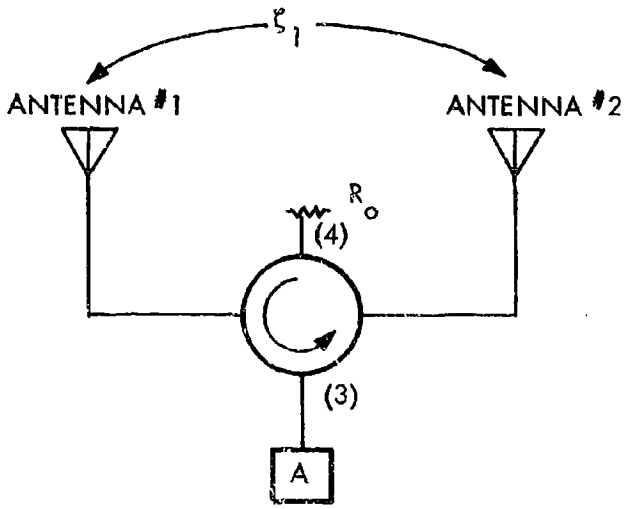

(a)

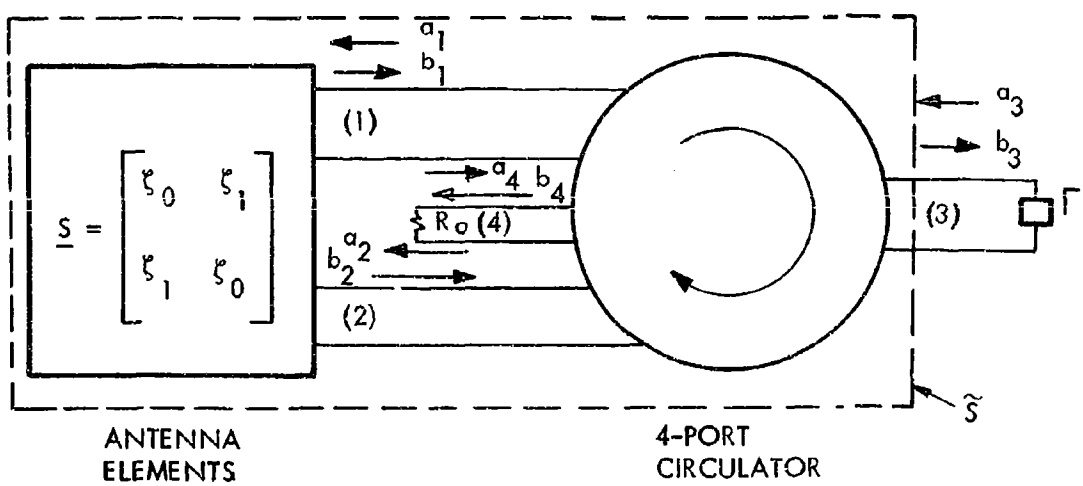

(b)

Figure 69. Two Element Unilateral Van Atta Array

Referring to Figure 68, let the antenna array be represented by

$$\begin{bmatrix} b_1 \\ b_2 \end{bmatrix} = \underline{S} \begin{bmatrix} a_1 \\ a_2 \end{bmatrix} \tag{211}$$

$$\underline{S} = \begin{bmatrix} \zeta_0 & \zeta_1 \\ \zeta_1 & \zeta_0 \end{bmatrix} \tag{212}$$

where ζ_0 and ζ_1 are measures of antenna match and mutual coupling. The scattering matrix of the 4-port circular has been presented in Eq. (129). Noting the direction of the incident and reflected waves in Figure 68(b), we have

$$\left[\begin{array}{c} a_1 \\ a_2 \\ \hline b_3 \\ b_4 \end{array}\right] = \left[\begin{array}{cc:cc} \gamma & \eta & \beta_1 & \alpha_2 \\ \eta & \gamma & \alpha_2 & \beta_1 \\ \hdashline \alpha_1 & \beta_2 & r_1 & n_2 \\ \beta_2 & \alpha_1 & n_2 & r_1 \end{array}\right] \left[\begin{array}{c} b_1 \\ b_2 \\ \hline a_3 \\ a_4 \end{array}\right] \tag{213}$$

Partitioning the 4 x 4 matrix as shown, we have

$$\begin{bmatrix} a_1 \\ a_2 \end{bmatrix} = \begin{bmatrix} \gamma & \eta \\ \eta & \gamma \end{bmatrix} \begin{bmatrix} b_1 \\ b_2 \end{bmatrix} + \begin{bmatrix} \beta_1 & \alpha_2 \\ \alpha_2 & \beta_1 \end{bmatrix} \begin{bmatrix} a_3 \\ a_4 \end{bmatrix} \tag{214}$$

$$\begin{bmatrix} b_3 \\ b_4 \end{bmatrix} = \begin{bmatrix} \alpha_1 & \beta_2 \\ \beta_2 & \alpha_1 \end{bmatrix} \begin{bmatrix} b_1 \\ b_2 \end{bmatrix} + \begin{bmatrix} \gamma & \eta \\ \eta & \gamma \end{bmatrix} \begin{bmatrix} a_3 \\ a_4 \end{bmatrix} \tag{215}$$

Substitution of Eqs. (211) and (214) into Eq. (215), we obtain

$$\begin{bmatrix} b_3 \\ b_4 \end{bmatrix} = \underline{S} \begin{bmatrix} a_3 \\ a_4 \end{bmatrix} \tag{216}$$

where $\underline{\tilde{S}}$ is the scattering matrix of equivalent 2-port [Figure 68(b)] given by

$$\underline{\tilde{S}} = \begin{bmatrix} \gamma & \eta \\ \eta & \gamma \end{bmatrix} + \begin{bmatrix} \alpha_1 & \beta_2 \\ \beta_2 & \alpha_1 \end{bmatrix} \left\{ \begin{bmatrix} \zeta_0 & \zeta_1 \\ \zeta_1 & \zeta_0 \end{bmatrix}^{-1} - \begin{bmatrix} \gamma & \eta \\ \eta & \gamma \end{bmatrix} \right\}^{-1} \begin{bmatrix} \beta_1 & \alpha_2 \\ \alpha_2 & \beta_1 \end{bmatrix} \tag{217}$$

The 1-port negative resistance amplifiers at port 3 and port 4 are described by

$$a_3 = \Gamma_3 b_3 \tag{218}$$

and

$$a_4 = \Gamma_4 b_4 \tag{219}$$

From (210), we now have

$$\det \left\{ \underline{\tilde{S}} - \begin{bmatrix} \frac{1}{\Gamma_3} & 0 \\ 0 & \frac{1}{\Gamma_4} \end{bmatrix} \right\} = 0 \tag{220}$$

where $\underline{\tilde{S}}$ is defined in Eq. (217). If $\Gamma_3 = \Gamma_4 = \Gamma$, then Eq. (220) is in the form of an eigenvalue problem of the 2 x 2 matrix $\underline{S}$, with

$\lambda = 1/\Gamma$. For this simple case, Eq. (220) can be solved analytically without assuming that $\Gamma_3 = \Gamma_4$, and explicit stability criteria can be obtained in terms of the antenna parameters ζ_0, ζ_1 and the circulator parameters.

For an ideal, but mismatched 4-port circular ($\gamma \neq 0$) we have from Eqs. (217) and (220) that

$$\left[1 - \left(\zeta_0\gamma + \zeta_1 \frac{\Gamma_3}{1 - \gamma\Gamma_3}\right)\right]\left[1 - \left(\zeta_0\gamma + \zeta_1 \frac{\Gamma_4}{1 - \gamma\Gamma_4}\right)\right]$$

$$- \left(\zeta_1\gamma + \zeta_0 \frac{\Gamma_3}{1 - \gamma\Gamma_3}\right)\left(\zeta_1\gamma + \zeta_0 \frac{\Gamma_4}{1 - \gamma\Gamma_4}\right) = 0 \qquad (221)$$

where the parameters ζ_0, ζ_1, and γ, as well as the reflection coefficients Γ_3 and Γ_4, can be functions of the complex frequency variable p. For stability, the characteristic equation (220) cannot have any zeros in the entire closed right-half p-plane. This is an explicit stability criterion which shows the interrelationship among the following parameters: antenna match (ζ_0), antenna mutual coupling (ζ_1), circulator reflection coefficient (γ), and the gain of the amplifiers (Γ_3 and Γ_4). If $\gamma = 0$, then the characteristic equation (221) simplifies to

$$\left(1 - \zeta_1\Gamma_3\right)\left(1 - \zeta_1\Gamma_4\right) - \zeta_0^2\,\Gamma_3\Gamma_4 = 0 \qquad (222)$$

If, in addition, $\Gamma_3 = \Gamma_4 = \Gamma$, then Eq. (222) reduces to

$$\left|1 - (\zeta_1 - \zeta_0)\Gamma\right|\,\left|1 - (\zeta_1 + \zeta_0)\Gamma\right| = 0 \qquad (223)$$

Thus, for this case, a sufficient stability condition is given by

$$\Gamma < \frac{1}{|\zeta_1| + |\zeta_0|} \qquad (224)$$

It is noted that for this simple bilateral case, stability is critically dependent on the antenna mutual coupling as well as the match of the antenna elements. There exists, in fact, a direct tradeoff between the gain of the system and the allowable mutual coupling between the antenna elements. The various gain equations persented in Section V are derived for the uncoupled case. When the antenna mutual coupling is taken into account, these results must be modified. In the modified gain equations, the expressions given in Eqs. (221) to (223) will appear in the denominator for the corresponding case.

6.5.2 Two-Element Unilateral Case

The simple two-element unilateral case is shown in Figure 69. This is simular to the bilateral case except that now only one negative resistance element is used and port 4 of the circulator is terminated in a matched dummy load R_0. Equations (212) to (216) are still valid. Instead of Eqs. (218) and (219), we now have

$$a_3 = \Gamma b_3 \tag{225}$$

and

$$a_4 = 0 \tag{226}$$

Using Eq. (226), the equivalent network is a simple 1-port. The characteristic equation for this case is given by

$$\tilde{S} - \frac{1}{\Gamma} = 0 \tag{227}$$

where $\tilde{S}$ is a scalar given by

$$\tilde{S} = \gamma + \begin{bmatrix} \alpha_1 & \beta_2 \end{bmatrix} \left\{ \begin{bmatrix} \zeta_0 & \zeta_1 \\ \zeta_1 & \zeta_0 \end{bmatrix}^{-1} - \begin{bmatrix} \gamma & \eta \\ \eta & \gamma \end{bmatrix} \right\}^{-1} \begin{bmatrix} \beta_1 \\ \alpha_2 \end{bmatrix} \quad (228)$$

For a 4-port circulator which is ideal except $\gamma \neq 0$, Eq. (227) becomes

$$\left(1 - \zeta_o\gamma\right)\left[1 - \left(\zeta_o\gamma + \zeta_1 \frac{\Gamma}{1 - \gamma\Gamma}\right)\right] - \zeta_1\gamma\left(\zeta_1\gamma + \zeta_o \frac{\Gamma}{1 - \gamma\Gamma}\right) = 0 \quad (229)$$

If $\gamma = 0$, then it further reduces to

$$1 - \zeta_1\Gamma = 0 \quad (230)$$

for this case, a sufficient condition for stability is

$$\zeta_1\Gamma < 1 \quad (231)$$

This condition is compared with Eq. (224) for the corresponding bilateral case. It is noted that with an ideal 4-port circulator, the stability of the unilateral case is independent of the match of the antenna elements (ζ_o). This is the sharp contrast to the bilateral case in which ζ_o has an important role in determining the stability.

In actual design of active Van Atta arrays, more general stability criteria such as Eqs. (221) and (229) should be used since the importance of the circulator parameters on the stability and gain sensitivity of the device has already been demonstrated in Section V. Techniques presented here can be used to obtain definitive results on the design of active Van Atta arrays.

6.5.3 Linear Four-Element Bilateral Array

A linear four-element bilateral array is shown in Figure 70. This array is equidistant with a separation of "d" between adjacent elements. The mutual coupling coefficients are ζ_1, ζ_2, and ζ_3. As functions of separation, we have

$$\begin{aligned} \zeta_1 &= \zeta(d) \\ \zeta_2 &= \zeta(2d) \\ \zeta_3 &= \zeta(3d) \end{aligned} \tag{232}$$

The general linear four-element array can be described by its scattering matrix $\underline{S}$, as follows:

$$\begin{bmatrix} b_1 \\ b_2 \\ b_3 \\ b_4 \end{bmatrix} = \underbrace{\begin{bmatrix} \zeta_o & \zeta_1 & \zeta_1 & \zeta_2 \\ \zeta_1 & \zeta_o & \zeta_2 & \zeta_1 \\ \zeta_1 & \zeta_2 & \zeta_o & \zeta_3 \\ \zeta_2 & \zeta_1 & \zeta_3 & \zeta_o \end{bmatrix}}_{\underline{S}} \begin{bmatrix} a_1 \\ a_2 \\ a_3 \\ a_4 \end{bmatrix} \tag{233}$$

The scattering matrix of the 4-port circulator, $\underline{S}^{(c)}$, is given by Eq. (129). We can partition this 4 x 4 matrix as

$$\underline{S}^{(c)} = \left[\begin{array}{c|c} \underline{S}_{11}^{(c)} & \underline{S}_{12}^{(c)} \\ \hline \underline{S}_{21}^{(c)} & \underline{S}_{22}^{(c)} \end{array}\right] \tag{234}$$

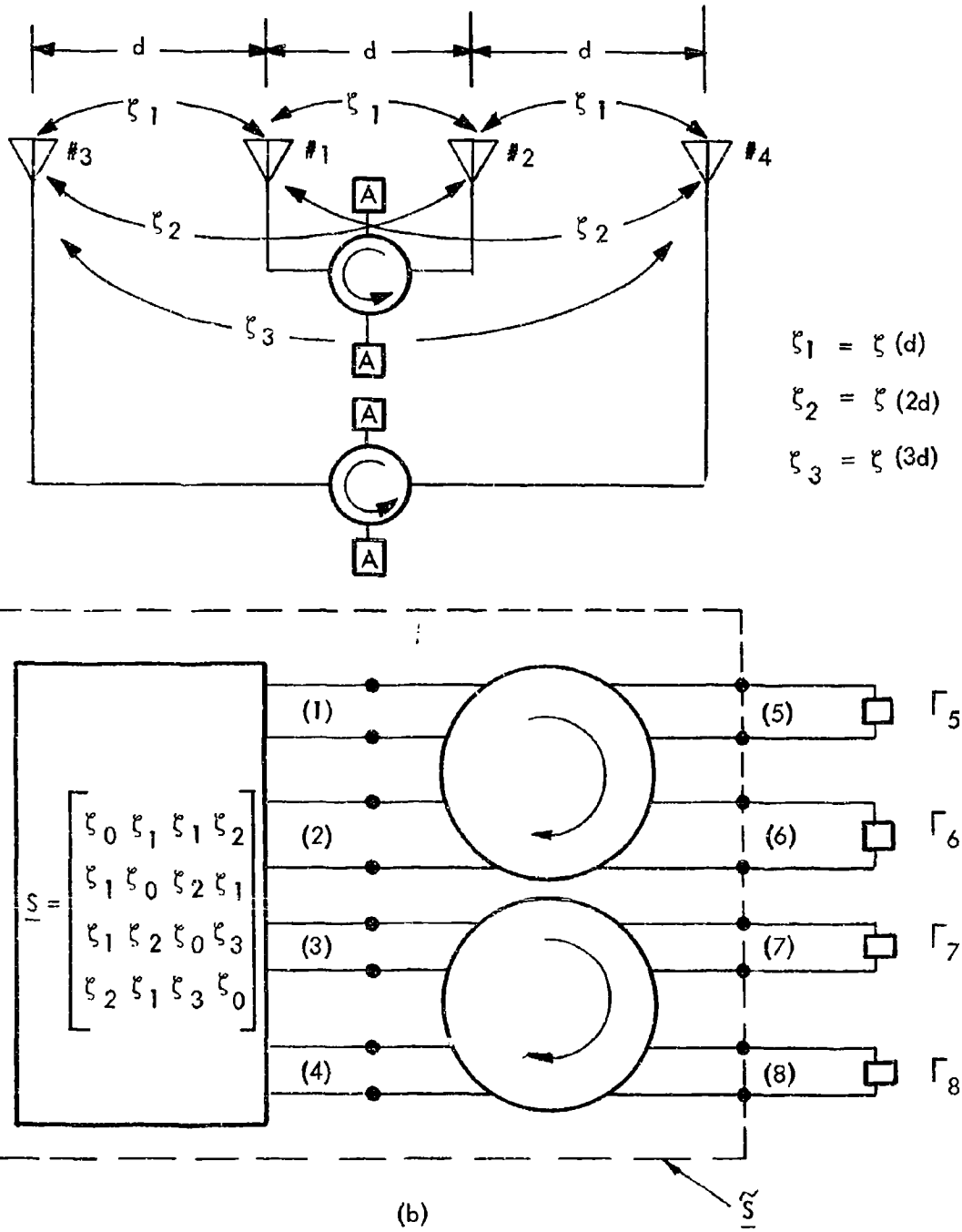

(b)

Figure 70. Linear Four Element Bilateral Active Van Atta Array

where

$$\underline{S}_{11}^{(c)} = \underline{S}_{22}^{(c)} = \begin{bmatrix} \gamma & \eta \\ \eta & \gamma \end{bmatrix} \tag{235}$$

$$\underline{S}_{12}^{(c)} = \begin{bmatrix} \beta_1 & \alpha_2 \\ \alpha_2 & \beta_1 \end{bmatrix} \tag{236}$$

$$\underline{S}_{21}^{(c)} = \begin{bmatrix} \alpha_1 & \beta_2 \\ \beta_2 & \alpha_1 \end{bmatrix} \tag{237}$$

From Figure 70(b), we have

$$\begin{bmatrix} a_1 \\ a_2 \\ \hline b_5 \\ b_6 \end{bmatrix} = \left[\begin{array}{c|c} \underline{S}_{11}^{(c)} & \underline{S}_{12}^{(c)} \\ \hline \underline{S}_{21}^{(c)} & \underline{S}_{22}^{(c)} \end{array}\right] \begin{bmatrix} b_1 \\ b_2 \\ \hline a_5 \\ a_6 \end{bmatrix} \tag{238}$$

$$\begin{bmatrix} a_3 \\ a_4 \\ \hline b_7 \\ b_8 \end{bmatrix} = \left[\begin{array}{c|c} \underline{S}_{11}^{(c)} & \underline{S}_{12}^{(c)} \\ \hline \underline{S}_{21}^{(c)} & \underline{S}_{22}^{(c)} \end{array}\right] \begin{bmatrix} b_3 \\ b_4 \\ \hline a_7 \\ a_8 \end{bmatrix} \tag{239}$$

Rearranging Eqs. (238) and (239), we obtain

$$\begin{bmatrix} a_1 \\ a_2 \\ \hline a_3 \\ a_4 \end{bmatrix} = \left[\begin{array}{c|c} \underline{S}_{11}^{(c)} & \underline{0} \\ \hline \underline{0} & \underline{S}_{11}^{(c)} \end{array}\right] \begin{bmatrix} b_1 \\ b_2 \\ \hline b_3 \\ b_4 \end{bmatrix} + \left[\begin{array}{c|c} \underline{S}_{12}^{(c)} & \underline{0} \\ \hline \underline{0} & \underline{S}_{12}^{(c)} \end{array}\right] \begin{bmatrix} a_5 \\ a_6 \\ \hline a_7 \\ a_8 \end{bmatrix} \tag{240}$$

$$\begin{bmatrix} b_5 \\ b_6 \\ \hline b_7 \\ b_8 \end{bmatrix} = \left[\begin{array}{c|c} \underline{S}_{21}^{(c)} & \underline{0} \\ \hline \underline{0} & \underline{S}_{21}^{(c)} \end{array}\right] \begin{bmatrix} b_1 \\ b_2 \\ \hline b_3 \\ b_4 \end{bmatrix} + \left[\begin{array}{c|c} \underline{S}_{22}^{(c)} & \underline{0} \\ \hline \underline{0} & \underline{S}_{22}^{(c)} \end{array}\right] \begin{bmatrix} a_5 \\ a_6 \\ \hline a_7 \\ a_8 \end{bmatrix} \tag{241}$$

From Eqs. (233) and (240),

$$\begin{bmatrix} b_1 \\ b_2 \\ \hline b_3 \\ b_4 \end{bmatrix} = \left\{ \underline{S}^{-1} - \left[\begin{array}{c|c} \underline{S}_{11}^{(c)} & \underline{0} \\ \hline \underline{0} & \underline{S}_{11}^{(c)} \end{array}\right] \right\}^{-1} \left[\begin{array}{c|c} \underline{S}_{12}^{(c)} & \underline{0} \\ \hline \underline{0} & \underline{S}_{12}^{(c)} \end{array}\right] \begin{bmatrix} a_5 \\ a_6 \\ \hline a_7 \\ a_8 \end{bmatrix} \tag{242}$$

Substitution of Eq. (242) into Eq. (241) yields the scattering matrix of the equivalent 4-port, $\underline{\tilde{S}}$

$$\begin{bmatrix} b_5 \\ b_6 \\ b7 \\ b_8 \end{bmatrix} = \underline{\tilde{S}} \begin{bmatrix} a_5 \\ a_6 \\ a_7 \\ a_8 \end{bmatrix} \tag{243}$$

where

$$\tilde{\underline{S}} = \left[\begin{array}{c|c} \underline{S}_{22}^{(c)} & \underline{0} \\ \hline \underline{0} & \underline{S}_{11}^{(c)} \end{array}\right] + \left[\begin{array}{c|c} \underline{S}_{21}^{(c)} & \underline{0} \\ \hline \underline{0} & \underline{S}_{21}^{(c)} \end{array}\right]$$

$$\left\{\underline{S}^{-1} - \left[\begin{array}{c|c} \underline{S}_{11}^{(c)} & 0 \\ \hline \underline{0} & \underline{S}_{11}^{(c)} \end{array}\right]\right\}^{-1} \left[\begin{array}{c|c} \underline{S}_{12}^{(c)} & \underline{0} \\ \hline \underline{0} & \underline{S}_{12}^{(c)} \end{array}\right] \tag{244}$$

In Eq. (244), $\underline{S}$ is the scattering matrix of the antenna array given by Eq. (233) and $\underline{S}_{11}^{(c)}$, $\underline{S}_{22}^{(c)}$, $\underline{S}_{12}^{(c)}$, and $\underline{S}_{21}^{(c)}$, are submatrices of the circulator defined in Eqs. (235) to (237).

Using

$$a_i = \Gamma_i \, b_i, \quad i = 5, 6, 7, 8 \tag{245}$$

and defining the diagonal matrix

$$\underline{\Gamma} = \text{diag}\left|\Gamma_5, \ \Gamma_6, \ \Gamma_7, \ \Gamma_8\right| \tag{246}$$

the characteristic equation for the stability of this array is given by

$$\det\left|\tilde{\underline{S}} - \underline{\Gamma}^{-1}\right| = 0 \tag{247}$$

This contains the complete solution of stability of the linear four-element active Van-Atta array using bilateral amplification. In this solution, the antenna mutual coupling is arbitrary, the circulators are nonideal, and the negative resistance elements are not assumed to be identical.

To illustrate this result consider the case where the 4-port circulators are assumed to be ideal. The characteristic equation (247) becomes

$$\det \begin{bmatrix} (1 - \zeta_1\Gamma_5) & -\zeta_o\Gamma_6 & -\zeta_2\Gamma_7 & -\zeta_1\Gamma_8 \\ -\zeta_o\Gamma_5 & (1 - \zeta_1\Gamma_6) & -\zeta_1\Gamma_7 & -\zeta_2\Gamma_8 \\ -\zeta_2\Gamma_5 & -\zeta_1\Gamma_6 & (1 - (\zeta_3\Gamma_7) & -\zeta_o\Gamma_8 \\ -\zeta_1\Gamma_5 & -\zeta_2\Gamma_6 & -\zeta_o\Gamma_7 & (1 - \zeta_3\Gamma_8) \end{bmatrix} = 0 \tag{248}$$

If, in addition, it is assumed that $\Gamma_5 = \Gamma_6 = \Gamma_7 = \Gamma_8 = \Gamma$, then Eq. (248) can be evaluated analytically as

$$\left[(1 - \zeta_1\Gamma)(1 - \zeta_3\Gamma) - \Gamma^2\left(\zeta_1^2 + \zeta_2^2\right)\right]^2 - \left(2\zeta_1\zeta_2\Gamma^2\right)^2 + \zeta_o\Gamma^2\left\{\zeta_o\Gamma^2\left[\zeta_o^2 - 2\left(\zeta_1^2 + \zeta_2^2\right)\right] - \left(\zeta_o + 4\zeta_1\zeta_2\Gamma\right)\left[(1 - \zeta_1\Gamma) + (1 - \zeta_3\Gamma)\right]\right\} = 0 \tag{249}$$

If, in addition, $\zeta_o = 0$, then Eq. (249) reduces to

$$\left[(1 - \zeta_1\Gamma)(1 - \zeta_3\Gamma) - \Gamma^2\left(\zeta_1^2 + \zeta_2^2\right)\right]^2 - \left(2\zeta_1\zeta_2\Gamma^2\right)^2 = 0 \tag{250}$$

The characteristic equations for these idealized cases can also be obtained by using signal flow-graph techniques. The loop gain is calculated by considering all the feedback paths. In the more general cases in which feedback paths through the circulators are taken into account, the signal flow technique becomes cumbersome.

The matrix eigenvalue technique is simpler and can be generalized to treat the stability of arrays of arbitrary complexity in a straightforward manner. Well-known numerical techniques are available to accurately compute the eigenvalues of large matrices.

6.5.4 Linear Four-Element Unilateral Array

A linear four-element unilateral array is shown in Figure 71. The mutual coupling coefficients are the same as that defined in Eq. (232). The techniques used in paragraph 6.5.3 are still applicable, but now the equivalent network $\underline{S}$ is a 2-port as shown in Figure 71. Instead of Eq. (245), we have

$$a_5 = \Gamma_5 \, b_5 \, , \qquad a_6 = \Gamma_6 \, b_6 \tag{251}$$

$$a_7 = 0 \, , \qquad a_8 = 0 \tag{252}$$

Using Eq. (252) we obtain

$$\begin{bmatrix} a_1 \\ a_2 \\ \hline b_5 \end{bmatrix} = \left[\begin{array}{cc:c} \gamma & \eta & \beta_1 \\ \eta & \gamma & \alpha_2 \\ \hline \alpha_1 & \beta_2 & \gamma \end{array}\right] \begin{bmatrix} b_1 \\ b_2 \\ \hline a_5 \end{bmatrix} \tag{253}$$

$$\begin{bmatrix} a_3 \\ a_4 \\ \hline b_6 \end{bmatrix} = \left[\begin{array}{cc:c} \gamma & \eta & \beta_1 \\ \eta & \gamma & \alpha_2 \\ \hline \alpha_1 & \beta_2 & \gamma \end{array}\right] \begin{bmatrix} b_3 \\ b_4 \\ \hline a_6 \end{bmatrix} \tag{254}$$

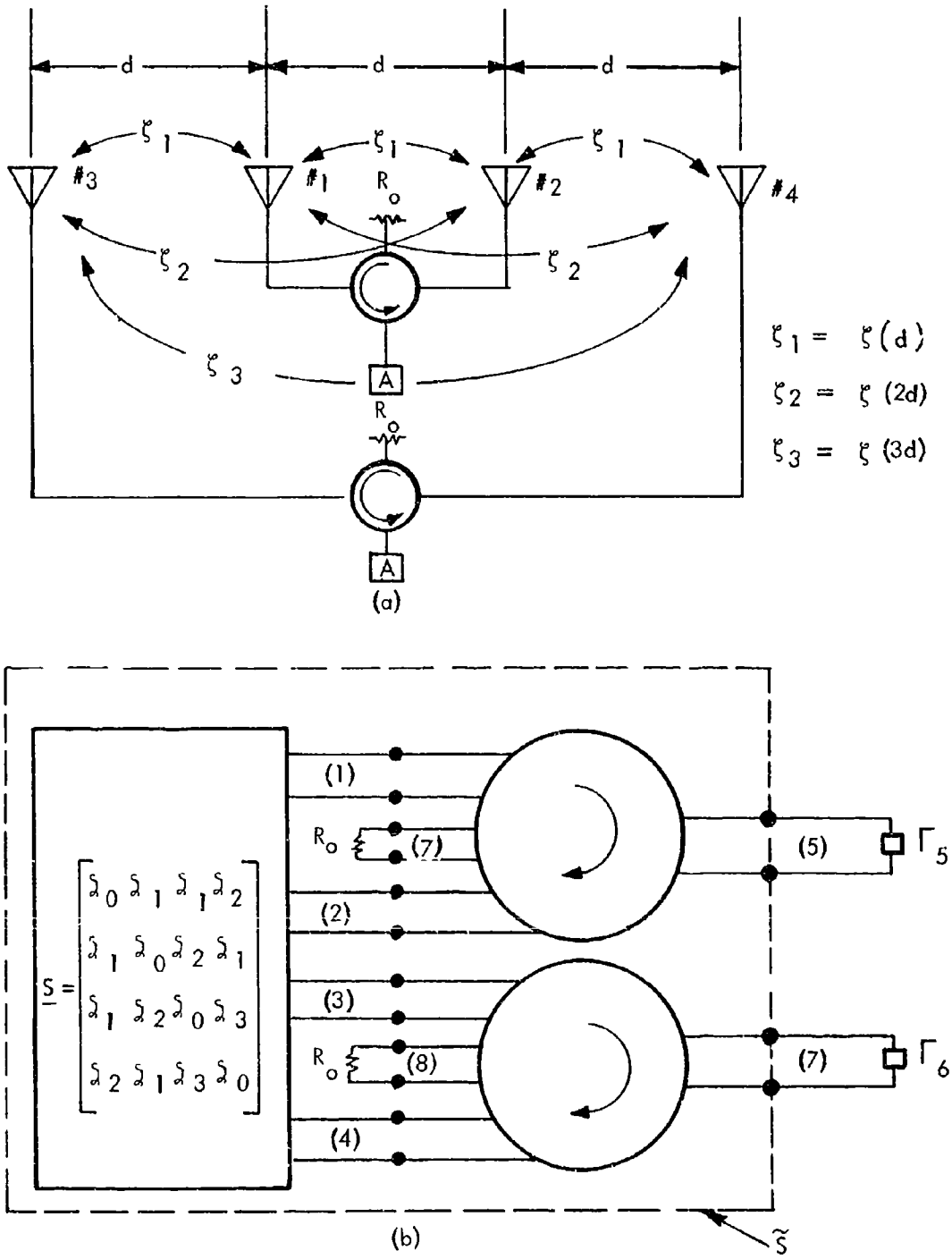

Figure 71. Linear Four Element Unilateral Active Van Atta Array

Rearranging Eqs. (253) and (254), we have

$$\begin{bmatrix} a_1 \\ a_2 \\ \hline a_3 \\ a_4 \end{bmatrix} = \left[\begin{array}{c|c} \underline{S}_{11}^{(c)} & \underline{0} \\ \hline \underline{0} & \underline{S}_{11}^{(c)} \end{array}\right] \begin{bmatrix} b_1 \\ b_2 \\ \hline b_3 \\ b_4 \end{bmatrix} + \left[\begin{array}{c|c} \beta_1 & 0 \\ \alpha_2 & 0 \\ \hline 0 & \beta_1 \\ 0 & \alpha_2 \end{array}\right] \begin{bmatrix} a_5 \\ \hline a_6 \end{bmatrix} \tag{255}$$

$$\begin{bmatrix} b_5 \\ \hline b_6 \end{bmatrix} = \left[\begin{array}{cc|cc} \alpha_1 & \beta_2 & 0 & 0 \\ \hline 0 & 0 & \alpha_1 & \beta_2 \end{array}\right] \begin{bmatrix} b_1 \\ b_2 \\ \hline b_3 \\ b_4 \end{bmatrix} + \left[\begin{array}{c|c} \gamma & 0 \\ \hline 0 & \gamma \end{array}\right] \begin{bmatrix} a_5 \\ \hline a_6 \end{bmatrix} \tag{256}$$

From Eqs. (253) and (259),

$$\begin{bmatrix} b_1 \\ b_2 \\ \hline b_3 \\ b_4 \end{bmatrix} = \left\{ \underline{S}^{-1} - \left[\begin{array}{c|c} \underline{S}_{11}^{(c)} & \underline{0} \\ \hline \underline{0} & \underline{S}_{11}^{(c)} \end{array}\right] \right\}^{-1} \left[\begin{array}{c|c} \beta_1 & 0 \\ \alpha_2 & 0 \\ \hline 0 & \beta_1 \\ 0 & \alpha_2 \end{array}\right] \begin{bmatrix} a_5 \\ \hline a_6 \end{bmatrix} \tag{257}$$

Substituion of Eq. (257) into Eq. (256) yields the scattering matrix of the equivalent 2-port, $\underline{\tilde{S}}$.

$$\begin{bmatrix} b_5 \\ b_6 \end{bmatrix} = \underline{\tilde{S}} \begin{bmatrix} a_5 \\ a_6 \end{bmatrix} \tag{258}$$

where

$$\tilde{\underline{S}} = \begin{bmatrix} \gamma & 0 \\ 0 & \gamma \end{bmatrix} + \left[\begin{array}{cc:cc} \alpha_1 & \beta_2 & 0 & 0 \\ 0 & 0 & \alpha_1 & \beta_2 \end{array}\right] \left\{ \underline{S}^{-1} - \begin{bmatrix} \underline{S}_{11}^{(c)} & \underline{0} \\ \underline{0} & \underline{S}_{11}^{(c)} \end{bmatrix} \right\}^{-1} \left[\begin{array}{c:c} \beta_1 & 0 \\ \alpha_2 & 0 \\ \hdashline 0 & \beta_1 \\ 0 & \alpha_2 \end{array}\right] \tag{259}$$

Using Eq. (251) and defining

$$\underline{\Gamma} = \text{diag} \left| \Gamma_5, \ \Gamma_6 \right| \tag{260}$$

the characteristic equation for stability is given by

$$\det \left| \tilde{\underline{S}} - \underline{\Gamma}^{-1} \right| = 0 \tag{261}$$

where $\tilde{\underline{S}}$ is presented in Eq. (259). Thus, the stability of the linear four-element unilateral Van Atta array is completely delineated by the determinantal equation of an equivalent 2 x 2 matrix.

To illustrate this general result, consider the case where the 4-port circulators are assumed to be ideal. The characteristic equation is given by

$$\left(1 - \zeta_1 \Gamma_5\right)\left(1 - \zeta_3 \Gamma_6\right) - \zeta_2^2 \Gamma_5 \Gamma_6 = 0 \tag{262}$$

It is noted that for the ideal circulator case, the parameter ζ_0 does not affect the stability of the unilateral array.

If, in addition, $\Gamma_5 = \Gamma_6 = \Gamma$, then Eq. (262) becomes

$$(1 - \varsigma_1\Gamma)(1 - \varsigma_3\Gamma) - \varsigma_2^2\Gamma^2 = 0 \tag{263}$$

This condition should be compared with the result of the corresponding bilateral case presented in Eq. (249).

6.5.5 Planar Four-Element Unilateral Array

Consider the planar four-element Van Atta array shown in Figure 72(a). All the results presented in paragraphs 6.5.3 and 6.5.4 can be applied by redefining the scattering matrix of the array. Instead of Eqs. (232) and (233), we have

$$\begin{aligned} \varsigma_1 &= \varsigma(d) \\ \varsigma_2 &= \varsigma(\sqrt{2}d) \end{aligned} \tag{264}$$

and the scattering matrix of the planar four-element array is given by

$$\underline{S} = \begin{bmatrix} \varsigma_0 & \varsigma_2 & \varsigma_1 & \varsigma_1 \\ \varsigma_3 & \varsigma_0 & \varsigma_1 & \varsigma_1 \\ \varsigma_1 & \varsigma_1 & \varsigma_0 & \varsigma_2 \\ \varsigma_1 & \varsigma_1 & \varsigma_2 & \varsigma_0 \end{bmatrix} \tag{265}$$

To obtain the characteristic equation, Eq. (265) is substituted into Eqs. (244) and (259) respectively, for the bilateral and unilateral array.

For the unilateral case shown in Figure 72, we have

$$\left(1 - \zeta_2\Gamma_5\right)\left(1 - \zeta_2\Gamma_6\right) - \zeta_1^2\Gamma_5\Gamma_6 = 0 \tag{266}$$

which is similar to the result for the linear unilateral array presented in Eq. (262). Note, however, the definition of ζ_2 is different for the two cases (see Eqs. (232) and (264)).

If we assume that $\Gamma_5 = \Gamma_6 = \Gamma$, then Eq. (266) reduces to

$$\left(1 - \zeta_2\Gamma\right)^2 - \zeta_1^2\Gamma^2 = 0 \tag{267}$$

which corresponds to Eq. (263) for the corresponding linear array.

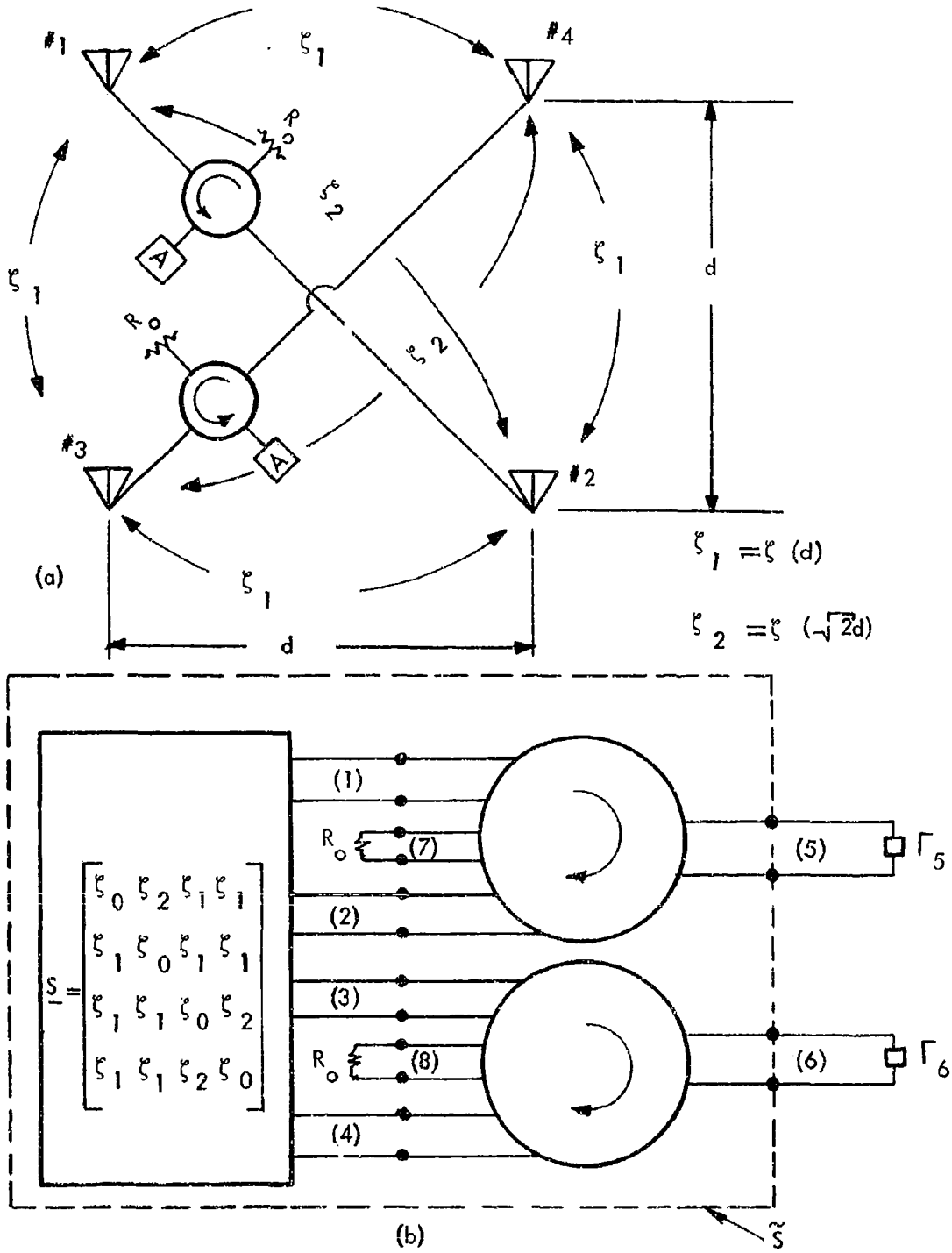

Figure 72. Planar Four Element Unilateral Active Van Atta Array

SECTION VII

CONCLUSIONS AND RECOMMENDATIONS

The present study of active bilateral Van Atta arrays accomplished a number of important objectives. The shunt-tunnel-diode amplifier design originally proposed was shown to be impractical for small arrays, due to the strong interaction of the retrodirected and specular beams. Computed data for the 4 x 4 element case show little evidence of retrodirectivity. It was also shown that "blind incident angles" appear for which no array return occurs at any output angle, in any high gain shunt-diode array for which the inter-antenna spacing exceeds one-half wavelength.

Investigation of the application of bilateral amplifiers to Van Atta arrays yielded several important results. It was learned that the relative values of the antenna element return loss (due to mismatch) and mutual coupling determine whether or not a bidirectional amplifier scheme is practical. For the cavity-backed equiangular spiral, it was shown experimentally that the isolation between antennas can be as high as 60 dB, compared to the 30 dB of return loss achievable with the same antenna and its associated connector. The 30-dB difference is roughly the gain advantage of a unilateral-amplifier array over the same array using bidirectional amplifiers, for comparable gain stability.

Economic considerations seem to dictate that a Van Atta array achieve its gain via its amplifiers rather than through a large number of elements. An increase in array gain of 6 dB can be had either by increasing the amplifier gains by 6 dB, or <u>doubling</u> the number of element pairs. The upper limit on gain (for a unilateral array) is set by the reciprocal of the largest inter-antenna coupling magnitude. Thus, the basic design problem is to devise an antenna system which gives the desired angle coverage, while maintaining the lowest possible coupling between individual elements. If the inter-element coupling sets a gain limit which is too low, or the power levels involved are too high for available amplifiers, then the number of elements must be increased to achieve the required gain. One may, of course, prefer array gain to amplifier gain for reasons of security or interference reduction, dictating the use of many low-gain elements.

Circulator-coupled avalanche-diode amplifiers and transistor amplifiers are very attractive for Van Atta array applications. These devices permit array operation at much higher power levels than is possible with tunnel diodes. The results obtained in the present study can be carried over directly to these devices.

Use of superregenerative circuits should be considered in future active-array investigations. Superregenerative operation of avalanche diodes or transistors will permit very high gains to be achieved in a single-stage circuit, without the gain-stability problems associated with ordinary reflection-type amplifiers. Superregenerative circuits have "built-in" modulation and frequency-shifting capabilities as well. The wide acceptance band and relatively poor noise performance of superregenerative circuits should in no way limit their usefulness for active arrays.

APPENDIX I

AUTOMATED DRAFTING OF SPIRAL ANTENNAS

The principal requirement to be met by the spiral antenna-balun combination considered in Section III was that it be closely matched to the interconnecting transmission line in the vicinity of 4.5 GHz. Flexibility in the fabrication of the antennas was highly desirable in view of the incomplete theoretical and experimental data available.[3] The necessary cut and try procedure was greatly accelerated by an analog computer process, which generated high-contrast negatives, suitable for direct contact-printing onto sensitized copper-clad dielectrics.

Spiral antenna negatives have been drawn by digital computers at Avco.[19] It occurred to us that a second-order linear differential equation could be used to generate spiral curves on an analog computer, and a photograph made of the resulting oscilloscope presentation. Consider the following differential equation for the impulse response x(t) of a second-order damped oscillatory system:

$$\dot{x}(t) + 2\alpha x(t) + \omega_o^2 \int_{-\infty}^{t} x(t)dt = u_o(t)x_o \qquad \text{(I-1)}$$

The solution to Eq. (I-1) is an exponentially damped sinusoid:

$$x(t) = \frac{x_o\, e^{-\alpha t}}{\cos\theta} \cos\left(\omega_d t + \theta\right) \qquad \omega_d \triangleq \sqrt{\omega_o^2 - \alpha^2}$$
$$\theta \triangleq \cos^{-1}\left(\frac{\omega_d}{\omega_o}\right) \qquad \text{(I-2)}$$

If x(t) is plotted in rectangular coordinates against y(t) [the corresponding function of $\sin\left(\omega_d t + \theta\right)$], the resulting point

traces out a spiral of radius $r_o\, e^{-\alpha t}$ at an angular rate ω_d. $y(t)$ is easily made up on the computer from $x(t)$ and $\dot{x}(t)$:

$$y(t) = \frac{x_o\, e^{-\alpha t}}{\cos\theta} \sin\left(\omega_d t + \theta\right) = \frac{-1}{\omega_d}\left[\dot{x}(t) + \alpha x(t)\right] \qquad \text{(I-3)}$$

$$\left|r(t)\right| = \sqrt{x^2(t) + y^2(t)} = \frac{x_o\, e^{-\alpha t}}{\cos\theta} = r_o\, e^{-\alpha t}$$

$$\phi(t) = \omega_d t + \theta \qquad \text{(I-4)}$$

Figure I-1 shows the analog computer program used to generate $x(t)$ and $y(t)$. The initial condition on the second integrator sets x_o, and hence r_o, the maximum radius of the spiral curve. The computer is operated repetitively, so that the system operates for a fixed length of time and then repeats. The operating time and the frequency, ω_d, fix the length of the spiral curve. The initial condition, x_o, is swept at a very slow rate, so that a series of closely nested spirals are drawn on the oscilloscope. The camera shutter is opened at the beginning of the initial-condition sweep cycle. The photo of the nested curves has a constant angular width, as required by the antenna design. Changing the sign of the initial condition on $x(t)$ causes the computer to draw the second antenna arm 180^o away from the first.

Some additional refinements were incorporated into the process. In order to obtain a uniform exposure over each antenna arm, it was necessary to use an exponential blanking-voltage variation, to compensate for the exponential decrease of antenna-arm area toward the center. Total blanking was also necessary between computer cycles. The initial condition was swept using a Tektronix Type T time-base unit, triggered by the repetitive-operation bus of the computer.

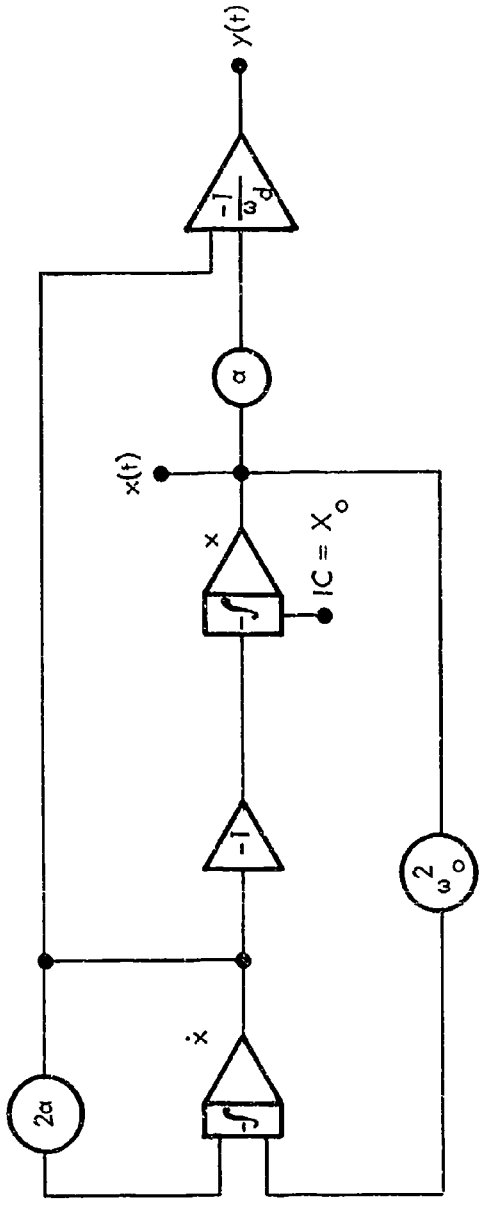

Figure 1-1. Analog Computer Program

REFERENCES

1. A. F. Snyder, "An Active Retrodirective Array with Bilateral Tunnel Diode Amplifiers," RADC-TR-67-163; August 1967.

2. B. Hershenov, "Microstrip Junction Circulator for Microwave Integrated Circuits," IEEE Trans. on Microwave Theory and Techniques, pp. 748-750; December 1967.

3. V. H. Rumsey, Frequency Independent Antennas, Academic Press, New York and London; 1966.

4. J. D. Dyson, "The Equiangular Spiral Antenna," IRE Trans. on Antennas and Propagation, vol. AP-7, pp. 181-187; April 1959.

5. J. W. Duncan and V. P. Minerva, "100:1 Bandwidth Balun Transformer," Proc. IRE, pp. 156-164; February 1960.

6. C. P. Wu, "Note on Integral Equations and Variational Expressions for Arbitrary Scanning of Regular Infinite Arrays," IEEE Trans. on Antennas and Propagation (Communications), vol. AP-16, pp. 136-138; January 1968.

7. K. K. Mei, "On the Integral Equations of Thin Wire Antennas," IEEE Trans. on Antennas and Propagation, vol. AP-13, pp. 374-379; May 1965.

8. R. W. P. King, The Theory of Linear Antennas, Harvard University Press, Cambridge, Mass., 1956, p. 16, pp. 76-85, pp. 381-396.

9. L. C. Van Atta, "Electromagnetic Reflector," U.S. Patent No. 2,908,002; October 6, 1959.

10. E. D. Sharp and M. A. Diab, "Van Atta Reflector Array," IRE Trans. on Antennas and Propagation, vol. AP-8, pp. 436-438; July 1960.

11. D. E. N. Davies, "Some Properties of Van Atta Arrays and the Use of 2-Way Amplification in the Delay Paths," Proc. IEE, vol. 110, pp. 507-512; March 1963.

REFERENCES - continued

12. IEEE Trans. on Antennas and Propagation, vol. AP-12, no. 2; March 1964.

13. T. W. Glynn, "Beam Steering of a Phased Array by Single Element Phase Shifting," IEEE Trans. on Antennas and Propagation, accepted for publication.

14. R. L. Lewis, "Efficient Wide-Angle Coverage Dipole Van Atta Array Design," IEEE Trans. on Antennas and Propagation (Communications), vol. AP-16, no. 2, p. 256; March 1968.

15. W. H. Ku, "Design of Transistor Amplifiers Using the Scattering Parameters of Active Two Ports," Proc. First Asilomar Conference on Circuits and Systems, pp. 100-111; November 1967.

16. W. H. Ku, "Negative Resistance Devices Using a Multiple Number of Tunnel Diodes or Varactors," NATCOM Proceedings, October 1965; and, IEEE Trans. on Communication Technology, vol. COM-14, no. 4, pp. 478-483; August 1966.

17. W. H. Ku, "Some Results on the Stability Theory of Active Antenna Arrays with Imbedded Tunnel Diodes -- Part I," ARL Research Note No. 678, Applied Research Laboratory; November 1966.

18. M. Marcus and H. Ming, A Survey of Matrix Theory and Matrix Inequalities, Allyn and Bacon, Inc.; 1964.

19. W. K. Cetauruk, "Computer Draws Art Work for Stripline Devices," Microwaves, pp. 48-52; November 1966.

20. R. C. Hansen, Microwave Scanning Antennas, vol. II, Academic Press, New York and London; 1966, p. 303.

21. J. A. Stratton, Electromagnetic Theory, McGraw Hill, New York and London; 1941, p. 452.

22. C. T. Tai, "The Optimum Directivity of Uniformly Spaced Broadside Arrays of Dipoles," IEEE Trans. on Antennas and Propagation, vol. AP-12, pp. 447-454.

23. J. L. Allen, "The Theory of Array Antennas," Lincoln Laboratory Report No. 323, p. 10; July 1963.

UNCLASSIFIED
Security Classification

DOCUMENT CONTROL DATA - R & D

(Security classification of title, body of abstract and indexing annotation must be entered when the overall report is classified)

1 ORIGINATING ACTIVITY (Corporate author)	2a. REPORT SECURITY CLASSIFICATION
Sylvania Electronic Systems Sylvania Electric Products Inc. 40 Sylvan Road, Waltham, Mass. 02154	Unclassified 2b. GROUP N/A

3 REPORT TITLE

ACTIVE ELEMENT ARRAY

4 DESCRIPTIVE NOTES (Type of report and inclusive dates)

Final Report - 2 Feb 1967 - 16 April 1968

5 AUTHOR(S) (First name, middle initial, last name)

Peter Ver Planck
Walter Ku
Thomas Glynn

6 REPORT DATE	7a. TOTAL NO. OF PAGES	7b. NO. OF REFS
October 1968	204	23

8a. CONTRACT OR GRANT NO.	9a. ORIGINATOR'S REPORT NUMBER(S)
F30602-67-C-0189 b. PROJECT NO. 4519 c. Task No. 451901 d.	9b. OTHER REPORT NO(S) (Any other numbers that may be assigned this report) RADC-TR-68-221

10. DISTRIBUTION STATEMENT

This document is subject to special export controls and each transmittal to foreign governments, foreign nationals or representatives thereto may be made only with prior approval of RADC (EMCRR), GAFB, N.Y. 13440.

11 SUPPLEMENTARY NOTES	12. SPONSORING MILITARY ACTIVITY
	Rome Air Development Center (EMCRR) Griffiss Air Force Base, New York 13440

13 ABSTRACT

This report describes the Active Element Array study which was conducted to determine the feasibility of constructing a 16-element microwave retrodirective array employing spiral antennas and bilateral tunnel diode amplifiers. The shunt-diode type of amplifier originally proposed was shown to be impractical for small arrays because of its inherent mismatch.

Better performance was indicated for matched bilateral amplifiers, but there is a serious gain limitation imposed by antenna-element mismatch which is absent in unilateral arrays. For the cavity-backed spiral antennas constructed under the present contract, the inter-antenna isolation exceeded the mismatch return loss by as much as 30 db, so that the 6-db gain advantage of the bilateral scheme was totally negated by the mismatch-imposed gain limitation.

The results of this study indicate that future investigation should concentrate on Van Atta arrays composed of a few well-isolated antenna elements interconnected by high-gain unilateral amplifiers.

DD FORM 1 NOV 65 1473

UNCLASSIFIED
Security Classification

Security Classification

14. KEY WORDS	LINK A		LINK B		LINK C	
	ROLE	WT	ROLE	WT	ROLE	WT
Retrodirective Arrays Van Atta Arrays Active Arrays Cross-Section Enhancement Active Reflectors						

UNCLASSIFIED

Security Classification